

DISS. ETH NO. 26020

**Synergistic Effects of Redox Processes and Ligand-Controlled  
Dissolution of Fe(III)(hydr)oxide Phases**

A thesis submitted to attain the degree of  
DOCTOR OF SCIENCES of ETH ZURICH  
(Dr. sc. ETH Zurich)

presented by

JAGANNATH BISWAKARMA

M.Sc. UZH in Environmental Sciences, University of Zurich

born on 26.12.1988

citizen of India

accepted on the recommendation of

Prof. Dr. Janet G. Hering (examiner)

Dr. Stephan J. Hug (co-examiner)

Dr. Walter D. C. Schenkeveld (co-examiner)

Prof. Dr. Stephan M. Kraemer (co-examiner)

Prof. Dr. Andreas Kappler (co-examiner)

2019

Dedicated to

My Elegant, Empowering, & Encouraging -

MOTHER, FATHER  
&  
GRANDMOTHERS



## ACKNOWLEDGEMENT

The journey as a doctoral student has been incredible for me. I am thankful to all of you who contributed to this journey.

It gives me immense pleasure to express my sincere thanks to Prof. Janet Hering. Janet's expertise, strong guidance, support and patience have enabled me to be creative, confident and extra-motivated. Janet has inspired me throughout this journey. I am heartily grateful to Janet for her contribution to my scientific growth. It is truly a memorable and wonderful experience working under Janet's guidance.

I am indebted to Dr. Stephan Hug for giving me an unique opportunity to pursue my doctoral studies under his supervision in Eawag/ETH Zurich. Stephan's careful supervision, critical feedback, valuable suggestions to develop understanding of the topic have contributed significantly to the production of this thesis. I am thankful to Stephan for his commitment to the success of this thesis.

My sincere thanks to Dr. Susan Borowski, Prof. Stephan Kraemer, Dr. Walter Schenkeveld and Kyounglim Kang for stimulating discussions, their valuable inputs on manuscripts and constant encouragements.

I express my sincere thanks to Prof. Andreas Kappler for reviewing and evaluating my thesis. I am grateful to Prof. Lenny Winkel for chairing the defense examination.

I am happy to thank Swiss National Science Foundation (SNF) for funding the project and giving me opportunities to travel for conferences and seminars.

I am very thankful to Dr. Andreas Voegelin for introducing me to the world of synchrotron based techniques and Dr. Ralf Kägi to electron microscopy.

I am very grateful to Thomas Rüttimann for his assistance in lab, care and moral support. I learnt many useful analytical skills from Thomas's technical expertise. Thomas's jokes kept me alive in long lab days. I am thankful to Ursi Schönenberger for her constant encouragements, for making our office space cheerful and for our friendship. I am delighted to thank Numa Pfenninger and Irene Brunner for their support in laboratories and for fun-filled activities.

My special thanks to Benita Schweiger who conducted her master's thesis under my co-supervision and brought exciting results for understanding iron precipitate dissolution.

I am grateful to Prof. Mario Schirmer for giving me an opportunity to collaborate on groundwater arsenic project. I thank Anja Bretzler for her support on the project.

I thank Prof. Geri Furrer for his constant support during studies and for valuable feedback on my defense talk. I had fun working with Geri in organizing IBP PhD Congress 2017.

I extend my thanks to the members of Water resources and Drinking water department. Silvan Wick, Reto Britt and Emanuel Muller provided great atmosphere throughout my time in Eawag. Anna Caterina Senn, Caroline de Meyer, Julie Tolu, Meret Aeppli and Elke Suess motivated me with their positivities and strong encouragement. Thanks to Bas Vriens, Dirk Radny, Stefano Basso and Christian Möck for their support during my early days at Eawag. I thank Ari Feinberg, Francesco Marafatto, Jonas Wielinski, Emiliano Stopelli and Caroline Stengel for enjoyable working environments.

I like to thank my friends who are not associated with my work place but have contributed for my overall development. Ajay Kumar, Bikul Mitra, Gagandeep Singh for enormous support and care; Tonči Novković, Jyotshna Mondal, Somil Miglani, Vidya Vishwanathan, Olivia Meier, Ekansh Anand for always being supportive of me; Nikolina Novković, Nicolas Ruffray, Ekaterina Nadibaidze, Meenakshi Ravichandran, Marko Peric, Corina Gorban, Manoj Naikade, Nicole Sani Kast, Jasmine Schönenberger for enjoyable times we spend outside academia; Jacinta Edibeli, Gitika Srivastava, Surendra Babu, Suresh Mali, Jérôme Frutiger for support and help; Mayank Paramar, Magdalena Kruza, Xinwei Fang, Michelle for encouragements beyond words. Thank you.

Especial thanks to my wonderful family in India. My younger brother's advices, help, and encouragements to my endeavors are invaluable. I am grateful to my each and every family members who are always there for me with open arms.

At last but not least, I express my humble regards to my parents for their commitment to my ambition and selfless sacrifices.

Jagannath Biswakarma  
Zurich, 25 April 2019

“The woods are lovely, dark and deep,

But I have promises to keep,

And miles to go before I sleep,

And miles to go before I sleep.”

- Robert Frost



# TABLE OF CONTENT

<b>Acknowledgement</b>	<b>III</b>
<b>Abstract</b>	<b>IX</b>
<b>Zusammenfassung</b>	<b>XIII</b>
<b>Chapter 1. Introduction</b>	<b>1-10</b>
<b>Chapter 2. Fe(II)-Catalyzed Ligand-Controlled Dissolution of Iron(hydr)oxides</b>	<b>11-62</b>
Abstract	12
Introduction	13
Materials and Method	15
Results and Discussion	18
Environmental Significance	31
Acknowledgement	32
References	32
Supporting Information	37
<b>Chapter 3. Linking Isotope-Exchange with Fe(II)-Catalyzed Dissolution of Iron(hydr)oxides in the Presence of the Bacterial Siderophore Desferrioxamine-B</b>	<b>63-94</b>
Abstract	64
Introduction	65
Materials and Method	66
Results and Discussion	69
Environmental Significance	82
Acknowledgement	83
References	83
Supporting Information	87
<b>Chapter 4. Photochemically Induced Fe(II)-Catalyzed Ligand-Controlled Dissolution of Iron(hydr)oxides</b>	<b>95-124</b>
Abstract	96
Introduction	97
Materials and Method	98
Results and Discussion	100
Environmental Implications	110
Acknowledgement	111
References	112
Supporting Information	115
<b>Chapter 5. Conclusion</b>	<b>125-142</b>
<b>Curriculum vitae</b>	<b>143</b>





## ABSTRACT

Dissolution of iron(III)(hydr)oxides is a key process in the biogeochemical cycle of iron (Fe) and biological Fe acquisition. Reactions that promote dissolution in the circumneutral pH-range, where Fe(III)(hydr)oxides are poorly soluble and dissolution is slow, are thus highly relevant. Previous studies have shown synergistic effects on ligand-controlled dissolution of Fe(III)(hydr)oxides with two or more ligands. More dramatic effects on ligand-controlled dissolution rates have been observed in a few studies conducted at low pH and under anoxic conditions, in which addition of small amounts of Fe(II) increased dissolution rates by factors of 10-100.

Despite its probable importance, Fe(II)-catalyzed dissolution has not been investigated in the environmentally relevant pH range of 6.0-8.5 under oxic as well as anoxic conditions. Moreover, suggested mechanisms for Fe(II)-catalyzed dissolution at low pH have not been further investigated and may not apply at higher pH. More recent studies have shown that adsorption of Fe(II) at higher pH can lead to phase transformations and recrystallization. Destabilization of Fe(III)-phases by transfer of negative charge from Fe(II) might provide an alternative pathway for accelerated dissolution.

This doctoral research examined the accelerating effects of Fe(II) on ligand-controlled dissolution of Fe(III)(hydr)oxide phases at pH 6.0, 7.0, and 8.5, under anoxic and oxic conditions. The main goal was to determine the extent to which catalytic concentrations of Fe(II) can accelerate ligand-controlled dissolution under environmentally relevant conditions. A more general goal was to improve our understanding of the mechanism of Fe(II)-catalyzed ligand-controlled dissolution processes.

For these purposes, two structurally different Fe(III)(hydr)oxide minerals, lepidocrocite ( $\gamma$ -FeOOH, Lp) and goethite ( $\alpha$ -FeOOH, Gt), were synthesized and used in experiments with two ligands with different functional groups, ethylenediamine tetra acetic acid (EDTA) and the biogenic ligand-desferrioxamine (DFOB). Batch experiments were conducted with 1.13 mM suspensions of Lp or Gt and 20  $\mu$ M and 50  $\mu$ M EDTA or DFOB. Fe(II) was added or produced *in-situ* by illumination with UV-A light on the surface of Lp or Gt. Experiments at pH 6.0 and 8.5 and some experiments at pH 7.0 were

conducted with 9.5 mM NaCl background solutions buffered with Good's buffers. Most experiments at pH 7.0 were buffered with 3 mM NaHCO<sub>3</sub> and 2% CO<sub>2</sub> in N<sub>2</sub> or air, to simulate natural conditions.

Fourier Transform Infrared spectroscopy coupled with Attenuated Internal Reflection (ATR-FTIR) was used to follow the adsorption of EDTA and the dissolution of the solids *in situ* as a function of time; structural changes on the surface and in the bulk mineral were followed simultaneously. These experiments showed strong catalytic effects of 0.2-10  $\mu$ M Fe(II) and 50  $\mu$ M EDTA on Lp dissolution under anoxic conditions. At pH 6.0, the catalytic effect of added Fe(II) on Lp dissolution was in the range of 7-31. The catalytic effect was also observed with Fe(II) produced photo-chemically. Introduction of oxygen decreased the rate of dissolution and eventually inhibited the dissolution process. No changes in bulk Lp were observed.

In batch experiments with Lp and 50  $\mu$ M DFOB under anoxic conditions, addition of 1-5  $\mu$ M Fe(II) accelerated the rate of dissolution by a factor of up to 80 at pH 7.0. A pseudo first order empirical model, in which the rate of Fe(II)-catalyzed dissolution was assumed to be directly proportional to the free ligand concentration, was applied to quantify dissolution rates. Whether Fe(II) was added before or after DFOB had no significant effect on the observed dissolution rates.

In contrast to the negligible effect on dissolution rates, the order of addition was found to have a significant effect on the fate of added Fe(II) in isotope exchange and dissolution studies conducted with <sup>57</sup>Fe and either EDTA or DFOB. When <sup>57</sup>Fe(II) addition occurred after DFOB or EDTA, most of the added <sup>57</sup>Fe remained in solution, suggesting that no or only minimal isotope exchange occurred when <sup>57</sup>Fe(II)-ligand complexes formed prior to or concurrent with adsorption on Lp. In contrast, when <sup>57</sup>Fe(II) was added before EDTA or DFOB, extensive isotopic exchange occurred within our experimental timeframe (minutes to hours) with Lp, but not with Gt. Upon ligand addition, the previously added <sup>57</sup>Fe reappeared in solution along with, but more slowly than, <sup>56</sup>Fe during Lp dissolution. With Gt, the rates of release of <sup>57</sup>Fe and <sup>56</sup>Fe were in similar range.

Photochemical experiments were conducted with both continuous and intermittent illumination (illumination periods of 5-15 min) with UV-A. At pH 7.0, continuous production of Fe(II) by UV-A increased rates of Lp dissolution by up to 30-fold under anoxic conditions and up to 5-fold even under oxic conditions. After intermittent illuminations, accelerated dissolution continued during subsequent dark periods under anoxic, but not under oxic, conditions, indicating that photoproduced Fe(II) was not protected from oxidation.

Kinetic models were applied to explore possible mechanisms leading to accelerated dissolution and isotope exchange. The main reactions that can describe the observed results are adsorption (of dissolved Fe(II)-ligand complexes, Fe(II), and/or of a ligand on Fe(II) already associated with a surface site), followed by electron transfer from surface Fe(II)-ligand complexes to surface Fe(III)-sites and detachment of Fe(III)-ligand complexes. Our experiments revealed a more complex picture than that previously suggested based on studies at lower pH. The observed isotope exchange and detachment of predominantly  $^{56}\text{Fe}$  after addition of  $^{57}\text{Fe}$  clearly indicate charge transfer at the Lp surface. The accelerating effect of adsorbed Fe(II) is thus most likely due to the presence of mobile charge (in the form of Fe(II) sites) on the surface. Complexation of Fe(II) surface sites with DFOB or EDTA is expected to lead to quick oxidation of the complexed site by electron transfer to a neighboring site, due to the low reduction potential of Fe(II)DOFB and Fe(II)EDTA. The resulting Fe(III) surface complex detaches faster in the presence of neighboring Fe(II) due to weaker Fe(II)-Fe(III) bonds than the corresponding Fe(III)-Fe(III) bonds in non-catalyzed ligand-controlled dissolution. The catalytic cycle continues until the excess dissolved ligand is used up or Fe(II) is oxidized by dissolved oxygen or other oxidants.

The results presented in this thesis demonstrate that sub-micromolar and micromolar concentrations of Fe(II) accelerate ligand controlled dissolution of FeOOH under environmentally relevant conditions. The catalytic effect of Fe(II) was roughly proportional to the concentration of added Fe(II). Under anoxic conditions, rates of Lp dissolution were accelerated more than 15-fold by  $1\text{ }\mu\text{M}$  added Fe(II) in the presence of EDTA at pH 6.0 and of DFOB at pH 7.0. Fe(II) produced by short

intermittent illumination with UV-A light showed roughly half the accelerating effect, presumably due to oxidation of formed Fe(II) by co-formed oxidants such as H<sub>2</sub>O<sub>2</sub>. The effects of Fe(II) were weaker at pH 8.5 than at pH 6.0 and 7.0. The dissolution at pH 8.5 under anoxic conditions with DFOB after intermittent illumination was still accelerated by a factor of two, which is in agreement with the effect observed with 2 μM added Fe(II) and DFOB.

Traces of Fe(II) in oxic environments and at redox interfaces could be formed by reducing ligands, by light, and by iron-reducing microorganisms. Fe(II)-catalyzed ligand-controlled dissolution with formation of dissolved Fe(III) complexes is thus likely important in many natural systems such as in soils, at oxic-anoxic interfaces in shallow lakes and ponds, in groundwater, and generally in environments subject to dynamic redox conditions.

## ZUSAMMENFASSUNG

Die Auflösung von Eisen(III)(hydr)oxiden ist ein grundlegender Prozess im biogeochemischen Eisenkreislauf und in der biologischen Eisenaquisition. Reaktionen, welche die Auflösung im neutralen pH-Bereich, in dem Eisen(III)(hydr)oxide schwer löslich sind und die Auflösung langsam ist, beschleunigen, sind deshalb von grossem Interesse. Frühere Studien zeigten synergistische Effekte zwischen zwei oder mehreren Liganden in der ligandenkontrollierten Auflösung von Fe(III)(hydr)oxiden. Ausgeprägtere Auswirkungen wurden in einigen Studien beobachtet, die bei tiefen pH-Werten und unter anoxischen Bedingungen durchgeführt wurden und in welchen geringe Konzentrationen von Fe(II) die Auflösungsraten mit Liganden um Faktoren von 10-100 erhöhten.

Trotz der zu erwartenden Bedeutung in Umweltsystemen wurde die Fe(II)-katalysierte Auflösung im umweltrelevanten pH-Bereich von 6.0-8.5 und unter oxischen und anoxischen Bedingungen bisher nicht untersucht. Ebenfalls sind die vorgeschlagenen Mechanismen für die Fe(II)-katalysierte Auflösung bei niedrigen pH-Werten nicht weiter untersucht worden und sind möglicherweise bei höheren pH-Werten nicht anwendbar. Neuere Studien haben gezeigt, dass bei höheren pH-Werten die Adsorption von Fe(II) zu Phasenumwandlungen und Rekristallisationen führen kann. Die beobachtete Destabilisierung von Fe(III)-Phasen durch die Übertragung negativer Ladung von adsorbiertem Fe(II) auf die Festphasen könnte eine alternative Erklärung für die beschleunigte Auflösung bieten.

Die vorliegende Doktorarbeit untersuchte die beschleunigenden Effekte von Fe(II) auf die ligandenkontrollierte Auflösung von Fe(III)(hydr)oxidphasen bei pH 6.0, 7.0 und 8.5, sowohl unter anoxischen und oxischen Bedingungen. Das Hauptziel dieser Studien war festzustellen, wie stark katalytische Konzentrationen von Fe(II) die ligandenkontrollierte Auflösung unter umweltrelevanten Bedingungen beschleunigen können. Ein allgemeineres Ziel war ein verbessertes Verständnis der Mechanismen der Fe(II)-katalysierten ligandenkontrollierten Auflösungsprozesse.

Zur Untersuchung dieser Fragen wurden zwei strukturell unterschiedliche Fe(III)(hydr)oxidmineralien, Lepidokrokit ( $\gamma$ -FeOOH, Lp) und Goethit ( $\alpha$ -FeOOH, Gt), synthetisiert und in Experimenten mit zwei Liganden mit unterschiedlichen funktionellen Gruppen,

Ethylendiamintetraessigsäure (EDTA) und Desferrioxamin (DFOB) eingesetzt. Die meisten Experimente wurden mit 1.13 mM Suspensionen von Lp und Gt mit 20  $\mu\text{M}$  und 50  $\mu\text{M}$  EDTA oder DFOB ausgeführt. Fe(II) wurde zugesetzt, oder durch Belichtung mit UV-A Licht direkt auf der Oberfläche von Lp oder Gt gebildet. Experimente bei pH 6.0, pH 8.5 und einige Experimente bei pH 7.0 wurden in 9.5 mM NaCl mit 5 mM nicht-interferierenden Good-Puffern ausgeführt. Die meisten Experimente bei pH 7.0 wurden mit 3 mM  $\text{NaHCO}_3$  und 2%  $\text{CO}_2$  in  $\text{N}_2$  oder Luft gepuffert, um möglichst natürliche Bedingungen zu simulieren.

Fourier-Transformations-Infrarot-Spektroskopie mit abgeschwächter Totalreflektion (ATR-FTIR) wurde verwendet, um die Adsorption von EDTA und die Auflösung der Feststoffe *in situ* und als Funktion der Zeit zu verfolgen. Mit ATR-FTIR konnten strukturelle Veränderungen an der Oberfläche und im Innern der Feststoffe gleichzeitig verfolgt werden. Diese Experimente zeigten starke katalytische Effekte durch 0.2-10  $\mu\text{M}$  zugesetztes Fe(II) auf die Auflösung von Lp mit 50  $\mu\text{M}$  EDTA unter anoxischen Bedingungen. Bei pH 6.0 lag der Faktor der Beschleunigung der Auflösung im Bereich von 7-31. Der katalytische Effekt wurde auch mit Fe(II) beobachtet, das durch photochemische Reaktionen erzeugt wurde. Die Zuführung von Sauerstoff verminderte die Auflösungsrate und hemmte schließlich den katalysierten Auflösungsprozess. Es wurden keine Veränderungen in der Lp Festphase beobachtet.

In Batch-Experimenten mit Lp (1.13 mM) beschleunigte die Zugabe von 1-5  $\mu\text{M}$  Fe(II) unter anoxischen Bedingungen die Auflösungsrate mit 50  $\mu\text{M}$  DFOB bei pH 7.0 um einen Faktor von bis zu 80. Ein empirisches Reaktionsmodell erster Ordnung, bei dem die Rate der Fe(II)-katalysierten Auflösung als direkt proportional zur Konzentration des freien Liganden angenommen wurde, diente zur Quantifizierung der Auflösungsraten. Die Reihenfolge der Zugabe von Fe(II) und DFOB hatte keinen signifikanten Einfluss auf die beobachteten Auflösungsraten.

Im Gegensatz zu den vernachlässigbaren Auswirkungen auf die Auflösungsraten hatte die Reihenfolge der Zugabe einen signifikanten Einfluss auf die Reaktionswege des zugesetzten Fe(II), wie sich in Isotopenaustausch- und Auflösungsstudien mit  $^{57}\text{Fe}$  zeigte. Wenn  $^{57}\text{Fe(II)}$  nach DFOB oder EDTA zugefügt wurde, blieb der größte Teil des zugesetzten  $^{57}\text{Fe}$  in Lösung, was darauf hindeutet, dass kein oder nur ein minimaler Isotopenaustausch stattfand, nachdem  $^{57}\text{Fe(II)}$ -Komplexe vor oder gleichzeitig mit der Adsorption an Lp gebildet wurden. Im Gegensatz dazu fand innerhalb

unseres experimentellen Zeitrahmens (Minuten bis Stunden) ein umfangreicher Isotopenaustausch mit Lp statt, wenn  $^{57}\text{Fe(II)}$  vor EDTA oder DFOB hinzugefügt wurde, nicht aber mit Gt. Nach dem Zufügen von EDTA oder DFOB erschien mit der Auflösung von Lp das zuvor zugegebene  $^{57}\text{Fe}$  zwar zusammen mit  $^{56}\text{Fe}$  (aus Lp) in der Lösung, aber langsamer als  $^{56}\text{Fe}$ . Mit Gt lagen die Freisetzungsraten von  $^{57}\text{Fe}$  und  $^{56}\text{Fe}$  hingegen in einem ähnlichen Bereich. Diese Ergebnisse deuten darauf hin, dass die Reaktionswege des hinzugefügten Fe(II) von der Reihenfolge der Zugabe und von der Struktur der FeOOH-Phase abhängig ist.

Photochemische Experimente wurden sowohl mit kontinuierlicher als auch mit unterbrochener Belichtung (Belichtungsperioden von 5-15 min) mit UV-A durchgeführt. Bei pH 7.0 führte die kontinuierliche photochemische Bildung von Fe(II) durch UV-A zu einer Erhöhung der Auflösungsraten von Lp um bis um das 30-fache unter anoxischen Bedingungen und bis um das 5-fache unter oxischen Bedingungen. Nach unterbrochener Belichtung setzte sich die beschleunigte Auflösung in den nachfolgenden Dunkelphasen unter anoxischen, aber nicht unter oxischen Bedingungen fort, was darauf hindeutet, dass durch photochemische Prozesse gebildetes Fe(II) nicht vor Oxidation geschützt war.

Mit kinetischen Modellen wurden mögliche Reaktionsmechanismen untersucht, die zu einer beschleunigten Auflösung und zum Isotopenaustausch führen können. Die Hauptreaktionen, welche die beobachteten Ergebnisse beschreiben können, sind Adsorption (von gelösten Fe(II)-Komplexen, Fe(II), und/oder von Liganden auf bereits mit Oberflächen assoziiertem Fe(II)), gefolgt von Elektronentransfer von Oberflächen-Fe(II)-Komplexen auf Fe(III) auf der Oberfläche und der Ablösung von Fe(III)-Komplexen. Unsere Experimente zeigten ein komplexeres Bild als die zuvor vorgeschlagenen Modelle basierend auf den Studien bei tieferen pH-Werten. Der beobachtete Isotopenaustausch und die Ablösung von überwiegend  $^{56}\text{Fe}$  nach Zugabe von  $^{57}\text{Fe}$  sind deutliche Indikatoren für Ladungstransfer auf der Oberfläche von Lp. Die beschleunigende Wirkung von adsorbiertem Fe(II) kann daher durch mobile Ladungsträger (in der Form von Fe(II) auf der Oberfläche von Lp) erklärt werden. Die Komplexierung von Fe(II) durch DFOB oder EDTA führt aufgrund des tiefen Redoxpotenzials von Fe(II)DOFB und Fe(II)EDTA erwartungsgemäss zu einer raschen Oxidation des komplexierten Fe(II) durch Elektronenübertragung auf ein Fe(III) Ion auf der Oberfläche. Der dabei gebildete Fe(III)-Oberflächenkomplex kann sich in Gegenwart des benachbart



gebildeten Fe(II) aufgrund der schwächeren Fe(II)-Fe(III) Bindungen schneller von der Oberfläche ablösen als von den entsprechenden Fe(III)-Fe(III) Bindungen in der nicht katalysierten Auflösung. Der katalytische Zyklus wird fortgesetzt, bis der überschüssige gelöste Ligand aufgebraucht ist oder das Fe(II) durch gelösten Sauerstoff oder andere Oxidantien oxidiert wird.

Die in dieser Arbeit beschriebenen Ergebnisse zeigen, dass submikromolare und mikromolare Konzentrationen von Fe(II) die ligandenkontrollierte Auflösung von FeOOH unter umweltrelevanten Bedingungen stark beschleunigen können. Die katalytische Wirkung von Fe(II) ist in erster Näherung proportional zur Konzentration des zugesetzten Fe(II). Unter anoxischen Bedingungen wurden die Raten der Auflösung von Lp durch 1  $\mu\text{M}$  Fe(II) in Gegenwart von 50  $\mu\text{M}$  EDTA bei pH 6.0 und 50  $\mu\text{M}$  DFOB bei pH 7.0 um mehr als das 15-fache beschleunigt. Fe(II), das durch kurzzeitige Belichtung mit UV-A-Licht erzeugt wurde, zeigte etwa die Hälfte des Beschleunigungseffekts, vermutlich aufgrund der Oxidation des gebildeten Fe(II) durch mitgebildete Oxidantien wie  $\text{H}_2\text{O}_2$ . Die Effekte von Fe(II) bei pH 8,5 waren schwächer als bei pH 6.0 und 7.0. Die Auflösung bei pH 8.5 unter anoxischen Bedingungen mit DFOB nach kurzer Beleuchtung wurde um den Faktor zwei beschleunigt, was mit dem beobachteten Effekt von 2  $\mu\text{M}$  zugesetztem Fe(II) übereinstimmt.

Spuren von Fe(II) unter oxischen Bedingungen und in Redox-Übergangszonen können durch reduktive Liganden, Licht und durch eisenreduzierende Mikroorganismen gebildet werden. Die Fe(II)-katalysierte ligandenkontrollierte Auflösung von Fe(III)(hydr)oxiden unter Bildung gelöster Fe(III)-Komplexe ist daher wahrscheinlich in zahlreichen natürlichen Systemen von Bedeutung, zum Beispiel im Böden, in oxisch-anoxischen Übergangszonen in Seen und anderen Oberflächenwässern, im Grundwasser und generell in Umweltsystemen mit dynamischen Redox-Bedingungen.

# **Chapter 1**

## **INTRODUCTION**

---

## Background

Iron (Fe), as an essential micronutrient, is critical to all living organisms. Fe is one of the most abundant elements on our planet; the biogeochemical cycling of Fe affects that of other elements, regulating the dynamics of associated nutrients or contaminants. Commonly, Fe occurs in the environment as either Fe(III) (ferric) or Fe(II) (ferrous) in the form of minerals. Under oxic conditions, the insoluble oxides, hydroxides and oxyhydroxides phases, here collectively termed as Fe(III)(oxyhydr)oxides, are predominant. Dissolution of Fe(III)(oxyhydr)oxide phases is one of the key processes in Fe cycling and biological Fe acquisition. Despite the abundance of Fe in the Earth's crust, low solubility and slow dissolution processes of Fe(III)(oxyhydr)oxides at circumneutral to alkaline pH can lead to Fe deficiencies for biota.<sup>1, 2</sup>

Under Fe-limiting conditions, plants and microorganism can acquire Fe by releasing ligands (L) that promote the dissolution of Fe(III)(oxyhydr)oxides.<sup>3, 4</sup> Previous studies of Fe(III)(oxyhydr)oxide dissolution processes have identified three main pathways for dissolution. Proton-promoted dissolution occurs under acidic conditions.<sup>5</sup> Ligand-controlled dissolution leads to formation of Fe(III)-ligand complexes in solution.<sup>6, 7</sup> Reductive<sup>8, 9</sup> and photo-reductive dissolution<sup>10-13</sup> leads to formation of Fe(II) or, in the presence of ligands, to Fe(II)-ligand complexes. Several previous studies have demonstrated that Fe availability and rates of Fe(III)(oxyhydr)oxide dissolution are increased by natural ligands (e.g. siderophores such as desferrioxamine-B (DFOB), and aerobactin)<sup>14, 15</sup> and by synthetic ligands (e.g. ethylenediaminetetraacetate (EDTA)).<sup>16, 17</sup> Ligand-controlled dissolution rates of Fe(III)(oxyhydr) oxides are slow in the circumneutral pH range but can be accelerated by synergistic effects of two or more ligands.<sup>14, 18-23</sup> For example, the dissolution rates of hematite<sup>20, 24</sup>, ferrihydrite<sup>25</sup>, and goethite with DFOB were accelerated 2-10 times by addition of oxalate<sup>18, 19, 22, 23</sup>, Suwannee river fulvic acid<sup>26</sup>, and ascorbate<sup>20</sup> at acidic pH conditions. Similar synergistic effects were observed for the release of trace elements associated with the dissolution of Fe(III)(hydr)oxides.<sup>27, 28 29</sup>

Earlier studies<sup>9, 16, 30-33</sup> conducted under anoxic conditions found that trace concentrations of Fe(II) accelerated the rate of EDTA-controlled dissolution by factors of 10-100 at low pH, a much greater effect than the 2-10-fold increase observed with synergistic ligands.<sup>19</sup> This catalytic effect was explained by following reaction steps<sup>9</sup>: (a) adsorption of ligands on mineral surface, resulting in formation of Fe(III)-ligand complex on the surface, (b) binding of added Fe(II) to the Fe(III) of mineral surface through the adsorbed ligand, resulting in formation of a ternary complex with the adsorbed ligand. (c) charge transfer from Fe(II) to the Fe(III) through the bridging ligand, resulting in detachment of Fe(III)-ligand complex, and finally (d) rate-determining detachment of Fe(II) from the surface. The detached Fe(II) forms a new ternary complex, leading to a catalytic cycle.

Accelerated dissolution of goethite was also observed under anoxic conditions at pH 6 when experiments were conducted in the presence of both a reductant (ascorbate, citrate or esculetin) and a ligand (DFOB or 2'-deoxymugineic acid), suggesting that dissolution was accelerated by formation of Fe(II).<sup>34, 35</sup>

Fe(II) can be formed not only by the addition of (thermal) reductants but also through photochemical processes. In the presence of light, photoreduction of Fe(III)(oxyhydr)oxides phases can lead to reductive dissolution (i.e., release of Fe(II) into solution) or to re-oxidation of Fe(II).<sup>12, 36</sup> Efficient reductive dissolution is possible only when the rate of Fe(II) detachment is faster than the competing re-oxidation processes. Photochemical experiments conducted in the presence of ligands demonstrated faster rates of dissolution than were observed in (thermal) reductive dissolution.<sup>11, 13, 36-38</sup>

Insight into the possible role of Fe(II) in dissolution can also be gained from studies of the adsorption and reactivity of Fe(II) on Fe(III)(oxyhydr)oxides surfaces conducted under conditions that did not promote net dissolution. Observed ET, isotope exchange and mineral recrystallization in these studies has been explained in terms of a conveyor belt model involving electron conduction through the bulk solid and resulting in release of Fe(II) at a distant surface site, with no net dissolution of the mineral.<sup>39-43</sup> In this model, mineral transformation is driven by crystal growth occurring at the site of initial Fe(II) adsorption. The possibility of such electron conduction through the bulk solid has not been considered in previous studies of Fe(III)(oxyhydr)oxide dissolution.

## Concept of this doctoral thesis

Previous studies suggest that Fe(II)-catalysis could be important in the dissolution of Fe(III)(oxyhydr)oxides phases in sub- and anoxic environments (e.g. in soils and sediments) and at the oxic-anoxic interface in shallow lakes, wetlands and irrigated fields. In the subset of these environments that are exposed to sunlight, photoproduction of Fe(II) could lead to accelerated dissolution. Under anoxic conditions (where Fe(II) would not be subject to re-oxidation), the effect of photoproduced Fe(II) might be expected to persist in the dark; this possibility has not been explored previously. In addition, bulk electron conduction, *if it occurs in such systems*, could potentially retard the re-oxidation of Fe(II) and thus allow catalysis by photo-produced Fe(II) to persist in the dark even under oxic conditions.

Therefore, a systematic investigation of the effects of Fe(II) on ligand-controlled Fe(III)(hydr)oxide dissolution was conducted to provide a better mechanistic understanding of dissolution processes. Experiments were conducted with both added and photo-produced Fe(II) under both anoxic and oxic conditions over the environmentally-relevant pH range 6-8.5.

This doctoral thesis addresses the following specific research questions:

1. What is the effect of added Fe(II) with dissolution-promoting ligands on Fe(III)(hydr)oxide on lepidocrocite (Lp) and goethite (Gt) dissolution?
2. What is the effect of Fe(II) on dissolution when produced *in situ* through photochemical reactions? In addition, does the effect of photo-produced Fe(II) persist in dark under oxic and anoxic conditions?
3. What is the fate of added Fe(II) during Fe(III)(hydr)oxide dissolution? Does the fate of added Fe(II) depends on the presence and absence of ligands?
4. Is the fate of Fe(II) dependent on Fe(III) phases? [There might be possible influence of mineralogy and structure on the interaction of Fe(II) with Fe(III)(hydr)oxide phases.]

The results of this thesis are described in following three chapters:

**Chapter 2: Fe(II)-catalyzed ligand-controlled dissolution of iron(hydr)oxides.** This chapter was published in Environmental Science & Technology, 2019, 53 (1), 88-97. This chapter describes the effect of Fe(II) on Lp ( $\gamma$ -FeOOH) dissolution that was examined in the presence and absence of a synthetic ligand EDTA under anoxic conditions. Most experiments were conducted at pH 6 with

Attenuated Total Reflectance Fourier Transform infrared spectroscopy (ATR-FTIR). Fe(II) was added or *in-situ* produced photochemically.  $^{57}\text{Fe(II)}$  isotope exchange (batch) experiments were conducted to assess the fate of added Fe(II) before and during dissolution. A kinetic model was developed to explain the accelerated FeOOH dissolution.

**Chapter 3: Linking isotope-exchange with Fe(II)-catalyzed dissolution of iron (hydr)oxides in the presence of bacterial siderophore desferrioxamine-B.** The effect of Fe(II) added at micromolar concentrations in the presence of the natural ligand DFOB on Lp dissolution was investigated at pH 7.0 (in carbonate-buffered suspensions). In addition,  $^{57}\text{Fe(II)}$  was added before and after DFOB in order to examine the isotope exchange before and during dissolution.  $^{57}\text{Fe(II)}$  isotope exchange experiments were conducted with Lp at pH 6.0 (MES-buffered), pH 7.0 (MOPS and carbonate-buffered) and pH 8.5 (PIPES-buffered) and with Gt at pH 7 (carbonate-buffered). Accelerated dissolution was observed and could be described, for the entire course of dissolution, with a simple pseudo first order empirical model. A mechanistic kinetic model was developed to describe the accelerated dissolution and also to quantify isotope-exchange before and during dissolution.

**Chapter 4. Photochemically induced Fe(II)-catalyzed ligand-controlled dissolution of iron (hydr)oxides.** The effect of photochemically produced Fe(II) on dissolution of Lp and Gt with the organic ligands EDTA and DFOB was examined, under both oxic and anoxic conditions. Lp dissolution experiments were conducted with EDTA at pH 6 and 7, and with DFOB at pH 7 and 8.5. Gt dissolution was examined with EDTA and DFOB only at pH 7. Bicarbonate buffer was used at pH 7. Fe(III)(hydr)oxide suspensions were subjected to intermittent or continuous irradiation with UV-A light (320-420 nm) to produce Fe(II) *in-situ* under both oxic and anoxic conditions. Photoproduction of Fe(II) was quantified in experiments conducted with a large excess of the strong Fe(II) complexing agent phenanthroline. The extent of accelerated dissolution was found to vary with the dissolution-promoting ligand (i.e., EDTA vs. DFOB), with the solid and with pH. The observed effects could be only partially explained by the concentration of photoproduced Fe(II).

Each of the three main chapters is supplemented by separate sections that provide supporting information. The final chapter provides a summary and synthesis of the findings of this thesis and their environmental significance, along with the outlook for possible future studies.

## References

1. Kraemer, S. M.; Hering, J. G., Biogeochemical controls on the mobility and bioavailability of metals in soils and groundwater. *Aquatic Sciences* **2004**, *66*, (1), 1-2.
2. Kraemer, S. M., Iron oxide dissolution and solubility in the presence of siderophores. *Aquatic Sciences* **2004**, *66*, (1), 3-18.
3. Watteau, F.; Berthelin, J., Microbial Dissolution of Iron and Aluminum from Soil Minerals - Efficiency and Specificity of Hydroxamate Siderophores Compared to Aliphatic-Acids. *European Journal of Soil Biology* **1994**, *30*, (1), 1-9.
4. Hersman, L.; Maurice, P.; Sposito, G., Iron acquisition from hydrous Fe(III)-oxides by an aerobic *Pseudomonas* sp. *Chemical Geology* **1996**, *132*, (1-4), 25-31.
5. Casey, W. H.; Ludwig, C., The mechanism of dissolution of oxide minerals. *Nature* **1996**, *381*, 506.
6. Furrer, G.; Stumm, W., The Coordination Chemistry of Weathering .1. Dissolution Kinetics of Delta-Al<sub>2</sub>O<sub>3</sub> and Beo. *Geochimica et Cosmochimica Acta* **1986**, *50*, (9), 1847-1860.
7. Kraemer, S. M.; Chiu, V. Q.; Hering, J. G., Influence of pH and competitive adsorption on the kinetics of ligand-promoted dissolution of aluminum oxide. *Environmental Science & Technology* **1998**, *32*, (19), 2876-2882.
8. Dos Santos Afonso, M.; Morando, P. J.; Blesa, M. A.; Banwart, S.; Stumm, W., The reductive dissolution of iron oxides by ascorbate. The role of carboxylate anions in accelerating reductive dissolution. *Journal of Colloid and Interface Science* **1990**, *138*, (1), 74-82.
9. Suter, D.; Banwart, S.; Stumm, W., Dissolution of Hydrous Iron(III) Oxides by Reductive Mechanisms. *Langmuir* **1991**, *7*, (4), 809-813.
10. Waite, T. D.; Morel, F. M. M., Photoreductive Dissolution of Colloidal Iron Oxides in Natural Waters. *Environmental Science & Technology* **1984**, *18*, (11), 860-868.
11. Litter, M. I.; Blesa, M. A., Photodissolution of iron oxides. I. Maghemite in EDTA solutions. *Journal of Colloid and Interface Science* **1988**, *125*, (2), 679-687.
12. Wells, M. L.; Mayer, L. M.; Donard, O. F. X.; Sierra, M. M. D.; Ackelson, S. G., The Photolysis of Colloidal Iron in the Oceans. *Nature* **1991**, *353*, (6341), 248-250.
13. Sulzberger, B.; Laubscher, H., Photochemical Reductive Dissolution of Lepidocrocite - Effect of pH. In *Aquatic Chemistry - Interfacial and Interspecies Processes*, Huang, C. P.; Omelia, C. R.; Morgan, J. J., Eds. American Chemical Society: Washington, 1995; Vol. 244, pp 279-290.
14. Sandy, M.; Butler, A., Microbial iron acquisition: Marine and terrestrial siderophores. *Chemical Reviews*. **2009**, *109*, (10), 4580-4595.
15. Kraemer, S. M.; Butler, A.; Borer, P.; Cervini-Silva, J., Siderophores and the dissolution of iron-bearing minerals in marine systems. In *Reviews in Mineralogy and Geochemistry*, 2005; Vol. 59, pp 53-84.

16. Blesa, M. A.; Borghi, E. B.; Maroto, A. J. G.; Regazzoni, A. E., Adsorption of EDTA and iron-EDTA complexes on magnetite and the mechanism of dissolution of magnetite by EDTA. *Journal of Colloid and Interface Science* **1984**, 98, (2), 295-305.
17. Suter, D.; Siffert, C.; Sulzberger, B.; Stumm, W., Catalytic dissolution of iron(III)(hydr)oxides by oxalic acid in the presence of Fe(II). *Naturwissenschaften* **1988**, 75, (11), 571-573.
18. Akafia, M. M.; Harrington, J. M.; Bargar, J. R.; Duckworth, O. W., Metal oxyhydroxide dissolution as promoted by structurally diverse siderophores and oxalate. *Geochimica et Cosmochimica Acta* **2014**, 141, 258-269.
19. Cheah, S. F.; Kraemer, S. M.; Cervini-Silva, J.; Sposito, G., Steady-state dissolution kinetics of goethite in the presence of desferrioxamine B and oxalate ligands: Implications for the microbial acquisition of iron. *Chemical Geology* **2003**, 198, (1-2), 63-75.
20. Dehner, C. A.; Awaya, J. D.; Maurice, P. A.; DuBois, J. L., Roles of Siderophores, Oxalate, and Ascorbate in Mobilization of Iron from Hematite by the Aerobic Bacterium *Pseudomonas mendocina*. *Applied Environmental Microbiology* **2010**, 76, (7), 2041-2048.
21. Lemanceau, P.; Bauer, P.; Kraemer, S.; Briat, J. F., Iron dynamics in the rhizosphere as a case study for analyzing interactions between soils, plants and microbes. *Plant Soil* **2009**, 321, (1-2), 513-535.
22. Loring, J. S.; Simanova, A. A.; Persson, P., Highly mobile iron pool from a dissolution-readsorption process. *Langmuir* **2008**, 24, (14), 7054-7057.
23. Reichard, P. U.; Kretzschmar, R.; Kraemer, S. M., Dissolution mechanisms of goethite in the presence of siderophores and organic acids. *Geochimica et Cosmochimica Acta* **2007**, 71, (23), 5635-5650.
24. Hersman, L.; Lloyd, T.; Sposito, G., Siderophore-Promoted Dissolution of Hematite. *Geochimica et Cosmochimica Acta* **1995**, 59, (16), 3327-3330.
25. Yoshida, T.; Hayashi, K.; Ohmoto, H., Dissolution of iron hydroxides by marine bacterial siderophore. *Chemical Geology* **2002**, 184, (1-2), 1-9.
26. Stewart, A. G.; Hudson-Edwards, K. A.; Dubbin, W. E., Mechanisms of goethite dissolution in the presence of desferrioxamine B and Suwannee River fulvic acid at pH 6.5. *Geochimica et Cosmochimica Acta* **2013**, 115, 1-14.
27. Wolff-Boenisch, D.; Traina, S. J., The effect of desferrioxamine B, enterobactin, oxalic acid, and Na-alginate on the dissolution of uranyl-treated goethite at pH 6 and 25 °C. *Chemical Geology* **2007**, 243, (3-4), 357-368.
28. Liu, X.; Fu, J. W.; Da Silva, E.; Shi, X. X.; Cao, Y.; Rathinasabapathi, B.; Chen, Y.; Ma, L. Q., Microbial siderophores and root exudates enhanced goethite dissolution and Fe/As uptake by As-hyperaccumulator *Pteris vittata*. *Environmental Pollution* **2017**, 223, 230-237.
29. Lee, J. C.; Kim, E. J.; Baek, K., Synergistic effects of the combination of oxalate and ascorbate on arsenic extraction from contaminated soils. *Chemosphere* **2017**, 168, 1439-1446.



30. Borghi, E. B.; Regazzoni, A. E.; Maroto, A. J. G.; Blesa, M. A., Reductive dissolution of magnetite by solutions containing EDTA and FeII. *Journal of Colloid and Interface Science* **1989**, *130*, (2), 299-310.
31. Wehrli, B.; Sulzberger, B.; Stumm, W., Redox processes catalyzed by hydrous oxide surfaces. *Chemical Geology*. **1989**, *78*, (3-4), 167-179.
32. Torres, R.; Blesa, M. A.; Matijević, E., Interactions of metal hydrous oxides with chelating agents. IX. Reductive dissolution of hermatite and magnetite by aminocarboxylic acids. *Journal of Colloid and Interface Science* **1990**, *134*, (2), 475-485.
33. Karametaxas, G.; Hug, S. J.; Sulzberger, B., Photodegradation of EDTA in the Presence of Lepidocrocite. *Environmental Science & Technology* **1995**, *29*, (12), 2992-3000.
34. Wang, Z.; Schenkeveld, W. D. C.; Kraemer, S. M.; Giammar, D. E., Synergistic Effect of Reductive and Ligand-Promoted Dissolution of Goethite. *Environmental Science & Technology* **2015**, *49*, (12), 7236-7244.
35. Schenkeveld, W. D. C.; Wang, Z.; Giammar, D. E.; Kraemer, S. M., Synergistic Effects between Biogenic Ligands and a Reductant in Fe Acquisition from Calcareous Soil. *Environmental Science and Technology* **2016**, *50*, (12), 6381-6388.
36. Goldberg, M. C.; Cunningham, K. M.; Weiner, E. R., Aquatic Photolysis - Photolytic Redox Reactions between Goethite and Adsorbed Organic-Acids in Aqueous-Solutions. *Journal of Photochemistry and Photobiology A: Chemistry*. **1993**, *73*, (2), 105-120.
37. Borer, P.; Kraemer, S. M.; Sulzberger, B.; Hug, S. J.; Kretzschmar, R., Photodissolution of lepidocrocite ( $\gamma$ -FeOOH) in the presence of desferrioxamine B and aerobactin. *Geochimica et Cosmochimica Acta* **2009**, *73*, (16), 4673-4687.
38. Borer, P.; Sulzberger, B.; Hug, S. J.; Kraemer, S. M.; Kretzschmar, R., Photoreductive Dissolution of Iron(III) (Hydr)oxides in the Absence and Presence of Organic ligands: Experimental Studies and Kinetic Modeling. *Environmental Science & Technology* **2009**, *43*, (6), 1864-1870.
39. Williams, A. G. B.; Scherer, M. M., Spectroscopic evidence for Fe(II)-Fe(III) electron transfer at the iron oxide-water interface. *Environmental Science & Technology* **2004**, *38*, (18), 4782-4790.
40. Pedersen, H. D.; Postma, D.; Jakobsen, R.; Larsen, O., Fast transformation of iron oxyhydroxides by the catalytic action of aqueous Fe(II). *Geochimica et Cosmochimica Acta* **2005**, *69*, (16), 3967-3977.
41. Yanina, S. V.; Rosso, K. M., Linked reactivity at mineral-water interfaces through bulk crystal conduction. *Science* **2008**, *320*, (5873), 218-222.
42. Handler, R. M.; Beard, B. L.; Johnson, C. M.; Scherer, M. M., Atom exchange between aqueous Fe(II) and goethite: An Fe isotope tracer study. *Environmental Science & Technology* **2009**, *43*, (4), 1102-1107.

43. Katz, J. E.; Zhang, X. Y.; Attenkofer, K.; Chapman, K. W.; Frandsen, C.; Zarzycki, P.; Rosso, K. M.; Falcone, R. W.; Waychunas, G. A.; Gilbert, B., Electron Small Polarons and Their Mobility in Iron (Oxyhydr)oxide Nanoparticles. *Science* **2012**, 337, (6099), 1200-1203.



## Chapter 2

# Fe(II)-Catalyzed Ligand-Controlled Dissolution of Iron(hydr)oxides

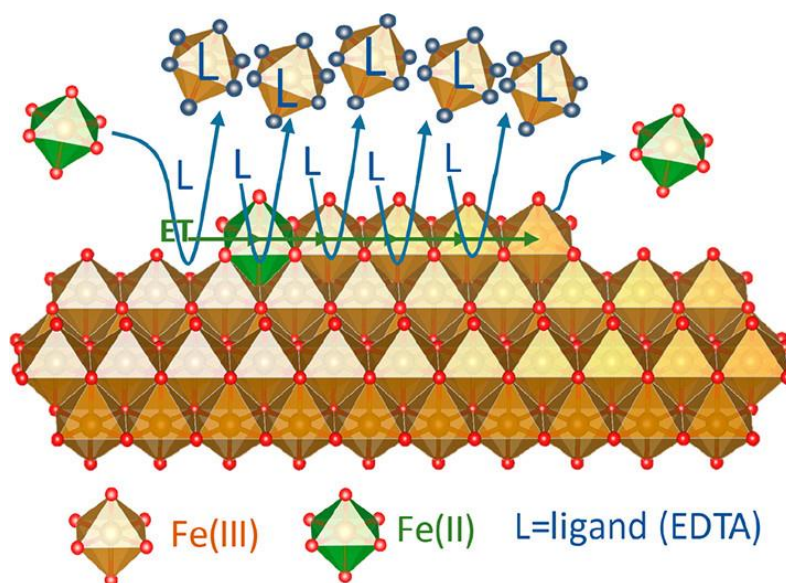
---

Jagannath Biswakarma, Kyounglim Kang, Susan C. Borowski,

Walter D.C. Schenkeveld, Stephan M. Kraemer, Janet G. Hering and Stephan J. Hug

*Published in Environmental Science and Technology, 2019, 53(1), 88-97*

*doi/10.1021/acs.est.8b03910*



*Published TOC*

## Abstract

Dissolution of iron(III)phases is a key process in soils, surface waters, and the ocean. Previous studies found that traces of Fe(II) can greatly increase ligand-controlled dissolution rates at acidic pH, but the extent that this also occurs at circumneutral pH and what mechanisms are involved are not known. We addressed these questions with infrared spectroscopy and  $^{57}\text{Fe}$  isotope exchange experiments with lepidocrocite (Lp) and 50  $\mu\text{M}$  ethylenediaminetetraacetate (EDTA) at pH 6 and 7. Addition of 0.2-10  $\mu\text{M}$  Fe(II) led to an acceleration of the dissolution rates by factors of 7-31. Similar effects were observed after irradiation with 365 nm UV light. The catalytic effect persisted under anoxic conditions, but decreased as soon as air or phenanthroline was introduced. Isotope exchange experiments showed that added  $^{57}\text{Fe}$  remained in solution, or quickly re-appeared in solution when EDTA was added after  $^{57}\text{Fe(II)}$ , suggesting that catalyzed dissolution occurred at or near the site of  $^{57}\text{Fe}$  incorporation at the mineral surface. Infrared spectra indicated no change in the bulk, but changes in the spectra of adsorbed EDTA after addition of Fe(II) were observed. A kinetic model shows that the catalytic effect can be explained by electron transfer to surface Fe(III) sites and rapid detachment of Fe(III)EDTA due to the weaker bonds to reduced sites. We conclude that the catalytic effect of Fe(II) on dissolution of Fe(III)(hydr)oxides is likely important under circumneutral anoxic conditions and in sunlit environments.

## Introduction

The bioavailability of iron in oxic environments with circumneutral pH is limited due to the low solubility and slow dissolution kinetics of iron (oxyhydr)oxide minerals<sup>1</sup> (here collectively termed Fe(III)(hydr)oxides). A common strategy of plants and micro-organisms for Fe acquisition involves the release of ligands (L) that promote the dissolution of Fe(III)(hydr)oxides. Laboratory and field studies have demonstrated that iron availability and rates of Fe(III)(hydr)oxide dissolution are increased by natural ligands (e.g. siderophores such as desferroxamine-B (DFOB) and aerobactin)<sup>2</sup> and by synthetic ligands (e.g. ethylenediaminetetraacetate (EDTA)).<sup>3</sup> It has been further found that dissolution rates can be accelerated by synergistic effects between different ligands, for example between oxalate and DFOB<sup>4, 5</sup> and other low molecular weight organic acids and siderophores.<sup>6, 7</sup> Similar synergistic effects were observed in the dissolution of Fe(III)(hydr)oxides associated with release of trace elements.<sup>8, 9</sup>

While the synergistic effects between ligands were reported to accelerate dissolution rates by factors of 2-10,<sup>4</sup> a group of earlier studies found that a trace of Fe(II) in presence of EDTA accelerated the rate of ligand-controlled dissolution by factors of 10-100 at low pH under anoxic conditions.<sup>10-16</sup> There were no follow-up studies on the catalytic effect of Fe(II) to our knowledge until recently, and it is not known if and under what conditions the strong catalytic effect is also efficient at circumneutral pH. In a recent study, Wang et al. observed a synergistic effect between DFOB or N,N'-di(2-hydroxybenzyl)-ethylenediamine-N,N'-diacetic acid (HBED) and the reducing ligand ascorbate in the dissolution of goethite at pH 6.<sup>17</sup> Similar synergistic effects were observed between ascorbate and DFOB, 2'-deoxymugineic acid, citrate and esculetin.<sup>18</sup> The Fe(II) concentrations resulting from ascorbate addition were not determined, but a careful analysis of the results showed that Fe(II) acted as a catalyst for accelerated dissolution. In a subsequent study using density function theory, Kubicki et al.<sup>19</sup> found that adsorption of Fe(II) near an Fe(III) corner site with adsorbed oxalate lead to a weakening of bonds between the corner site and the lattice, explaining a faster rate of detachment of this site from the lattice. A synergistic effect between oxalate and ascorbate was also recently reported in the extraction of arsenic from contaminated soils.<sup>20</sup>

The catalytic effect of Fe(II) in the earlier dissolution studies conducted at low pH has been explained as follows: Fe(II), either added or generated through reduction of surface Fe(III) by a reductant, can form ternary surface complexes, e.g.  $\equiv\text{Fe(III)-L-Fe(II)}$  (bonds to the lattice are symbolized by  $\equiv$ ). Electron transfer (ET) then leads to formation of  $\equiv\text{Fe(II)-L-Fe(III)}$  and rapid detachment of Fe(III)L into solution due to the relatively weaker Fe(II)-L bonds compared to Fe(III)-L bonds. Detachment of Fe(II) then leads to formation of new ternary surface complexes and to accelerated dissolution in a catalytic cycle.

Several more recent studies found that Fe(II) adsorption on Fe(III)(hydr)oxides, in the absence of ligands, can lead to isotopic exchange and recrystallization of the mineral <sup>21-28</sup> and suggested a mechanism for the recrystallization that might also provide alternative explanations for Fe(II) catalyzed dissolution. The recrystallization was explained by a model in which electrons transferred from adsorbed Fe(II) to the surface are mobile within the Fe(III)(hydr)oxide bulk solid. This leads to formation of Fe(III) and growth at the site of initial Fe(II) adsorption and to formation and detachment of Fe(II) and thus dissolution at a remote surface site. <sup>21</sup> Based on the studies on Fe(II)-catalyzed recrystallization and on the observations and suggestions by Wang et al. and Schenkeveld et al. <sup>17, 18</sup>, delocalization of charge in the mineral structure could play an important role in the accelerated Fe(II)-catalyzed dissolution of Fe(III)(hydr)oxides.

In a new approach to study dissolution of Fe(III)(hydr)oxides, we applied Attenuated Total Reflectance Fourier-transformed Infrared (ATR-FTIR) spectroscopy to examine the dissolution of lepidocrocite (Lp) and to observe structural changes in the bulk and on the surface before and during the dissolution process continuously with high time resolution (no filtration is required). We used ATR-FTIR previously to study the structure and the photoreactions of surface complexes of citrate,<sup>29</sup> DFOB and aerobactin <sup>30</sup> and of dicarboxylates, <sup>31</sup> but not to follow changes in Lp structure and its dissolution. In studies by Borer et al.,<sup>32-35</sup> we investigated light induced photo-reductive dissolution of Lp in the absence and presence of DFOB and aerobactin, considering Fe(II) as a reaction product but not its potential autocatalytic role. <sup>32-35</sup>. In the current study, we address the catalytic effect of Fe(II) in the non-reductive ligand-controlled dissolution in the dark, with added and photo-generated Fe(II). Isotope experiments with <sup>57</sup>Fe(II) were used to probe the fate of added Fe(II) and the importance of

charge migration and isotopic exchange. Further, we applied kinetic modeling to test if proposed mechanisms are able to describe experimental results. Lp was chosen due its relevance in the environment and EDTA as a model ligand for non-reducing siderophores with predominantly carboxylate groups and due to its applications in fertilizers to increase the solubility of iron in soils. Fe(II) catalyzed dissolution might be an important pathway in the dissolution of iron(III) phases in sub- and anoxic environments, e.g. in soils and sediments, and in the oxic-anoxic interface in shallow lakes, wetlands and irrigated fields. Photo-produced Fe(II) might accelerate dissolution of iron(III) phases in sunlit oxic environments, e.g. in the ocean and in the atmosphere. Studies addressing these questions at circumneutral pH (which have not been conducted so far) are of particular interest because the solubility of Fe(III) phases is minimal in this pH-range. In a parallel study, the effect of added Fe(II) is investigated with Lp, goethite, hematite and 2-line ferrihydrite and the ligands HBED and DFOB over a larger pH range.<sup>36</sup>

## **Materials and Methods**

### **Chemicals and Solutions**

All chemicals used were of analytical grade and are listed in Table S1. Aqueous solutions were prepared using high-purity doubly-deionized (DDI) water (Barnstead Nanopure). To perform studies on isotope exchange and Lp dissolution, a 20 mM <sup>57</sup>Fe(II) stock solution was prepared by dissolving 5.7 mg <sup>57</sup>Fe (Sigma-Aldrich, 95% pure) in 100 µl 2.5 M HCl and dilution to 5.00 ml with DDI H<sub>2</sub>O. The <sup>57</sup>Fe powder was 99% pure in Fe, with an isotopic composition of 95.06 % <sup>57</sup>Fe, 3.04% <sup>56</sup>Fe and 1.86% <sup>58</sup>Fe (Certificate of Analysis of the supplier).

### **Lp (γ-FeOOH) synthesis and characterization**

The synthesis of Lp was modified from Schwertmann<sup>37</sup> and is described in more detail in the Supporting Information (SI). Briefly, 60 mM FeCl<sub>2</sub> was purged with a stream of air and titrated with 1M NaOH to within a pH range of 6.65 - 6.76 in a strongly stirred solution, until NaOH consumption ceased. After 2 h, the bright orange suspended particles were collected by centrifugation and repeatedly washed by resuspension and centrifugation with DDI water. Finally, the solid was collected and dried with stream of N<sub>2</sub>. The purity and the properties of the synthesized Lp were



determined by X-ray diffraction (XRD), ATR-FTIR, and scanning electron microscopy (SEM), see SI, Figures S1-S3. The specific surface area of Lp was measured as 63 m<sup>2</sup>/g by a multipoint N<sub>2</sub> Brunauer–Emmett–Teller (BET) adsorption method (Quantachrome Nova 3200).

### ATR-FTIR measurements

ATR-FTIR spectroscopy was employed to investigate the adsorption of EDTA onto Lp and to follow the dissolution of Lp at pH 6 and 7. Measurements were performed on a Biorad FTS 575C instrument equipped with a liquid N<sub>2</sub>-cooled mercury cadmium telluride (MCT) detector and a nine reflection diamond ATR unit (SensIR Technologies, Danbury, CT), as described in detail in the SI. Briefly, a thin layer of 40-60 µg Lp was deposited on the ATR crystal (diamond,  $\phi$  4 mm). IR absorbance spectra of the layer were recorded after drying with a gentle stream of N<sub>2</sub>. Subsequently, the layer was covered with 40 ml 9.5 mM NaCl (38 ml 10 mM NaCl) and 5 mM MES/MOPS (2 ml 100 mM MES/MOPS stock solution). Continuous purging of the aqueous solution with high purity N<sub>2</sub> gas led to removal of dissolved O<sub>2</sub> and desorption of adsorbed CO<sub>2</sub> and served to stir the solution during measurements. Residual O<sub>2</sub> concentrations after 3 h were < 10 nM (measured with a photo-luminescent probe directly in the reaction cell, see SI). At this point, a single-beam background spectrum with the Lp-layer in contact with the anoxic background electrolyte was recorded. Subsequently, difference absorbance ( $\Delta A$ ) spectra were measured continuously, every 43 s or 71 s.

**EDTA and Fe(II) addition.** 50 µM EDTA (400 µl 5 mM EDTA deoxygenated stock solution) was added 180-200 s after the background spectrum was measured. Fe(II) (0.2-10 µM) was added 1800 s after EDTA addition. Toward the end of the measurement after 6300 s, synthetic air or 1mM phenanthroline was added to examine the effect of O<sub>2</sub> or phenanthroline on dissolution. The same experiments were performed with addition of Fe(II) 1800 s before addition of EDTA. Experiments at each of the seven different Fe(II) concentrations were performed in duplicate. All procedures except the illumination with UV-light were performed under weak yellow light (>550 nm), to avoid photochemical reactions with solid and dissolved Fe(III) species.

**Photochemically produced Fe(II).** A UV (365 nm, bandwidth 10 nm) light-emitting diode (Dr. Groebel UVElektronik GmbH) was used to produce Fe(II) at the Lp surface under both anoxic (N<sub>2</sub>) and oxic conditions (synthetic, CO<sub>2</sub>-free air). The Lp-layer immersed in the aqueous solution, was

illuminated at a distance of 7.25 cm from the lamp through a UV-transparent glass plate covering the solution. Illumination was done twice for 900 s: (a) 2700-3600 s and (b) 6200-7100 s. The light intensity of the irradiation at the Lp-layer was  $150 \text{ W/m}^2$  (approximately double the irradiance of natural sunlight in the range of 300-450 nm) as measured by ferrioxalate actinometry (see SI).

### **$^{57}\text{Fe(II)}$ isotope exchange and Lp dissolution with ICP-MS analysis.**

$^{57}\text{Fe(II)}$  was used to investigate the fate of the added Fe(II) during the dissolution process. Batch dissolution experiments were conducted under anoxic conditions at pH 6 at room temperature. Lp suspensions ( $1125 \text{ } \mu\text{M} \approx 0.100 \text{ g L}^{-1}$ ) were prepared by dispersing 10.0 mg Lp in 100 ml aqueous solution (9.5 mM NaCl and 5 mM MES). Suspensions were purged with  $\text{N}_2$  for at least 4 h before addition of EDTA or  $^{57}\text{Fe(II)}$ . Fe(II) was either applied after or before EDTA: (a)  $1.2 \text{ } \mu\text{M}$   $^{57}\text{Fe(II)}$  was injected 30 min after 50  $\mu\text{M}$  EDTA addition, and (b) 1.0 or 1.2  $\mu\text{M}$   $^{57}\text{Fe(II)}$  was added 30 min before EDTA addition. The time between Fe(II) and EDTA addition made it possible to a) examine Lp dissolution in the presence of EDTA and b) to investigate isotope exchange in the absence of EDTA. Aliquots of 1.5 ml were withdrawn periodically, filtered through a 0.1  $\mu\text{m}$  nylon filters (Whatman® Puradisc 13 syringe filters) and diluted in 1%  $\text{HNO}_3$  (Merck, suprapure) for inductively coupled plasma-mass spectrometry (ICP-MS, Agilent 7500ce) analysis. The dissolution of Lp was followed at mass 56, with counts calibrated to represent the total concentration of all iron isotopes from Lp. Dissolution rates were determined as the slope of the linear fit of the dissolved Fe concentration as a function of time over the time-interval 600-2400s after Fe(II) addition. We use the following definitions:

$[\text{}^{56}\text{Fe}]^*_{\text{diss}}$  Concentration of dissolved  $^{56}\text{Fe}$  multiplied with 1.092 to represent the total dissolved iron (sum of all iron isotopes) released from Lp. (5.85%  $^{54}\text{Fe}$ , 91.57%  $^{56}\text{Fe}$ , 2.12%  $^{57}\text{Fe}$ , 0.28%  $^{58}\text{Fe}$ ). This is the concentration of Fe as usually measured with ICP-MS at mass 56, with counts calibrated with certified standard solutions.  $^{56}\text{Fe}$  comes from dissolution of Lp or from exchange of added  $^{57}\text{Fe}$  with  $^{56}\text{Fe}$  from Lp. We corrected for the 3%  $^{56}\text{Fe}$  impurity in 1-1.2  $\mu\text{M}$  added  $^{57}\text{Fe}$ . This correction is small ( $<0.04 \text{ } \mu\text{M}$ ) compared to the concentrations of  $^{56}\text{Fe}$  released from Lp by isotope exchange and dissolution.

$[^{57}\text{Fe}]_{\text{diss}}$  Concentration of dissolved  $^{57}\text{Fe}$ . Measured with ICP-MS at mass 57 and calibrated with normal certified Fe standards, considering that they contain 2.12%  $^{57}\text{Fe}$ .

$[^{57}\text{Fe}]_{\text{tracer, diss}}$  To follow the concentration of  $^{57}\text{Fe}$  added as a tracer, we subtracted the  $^{57}\text{Fe}$  coming from dissolution or isotope exchange with Lp:

$$[^{57}\text{Fe}]_{\text{tracer, diss}} = [^{57}\text{Fe}]_{\text{diss}} - 0.0212[^{56}\text{Fe}]_{\text{diss}}^*$$

(The subtracted concentration of  $^{57}\text{Fe}$  from dissolution of Lp is 1.06  $\mu\text{M}$ , when 50  $\mu\text{M}$  Fe(III) is dissolved in the presence of 50  $\mu\text{M}$  EDTA).

## Results and Discussion

### Lp dissolution monitored with ATR-FTIR

Fig 1A shows the ATR-FTIR absorbance spectrum of a Lp layer and a SEM image of the Lp in the inset. The Lp consists of plate-like (50-100 nm width and 200-500 nm length) aggregates of 200-500 nm long rods of 10 nm width and less than 10 nm thickness. The IR spectrum shows the characteristic vibrations of Lp at 1160  $\text{cm}^{-1}$ , 1021  $\text{cm}^{-1}$ . The full spectrum shown in Figure S1 also shows the characteristic band of rod-shaped Lp at 752  $\text{cm}^{-1}$  (in contrast to plate-shaped Lp where this band is located at 742  $\text{cm}^{-1}$ ).<sup>38</sup> Figure 1B shows ATR-FTIR difference absorbance ( $\Delta A$ ) spectra recorded during EDTA adsorption over 1800 seconds at pH 6 under anoxic condition. Addition of 50  $\mu\text{M}$  EDTA at  $t=180-220$  s lead to characteristic IR absorbance bands in the range of 1700-1200  $\text{cm}^{-1}$  that increased in the first few minutes and then reached a stable level. There are two distinct peaks of adsorbed EDTA at 1570  $\text{cm}^{-1}$  and 1408  $\text{cm}^{-1}$ , which were assigned to the asymmetric and symmetric vibrations of carboxylate groups, respectively.<sup>39</sup> There was an increase, but no significant change in the shape of the spectra during EDTA adsorption. This shows that at pH 6.0 one single surface complex, or several complexes in constant proportions, were formed on the Lp layer. Complexes with different spectral characteristics are formed at lower pH (SI, Figure S4). The adsorption of EDTA led to a small decrease to the left of and a small increase to the right of the absorbance peak of Lp. These small changes in absorbance must be due to local changes in the coordination environment of the Lp lattice at the surface related to adsorption of EDTA, but are not interpreted further. Importantly, there was only a minimal decrease at 1021  $\text{cm}^{-1}$  for the entire duration of the first 1800 s, indicating that there was only minor dissolution of Lp in the presence of EDTA alone.

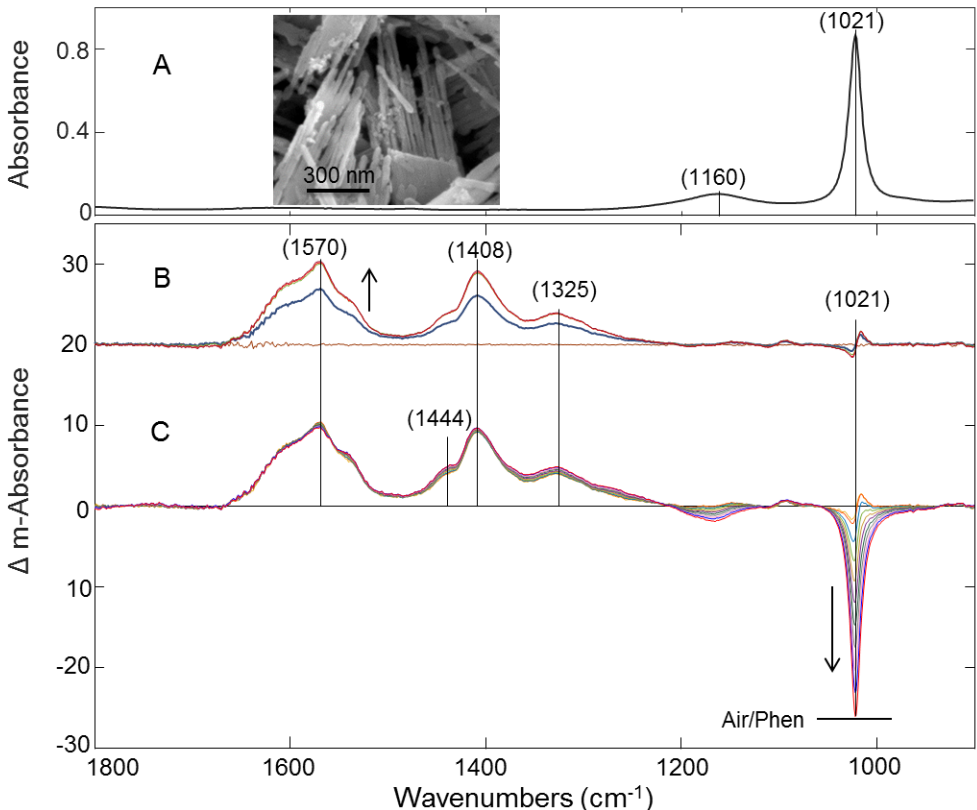


**Figure 1.** (A) ATR-FTIR absorbance spectrum of lepidocrocite (Lp) and SEM image of Lp (inset). (B) Difference absorbance spectra recorded during EDTA adsorption (offset by 20 units), upon addition of 50  $\mu\text{M}$  EDTA to a layer of 40-60  $\mu\text{g}$  Lp in contact with 40 ml aqueous solution (10 mM NaCl and 5 mM MES, pH 6.0). (C) Dissolution of Lp after addition of 1  $\mu\text{M}$  Fe(II) in presence of 50  $\mu\text{M}$  EDTA. Spectra were recorded continuously every 43 s. Averages of every 10 continuous spectra are shown for clarity. All measurements were conducted at pH 6 under anoxic condition by purging the solution with high purity  $\text{N}_2$ . The group of spectra in (B) shows adsorption of EDTA by the increase of peaks at  $1570\text{ cm}^{-1}$  and  $1408\text{ cm}^{-1}$ . The spectra in (C) show the strongly accelerated dissolution of Lp by the decrease of the absorbance of Lp at  $1021\text{ cm}^{-1}$  after addition of 1  $\mu\text{M}$  Fe(II) ( $t_{\text{Fe(II) addition}}=1843\text{ s}$ ). Introduction of synthetic air or 1 mM phenanthroline (Phen) (at  $t = 6300\text{ s}$ ) stopped the dissolution.

The group of spectra in (C) show a decrease in absorbance at  $1021\text{ cm}^{-1}$ , indicating a strong acceleration in dissolution of Lp after addition of  $1\text{ }\mu\text{M}$  Fe(II). Minor spectral changes (which will be discussed later) were recorded in the spectra of adsorbed EDTA upon addition of  $1\text{ }\mu\text{M}$  Fe(II). Introduction of synthetic air or  $1\text{ mM}$  phenanthroline at  $6300\text{ s}$  stopped the accelerated dissolution of Lp. The effect of air indicates a rapid oxidation of Fe(II) at the surface, which ends the catalytic effect of Fe(II) on dissolution. Phenanthroline addition caused rapid formation of Fe(II)-phenanthroline complexes in the solution and apparently also fast desorption of Fe(II) from the surface or

complexation of Fe(II) at the surface, which ended the catalytic action of Fe(II). These results show the importance of the presence of Fe(II) or Fe(II)EDTA for the catalytic effect on the dissolution processes. Similar observations were made when 10  $\mu\text{M}$  Fe(II) was added 3000 s after 50  $\mu\text{M}$  EDTA at pH 7 (see SI, Fig S5).

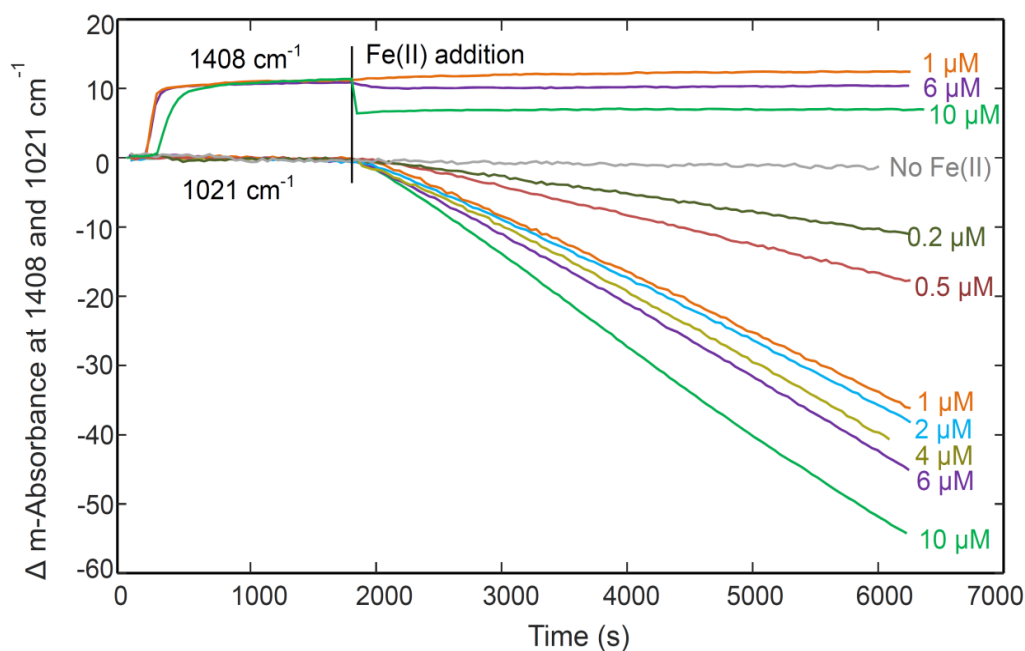


**Fig.2.** Kinetics of EDTA adsorption and Lp dissolution (pH 6.0, anoxic conditions) monitored with ATR-FTIR. Adsorption of EDTA was monitored at  $1408\text{ cm}^{-1}$  and dissolution of Lp at  $1021\text{ cm}^{-1}$ . 50  $\mu\text{M}$  EDTA was added (at  $t=180\text{--}200\text{ s}$ ) after purging the aqueous solution covering the Lp layer with  $\text{N}_2$  for at least 3-4 h, followed by addition of Fe(II) (0.2-10  $\mu\text{M}$ ) after 1800 s. EDTA adsorbed rapidly and reached equilibrium in  $< 600\text{ s}$ . Fe(II) additions lead to accelerated dissolution of Lp. Slopes (at  $1021\text{ cm}^{-1}$ ) were determined from 3000-5000 s.

Fig. 2 shows the kinetics of EDTA adsorption and Lp dissolution at pH 6 under anoxic condition (data points every 43 s). EDTA adsorption was examined at  $1408\text{ cm}^{-1}$  and Lp dissolution at  $1021\text{ cm}^{-1}$ . EDTA adsorbed rapidly and reached equilibrium within 600 s after EDTA addition. There is virtually no decrease of the absorbance at  $1021\text{ cm}^{-1}$ , indicating a low rate of dissolution in the presence of only EDTA. Increasing concentrations of Fe(II) (0.2-10  $\mu\text{M}$ ) were added 1800 s after 50  $\mu\text{M}$  EDTA addition. A clear catalytic effect was observed already for sub-micro molar concentrations of added Fe(II) with a strongly accelerated decrease of absorbance at  $1021\text{ cm}^{-1}$ . The same effect at sub-micromolar concentrations were observed in a parallel study with two different ligands (HBED and DFOB) and several Fe(III)(hydr)oxides<sup>36</sup>. The plots in Fig. 2 show that the dissolution rates

started to increase quickly after addition of Fe(II) and that the decrease in absorbance after Fe(II) addition was linear over time from 3000-6000 s. At the same time, the absorbance of EDTA at 1408  $\text{cm}^{-1}$  showed no visible change for 0.2-1.0  $\mu\text{M}$  added Fe(II). With 6-10  $\mu\text{M}$  added Fe(II), the absorbance decreased quickly and then remained at a stable level. This indicates that a steady-state dissolution rate was reached within 30-120 s, which remained constant throughout our ATR-FTIR experiments. The fast decrease in absorbance at 1408  $\text{cm}^{-1}$  and the changes in the spectra of adsorbed EDTA for 6  $\mu\text{M}$  and 10  $\mu\text{M}$  Fe(II) will be discussed in the last section. The order in which EDTA and Fe(II) were added did not alter the main observations. When 1  $\mu\text{M}$  Fe(II) was added 1800 s before 50  $\mu\text{M}$  EDTA, no changes were recorded for Lp at 1021  $\text{cm}^{-1}$  (see SI, Fig. S6). After EDTA was added, approximately the same rate of decline in absorbance (-0.033 units after 6000 s) was reached as when EDTA was added first (-0.032 units after 6000s). 1 mM phenanthroline addition after  $\sim 8800$  s again stopped the accelerated Lp dissolution.

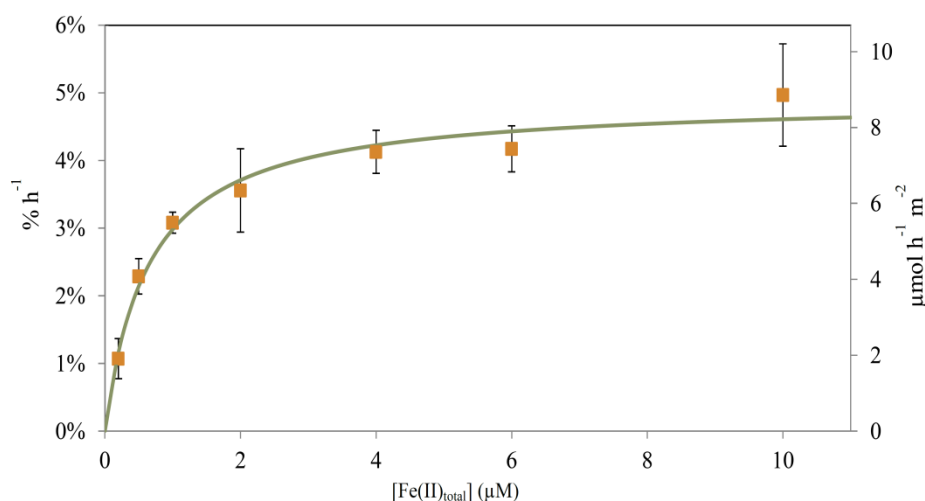


**Fig.3.** Rates of Lp dissolution as a function of added (total) Fe(II) concentrations. Rates expressed as  $\% \text{ h}^{-1}$  (left Y-axis) were calculated from the slopes of the lines in Fig. 2 divided by the initial absorbance of Lp (at 1021  $\text{cm}^{-1}$ ) for each experiment. Rates expressed as  $\mu\text{mol h}^{-1} \text{ m}^{-2}$  (right Y-axis) were calculated using the molecular weight ( $88.85 \text{ g mol}^{-1}$ ) and surface area ( $63 \text{ m}^2 \text{ g}^{-1}$ ) of Lp. The solid line corresponds to a kinetic model (Table 1) as described in the text.

To determine dissolution rates, slopes were calculated from the linear ranges of the decreasing absorbances at 1021  $\text{cm}^{-1}$  in Figure 2. (The ranges were 900-1200 s for EDTA only and 3000-5000 s in the presence of Fe(II)). The rates of Lp dissolution expressed in % of Lp dissolved per time were calculated from the slopes divided by the initial absorbance of Lp at 1021  $\text{cm}^{-1}$  for each

experiment. The initial absorbances of the Lp layers in the different experiments varied in the range of 0.7-0.9 and are listed in SI, Table S2. Figure 3 presents the rate of Lp dissolution as a function of added Fe(II) concentrations. In the range of 0.2-2  $\mu\text{M}$  Fe(II), the rate of Lp dissolution increased close to linearly with increasing concentrations of added Fe(II), after which the increase leveled off. The solid line corresponds to a fit with a kinetic model which is described in a later section.

**Photochemically produced Fe(II).** The kinetics of EDTA adsorption and Lp dissolution, during experiments in which Fe(II) was photo-chemically generated at pH 6.0, are shown in Fig. 4.. EDTA (50  $\mu\text{M}$ ) was added after 180-220 s and EDTA adsorption reached an equilibrium within 600 s under both anoxic and oxic conditions. Again, there was only very minimal Lp dissolution in the presence of EDTA alone. Under UV-illumination (for 900 s) absorbances at 1408 and 1021  $\text{cm}^{-1}$  immediately started to change. The absorbance at 1408  $\text{cm}^{-1}$  (adsorbed EDTA) decreased and stabilized at a lower level during illumination, while the absorbance at 1021  $\text{cm}^{-1}$  (Lp) decreased linearly under both anoxic and oxic conditions. We attribute this mainly to photolysis of Fe(III)-EDTA surface complexes and formation of Fe(II) directly on the Lp surface, due to the high photoreactivity of the adsorbed EDTA,<sup>16</sup> but intrinsic photo-processes of Lp with formation of Fe(II) and OH-radicals could also have contributed to EDTA degradation.<sup>34</sup> From the decrease in the absorbance of Lp, we estimate that 0.14-0.25  $\mu\text{M}$  Fe(II) were formed during each illumination (see SI). After the illumination stopped, photolyzed EDTA was replaced by EDTA from solution which can be seen by the recovery of the absorbance at 1408  $\text{cm}^{-1}$ . Also, Lp dissolution under oxic condition almost instantly came to a halt after illumination. In contrast, under anoxic conditions, Lp dissolution continued in the dark, yet at a slower rate. During a second UV-illumination (from 6200-7100 s) under anoxic conditions, more Lp was dissolved than during the first illumination and the subsequent dissolution rate in the dark continued at a faster rate. Apparently, Fe(II) produced during the second illumination was added to Fe(II) formed in the first illumination and thus increased the concentration of photogenerated Fe(II) and the catalytic effect of Fe(II) during and after the illumination.

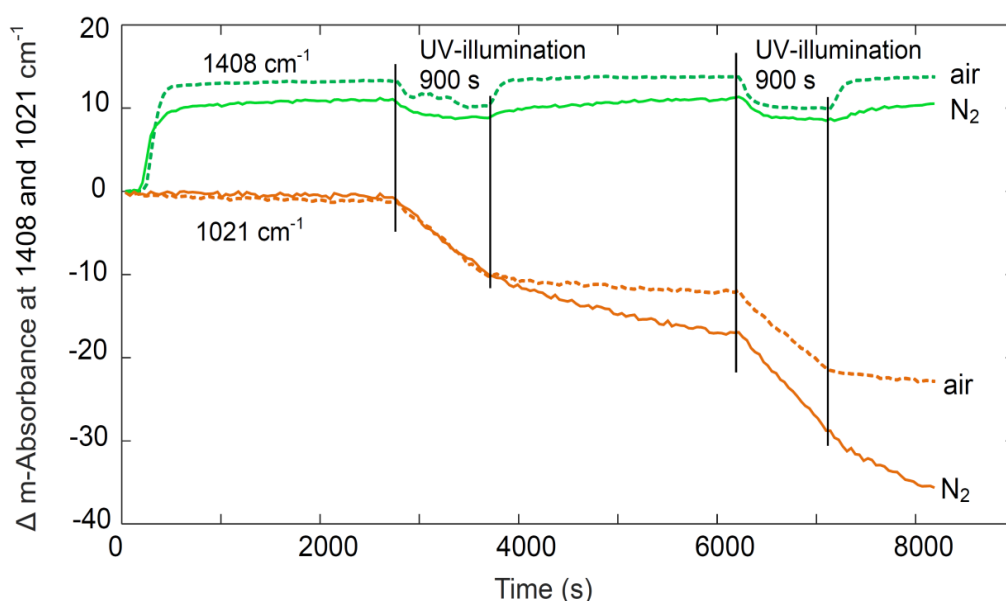


**Fig.4.** Kinetics of EDTA adsorption (monitored at  $1408\text{ cm}^{-1}$ ) and dissolution of Lp (monitored at  $1021\text{ cm}^{-1}$ ) at pH 6 ( $I=0.01\text{ M}$ ) during photochemical experiments. Dashed lines represent experiments performed under oxic conditions and solid lines under anoxic conditions. EDTA ( $50\text{ }\mu\text{M}$ ) was added at 180-220 s. During UV-illumination (for 900 s) with a 365 nm UV-LED lamp, adsorbed EDTA is photolyzed at the surface. After irradiation, photo-transformed EDTA is replaced by EDTA from solution. Lp dissolution was strongly accelerated by UV-illumination under both oxic and anoxic conditions. After irradiation stopped, there was no or very minimal continuing Lp dissolution under oxic condition. In contrast, under anoxic condition, dissolution of Lp continued.

The catalytic effect was not observed under oxic conditions, where the second illumination lead to the same rate and amount of dissolution as the first illumination and to essentially no dissolution in the absence of light. We ascribe this to fast oxidation of the formed adsorbed Fe(II) by dissolved  $\text{O}_2$ . Similar observations were made in experiments at pH 7 (see SI, Fig S7). These results demonstrate a continuing catalytic effect of photochemically produced Fe(II) on non-reductive ligand-controlled dissolution at pH 6 and 7 after illumination stops under anoxic conditions. Qualitatively, the dissolution rates after illumination are similar to those with  $0.2\text{--}0.5\text{ }\mu\text{M}$  added Fe(II) immediately after the illumination stops, and about half of these rates a few minutes later. Since Fe(II) is formed directly at the surface and equilibration with the solution might take a few minutes, the observed Fe(II) catalyzed dissolution rates agree well with the effect of the estimated  $0.14\text{--}0.25\text{ }\mu\text{M}$  Fe(II) in the solution volume of 40 ml.



### **$^{57}\text{Fe}$ isotope exchange and Lp (lepidocrocite) dissolution**

To determine the fate of Fe added as Fe(II) before and during Lp dissolution, we performed dissolution experiments in which we added Fe(II) as  $^{57}\text{Fe(II)}$ .

Figure 5A shows Lp dissolution as a function of time before and after addition of 1.2  $\mu\text{M}$   $^{57}\text{Fe(II)}$  to a Lp suspension (1125  $\mu\text{M}$ ) containing 50  $\mu\text{M}$  EDTA at pH 6.0 under anoxic conditions. The dissolved concentrations of iron coming from dissolution of Lp,  $[\text{}^{56}\text{Fe}]_{\text{diss}}^*$ , are plotted as purple triangles on the right y-axis. In agreement with the FTIR results, the dissolution of Lp was very slow in the absence of Fe(II). After addition of  $^{57}\text{Fe(II)}$ , the dissolution was strongly accelerated and  $[\text{}^{56}\text{Fe}]_{\text{diss}}^*$  reached 42  $\mu\text{M}$  after 16000s, approaching the expected limit of Fe(III) solubility with 50  $\mu\text{M}$  EDTA. The dissolved concentrations of added  $^{57}\text{Fe}$  are plotted as orange squares on the left y-axis ( $[\text{}^{57}\text{Fe}]_{\text{tracer, diss}}$ ). Importantly, added  $^{57}\text{Fe}$  remained in the solution in the presence of EDTA. This shows that the added  $^{57}\text{Fe}$  (added as  $^{57}\text{Fe(II)}$ ) was not incorporated into the surface or bulk during dissolution. A decrease in  $[\text{}^{57}\text{Fe}]_{\text{tracer, diss}}$  would have been observed if adsorption of  $^{57}\text{Fe(II)}$  and incorporation as  $^{57}\text{Fe(III)}$  by electron transfer would have led to preferential dissolution of surface sites or surfaces which are different from the sites of adsorption and incorporation.

In the presence of EDTA, rapid electron transfer at the Lp-surface could have resulted in oxidation of added  $^{57}\text{Fe(II)}$  to  $^{57}\text{Fe(III)}$ . We cannot comment on the oxidation state of  $^{57}\text{Fe}_{\text{tracer, diss}}$  in the presence of EDTA; addition of phenanthroline (phen) to filtered solutions resulted in only very low and inconsistent UV absorbance, which did not allow quantification of  $\text{Fe(II)(phen)}_3$ . Even so, it is clear that  $^{57}\text{Fe}$  added in the presence of EDTA was not incorporated into the solid.

Figure 5B shows  $^{57}\text{Fe}$  isotope exchange and Lp dissolution with reversed addition of  $^{57}\text{Fe(II)}$  and EDTA. In the following, we first discuss the observations before addition of EDTA, when the oxidation state of measurable dissolved Fe can only be Fe(II), followed by the observations after EDTA addition, where the oxidation state of dissolved Fe is mixed, but predominantly Fe(III).

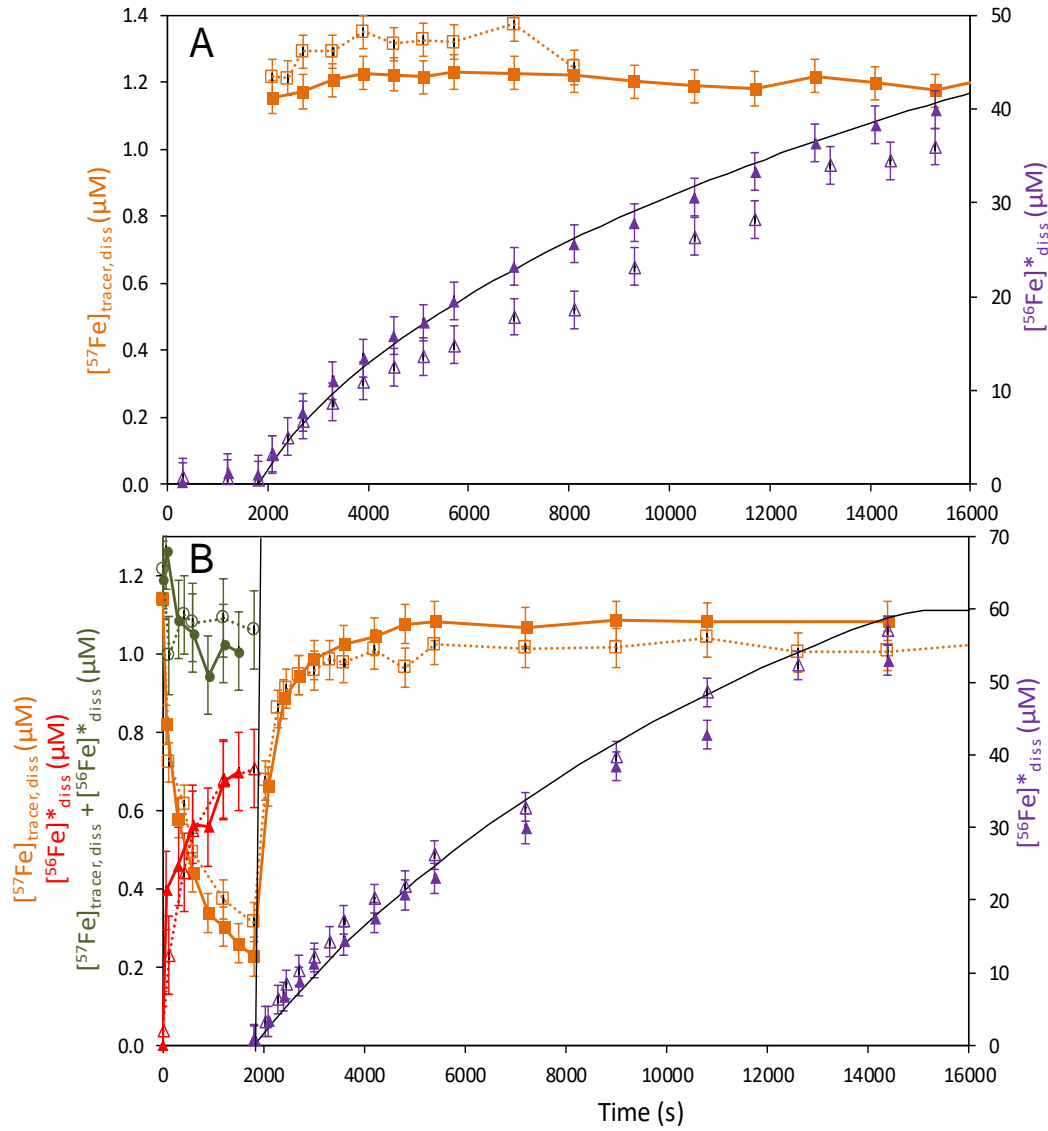


**Figure 5.** Dissolution of (1125 μM) Lp at pH 6.0 under anoxic conditions catalyzed by addition of 1.2 μM Fe(II) as  $^{57}\text{Fe(II)}$  either (a) 1800 s after the addition of 50 μM EDTA or (b) before EDTA addition. Adsorption and isotopic exchange of added  $^{57}\text{Fe(II)}$  were observed when (b) 60 μM EDTA was added 1800 s after Fe(II). Symbols: (purple triangles, right axis) concentration of Fe released into solution by Lp dissolution (reported values of  $^{56}\text{Fe}^*_{\text{diss}}$  correspond to the sum of all Fe-isotopes from Lp as described in Materials and Methods); (orange squares, left axis) concentration of the  $^{57}\text{Fe}$  tracer remaining in or released back into solution where  $^{57}\text{Fe}_{\text{tracer,diss}}$  was corrected for  $^{57}\text{Fe}$  released from Lp; (red triangles, left axis) concentration of  $^{56}\text{Fe}$  in solution resulting from isotopic exchange of added  $^{57}\text{Fe}$  with  $^{56}\text{Fe}$  in Lp ( $t < 1800$  s); (green circles, left axis) sum of dissolved Fe measured as  $^{57}\text{Fe}_{\text{tracer,diss}}$  and  $^{56}\text{Fe}^*_{\text{diss}}$ . Results of duplicate experiments are shown in open and closed symbols (note that results shown in Fig. 5b with filled symbols were scaled to compensate for the addition of a lower concentration (1.0 μM) of  $^{57}\text{Fe(II)}$  in this experiment). Error bars correspond to the standard deviations of ICP-MS measurements obtained from repeated calibrations. Solid black lines show kinetic model fits (Table 1).

In contrast to addition of  $^{57}\text{Fe}(\text{II})$  in the presence of EDTA, we observed an immediate decrease in the concentration of the added  $1.0\text{--}1.2\ \mu\text{M}$   $^{57}\text{Fe}(\text{II})$  (orange squares, left y-axis) in the absence of EDTA, presumably by adsorption. This was followed by a slower decrease in  $[^{57}\text{Fe}(\text{II})]$ , coupled with an increase of  $[^{56}\text{Fe}(\text{II})]_{\text{diss}}^*$  (red triangles, left y-axis), indicating isotope exchange between  $\text{Fe}(\text{II})$  in solution and  $\text{Fe}$  from Lp over the 1800 s before EDTA was added. The sum of these concentrations (green circles on the left y-axis) was  $1.0\text{--}1.1\ \mu\text{M}$ , meaning that  $0.1\text{--}0.2\ \mu\text{M}$  of the added  $\text{Fe}(\text{II})$  remain adsorbed. Since  $[^{56}\text{Fe}]_{\text{diss}}^*$  increased from 0 to  $0.7\ \mu\text{M}$ , up to  $0.7\ \mu\text{M}$   $^{57}\text{Fe}(\text{II})$  must have been incorporated into the surface as  $^{57}\text{Fe}(\text{III})$ . Thus, before EDTA addition, both adsorption and isotope exchange, but no dissolution was observed. This is in agreement with studies showing isotope exchange between dissolved  $\text{Fe}(\text{II})$  and  $\text{FeOOH}$  that leads to recrystallization on longer time scales<sup>21-28</sup>

After addition of EDTA, a rapid increase of  $[^{56}\text{Fe}]_{\text{diss}}^*$  (purple triangles, right axis ) due to catalyzed Lp dissolution was observed. At the same time, the added (tracer)  $^{57}\text{Fe}$  that was previously adsorbed and/or exchanged was released back into solution. Over 80% of the adsorbed/exchanged  $^{57}\text{Fe}$  was in solution after dissolution of  $10\ \mu\text{M}$  Lp within the first 1000 s after addition of EDTA.

This observation shows that added  $^{57}\text{Fe}$  was not preferentially incorporated into surface sites or surfaces that were less prone to dissolution upon addition of EDTA. Although this observation does not exclude ET to other sites and other surfaces, such ET (if it occurs) does not result in the preferential dissolution of those other sites or surfaces.

We can, in the main, exclude preferential dissolution distant from the site at which added  $^{57}\text{Fe}$  was adsorbed, since addition of EDTA resulted in release of  $>80\%$  of the added tracer  $^{57}\text{Fe}$  back into solution. The initially adsorbed  $^{57}\text{Fe}$  (i.e.,  $1\ \mu\text{M}$  of the added  $1.2\ \mu\text{M}$   $^{57}\text{Fe}$ ) corresponds to only 5.7 % of the total active surface site concentration of  $17.5\ \mu\text{M}$  (calculated for  $100\ \text{mg Lp/L}$  with a surface area of  $6.3 \cdot 10^{18}\ \text{nm}^2/\text{L}$  assuming 1.67 active site per  $\text{nm}^2$ .<sup>40</sup> If ET had resulted in preferential dissolution at different surface sites and surfaces (with only the natural abundance of  $^{57}\text{Fe}$ ) then no increase in  $[^{57}\text{Fe}]_{\text{tracer, diss}}$  should have been observed (recall that the reported  $[^{57}\text{Fe}]_{\text{tracer, diss}}$  was corrected for the natural abundance of  $^{57}\text{Fe}$  in Lp). Even if dissolution had occurred randomly at all surface sites (enriched to 5.7 %  $^{57}\text{Fe}$ ), dissolution of  $10\ \mu\text{M}$  Lp would have resulted in a maximum tracer concentration  $[^{57}\text{Fe}]_{\text{tracer, diss}}$  of  $0.57\ \mu\text{M}$ . Incorporation of a minor fraction of  $^{57}\text{Fe}$  (added before

EDTA) into more stable sites and surfaces is, however, consistent with the association of 10-20% of the added  $^{57}\text{Fe}$  with the solid even after dissolution of 50  $\mu\text{M}$  Lp (i.e., measured as  $[\text{}^{56}\text{Fe}]_{\text{diss}}^*$ ).

Our observations do not exclude charge injection and charge migration in the Lp surface and bulk lattice that lead to recrystallization on a longer time scale. In the presence of a ligand that promotes dissolution, mobile charge can be transferred back to previously adsorbed or incorporated  $^{57}\text{Fe}$  and accelerate its dissolution. An alternative explanation for the fast dissolution of the added  $^{57}\text{Fe}$  is the formation of a less crystalline or amorphous  $^{57}\text{Fe(III)}$  phases that are dissolved more quickly than Lp after addition of EDTA. However, a surface precipitate with addition of only 1-1.2  $\mu\text{M}$  Fe(II) to a Lp suspension with estimated 17.5  $\mu\text{M}$  surface sites seems less likely than adsorption and isotope exchange by incorporation of  $^{57}\text{Fe}$  into the surface.

### Possible phase changes

We observed no evidence for transformation of Lp to goethite or magnetite with 0.2-10  $\mu\text{M}$  added Fe(II) (to which FTIR is very sensitive, see Figure S3) in our experiments. Previous studies found exchange of  $^{55}\text{Fe}$  between Lp and dissolved (0.2-1.0 mM) Fe(II) at pH 6.5,<sup>41, 42</sup> but only minor formation of magnetite even with 1mM dissolved Fe(II) after 2 days<sup>41</sup> and no formation of goethite over 7 days.<sup>42</sup>

### Kinetic model for the catalytic effect of Fe(II)

In our experiments, ligand controlled dissolution was slow compared to Fe(II)-catalyzed dissolution. We define the measured catalytic effect (CE) as  $R_{\text{diss,L,Fe(II)}} / R_{\text{diss,L}}$ , where  $R_{\text{diss,L,Fe(II)}}$  and  $R_{\text{diss,L}}$  are the dissolution rates in the presence and absence of Fe(II), respectively. As defined, CE was 1 without added Fe(II) and ranged from 7-31 with 0.2-10  $\mu\text{M}$  added Fe(II), as listed in Table S3.

To explore reaction mechanisms that can explain the catalytic effect of Fe(II), a kinetic model was developed that allowed us to fit the model outputs to measured data by optimizing rate coefficients and concentrations of active surface sites in the model. Tentative reaction mechanisms for Fe(II) catalyzed dissolution have been presented before for dissolution at low pH,<sup>10, 43, 44</sup> but it has not been shown that they can quantitatively explain experimental results. The model with reaction equations is presented in Table 1 and is described in more detail in the SI.

**Table. 1.** Kinetic model with list of reactions and fitted equilibrium constants, rate coefficients and surface site concentrations for pH 6.0 and 9.5 mM NaCl.

Nr.	Reaction			Nr. of K or k	Description	Fixed or fitted log(K) or log(k)
R1	$\text{Fe}^{\text{II}} + \text{L}$	$\rightleftharpoons$	$\text{Fe}^{\text{II}}\text{L}$	$K_1$	Complexation of $\text{Fe}^{\text{II}}$ in solution	10.3 <sup>(a)</sup>
R2	$\equiv\text{Fe}^{\text{III}} + \text{L}$	$\rightleftharpoons$	$\equiv\text{Fe}^{\text{III}}\text{-L}$	$K_2$	Adsorption of ligand (L)	5.0 <sup>(b)</sup>
R3	$\equiv\text{Fe}^{\text{III}} + \text{Fe}^{\text{II}}$	$\rightleftharpoons$	$\equiv\text{Fe}^{\text{III}}\text{-Fe}^{\text{II}}$	$K_3$	Adsorption of $\text{Fe}^{\text{II}}$	5.5 <sup>(c)</sup>
R4	$\equiv\text{Fe}^{\text{III}}\text{-Fe}^{\text{II}} + \text{L}$	$\rightleftharpoons$	$\equiv\text{Fe}^{\text{III}}\text{-Fe}^{\text{II}}\text{-L}$	$K_4$	Adsorption of L on adsorbed $\text{Fe}^{\text{II}}$	4.7 <sup>(d)</sup>
R5	$\equiv\text{Fe}^{\text{III}} + \text{Fe}^{\text{II}}\text{L}$	$\rightleftharpoons$	$\equiv\text{Fe}^{\text{III}}\text{-Fe}^{\text{II}}\text{L}$	$K_5$	Adsorption of $\text{Fe}^{\text{II}}\text{L}$	5.4
R6	$\equiv\text{Fe}^{\text{III}} + \text{Fe}^{\text{III}}\text{L}$	$\rightleftharpoons$	$\equiv\text{Fe}^{\text{III}}\text{-Fe}^{\text{III}}\text{L}$	$K_6$	Competing adsorption of $\text{Fe}^{\text{III}}\text{L}$	5.7 <sup>(c)</sup>
R7	$\equiv\text{Fe}^{\text{III}}\text{-Fe}^{\text{II}}\text{-L}$	$\rightarrow$	$\equiv\text{Fe}^{\text{II}}\text{-Fe}^{\text{III}}\text{-L}$	$k_{7(\text{ET})}$	Electron transfer	1
R8	$\equiv\text{Fe}^{\text{II}}\text{-Fe}^{\text{III}}\text{-L}$	$\rightarrow$	$\equiv\text{Fe}^{\text{II}} + \text{Fe}^{\text{III}}\text{L}$	$k_8$	Fe(II)-catalyzed detachment of $\text{Fe}^{\text{III}}\text{-L}$	-0.64
R9	$\equiv\text{Fe}^{\text{II}} + \text{Lp}_{\text{bulk}}$	$\rightarrow$	$\equiv\text{Fe}^{\text{II}}\text{-Fe}^{\text{II}}$	$k_9$	Formation of new surface site	6 <sup>(e)</sup>
R10	$\equiv\text{Fe}^{\text{III}}\text{-L}$	$\rightarrow$	$\equiv + \text{Fe}^{\text{III}}\text{L}$	$k_{10}$	Detachment of $\text{Fe}^{\text{III}}\text{-L}$	-2.5
R11	$\equiv + \text{Lp}_{\text{bulk}}$	$\rightarrow$	$\equiv\text{Fe}^{\text{III}}$	$k_{11}$	Formation of new surface site	6 <sup>(e)</sup>
Fitted active surface site conc. (last column, $[\equiv\text{Fe}^{\text{III}}]/[\text{Lp}]$ (M/M) and $\equiv\text{Fe}^{\text{III}}/\text{nm}^2$ ) for dissolution, and surface site conc. for adsorption of EDTA, Fe(II) and Fe(III)EDTA in batch experiments						
	$\equiv\text{Fe}^{\text{III}}$			$p_1$	Dissolution in batch and FTIR experiments	6.3e-5 <sup>(f)</sup> 6.7e-3 $\equiv\text{Fe}^{\text{III}}/\text{nm}^2$
	$\equiv\text{Fe}^{\text{III}}$			$p_2$	Adsorption of EDTA with FTIR (10 $\mu\text{M}$ Lp)	7.4e-3 <sup>(b)</sup> 0.79 $\equiv\text{Fe}^{\text{III}}/\text{nm}^2$
	$\equiv\text{Fe}^{\text{III}}$			$p_3$	Ads. of Fe(II) in batch experiments	1.0e-3 <sup>(c)</sup> 0.11 $\equiv\text{Fe}^{\text{III}}/\text{nm}^2$
	$\equiv\text{Fe}^{\text{III}}$			$p_4$	Ads. of Fe(III)EDTA	1.3e-3 <sup>(c)</sup> 0.14 $\equiv\text{Fe}^{\text{III}}/\text{nm}^2$

Surface sites  $\equiv\text{Fe}^{\text{III}}\text{-OH}$  are abbreviated as  $\equiv\text{Fe}^{\text{III}}$  and surface complexes  $\equiv\text{Fe}^{\text{III}}\text{-O-Fe}^{\text{II}}$  as  $\equiv\text{Fe}^{\text{III}}\text{-Fe}^{\text{II}}$ .

Surface complexes that involve both ligand and Fe(II) in close proximity are formulated as  $\equiv\text{Fe}^{\text{III}}\text{-Fe}^{\text{II}}\text{-L}$ .

This could mean a ternary surface complexes or adsorbed EDTA next to a reduced site.

<sup>(a)</sup> Conditional complex formation constant for Fe(II)EDTA at pH 6 (see SI). (Over 99.8% of Fe(II) is present as  $\text{Fe}^{\text{II}}\text{EDTA}^{2-}$  with 50  $\mu\text{M}$  EDTA).

<sup>(b)</sup> Best fits to adsorption isotherm for EDTA determined with FTIR, see SI Figures S10 and S11.

<sup>(c)</sup> Best fits to adsorption isotherms of Fe(II) and Fe(III)EDTA, see SI Table S5 and Figure S11.

<sup>(d)</sup> The rate coefficients of R4 are interdependent with the rate of  $\text{Fe}^{\text{II}}$  detachment (back reaction R3), formation of  $\text{Fe}^{\text{II}}\text{L}$  (R1) and adsorption of  $\text{Fe}^{\text{II}}\text{L}$  (R5), see SI.

<sup>(e)</sup> Arbitrary, fast and non-rate determining rate coefficients.

<sup>(f)</sup> Best fits to Lp-dissolution in batch (1.13 mM Lp) and FTIR (10  $\mu\text{M}$  Lp = 35.6  $\mu\text{g}/40\text{ml}$ ) experiments, see SI.

We assumed that all equilibrium reactions are fast and not rate determining for dissolution on the investigated time scale. As consequence of the fast equilibration in reactions R1-R5, the order of the addition of EDTA and Fe(II) should not change the observation of the catalytic effect, as was experimentally observed (Figure S6). The competitive adsorption of formed Fe(III)EDTA (R6) can explain the non-linear dissolution in the batch-experiments, with dissolution rates that decrease more strongly from 1800-5000 s (Figure 5) than expected from the decreasing concentration of uncomplexed EDTA. In the dissolution measured with FTIR (Figure 2) this effect was not observed and dissolution proceeded linearly, which can be explained by the much lower Lp concentrations in the AFR-FTIR experiments. With maximally 8% dissolution of 60  $\mu\text{g}$  Lp in 40 ml, dissolved Fe(III)EDTA concentration remained below 1.4  $\mu\text{M}$ . When 20  $\mu\text{M}$  Fe(III) was added (Figure S8) the dissolution rate also decreased. Similar non-linear dissolution kinetics were observed previously in the photo-reductive dissolution of Lp with aerobactin,<sup>33</sup> where decreasing rates in the presence of added and formed Fe(III) were also ascribed to competing adsorption of formed Fe(III)-ligand complexes with the free ligand. By variation of rate coefficients (see SI), we found that either the electron transfer (ET) in R7 or the detachment of Fe(III)L can be defined as the rate determining step in this model. Since Fe(II)EDTA is strongly reducing, we assumed that ET is the faster step and adjusted the rate coefficient for detachment of Fe(III)L ( $k_8$ ) in reaction R8 as the rate determining step. The listed fitted rate coefficients lead to good fits of the currently available data, but they are tentative because the rate coefficients for reactions R4 and R5 correspond to reactions (i.e., adsorption of EDTA on adsorbed Fe(II) or adsorption of Fe(II)EDTA) that yield the same surface complex in our model. Since more than 99.8% of Fe(II) is complexed by EDTA, the rate coefficients for these reactions are not independent, as explained in more detail in the SI.

Important parameters in the model are the concentrations of active sites for the dissolution reactions ( $p_1$  to  $p_4$ ). The site concentrations for the adsorption of Fe(II), EDTA and Fe(III)EDTA were obtained from adsorption data as shown in Figure S11. They agree with ranges for iron(hydr)oxides reported in the literature.<sup>45, 46</sup> A lower concentration of sites that are active for dissolution has been used in models describing the dissolution of hematite<sup>47</sup> and agrees with the understanding that

dissolution proceeds on kink and step sites<sup>48</sup> whose concentrations are smaller than the sum of adsorption sites measured in adsorption experiments.

**Structure of surface complexes.** In the kinetic model, we formulate the surface complexes that involve both Fe(II) and EDTA as  $\equiv\text{Fe}^{\text{III}}\text{-Fe}^{\text{II}}\text{-L}$ , but they could alternatively be formulated as  $\equiv\text{Fe}^{\text{III}}\text{-L-Fe}^{\text{II}}$  or as complexes with Fe(II) adsorbed next to a site where EDTA is adsorbed. Ideally, the infrared spectra could provide information about the structure of the complex involving both Fe(II) and EDTA. Addition of Fe(II) caused shifts in the spectra of adsorbed EDTA to higher energy and induced spectral changes around several peak positions (see SI, Fig. S9, SI Table S4). This clearly indicates that the interaction of Fe(II) with adsorbed EDTA led to formation of additional complexes at the surface, or that additional complexes were formed by adsorption of Fe(II)EDTA from solution. However, the shifts could not be interpreted in terms of structures. In a recently published study on the formation of oxalate complexes on Lp, we found that several surface complexes with different structures were formed. For oxalate, detailed DFT calculations allowed us to draw conclusions about the structures of these different surface complexes.<sup>49</sup> DFT calculations with the larger ligand EDTA in the presence of Fe(II) are computationally more demanding and were not attempted in this study.

### Reaction mechanisms and possible implications

Fe(II) accelerates the dissolution of Lp by EDTA when added before or after addition of EDTA. At pH 6, most of the added Fe(II) (>80%) remains in solution even in the absence of EDTA. In the presence of 50  $\mu\text{M}$  EDTA, over >99.8% of dissolved Fe(II) and >99.9% of Fe(III) are complexed with EDTA (Table S5). Most likely, the Fe(II) catalyzed dissolution is driven by adsorption of Fe(II)EDTA and formation of mixed Fe(II)-Fe(III) ternary surface complexes (reaction R5 in Table 1), followed by electron transfer and detachment of Fe(III)EDTA (R7-R8). We can currently not determine the fraction of adsorbed Fe(II)EDTA and whether the newly formed Fe(II) (R9) is complexed with EDTA directly at the surface (reaction R4) or leaves the surface (back reaction of R3) and reabsorbs as Fe(II)EDTA (R5) to continue the catalytic cycle. The model constitutes a useful list of possible reactions that can explain our observation, but more work is required to quantitatively determine the contribution of each of these reactions and to determine the corresponding rate coefficients.

## Environmental significance

We observed that added and photo-produced Fe(II) can accelerate the dissolution of Lp with EDTA by a factor of 7-31 at pH 6 and at pH 7 under anoxic conditions. Fe(II) catalyzed dissolution could be an efficient strategy for accelerated mobilization and uptake of iron in environments with changing redox conditions and in sunlit environments where Fe(II) is produced photochemically. Examples are soils where reducing conditions are not sufficient for reductive dissolution of Fe-bearing phases, but where traces of Fe(II) could lead to strongly accelerated Fe(II)-catalyzed dissolution in the presence of synthetic or natural ligands (e.g. siderophores),<sup>18</sup> as also shown in our parallel study for a range of minerals with HBED and DFOB.<sup>36</sup> Other environments where Fe(II)-catalyzed dissolution could be important are oxic-anoxic transition zones in lakes, wetlands, and irrigated agricultural fields. Added Fe(II) and photoproduced Fe(II) did not appear lead to formation of mobile charge or Fe(II) that is protected from oxidation by oxygen, e.g. by charge residing in the bulk of the solid, at least not with Lp. Nevertheless, steady state concentrations of photo-produced Fe(II) at the surface of iron oxide particles under sunlit conditions could make Fe(II)-catalyzed dissolution an important pathway in their photoreductive dissolution. It is also possible that negative charge from added or produced Fe(II) can persist longer in the bulk of more conductive iron(hydr)oxide minerals and that this results in a longer lasting catalytic effect of Fe(II) under oxic conditions. The time resolved ATR-FTIR measurements and <sup>57</sup>Fe isotope experiments presented here have proven useful and will be used to investigate the effect of Fe(II) on the dissolution of other Fe(III)(hydr)oxide phases in different environments.

## Associated Content

Supporting Information. List of chemicals; lepidocrocite synthesis and characterization (XRD and FTIR spectra); details on ATR-FTIR measurements, list of duplicate experiments; FTIR spectra of adsorbed EDTA with pH and concentration dependence, spectral changes with added Fe(II)); input file for kinetic model, model fits for dissolution kinetics and adsorption isotherms. (5 Tables, 12 Figures).



## Acknowledgements

We thank Thomas Rüttimann (Eawag) for ICP-MS analyses and for technical assistance. We also thank Numa Pfenninger (Eawag) for BET and XRD measurements and Dr. Ralf Kägi (Eawag) for SEM images. This project was financially supported by the Swiss National Science Foundation, project number 200021L\_150150 “Synergistic effects of redox processes and ligand controlled dissolution of iron(hydr)oxide phases” Mathematics, Natural sciences and Engineering (division II). SK, WS and KK were supported by the Austrian Science Fund (FWF, Grant No.: I 1528-N19).

## References

1. Kraemer, S. M., Iron oxide dissolution and solubility in the presence of siderophores. *Aquat. Sci.* **2004**, *66* (1), 3-18.
2. Sandy, M.; Butler, A., Microbial iron acquisition: Marine and terrestrial siderophores. *Chem. Rev.* **2009**, *109* (10), 4580-4595.
3. Shenker, M.; Chen, Y., Increasing Iron Availability to Crops: Fertilizers, Organo-Fertilizers, and Biological Approaches. *J. Soil Sci. Plant Nutr.* **2005**, *51*, (1), 1-17.
4. Cheah, S. F.; Kraemer, S. M.; Cervini-Silva, J.; Sposito, G., Steady-state dissolution kinetics of goethite in the presence of desferrioxamine B and oxalate ligands: Implications for the microbial acquisition of iron. *Chem. Geol.* **2003**, *198* (1-2), 63-75.
5. Cervini-Silva, J.; Sposito, G., Steady-state dissolution kinetics of aluminum-goethite in the presence of desferrioxamine-B and oxalate ligands. *Environ. Sci. Technol.* **2002**, *36*, (3), 337-342.
6. Reichard, P. U.; Kraemer, S. M.; Frazier, S. W.; Kretzschmar, R., Goethite dissolution in the presence of phytosiderophores: Rates, mechanisms, and the synergistic effect of oxalate. *Plant Soil* **2005**, *276* (1-2), 115-132.
7. Reichard, P. U.; Kretzschmar, R.; Kraemer, S. M., Dissolution mechanisms of goethite in the presence of siderophores and organic acids. *Geochim. Cosmochim. Acta* **2007**, *71* (23), 5635-5650.
8. Wolff-Boenisch, D.; Traina, S. J., The effect of desferrioxamine B, enterobactin, oxalic acid, and Na-alginate on the dissolution of uranyl-treated goethite at pH 6 and 25°C. *Chem. Geol.* **2007**, *243*, (3-4) 357-368.
9. Liu, X.; Fu, J. W.; Da Silva, E.; Shi, X. X.; Cao, Y.; Rathinasabapathi, B.; Chen, Y.; Ma, L. Q., Microbial siderophores and root exudates enhanced goethite dissolution and Fe/As uptake by As-hyperaccumulator *Pteris vittata*. *Environ. Pollut.* **2017**, *223*, 230-237.

10. Blesa, M. A.; Borghi, E. B.; Maroto, A. J. G.; Regazzoni, A. E., Adsorption of EDTA and iron-EDTA complexes on magnetite and the mechanism of dissolution of magnetite by EDTA. *J. Colloid Interface Sci.* **1984**, 98 (2), 295-305.
11. Suter, D.; Siffert, C.; Sulzberger, B.; Stumm, W., Catalytic dissolution of iron(III)(hydr)oxides by oxalic acid in the presence of Fe(II). *Naturwissenschaften* **1988**, 75 (11), 571-573.
12. Borghi, E. B.; Regazzoni, A. E.; Maroto, A. J. G.; Blesa, M. A., Reductive dissolution of magnetite by solutions containing EDTA and FeII. *J. Colloid Interface Sci.* **1989**, 130 (2), 299-310.
13. Wehrli, B.; Sulzberger, B.; Stumm, W., Redox processes catalyzed by hydrous oxide surfaces. *Chem. Geol.* **1989**, 78 (3-4), 167-179.
14. Torres, R.; Blesa, M. A.; Matijević, E., Interactions of metal hydrous oxides with chelating agents. IX. Reductive dissolution of hematite and magnetite by aminocarboxylic acids. *J. Colloid Interface Sci.* **1990**, 134 (2), 475-485.
15. Suter, D.; Banwart, S.; Stumm, W., Dissolution of Hydrous Iron(III) Oxides by Reductive Mechanisms. *Langmuir* **1991**, 7 (4), 809-813.
16. Karametaxas, G.; Hug, S. J.; Sulzberger, B., Photodegradation of EDTA in the Presence of Lepidocrocite. *Environ. Sci. Technol.* **1995**, 29 (12), 2992-3000.
17. Wang, Z.; Schenkeveld, W. D. C.; Kraemer, S. M.; Giammar, D. E., Synergistic Effect of Reductive and Ligand-Promoted Dissolution of Goethite. *Environ. Sci. Technol.* **2015**, 49, (12), 7236-7244.
18. Schenkeveld, W. D. C.; Wang, Z.; Giammar, D. E.; Kraemer, S. M., Synergistic Effects between Biogenic Ligands and a Reductant in Fe Acquisition from Calcareous Soil. *Environ. Sci. Technol.* **2016**, 50 (12), 6381-6388.
19. Kubicki, J. D.; Tunega, D.; Kraemer, S., A density functional theory investigation of oxalate and Fe(II) adsorption onto the (010) goethite surface with implications for ligand- and reduction-promoted dissolution. *Chem. Geol.* **2017**, 464, 14-22.
20. Lee, J. C.; Kim, E. J.; Baek, K., Synergistic effects of the combination of oxalate and ascorbate on arsenic extraction from contaminated soils. *Chemosphere* **2017**, 168, 1439-1446.
21. Handler, R. M.; Beard, B. L.; Johnson, C. M.; Scherer, M. M., Atom exchange between aqueous Fe(II) and goethite: An Fe isotope tracer study. *Environ. Sci. Technol.* **2009**, 43 (4), 1102-1107.
22. Gorski, C. A.; Scherer, M. M., Fe<sup>2+</sup> sorption at the Fe oxide-water interface: A revised conceptual framework. In *ACS Symposium Series*, American Chemical Society: 2011; Vol. 1071, pp 315-343.
23. Gorski, C. A.; Handler, R. M.; Beard, B. L.; Pasakarnis, T.; Johnson, C. M.; Scherer, M. M., Fe atom exchange between aqueous Fe<sup>2+</sup> and magnetite. *Environ. Sci. Technol.* **2012**, 46 (22), 12399-12407.

24. Latta, D. E.; Gorski, C. A.; Scherer, M. M., Influence of Fe<sup>2+</sup>-catalysed iron oxide recrystallization on metal cycling. *Biochem. Soc. Trans.* **2012**, *40*, (6), 1191-1197.
25. Handler, R. M.; Friedrich, A. J.; Johnson, C. M.; Rosso, K. M.; Beard, B. L.; Wang, C.; Latta, D. E.; Neumann, A.; Pasakarnis, T.; Premaratne, W. A. P. J.; Scherer, M. M., Fe(II)-catalyzed recrystallization of goethite revisited. *Environ. Sci. Technol.* **2014**, *48* (19), 11302-11311.
26. Joshi, P.; Fantle, M. S.; Larese-Casanova, P.; Gorski, C. A., Susceptibility of Goethite to Fe<sup>2+</sup>-Catalyzed Recrystallization over Time. *Environ. Sci. Technol.* **2017**, *51* (20), 11681-11691.
27. Joshi, P.; Gorski, C. A., Anisotropic Morphological Changes in Goethite during Fe<sup>2+</sup>-Catalyzed Recrystallization. *Environ. Sci. Technol.* **2016**, *50* (14), 7315-7324.
28. Zarzycki, P.; Rosso, K. M., Stochastic Simulation of Isotopic Exchange Mechanisms for Fe(II)-Catalyzed Recrystallization of Goethite. *Environ. Sci. Technol.* **2017**, *51* (13), 7552-7559.
29. Borer, P.; Hug, S. J.; Sulzberger, B.; Kraemer, S. M.; Kretzschmar, R., Photolysis of citrate on the surface of lepidocrocite: An in situ attenuated total reflection infrared spectroscopy study. *J. Phys. Chem. C* **2007**, *111* (28), 10560-10569.
30. Borer, P.; Hug, S. J.; Sulzberger, B.; Kraemer, S. M.; Kretzschmar, R., ATR-FTIR spectroscopic study of the adsorption of desferrioxamine B and aerobactin to the surface of lepidocrocite ( $\gamma$ -FeOOH). *Geochim. Cosmochim. Acta* **2009**, *73* (16), 4661-4672.
31. Borer, P.; Hug, S. J., Photo-redox reactions of dicarboxylates and  $\alpha$ -hydroxydicarboxylates at the surface of Fe(III)(hydr)oxides followed with in situ ATR-FTIR spectroscopy. *J. Colloid Interface Sci.* **2014**, *416*, 44-53.
32. Borer, P. M.; Sulzberger, B.; Reichard, P.; Kraemer, S. M., Effect of siderophores on the light-induced dissolution of colloidal iron(III) (hydr)oxides. *Mar. Chem.* **2005**, *93*, 179– 193.
33. Borer, P.; Kraemer, S. M.; Sulzberger, B.; Hug, S. J.; Kretzschmar, R., Photodissolution of lepidocrocite ( $\gamma$ -FeOOH) in the presence of desferrioxamine B and aerobactin. *Geochim. Cosmochim. Acta* **2009**, *73* (16), 4673-4687.
34. Borer, P.; Sulzberger, B.; Hug, S. J.; Kraemer, S. M.; Kretzschmar, R., Wavelength-dependence of photoreductive dissolution of lepidocrocite ( $\gamma$ -FeOOH) in the absence and presence of the siderophore DFOB. *Environ. Sci. Technol.* **2009**, *43* (6), 1871-1876.
35. Borer, P.; Sulzberger, B.; Hug, S. J.; Kraemer, S. M.; Kretzschmar, R., Photoreductive dissolution of iron(III) (Hydr)oxides in the absence and presence of organic ligands: Experimental studies and kinetic modeling. *Environ. Sci. Technol.* **2009**, *43* (6), 1864-1870.
36. Kang, K.; Schenkeveld, W. D. C.; Biswakarma, J.; Borowski, S. C.; Hug, S. J.; Hering, J. G.; Kraemer, S. M., Low Fe(II) concentrations catalyze the dissolution of various Fe(III) (hydr)oxide minerals in the presence of diverse ligands and over a broad pH range. *Environ. Sci. Technol.* **2018**.
37. Schwertmann, U.; Cornell, R. M., *Iron Oxides in the Laboratory*. 2nd, Completely Revised and Extended Edition ed.; Wiley-VCH Weinheim, Germany, 2000.

38. Cornell, R. M.; Schwertmann, U., *The Iron Oxides: Structure, Properties, Reactions, Occurrences, and Uses*. 2nd ed.; ed.; Wiley-VCH: New York, NY, USA, 2003.
39. Norén, K.; Loring, J. S.; Bargar, J. R.; Persson, P., Adsorption mechanisms of EDTA at the water-iron oxide interface: Implications for dissolution. *J. Phys. Chem. C* **2009**, *113*, (18), 7762-7771.
40. Zhang, Y.; Charlet, L.; Schindler, P. W., Adsorption of protons, Fe(II) and Al(III) on lepidocrocite ( $\gamma$ -FeOOH). *Colloids Surf.* **1992**, *63*, (3-4), 259-268.
41. Pedersen, H. D.; Postma, D.; Jakobsen, R.; Larsen, O., Fast transformation of iron oxyhydroxides by the catalytic action of aqueous Fe(II). *Geochim. Cosmochim. Acta* **2005**, *69*, (16), 3967-3977.
42. Jones, A. M.; Collins, R. N.; Rose, J.; Waite, T. D., The effect of silica and natural organic matter on the Fe(II)-catalysed transformation and reactivity of Fe(III) minerals. *Geochim. Cosmochim. Acta* **2009**, *73* (15), 4409-4422.
43. Ballesteros, M. C.; Rueda, E. H.; Blesa, M. A., The influence of iron (II) and (III) on the kinetics of goethite dissolution by EDTA. *J. Colloid Interface Sci.* **1998**, *201*, (1), 13-19.
44. Banwart, S.; Davies, S.; Stumm, W., The role of oxalate in accelerating the reductive dissolution of hematite ( $\alpha$ -Fe<sub>2</sub>O<sub>3</sub>) by ascorbate. *Colloids Surf.* **1989**, *39* (2), 303-309.
45. Nowack, B.; Lutzenkirchen, J.; Behra, P.; Sigg, L., Modeling the adsorption of metal-EDTA complexes onto oxides. *Environ. Sci. Technol.* **1996**, *30* (7), 2397-2405.
46. Nowack, B.; Sigg, L., Adsorption of EDTA and metal-EDTA complexes onto goethite. *J. Colloid Interface Sci.* **1996**, *177* (1), 106-121.
47. Samson, S. D.; Eggleston, C. M., The depletion and regeneration of dissolution-active sites at the mineral-water interface: II. Regeneration of active sites on  $\alpha$ -Fe<sub>2</sub>O<sub>3</sub> at pH 3 and pH 6. *Geochim. Cosmochim. Acta* **2000**, *64* (21), 3675-3683.
48. Wehrli, B., Monte Carlo simulations of surface morphologies during mineral dissolution. *J. Colloid Interface Sci.* **1989**, *132* (1), 230-242.
49. Borowski, S. C.; Biswakarma, J.; Kang, K.; Schenkeveld, W. D. C.; Hering, J. G.; Kubicki, J. D.; Kraemer, S. M.; Hug, S. J., Structure and reactivity of oxalate surface complexes on lepidocrocite derived from infrared spectroscopy, DFT-calculations, adsorption, dissolution and photochemical experiments. *Geochim. Cosmochim. Acta* **2018**, *226*, 244-262.



# Supporting Information

---

Text S1. Synthesis of lepidocrocite

Text S2. Lepidocrocite characterization

Text S3. Details on ATR-FTIR measurements

Text S4. Actinometry

Text S5. Estimation of photochemically produced Fe(II)

Text S6. Kinetic model

Text S7. Structures and photo-reactivity

Text S8. References

Table S1. List of chemicals used in the study

Table S2. Initial absorbances of lepidocrocite

Table S3. Dissolution rates of lepidocrocite and catalytic effects

Table S4. Comparison of experimental IR frequencies

Table S5. Kinetic model input for ACUCHEM

Figure S1. ATR-FTIR spectra of lepidocrocite

Figure S2. XRD-Diffractogram of lepidocrocite

Figure S3. ATR-FTIR spectra of mixtures of lepidocrocite, goethite and magnetite

Figure S4. ATR-FTIR difference spectra of adsorbed EDTA and kinetics- pH dependence

Figure S5. ATR-FTIR difference absorbance spectra of adsorbed EDTA, followed by 10  $\mu$ M Fe(II)-catalyzed lepidocrocite dissolution at pH 7

Figure S6. Lp dissolution at pH 6 when Fe(II) was added before EDTA

Figure S7. Kinetics of EDTA adsorption and Lp dissolution during photochemical experiment at pH7

Figure S8. Effect of Fe(III) in Fe(II)-catalyzed dissolution

Figure S9. Comparison of various ATR-FTIR spectra: aqueous Fe(II)-EDTA, Fe(III)-EDTA, adsorbed EDTA followed by addition of Fe(II) and adsorbed Fe(III)-EDTA at pH

Figure S10. ATR-FTIR absorbance spectra of adsorbed EDTA-concentration dependence

Figure S11. Adsorption isotherm of EDTA estimated from ATR-FTIR measurements

Figure S12. Kinetic fits to experimental data.

**Text S1. Synthesis of Lepidocrocite**

The method for synthesis of lepidocrocite (Lp) was modified from Schwertmann.<sup>5</sup> Briefly, 60 mM solution of  $\text{FeCl}_2$  (71.6 g of  $\text{FeCl}_2 \cdot 4\text{H}_2\text{O}$  in 6 L DDI water, with a pH between 3.53 - 3.79) was purged with  $\text{N}_2$  for 2 h. NaOH (~15 mL, 1 M) was titrated slowly to the strongly stirred solution to increase the pH to a range of 6.65 - 6.76. When the pH had stabilized, oxygen was bubbled through the solution to initiate the Fe(II) oxidation process. During the synthesis, the solution was continuously and vigorously stirred and temperature was kept at 15°C. The flow of oxygen was adjusted in the range of 360-1200 ml/min, keeping the base addition constant at 6 ml/min. The pH was kept between 6.60- 6.75 throughout the synthesis with NaOH (731 ml, 1 M). During the synthesis, the color changed from the initial green-yellow to green-blue, black and then to brown-orange. After 2 h, a bright orange suspension was formed. The suspended particles were collected by centrifugation and repeatedly washed by resuspension and centrifugation with DDI water until the electrical conductivity of the suspension had decreased from 2500  $\mu\text{S}/\text{cm}$  to 46  $\mu\text{S}/\text{cm}$ . Finally, the solid was collected and dried with stream of  $\text{N}_2$ . Vigorous stirring and slow addition of NaOH to the reaction mixture, in between the center and the walls of the reaction vessel right above the stirrer were essential to avoid formation of goethite and magnetite as byproducts.

**Text S2. Lepidocrocite characterization**

X-ray Diffraction. The dried samples of lepidocrocite were analyzed by X-ray diffraction analysis (X'Pert powder diffractometer with XCelerator, PANalytical, Almelo, the Netherlands) to determine the phase purity and to estimate the particle size.

ATR-FTIR spectroscopy. A suspension of synthesized lepidocrocite (30 mg/ml) was prepared in DDI  $\text{H}_2\text{O}$ . One  $\mu\text{l}$  from the suspension was air dried on the ATR-element prior to record a FTIR spectra on Biorad FTS 755C instrument equipped with a liquid  $\text{N}_2$ -cooled mercury cadmium telluride (MCT) detector and a nine reflection ATR unit (SensIR Technologies, Danbury, CT).

Transmission Electron Microscopy. Direct imaging of lepidocrocite was taken in the transmission electron microscope (HD2700Cs, Hitachi, Japan) to estimate the particle shapes and dimensions.

**Text S3. Details on ATR-FTIR measurements**

FTIR spectra ( $4000\text{--}400\text{ cm}^{-1}$ ,  $2\text{ cm}^{-1}$  resolution, 32 or 64 scans) were recorded on a Biorad FTS 575C instrument equipped with a liquid  $\text{N}_2$ -cooled mercury cadmium telluride (MCT) detector and a nine reflection diamond ATR unit (SensIR Technologies, Danbury, CT). Absorbance spectra were obtained from single beam background spectra ( $I_0$ ) and single beam sample spectra ( $I_s$ ), with the relation  $\text{absorbance} = \log_{10}(I_0/I_s)$ . FTIR spectral analysis were performed with routines written in Matlab.

The following procedure was employed before performing any dissolution experiments. A single-beam spectrum of the blank ATR crystal was measured as the background spectrum for the calculation of absorbance spectra of an initial Lp layer. A thin layer of  $40\text{--}60\text{ }\mu\text{g}$  Lp was formed on the ATR crystal (diamond,  $\phi\text{ }4\text{ mm}$ ) by spraying  $2\text{ }\mu\text{L}$  of a  $30\text{ mg/mL}$  Lp suspension with an ultrasonic tip (Sonozap ultrasonic atomizer). IR absorbance spectra of the Lp layer were recorded after drying the layer with a gentle stream of  $\text{N}_2$ . The layer was rinsed several times with a gentle stream of DDI water and subsequently dried, until the absorbance did not decrease due to detachment of loosely adhering particles. Subsequently, a  $50\text{ mL}$  polypropylene beaker was mounted onto the ATR unit and the layer was covered with  $40\text{ mL}$  aqueous solution of  $9.5\text{ mM}$  NaCl ( $38\text{ mL}$   $10\text{ mM}$  NaCl) and  $5\text{ mM}$  MES/MOPS ( $2\text{ mL}$   $100\text{ mM}$  MES/MOPS stock solution).

Continuous purging of the aqueous solution with high purity  $\text{N}_2$  gas (Alpha gas  $\text{N}_2$ , 99.999% pure,  $\text{O}_2 < 0.1\text{ ppm}$ ,  $\text{H}_2\text{O} < 0.5\text{ ppm}$ ) lead to desorption of adsorbed  $\text{CO}_2$  from Lp and served to stir the solution during measurements.  $\text{O}_2$  concentrations were optically measured using PreSens Fibox 4 trace oxygen sensor (PreSens precision sensing GmbH, Germany). Oxygen is measured with a luminescent oxygen sensor spot fixed on the inner wall of the reaction cell. Residual oxygen concentrations after 3 h of purging with  $\text{N}_2$  were  $< 10\text{ nM}$ . At this point a new single-beam background spectrum with the Lp-layer in contact with the anoxic background electrolyte was recorded. Subsequently, absorbance spectra were measured continuously, every  $43\text{ s}$  or  $71\text{ s}$ . Since these absorbance spectra display the differences developing with the addition of EDTA and Fe(II), they are termed difference absorbance ( $\Delta A$ ) spectra.



To measure the adsorption isotherm of EDTA on lepidocrocite at pH 6, 10-200  $\mu\text{M}$  EDTA were added to the deoxygenated aqueous solution (40ml 10 mM NaCl, 5 mM MES) covering lepidocrocite layer in the ATR unit. FTIR spectra were recorded continuously to follow the characteristic changes (increase/decrease) of absorbance. In an another experiment, 50  $\mu\text{M}$  EDTA was added to lepidocrocite layer at different pH ranges (pH 3-6) to observe the spectral changes of adsorbed EDTA due to (de/)protonation.

#### **Text S4. Actinometry**

An actinometer solution (1 ml of 1.2 M  $\text{K}_2\text{C}_2\text{O}_4$  and 1 ml of 400 mM  $\text{FeCl}_3 \cdot 6\text{H}_2\text{O}$  diluted to 20 ml with DDI  $\text{H}_2\text{O}$ ), was stirred with magnetic stirrer and irradiated with the UV-LED lamp through a mask with a circular opening with 4 mm diameter at a distance of 7.25 cm for 120 s (the same distance of the UV-lamp from the 4 mm diameter ATR-diamond crystal). After irradiation, 300  $\mu\text{L}$  of the actinometer solution was withdrawn and mixed with 150  $\mu\text{L}$  600 mM acetate buffer and with 600  $\mu\text{L}$  10 mM phenanthroline and diluted to 3.0 ml with DDI  $\text{H}_2\text{O}$ . A UV-visible absorption spectrum of this mixture in 1 cm quartz cell was then measured at 510 nm and the photon flux calculated as described previously. The determined photon flux was  $3.55 \times 10^{15}$  photons/s corresponding to an irradiation of  $150 \text{ W/m}^2$ .

#### **Text S5. Estimation of photochemically produced Fe(II)**

The decrease of the absorbance of Lp during the two irradiation periods was 0.01-0.012 absorbance units, which corresponds to 1.4-1.7% dissolution of the 40-60  $\mu\text{g}$  Lp (initial absorbance of ca. 0.8, see Table S2). Assuming that photo-reductive dissolution is the dominant process during illumination, we thus formed 0.14-0.25  $\mu\text{M}$  Fe(II) calculated over the solution volume of 40 ml. We note that in all ATR-FTIR measurements, EDTA was in excess (40 ml of 50  $\mu\text{M}$  EDTA = 2  $\mu\text{mol}$ ) compared to Lp in the layer (40-60  $\mu\text{g}$  = 0.45-0.68  $\mu\text{mol}$  Lp and 21-32 nmol surface sites with  $63 \text{ m}^2 \text{ g}^{-1}$  and 5 sites  $\text{nm}^{-2}$ ). EDTA was also in large excess over photoproducts formed. During illumination, we observe mainly photo-reductive dissolution as described in previous studies <sup>2, 6</sup> and possibly some additional Fe(II)-catalyzed non-reductive dissolution, while we observe only the latter after illumination stops.

## Text S6. Kinetic model

Equilibrium reactions in the model are described as forward and back reactions in the input file of the kinetic program ACUCHEM (see Table S5). This means that all equations with a double arrow consist of two equations in the program code and the corresponding equilibrium constant is the ratio of the forward over back-reaction rate coefficients ( $k_f/k_b$ ). Since we did not aim to determine the kinetics of complex formation for dissolved or adsorbed complexes, we entered a value of  $1 \cdot 10^6 \text{ s}^{-1}$  for the unimolecular back reactions and an adjustable parameter for the forward reaction. This makes all equilibrium reactions fast and not rate determining on the investigated time scale. The rate-determining reactions are either the electron transfer (R7) or the detachment of Fe(III)EDTA from the reduced surface site (R8). By variation of rate coefficients, we found that either R7 or R8 or a combination of both steps could be rate determining. Experimentally, we can only measure the rate of formation of dissolved Fe(III)L and we have currently no technique to measure the kinetics of the ET and detachment separately. Since Fe(II) complexed to EDTA is a strongly reducing species, we assigned a fixed value to  $k_{7(\text{ET})}$  that is higher than the value for  $k_8$  and adjusted the rate coefficient  $k_8$  for the detachment of Fe(III)L as the rate determining step. When reactions R7 and R8 are combined into one reaction ( $\equiv \text{Fe}^{\text{III}}\text{-Fe}^{\text{II}}\text{-L} \rightarrow \equiv \text{Fe}^{\text{II}} + \text{Fe}^{\text{III}}\text{L}$ ), the same value for the combined rate coefficient is obtained as the value for the Fe(II)-catalyzed detachment ( $k_8$ ) listed in Table 1 ( $\log(k_8) = -0.64$ ). Important parameters in the model are the concentration of active sites for the dissolution reactions ( $p_1$  to  $p_4$ ). The site concentration for the adsorption of Fe(II), EDTA and Fe(III)EDTA were obtained from adsorption data and fits as shown in Figure S10. They agree with ranges for iron(hydr)oxides reported in the literature.<sup>7, 8</sup> The fitted concentration of active sites determined from dissolution experiments were a factor of 50-75 smaller than for the sites for adsorption. Increasing their concentration could be compensated by decreasing  $k_{\text{ET}}$ , but only in a narrow range. More than a doubling of this site concentration lead to significantly worse fits. A lower concentration of sites that are active for dissolution has been used in models describing the dissolution of hematite<sup>9</sup> and agrees with the understanding that dissolution proceeds on kink and step sites<sup>10</sup> whose concentrations are smaller than the sum of adsorption sites measured in adsorption experiments.

It is important to point out that the purpose of the model is to show that the suggested reactions can explain the experimental results and to explore the importance of the listed reactions, not to determine rate coefficients. We currently don't have sufficient data to uniquely determine the listed rate coefficients.

### **Text S7. Structures and photo-reactivity**

The observation that the photolysis of adsorbed EDTA starts with the onset of UV-irradiation (Fig. 4) is an indication for inner-sphere complexation of EDTA with Fe(III) at the surface. Un-complexed EDTA is not photo-reactive and the yield of OH-radicals by UV-illumination of Fe(III)hydroxides is low <sup>11</sup> The EDTA must be bound as an inner-sphere complex with a metal to ligand charge transfer (MLCT) absorption band that allows rapid light-induced charge transfer from a bound ligand carboxylate group to a surface Fe(III) site. The photoproduct of EDTA, ED3A <sup>6</sup> with a lower IR- absorbance (due to fewer carboxylate groups) is partly replaced by excess EDTA from solution in a steady state exchange during UV-illumination and completely after the illumination stops. The continuous formation of Fe(II) on the surface ligand during photo-induced charge transfer lead to both photodissolution and Fe(II)-catalyzed ligand-promoted dissolution during illumination, under both oxic and anoxic conditions. After illumination the Fe(II)-catalyzed dissolution continued under anoxic conditions, but not under oxic conditions. In experiments with phenanthroline (not shown) the same behavior was observed as under oxic conditions. These observations show that Fe(II) formed by UV- irradiation is not protected from oxidation by O<sub>2</sub> and that it can easily be desorbed or complexed by phenanthroline. Added and photo-produced Fe(II) appear to have the same effect on the dissolution of Lp.

Table S1. List of chemicals used in the current study

Chemical name	Chemical formula	Supplier	Purity	Stock solution (mM)
NaCl	NaCl	Merck	>99%	10
Fe(II)	FeCl <sub>2</sub> · 4H <sub>2</sub> O	Sigma-Aldrich	>99%	10
Fe(III)	FeCl <sub>3</sub> · 6H <sub>2</sub> O	Sigma-Aldrich	>98%	10
MES (2-morpholino-ethanesulfonic acid monohydrate)	C <sub>6</sub> H <sub>13</sub> NO <sub>4</sub> S · H <sub>2</sub> O	Sigma-Aldrich	>99%	100
MOPS (3-(N-) morpholino propanesulfonic acid)	C <sub>7</sub> H <sub>15</sub> NO <sub>4</sub> S	Sigma-Aldrich	>99%	100
EDTA (Ethylenediamine tetra acetic disodium dihydrate)	C <sub>10</sub> H <sub>14</sub> N <sub>2</sub> Na <sub>2</sub> O <sub>8</sub> · 2H <sub>2</sub> O	Merck	>99%	100
Phenanthroline	C <sub>12</sub> H <sub>8</sub> N <sub>2</sub> · H <sub>2</sub> O	Fluka	>99%	10
Iron-10,000 µg/ml		J.T Baker	For ICPMS standard	

Table S2. Initial IR absorbances of Lp at  $1021\text{ cm}^{-1}$ , before conducting Fe(II) added Lp dissolution study. Experiments were conducted in duplicates. Each experiment is listed below as  $n_1$  and  $n_2$ .

(To record the initial absorbance, a thin layer of 40-60  $\mu\text{g}$  Lp was formed on the ATR element (diamond,  $\phi$  4 mm) by spraying 2  $\mu\text{L}$  of a 30 mg/mL Lp suspension with an ultra-sonicator tip and drying with a gentle stream of  $\text{N}_2$  (The background single-beam spectrum for the calculation of the absorbance spectrum was the spectrum of the blank ATR-crystal).

Added Fe(II) concentration ( $\mu\text{M}$ )	Lp IR-Absorbance	
	$n_1$	$n_2$
0	0.80	0.87
0.2	0.84	0.86
0.5	0.88	0.60
1	0.80	0.87
2	0.87	0.72
4	0.75	0.87
6	0.78	0.87
10	0.90	1.05

Table S3. Dissolution rates of lepidocrocite in presence of 50  $\mu\text{M}$  EDTA with varied added Fe(II) concentrations. All experiments were conducted at pH 6 under anoxic condition and in duplicates. Each experiment is listed below as  $n_1$  and  $n_2$ .

Added [Fe(II)] (μM)	Lp dissolution rate (% h <sup>-1</sup> )			Catalytic Effect (CE)*
	ATR-FTIR measurements <sup>a</sup> (Fig.3)			
	n <sub>1</sub>	n <sub>2</sub>	Average (n <sub>1</sub> :n <sub>2</sub> )	
0.0	0.17	0.14	0.16	1
0.2	0.86	1.28	1.07	7
0.5	2.10	2.47	2.29	14
1.0	2.97	3.19	3.08	19
2.0	3.12	3.99	3.56	22
4.0	3.90	4.35	4.13	26
6.0	4.41	3.93	4.17	26
10.0	5.50	4.43	4.97	31
Batch measurements <sup>b</sup> (Fig. 5)			n <sub>1</sub>	CE
Only in presence of EDTA			0.16	1
1.2 μM <sup>57</sup> Fe(II) was added 1800 s after EDTA addition			2.14	13
1.2 μM <sup>57</sup> Fe(II) was added 1800 s before EDTA addition <sup>c</sup>			2.40	15

$$*\text{CE} = R_{\text{diss,L,Fe(II)}} / R_{\text{diss,L}}$$

$R_{\text{diss,L,Fe(II)}}$  is the rate of Fe(II)-catalyzed dissolution in presence of a ligand and Fe(II).  $R_{\text{diss,L}}$  is the rate of dissolution in presence of a ligand alone.

With this definition, the CE is 1 if there is no catalytic effect.

<sup>a</sup> In ATR-FTIR measurements, Lp concentration was 10-17  $\mu\text{M}$ . 50  $\mu\text{M}$  EDTA was added 1800 s before Fe(II) addition. Slopes for determining rates were calculated within 3000-5000 s (EDTA addition considered as  $t=0$ ).

<sup>b</sup> In isotope exchange and dissolution batch studies, Lp concentration was 1125  $\mu\text{M}$ . Slopes were calculated within 2400-4200 s to determine the dissolution rates.

<sup>c</sup> In ATR-FTIR measurements, when 1  $\mu\text{M}$  Fe(II) was added 1800 s before EDTA addition, the rate of Lp dissolution was calculated 2.20 %  $\text{h}^{-1}$  (Fig. S6).

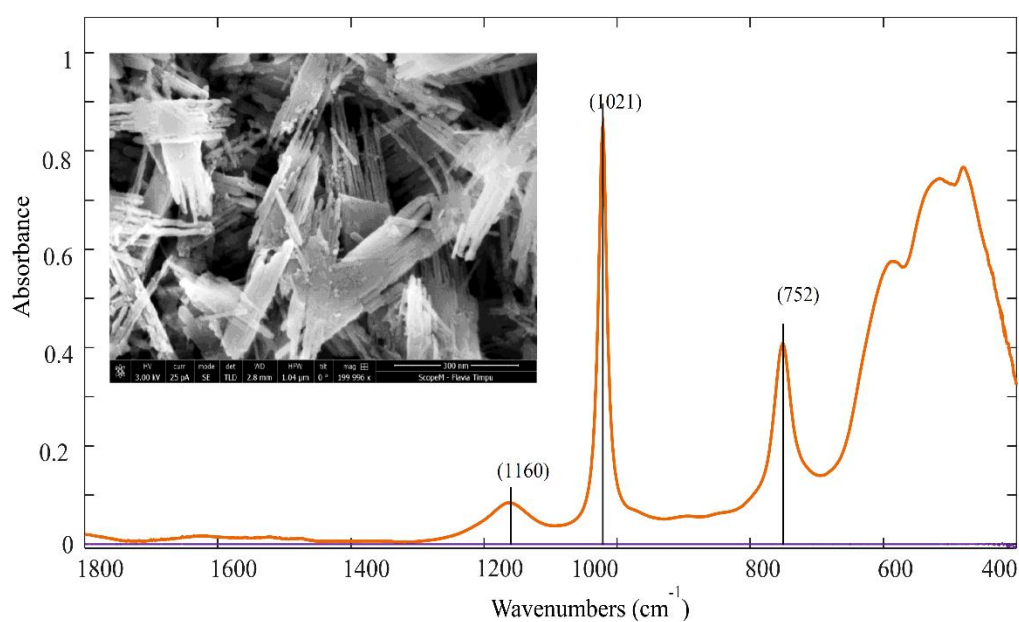


Figure S1. ATR-FTIR absorbance spectrum of synthesized Lp (lepidocrocite). A thin layer of 40-60  $\mu\text{g}$  Lp was formed on the ATR element (diamond,  $\phi$  4 mm) by spraying 2  $\mu\text{L}$  of a 30 mg/mL Lp suspension with an ultra-sonicator tip and drying with a gentle stream of  $\text{N}_2$  (The background single-beam spectrum for the calculation of the absorbance spectrum was the spectrum of the blank ATR-crystal).

The characteristic peaks at 1160 and 1021  $\text{cm}^{-1}$  correspond to in-plane bending ( $\delta\text{-OH}$ ) and 752  $\text{cm}^{-1}$  to outer-plane bending ( $\delta\text{-OH}$ ) of Lp structure.

The inset is the transmission electron microscope image of Lp structure.

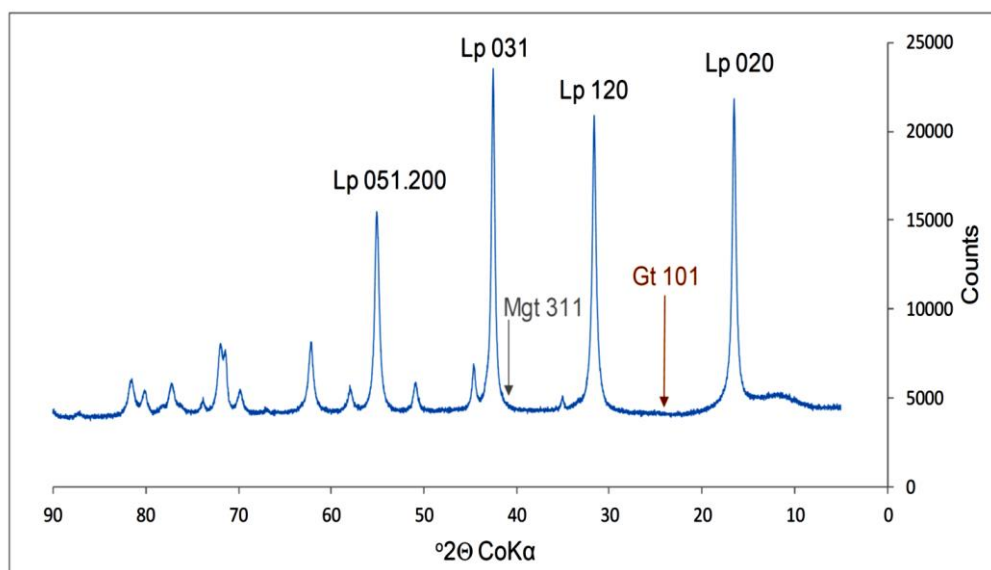


Figure S2. XRD powder diffractogram of the synthesized Lp (lepidocrocite) measured on X’Pert powder diffractometer with XCelerator, PANalytical, Almelo, the Netherlands. The diffractogram is in excellent agreement with lepidocrocite spectra reported by Cornell and Schwertmann.<sup>5</sup> Lines of magnetite (Mgt) and of goethite (Gt), which are common impurities in synthesized Lp, are not detectable.



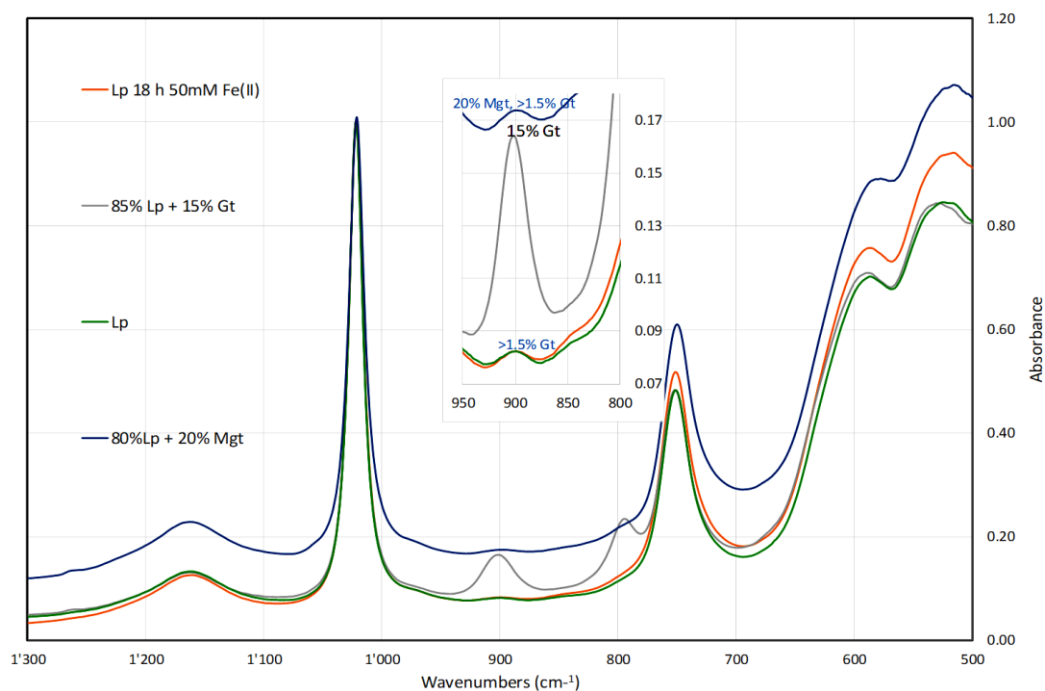


Figure S3. ATR-FTIR spectra of dried layers of various samples: Lp: freshly made Lp- suspension, Lp 18 h 50 mM Fe(II): Lp suspension with 10 mg Lp /100 ml exposed to 50  $\mu$ M Fe(II) at pH 8.0 under anoxic conditions for 18h, 85% Lp + 15 % Gt: Lp- and goethite (Gt) suspensions were mixed to achieve the indicated mass % mixture. Goethite was synthesized as described in Kang et al.<sup>12</sup>. 80% Lp + 20% magnetite (Mgt): suspensions mixed to achieve the % in weight. Magnetite was from MK-nano, Fe<sub>3</sub>O<sub>4</sub>, 99% Pure, APS: 25 nm (<https://www.mknano.com/Nanoparticles/Single-Element-Oxides>).

Samples of 2 ml suspensions were filtered through 0.2  $\mu$ m nylon filters and washed with 2 ml nanopure H<sub>2</sub>O. The filtrate was re-suspended in 2-5  $\mu$ l H<sub>2</sub>O and transferred onto the ATR-diamond disk and dried in a stream of N<sub>2</sub> before absorbance spectra were measured. Traces of goethite in lepidocrocite and changes in goethite fractions can be detected with a sensitivity of better than 1%. Formation of magnetite can be detected by a broad increase of absorbance.

In our experiments with 1-10  $\mu$ M added Fe(II), we did not detect formation of goethite or magnetite on the time scale of our experiments. Our synthesized Lp contained a fraction of < 1.5% Gt impurity (which was detectable with FTIR, but not in the XRD diffractogram). This fraction did not change during our experiments. We did not observe formation of Gt or Mgt during our experiments with 0.2-10  $\mu$ M Fe(II).

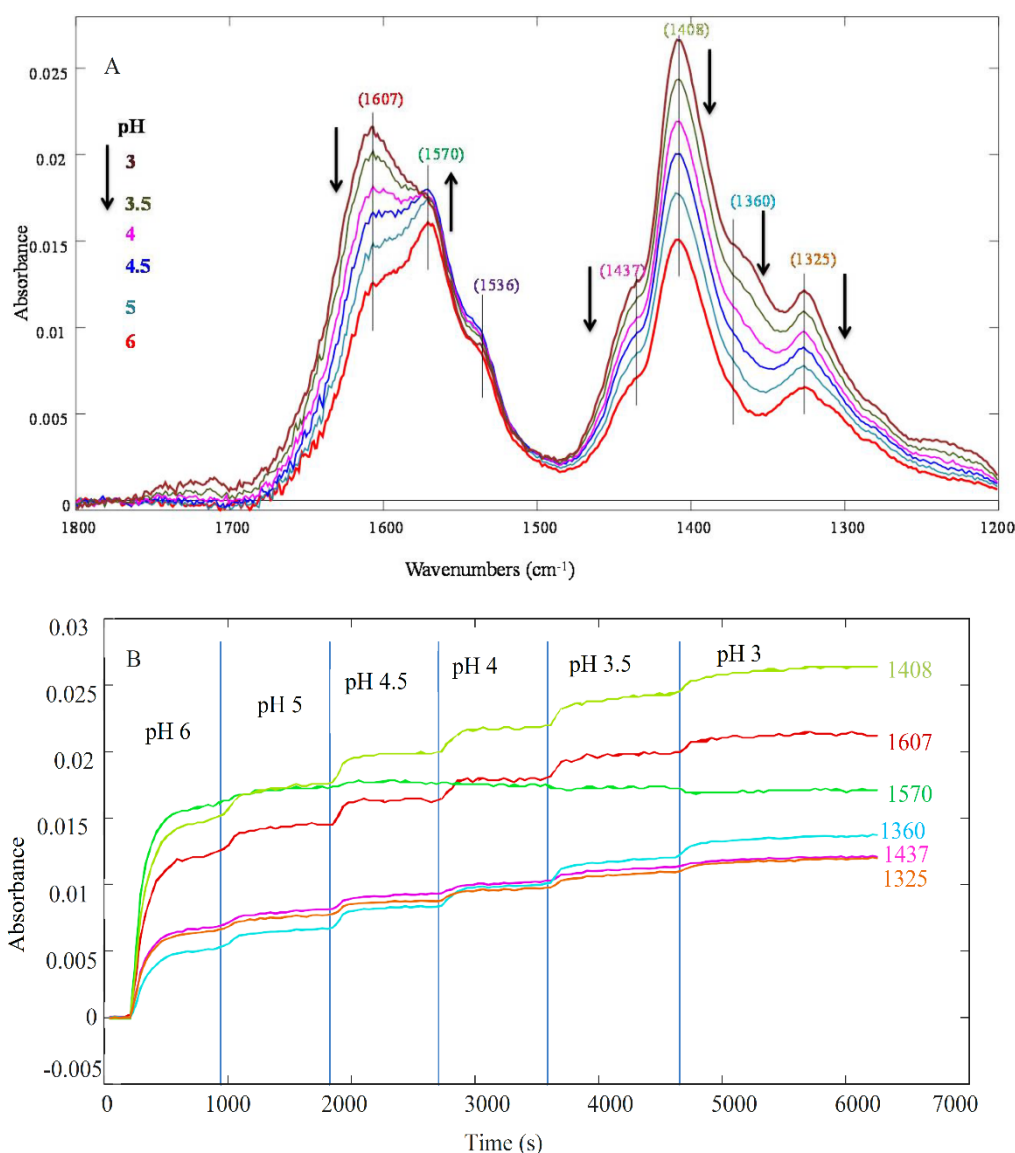


Figure S4. ATR-FTIR difference (background subtracted) (A) absorbance spectra recorded during EDTA adsorption onto lepidocrocite (Lp) and (B) kinetics at pH 3-6 under anoxic condition. The spectrum of Lp in contact with 40 ml aqueous solution (0.01 M NaCl and 0.005 M MES) after purging with high purity  $\text{N}_2$  for 3-4 h, before addition of 50  $\mu\text{M}$  EDTA, was defined as background. The pH adjustments were done with minute addition of 0.1 M HCl or NaOH only when EDTA adsorption reached equilibrium at each pH.

The amplitude of EDTA absorbance (recorded as indicated wavenumbers) decreases with increasing pH (pH 3-6), except at 1570  $\text{cm}^{-1}$ . The spectral changes occurred upon pH variations indicate that the type of surface complex formed at the surface of lepidocrocite is pH dependent

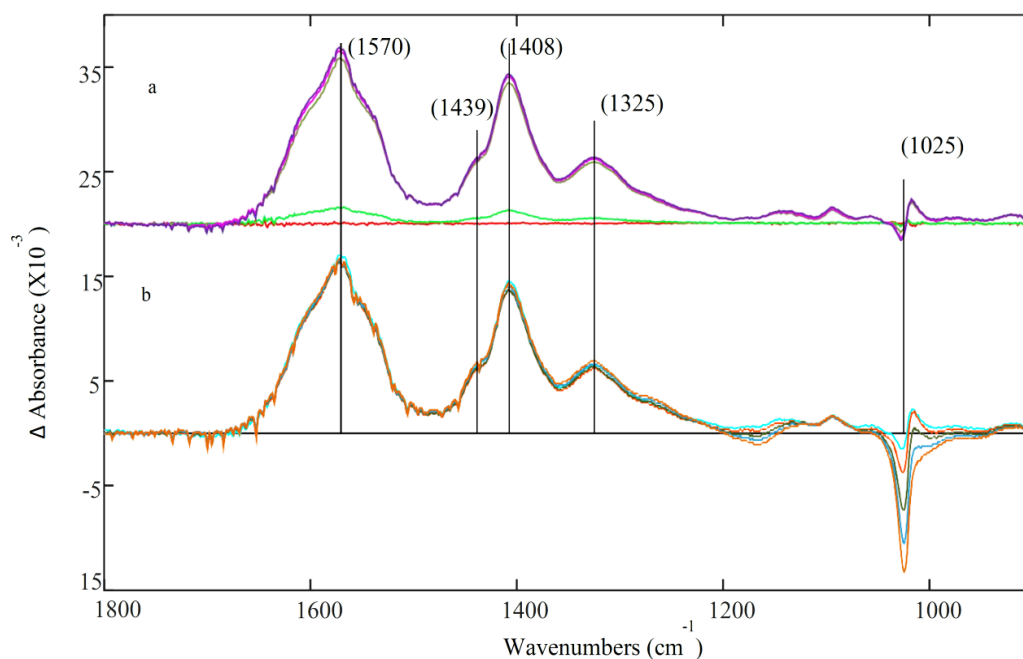


Figure S5. ATR-FTIR difference absorbance spectra (background subtracted), at pH 7, recorded during a) EDTA adsorption (offset by 20 units), upon addition of 50  $\mu\text{M}$  EDTA to a layer of 50-60  $\mu\text{g}$  lepidocrocite (Lp) in contact with 40 ml aqueous solution, and b) dissolution of Lp after addition of 10  $\mu\text{M}$  Fe(II) in presence of 50  $\mu\text{M}$  EDTA (no offset). The spectrum of Lp in contact with aqueous solution (0.01 M NaCl and 0.005 M MOPS) after purging with high purity  $\text{N}_2$  for 3-4 h, before addition of EDTA, was defined as background. Spectra were recorded continuously every 71 s. Averages of every 6-10 continuous spectra are shown for clarity.

The group of spectra in a) shows two characteristic peaks of adsorbed EDTA at 1570  $\text{cm}^{-1}$  and 1408  $\text{cm}^{-1}$  upon addition of EDTA and very minor dissolution of Lp at 1025  $\text{cm}^{-1}$ . The group of spectra in b) shows the strongly accelerated dissolution of Lp at 1025  $\text{cm}^{-1}$  after addition of 10  $\mu\text{M}$  Fe(II) ( $t_{\text{Fe(II) addition}}=3000$  s, when  $t_{\text{EDTA addition}}=800-900$  s).

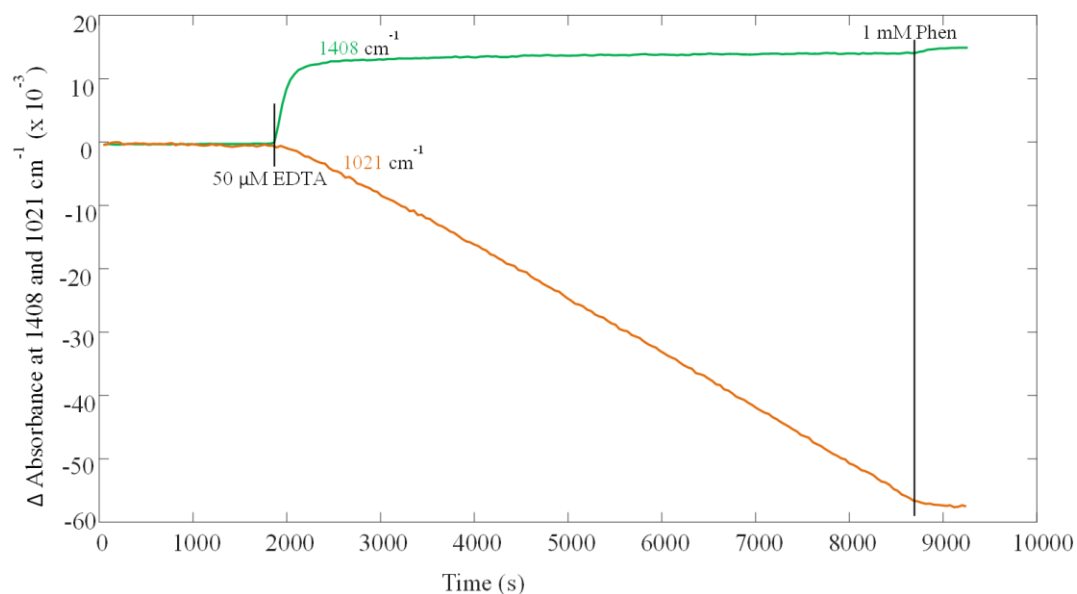


Figure S6. Kinetics of EDTA adsorption (monitored at  $1408\text{ cm}^{-1}$ ) and lepidocrocite (Lp) dissolution (monitored at  $1021\text{ cm}^{-1}$ ) with ATR-FTIR at pH 6 under anoxic conditions.  $50\text{ }\mu\text{M}$  EDTA was added 1800 s after  $1\text{ }\mu\text{M}$  Fe(II) was added, followed by addition of  $1\text{ mM}$  phenanthroline (Phen) after 8600 s. The data are shown without normalizing to initial Lp absorbance ( $0.7\text{--}0.9$  at  $1021\text{ cm}^{-1}$ ). Fe(II) addition didn't cause any significant changes to Lp in absence of EDTA. EDTA addition at 1800 s immediately caused the accelerated dissolution of Lp. EDTA adsorbed fast and reached equilibrium in  $< 200\text{ s}$ . Phen addition stopped the accelerated dissolution of Lp.

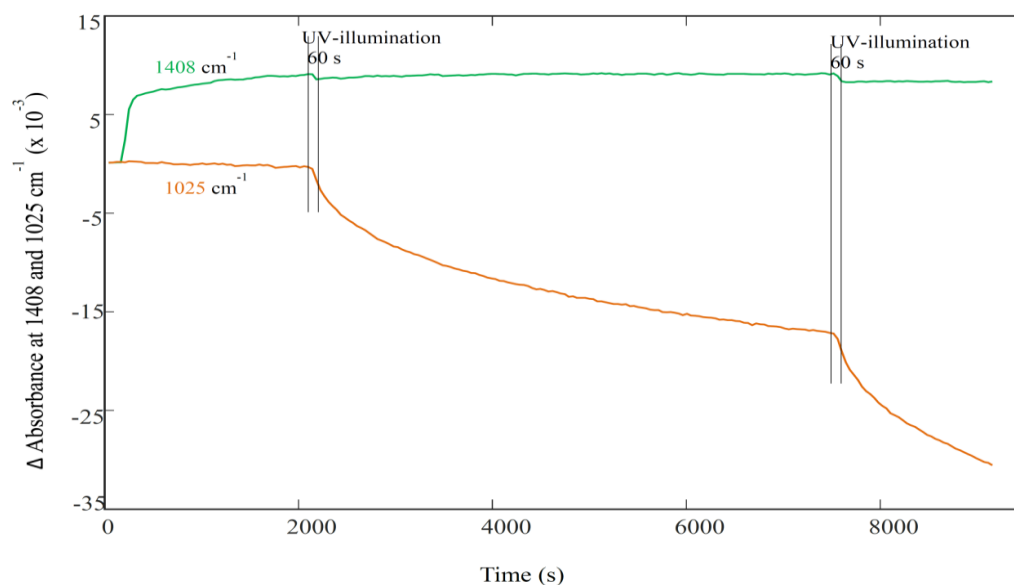


Figure S7. Kinetics of EDTA adsorption (monitored at  $1408\text{ cm}^{-1}$ ) and dissolution of lepidocrocite (Lp) (monitored at  $1025\text{ cm}^{-1}$ ) at pH 7 ( $I=0.01\text{ M}$ ) under anoxic conditions during photochemical experiments. EDTA ( $50\text{ }\mu\text{M}$ ) was added at 180-220 s. During UV-illumination (for 60 s, 2 times) with a 365 nm UV-LED lamp, adsorbed EDTA is photolyzed at the surface. After irradiation, photo-transformed EDTA is replaced by EDTA from solution. Lp dissolution was strongly accelerated by UV-illumination. After irradiation stops under anoxic condition, Lp dissolution continued.

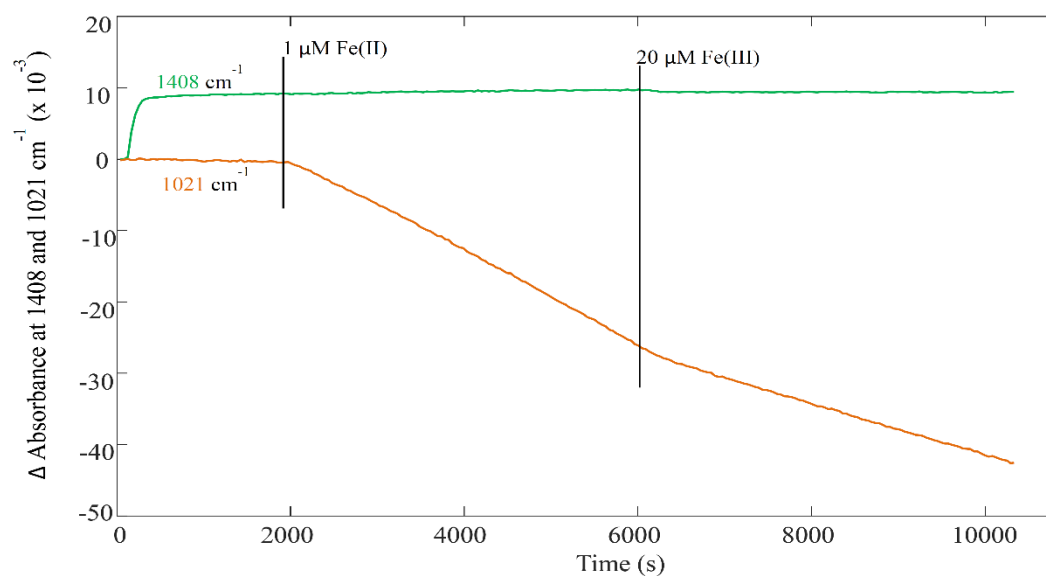


Figure S8. Kinetics of EDTA adsorption (monitored at 1408 cm<sup>-1</sup>) and lepidocrocite (Lp) dissolution (monitored at 1021 cm<sup>-1</sup>) with ATR-FTIR at pH 6 under anoxic conditions. 50 μM EDTA was added (at t=180-200 s) after purging the aqueous solution covering the Lp layer with N<sub>2</sub> for at least 3-4 h, followed by addition of 1 μM Fe(II) after 1800 s and addition of 20 μM Fe(III) after 6000 s. The data are shown without normalizing to initial Lp absorbance (0.7-0.9 at 1021 cm<sup>-1</sup>).

EDTA adsorbed fast and reached equilibrium in < 200 s. 1 μM Fe(II) addition lead to accelerated dissolution of Lp. Addition of 20 μM Fe(III) slowed down the accelerated dissolution.

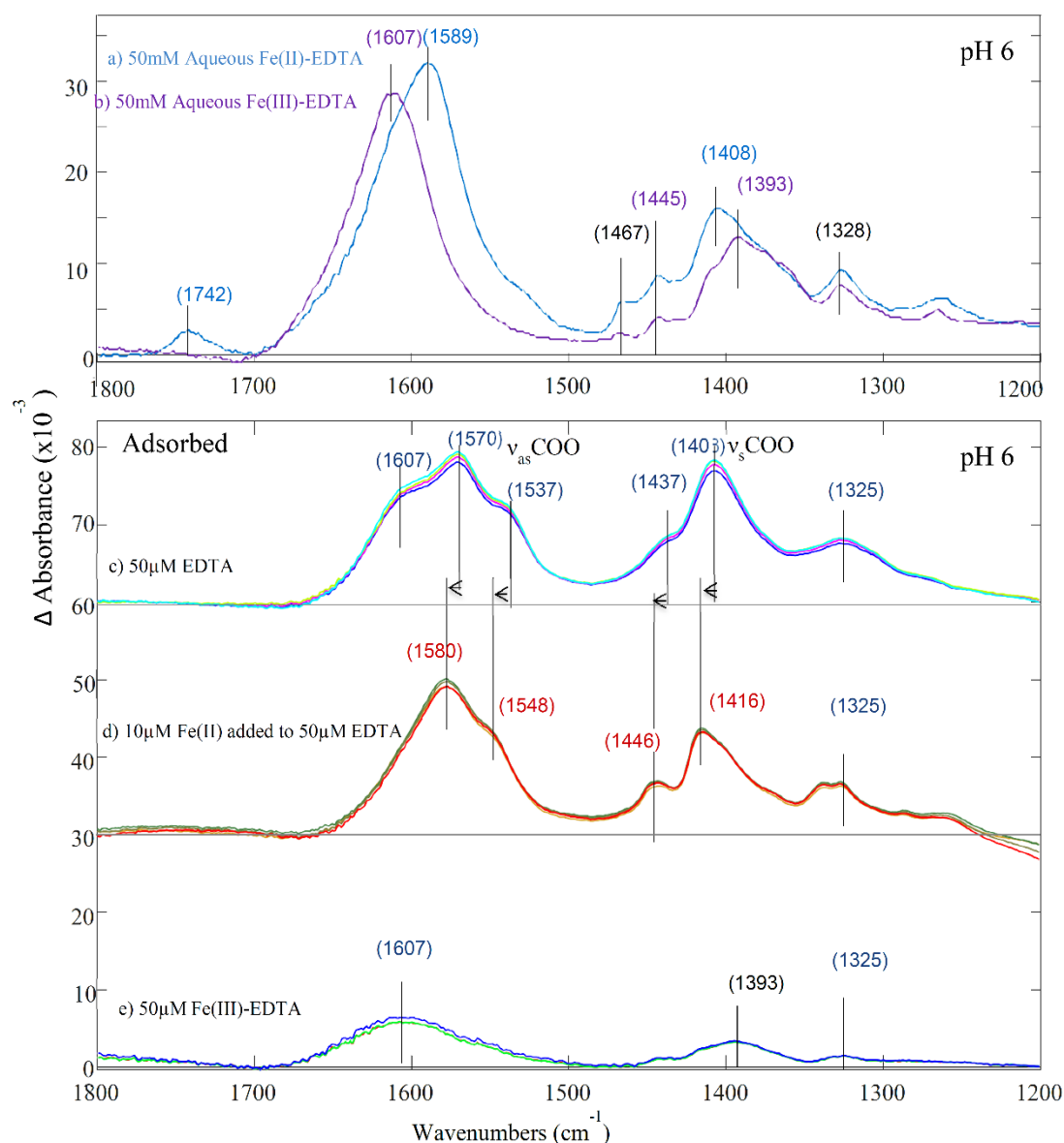


Figure S9. ATR-FTIR spectra of aqueous 1:1 complex of 50 mM (a) Fe(II)-EDTA and (b) Fe(III)-EDTA in top panel. In bottom panel, ATR-FTIR difference absorbance spectra recorded during (c) EDTA adsorption (offset by 60 units), upon addition of 50  $\mu$ M EDTA to a layer of 50-60  $\mu$ g lepidocrocite (Lp) in contact with 40 ml aqueous solution, (d) EDTA adsorption, upon addition of 10  $\mu$ M Fe(II) after 1800 sec of 50  $\mu$ M EDTA was added (offset by 30 units), and (e) adsorption of 1:1 aqueous complex of 50  $\mu$ M Fe(III)-EDTA onto lepidocrocite (no offset). All the measurements were conducted at pH 6 under anoxic condition (also see Table S4).

Table S4. Comparison of experimental IR frequencies

Assignments	Aqueous EDTA	Aqueous Fe(II)-EDTA	Aqueous Fe(III)-EDTA	Adsorbed EDTA	Addition of 10 $\mu$ M Fe(II) to Lp in the presence of EDTA	Adsorbed Fe(III)-EDTA
		1742				
$\nu_{\text{as}}$ C-O *	1613		1607	1607		1607
$\nu_{\text{as}}$ C-O *	1575	1589		1570	1580	
$\nu_{\text{s}}$ C-O *	1456	1467	1467	1537	1548	
$\nu_{\text{s}}$ C-O *	1433	1445	1445	1437	1446	
$\nu_{\text{s}}$ C-O *	1402	1408	1393	1408	1416	1393
n.a.	1357					
n.a.	1322	1328	1328	1325	1325	1325

\*  $\nu_{\text{as}}$ C-O and  $\nu_{\text{s}}$ C-O are simplified labels. They describe the asymmetric and symmetric carboxylate C-O stretching vibrations that contribute most to the intensity in these spectral regions. The vibrational modes giving rise to the several peaks and shoulders that also contain various contributions of  $\nu$ C-C,  $\delta$ N-H,  $\delta$ CH<sub>2</sub> and other vibrations.

n.a. = non-assigned.



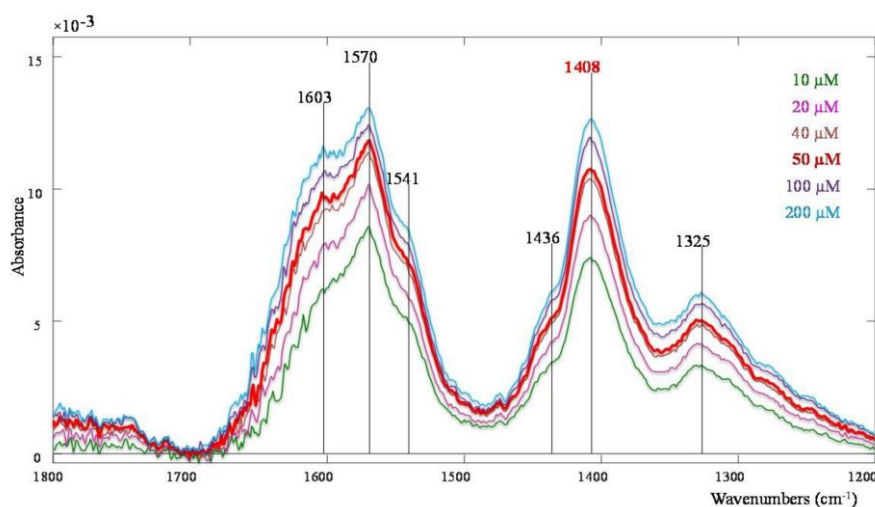


Figure S10. ATR-FTIR difference (background subtracted) absorbance spectra recorded during EDTA (10-200  $\mu\text{M}$ ) adsorption onto a layer of 50-60  $\mu\text{g}$  lepidocrocite (Lp) in contact with 40 ml aqueous solution at pH 6 under anoxic condition. The spectrum of Lp in contact with aqueous solution (0.01 M NaCl and 0.005 M MES) after purging with high purity N<sub>2</sub> for 3-4 h, before addition of EDTA, was defined as background. The spectra shown here are the spectra of EDTA when it reached adsorption equilibrium at each concentration.

The spectra show characteristic absorbance of EDTA onto Lp in the range of 1700-1200  $\text{cm}^{-1}$ . The two characteristic peaks of adsorbed EDTA at 1570  $\text{cm}^{-1}$  and 1408  $\text{cm}^{-1}$  correspond to asymmetric and symmetric vibrations of carboxylic group, respectively. The spectra show that increasing concentrations (10-200  $\mu\text{M}$ ) of aqueous EDTA do not cause significant spectral changes of adsorbed EDTA, except a small increase of the shoulder at 1603  $\text{cm}^{-1}$  (which might indicate a slightly higher contribution of protonated surface complex, see Fig. S2), indicating that the type of surface complex formed at the surface of Lp at pH 6 is largely independent of EDTA concentration.

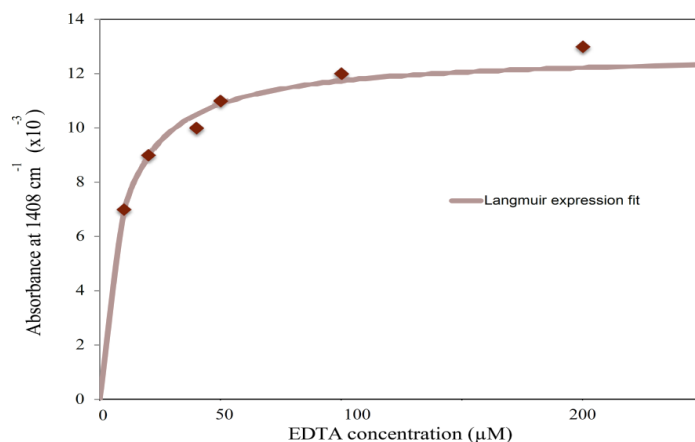


Figure S11. The maximum (absorbance) of EDTA adsorption monitored at  $1408\text{ cm}^{-1}$  on lepidocrocite (Lp), with ATR-FTIR at pH 6, plotted as a function of added EDTA concentrations. 10-200  $\mu\text{M}$  EDTA were added after purging the aqueous solution (10 mM NaCl and 5 mM MES) covering the Lp layer (60  $\mu\text{g}$ ) with  $\text{N}_2$  for at least 3-4 h. The absorbance at  $1408\text{ cm}^{-1}$  was fitted with a Langmuir type model (line) to estimate the equilibrium constant for the adsorption of EDTA (see kinetic model). Note that added and equilibrium EDTA concentrations are to within 1% the same in these experiments with only 60  $\mu\text{g}$  Lp and 40 ml aqueous solution (e.g. 6.3 nmol surface sites with  $1\text{ site/nm}^2$  versus 800 nmol EDTA in solution with 20  $\mu\text{M}$  EDTA). The surface was considered saturated at  $[\text{EDTA}]_{\text{aq}} = 200\text{ }\mu\text{M}$ . With  $[\text{FeOOH}] = 10\text{ }\mu\text{M}$  in the FTIR experiments and a surface site of concentration of  $0.79\text{ sites/nm}^2$  determined by batch experiments gives  $0.072\text{ }\mu\text{M}$  for  $[\text{EDTA}]_{\text{ads}}$  at saturation. A saturated surface concentration of  $0.79\text{ sites/nm}^2$  was similar to  $1.12\text{ site/nm}^2$  obtained by Nowack et al.<sup>8</sup>

Table S5. Kinetic model: input-file for ACUCHEM <sup>(a)</sup>

; INPUT file for ACUCHEM (AC99.EXE)

; Question marks are replaced by adjustable numerical values (fitting parameter or initial conc.)

;

input 0010

;

R1f,  $\text{Fe2} + \text{L} = \text{Fe2L}$ , 2.17e+16; 1 Dissolved Fe2L complex formation <sup>(b)</sup>R1b,  $\text{Fe2L} = \text{Fe2} + \text{L}$ , 1e6

;

R2f,  $(\text{SFe3}) + \text{L} = (\text{SFe3})\text{L}$ , ? ; 2 Adsorption of ligandR2b,  $(\text{SFe3})\text{L} = (\text{SFe3}) + \text{L}$ , 1e6

;

R3f,  $(\text{SFe3}) + \text{Fe2} = (\text{SFe3})\text{Fe2}$ , ? ; 3 Adsorption of Fe2R3b,  $(\text{SFe3})\text{Fe2} = (\text{SFe3}) + \text{Fe2}$ , 1e6

;

R4f,  $(\text{SFe3})\text{Fe2} + \text{L} = (\text{SFe3})\text{Fe2L}$ , ? ; 4 Adsorption of L on adsorbed Fe2R4b,  $(\text{SFe3})\text{Fe2L} = (\text{SFe3})\text{Fe2} + \text{L}$ , 1e6

;

R5f,  $(\text{SFe3}) + \text{Fe2L} = (\text{SFe3})\text{Fe2L}$ , ? ; 5 Adsorption of Fe2LR5b,  $(\text{SFe3})\text{Fe2L} = (\text{SFe3}) + \text{Fe2L}$ , 1e6

;

R6f,  $(\text{SFe3}) + \text{Fe3L} = (\text{SFe3})\text{Fe3L}$ , ? ; 6 Competing adsorption of Fe3LR6b,  $(\text{SFe3})\text{Fe3L} = (\text{SFe3}) + \text{Fe3L}$ , 1e6

;

R7f,  $(\text{SFe3})\text{Fe2L} = (\text{SFe2})\text{Fe3L}$ , 10 ; 7 Electron transferR8f,  $(\text{SFe2})\text{Fe3L} = (\text{SFe2}) + \text{Fe3L}$ , ? ; 8 Detachment of Fe3L  
(rate-determining)R9f,  $(\text{SFe2}) + \text{bulk} = (\text{SFe3})\text{Fe2}$ , 1e6 ; 9 Formation of new surface site  
(non-rate determining)

;

R10f,  $(\text{SFe3})\text{L} = (\text{S}) + \text{Fe3L}$ , ? ; 10 Detachment of Fe3LR11f,  $(\text{S}) + \text{bulk} = (\text{SFe3})$ , 1e6 ; 11 Formation of new surface site

end

;

Initial concentrations

 $(\text{SFe3})$ , ? ; 8 $\text{Fe2}$ , ? ; 9 $\text{L}$ , ? ; 10

bulk,? ; 11  
Fe3L,? ; 12  
end  
0.0001  
? ; 13 longest time-point (of 50) in the model in seconds  
end  
& Additional information for output which is not used by AC99.EXE  
9  
Fe3L  
Fe2L  
L  
Fe2  
(SFe2)Fe3L  
(SFe3)L  
bulk  
(SFe3)Fe2  
(SFe3)Fe3L

(a) W. Braun, J.T. Herron, D.K. Kahaner, Acuchem: a computer program for modeling complex chemical reaction systems, Int. J. Chem. Kinet. 20 (1988) 51–62.

(b) The conditional equilibrium constant for the complex formation of EDTA with Fe(II) at pH 6.0 in 9.5 mM NaCl was calculated with Visual Minteq (<https://vminteq.lwr.kth.se/>). With 50  $\mu\text{M}$  EDTA and 1-10  $\mu\text{M}$  dissolved Fe(II), 99.86% of Fe(II) is present as  $\text{Fe}^{\text{II}}\text{EDTA}^{2-}$ , and only 5·10<sup>-12</sup> M is present as non-complexed  $\text{Fe}^{2+}$ . Towards the end of Lp-dissolution with 50  $\mu\text{M}$  EDTA with 1-2  $\mu\text{M}$  dissolved Fe(II) and 45  $\mu\text{M}$  dissolved Fe(III), 99.86% of dissolved Fe(II) is still present as  $\text{Fe}^{\text{II}}(\text{EDTA})^{2-}$  and Fe(III) is to 97.96% present as  $\text{Fe}^{\text{III}}(\text{EDTA})^-$  and to 2.06% as  $\text{Fe}^{\text{III}}(\text{OH})(\text{EDTA})^{2-}$ .

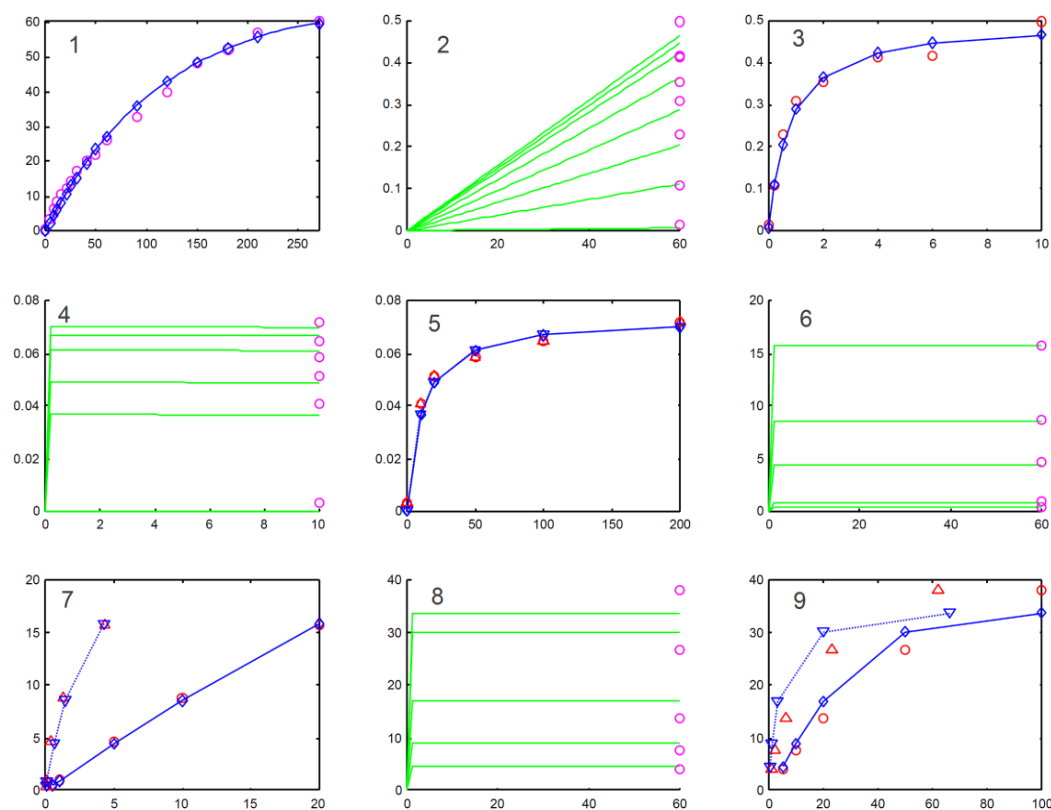


Figure S12. Kinetic model: data and model output

Data (red and magenta symbols) and model output (blue symbols and blue or green lines).

The x-axes indicate time (min) or concentrations ( $\mu\text{M}$ ) as indicated for the different panels below. The y-axes indicate concentrations ( $\mu\text{M}$ ). The red circles in panels 5, 7 and 9 show the measured concentrations of adsorbed EDTA, Fe(II) and Fe(III)EDTA as a function of added concentrations, the red triangles as a function of measured dissolved concentrations in equilibrium. The blue diamonds show the modeled adsorbed equilibrium concentrations as function of added concentrations, the blue triangles as a function of the calculated dissolved equilibrium concentrations.

- 1 Batch dissolution experiment:  $[\text{Fe(III)EDTA}]$  vs. time after addition of Fe(II).  $[\text{Lp}]_0 = 1.13 \text{ mM}$ .
- 2 FTIR dissolution experiments with added FeII:  $[\text{Fe(III)EDTA}]_{\text{diss.}}$  vs. time.  $[\text{Lp}]_0 = 10 \mu\text{M}$ .
- 3 FTIR dissolution experiments with added FeII:  $[\text{Fe(III)EDTA}]_{\text{diss.}}$  at  $t=3600$  vs. added  $[\text{Fe(II)}]$ .  $[\text{Fe(III)EDTA}]_{\text{diss.}}$  was calculated from dissolution rates measured by FTIR.  $[\text{Lp}]_0 = 10 \mu\text{M}$ .
- 4  $[\text{EDTA}]_{\text{ads}}$  vs. time for fast equilibrium.  $[\text{Lp}]_0 = 10 \mu\text{M}$ .
- 5  $[\text{EDTA}]_{\text{ads}}$  vs. added and equilibrium conc. of  $[\text{EDTA}]_{\text{diss.}}$ .  $[\text{Lp}]_0 = 10 \mu\text{M}$ .
- 6  $[\text{Fe(II)}]_{\text{ads}}$  vs. time for fast equilibrium.  $[\text{Lp}]_0 = 28.1 \text{ mM}$ .
- 7  $[\text{Fe(II)}]_{\text{ads}}$  vs. added and equilibrium conc. of  $[\text{EDTA}]_{\text{diss.}}$ .  $[\text{Lp}]_0 = 28.1 \text{ mM}$ .
- 8  $[\text{Fe(III)EDTA}]_{\text{ads}}$  vs. time for fast equilibrium.
- 9  $[\text{Fe(III)EDTA}]_{\text{ads}}$  vs. added and equilibrium conc. of  $[\text{Fe(III)EDTA}]_{\text{diss.}}$ .  $[\text{Lp}]_0 = 28.1 \text{ mM}$ .

Adsorption isotherms for Fe(II) and Fe(III)EDTA were measured in batch experiments with 2.5 g Lp/L (10 mM NaCl, 5 mM MES pH 6.0), reaction time 30 min. Fe-concentrations were measured with ICP-MS (Agilent 7500ce).<sup>12</sup>

## Text S8. References

1. Borer, P. M.; Sulzberger, B.; Reichard, P.; Kraemer, S. M., Effect of siderophores on the light-induced dissolution of colloidal iron(III) (hydr)oxides. *Mar. Chem.* **2005**, *93*, 179–193.
2. Borer, P.; Kraemer, S. M.; Sulzberger, B.; Hug, S. J.; Kretzschmar, R., Photodissolution of lepidocrocite ( $\gamma$ -FeOOH) in the presence of desferrioxamine B and aerobactin. *Geochim. Cosmochim. Acta* **2009**, *73*, (16), 4673-4687.
3. Borer, P.; Sulzberger, B.; Hug, S. J.; Kraemer, S. M.; Kretzschmar, R., Wavelength-dependence of photoreductive dissolution of lepidocrocite ( $\gamma$ -FeOOH) in the absence and presence of the siderophore DFOB. *Environ. Sci. Technol.* **2009**, *43*, (6), 1871-1876.
4. Borer, P.; Sulzberger, B.; Hug, S. J.; Kraemer, S. M.; Kretzschmar, R., Photoreductive dissolution of iron(III) (Hydr)oxides in the absence and presence of organic ligands: Experimental studies and kinetic modeling. *Environ. Sci. Technol.* **2009**, *43*, (6), 1864-1870.
5. Schwertmann, U.; Cornell, R. M., *Iron Oxides in the Laboratory*. 2nd, Completely Revised and Extended Edition ed.; Wiley-VCH Weinheim, Germany, 2000.
6. Karametaxas, G.; Hug, S. J.; Sulzberger, B., Photodegradation of EDTA in the Presence of Lepidocrocite. *Environ. Sci. Technol.* **1995**, *29*, (12), 2992-3000.
7. Nowack, B.; Lutzenkirchen, J.; Behra, P.; Sigg, L., Modeling the adsorption of metal-EDTA complexes onto oxides. *Environ. Sci. Technol.* **1996**, *30*, (7), 2397-2405.
8. Nowack, B.; Sigg, L., Adsorption of EDTA and metal-EDTA complexes onto goethite. *J. Colloid Interface Sci.* **1996**, *177*, (1), 106-121.
9. Samson, S. D.; Eggleston, C. M., The depletion and regeneration of dissolution-active sites at the mineral-water interface: II. Regeneration of active sites on alpha-Fe<sub>2</sub>O<sub>3</sub> at pH 3 and pH 6. *Geochim. Cosmochim. Acta* **2000**, *64*, (21), 3675-3683.
10. Wehrli, B., Monte Carlo simulations of surface morphologies during mineral dissolution. *J. Colloid Interface Sci.* **1989**, *132*, (1), 230-242.
11. Bhandari, N.; Hausner, D. B.; Kubicki, J. D.; Strongin, D. R., Photodissolution of Ferrihydrite in the Presence of Oxalic Acid: An In Situ ATR-FTIR/DFT Study. *Langmuir* **2010**, *26*, (21), 16246-16253.
12. Kang, K.; Schenkeveld, W. D. C.; Biswakarma, J.; Borowski, S. C.; Hug, S. J.; Hering, J. G.; Kraemer, S. M., The catalytic role of low Fe(II) concentrations in ligand-controlled dissolution of Fe(III) (hydr)oxide minerals submitted to *Environ. Sci. Technol.* 2018.



## Chapter 3

# Linking Isotope-Exchange with Fe(II)-Catalyzed Dissolution of Iron(hydr)oxides in the Presence of the Bacterial Siderophore Desferrioxamine-B

---

Jagannath Biswakarma, Kyounglim Kang, Walter D.C. Schenkeveld,

Stephan M. Kraemer, Janet G. Hering and Stephan J. Hug

*Revised version of this chapter published in*

*Environmental Science & Technology*, 2020, 54(2), 768-777

*doi/10.1021/acs.est.9b04235*



## Abstract

Dissolution of Fe(III) phases is a key process in making iron available to biota and in the mobilization of associated trace elements. Recently we demonstrated that submicromolar concentrations of Fe(II) can significantly accelerate rates of ligand-controlled dissolution of iron(oxyhydr)oxide phases at circumneutral pH. In our previous work, we could estimate the extent of charge (associated with Fe(II) adsorption) over the surface in dissolution experiments with lepidocrocite (Lp) and the synthetic ligand ethylenediaminetetraacetate (EDTA) at pH 6.0. Here, we extend these studies by conducting experiments with Lp at pH 6.0, 7.0 and 8.5 and with goethite (Gt) at pH 7.0 and the bacterial siderophore desferrioxamine-B (DFOB), and by applying a kinetic model that can account for the observed isotope exchange and catalytic effect of Fe(II).

The fate of added Fe(II) was strongly dependent on the order of addition of Fe(II) and ligand. <sup>57</sup>Fe(II) added after DFOB remained in solution and accelerated dissolution occurred by formation of dissolved Fe(II)DFOB followed by transfer of negative charge to the surface. When <sup>57</sup>Fe(II) was added first, isotope exchange in solution could be observed at pH 6.0, while at pH 7.0, <sup>57</sup>Fe(II) was almost completely adsorbed. Phenanthroline added after 30 min desorbed predominantly <sup>56</sup>Fe(II) from Lp, in contrast to predominantly <sup>57</sup>Fe(II) desorption from Gt. This shows that electron transfer from adsorbed <sup>57</sup>Fe to <sup>56</sup>Fe of the mineral surface occurred extensively on a time scale of hours on Lp, but much less on Gt. During dissolution of Lp with DFOB, ratios of released <sup>56</sup>Fe and <sup>57</sup>Fe were largely independent of added Fe(II) and DFOB concentrations. Our results show that addition of Fe(II) leads to a highly dynamic system of charge transfer between dissolved and adsorbed species and to isotope exchange at the surface, with the dissolution of Lp by ligands accelerated by factors up to over 50. Our experiments were conducted in the environmentally important pH range from 6.0-8.5, in solutions buffered with carbonate at pH 7. The role of Fe(II) in the dissolution of Fe(III) phases (which is not yet sufficiently recognized) likely plays an important role at anoxic/oxic interfaces in aquatic systems.

## Introduction

Iron (Fe) mobilization by natural ligands (e.g. siderophores) from poorly soluble Fe(III)(oxyhydr)oxide phases is a key Fe-acquisition strategy for organisms in Fe-deficient conditions.<sup>1-11</sup> Siderophore-promoted dissolution rates of Fe(III)(oxyhydr)oxides have been reported to be slow at circumneutral pH ranges but can be accelerated by synergistic effects of two or more ligands.<sup>12-18</sup> For example, the dissolution rates of hematite<sup>14, 19</sup>, ferrihydrite<sup>20</sup>, and goethite with bacterial siderophore deferoxamine-B (DFOB) was accelerated 2-10 times by addition of oxalate<sup>12, 13, 16, 17</sup>, Suwannee river fulvic acid<sup>21</sup>, and ascorbate<sup>14</sup> at acidic pH conditions.

Very recently, we demonstrated that, at circumneutral pH, submicromolar concentrations of added Fe(II) significantly accelerate dissolution rates of Fe(III)(oxyhydr)oxides with the synthetic ligands ethylenediaminetetraacetate (EDTA) and hydroxybenzyl ethylenediaminediacetic acid (HBED) and also with the bacterial siderophore desferrioxamine-B (DFOB).<sup>22, 23</sup> The catalytic effect of Fe(II) at pH 6 with EDTA could be described by a kinetic model in which accelerated dissolution was attributed to electron transfer (ET) to surface Fe(III) followed by detachment of Fe(III)EDTA.

In other studies, recrystallization of Fe(III)(oxyhydr)oxides minerals observed in <sup>57</sup>Fe isotope tracer studies was attributed to adsorption of added <sup>57</sup>Fe(II) followed by interfacial ET and bulk conduction.<sup>24-28</sup> Thus, during recrystallization, mineral growth occurs at the adsorption site and bulk ET leads to Fe(II) release at a distant site with zero net dissolution of the mineral.<sup>29-35</sup> Although Fe(II) adsorption is pH-dependent, the net interfacial ET per adsorbed Fe(II) was found to be independent of solution pH.<sup>32, 35</sup>

We included these processes in interpreting the release of <sup>57</sup>Fe at pH 6 that we observed in our recent study<sup>22</sup> of lepidocrocite (Lp) dissolution with <sup>57</sup>Fe(II) and EDTA. The kinetic model used in that study, however, did not explicitly include isotope exchange nor did we quantify the ratio of <sup>57</sup>Fe release over <sup>56</sup>Fe release during dissolution.

Here we addressed these questions by performing experiments under anoxic conditions (pH 6.0, 7.0 and 8.5) with Lp and varying concentrations of Fe(II), <sup>57</sup>Fe(II) and DFOB. Experiments were buffered with MES (pH 6.0) and PIPES (pH 8.5). At pH 7.0, experiments were conducted using a carbonate system since this is more relevant for environmental systems and avoids the possible

interference<sup>36</sup> associated with Goods buffers; some experiments were conducted with MOPS for comparison. We used an empirical kinetic model to compare rates of dissolution from initiation to completion with initial rates that we reported previously. We used a mechanistic kinetic model to describe isotopic exchange before and during Lp dissolution in the presence and absence of  $^{57}\text{Fe(II)}$  and DFOB at pH 6.0 and 7.0. We also conducted some experiments with goethite (Gt) in order to assess the effect of the solids (Gt and Lp) on the fate of added  $^{57}\text{Fe(II)}$ . Finally, we conducted experiments with both Lp and Gt in the presence of phenanthroline to examine isotopic exchange in the absence of dissolution.

## **Materials and Methods**

### **Chemicals and Solutions**

Aqueous solutions were prepared using high-purity doubly-deionized (DDI) water (Barnstead Nanopure). All chemicals used were of analytical grade and are listed in the supporting information (SI), Table S1. The detailed synthesis procedure and characterization of Lp and Gt were described in our recent studies.<sup>22, 23</sup> Pure crystalline Lp and Gt were synthesized; surface areas as measured by BET were  $63 \text{ m}^2 \text{ g}^{-1}$  for Lp and  $105 \text{ m}^2 \text{ g}^{-1}$  for Gt. A 20 mM  $^{57}\text{Fe(II)}$  stock solution was prepared by dissolving 5.7 mg  $^{57}\text{Fe}$  (Sigma-Aldrich, 95% pure) in 100  $\mu\text{l}$  2.5 M HCl and dilution to 5.00 ml with DDI  $\text{H}_2\text{O}$  for conducting studies on isotope exchange and dissolution.

### **Iron (hydr)oxide Dissolution in Batch Experiments with Fe(II) or $^{57}\text{Fe(II)}$**

Batch dissolution experiments were conducted under anoxic conditions at room temperature (22-24 °C) with suspensions of 1125  $\mu\text{M}$  Lp or Gt, 20 or 50  $\mu\text{M}$  DFOB, and varied concentrations of Fe(II) (1, 2, 5  $\mu\text{M}$ ). Isotope experiments were conducted with 2  $\mu\text{M}$  of  $^{57}\text{Fe(II)}$ . Most experiments were conducted at pH 7.0 in 3 mM  $\text{NaHCO}_3$  solution, purged with a high purity gas mixture of 2 %  $\text{CO}_2$  in  $\text{N}_2$ . Additional experiments were conducted at pH 6.0 (5 mM MES), pH 7.0 (5mM MOPS) and at pH 8.5 (5 mM PIPES). In the series of connected experiments with different Fe(II) concentrations, each experiment was conducted once. All  $^{57}\text{Fe(II)}$  isotope experiments were conducted in duplicate. Specifics of the conditions for all experiments are summarized in Table S2.

Briefly, suspensions were prepared by dispersing 10 mg Lp or Gt in 100 ml aqueous solution. The 130 ml reaction flasks were sonicated for 10-15 min to obtain homogeneous suspensions. All suspensions were purged with high purity N<sub>2</sub> (either with or without 2% CO<sub>2</sub>) for at least 3 h before initiation of the experiments (t=0). After dissolved O<sub>2</sub> concentrations dropped to below 20 nM (monitored with a PreSens Fibox 4 trace oxygen sensor), experiments were started by addition of small volumes of N<sub>2</sub>-purged stock solutions to reach 20 or 50 µM DFOB and 0-5 µM Fe(II). In one set of experiments Fe(II) was added first, followed by addition of DFOB after 1800 s; in a second set, DFOB was added first, followed by addition of Fe(II) after 1800 s. 2 ml samples were withdrawn periodically, filtered through 0.1 µm nylon filters (Whatman® Puradisc 13 syringe filters) and diluted in 1% HNO<sub>3</sub> (Merck, suprapure) for inductively coupled plasma-mass spectrometry (ICP-MS, Agilent 7500cx) analysis. The dissolved concentrations of Fe ([Fe]<sub>diss</sub>) was measured with repeated ICP-MS measurements.

**Isotope Exchange and Dissolution studies.** To investigate the fate of added Fe(II), we added an <sup>57</sup>Fe(II) tracer 1800 s before or after DFOB addition to Lp or Gt suspension. Solid dissolution was followed by measuring the concentration of dissolved iron ([<sup>56</sup>Fe]<sub>diss</sub><sup>\*</sup>) with ICP-MS at mass 56, calibrated to represent the concentration of the total natural abundance iron (5.85% <sup>54</sup>Fe, 91.75% <sup>56</sup>Fe, 2.12% <sup>57</sup>Fe, 0.28% <sup>58</sup>Fe). This is the concentration of Fe released from the solid during isotope exchange and dissolution, which is referred to as <sup>56</sup>Fe for ease of reading.

The dissolved concentration of <sup>57</sup>Fe ([<sup>57</sup>Fe]<sub>diss</sub>) was measured with ICP-MS at mass 57. The concentration of <sup>57</sup>Fe released from the solid during isotope exchange and dissolution (0.0212[<sup>56</sup>Fe]<sub>diss</sub><sup>\*</sup>) was subtracted from [<sup>57</sup>Fe]<sub>diss</sub> to obtain the dissolved concentration of tracer <sup>57</sup>Fe ([<sup>57</sup>Fe]<sub>tracer, diss</sub>).

**<sup>57</sup>Fe isotope exchange without dissolution.** In order to assess isotopic exchange at pH 7.0 without dissolution, we added phenanthroline (100 µM) 1800 s after <sup>57</sup>Fe(II) (2 µM) addition to Lp or Gt suspension. Since phenanthroline has a high affinity for Fe(II), we assume that it complexed both Fe(II) in solution as well as surface-bound Fe(II) that was easily released from the surface. The resulting (total) Fe(II) in solution was measured with ICP-MS.

## Kinetic modeling

In the present work and our previous studies,<sup>23</sup> we have used a variety of approaches for kinetic modeling: (i) empirical modeling based on initial dissolution rates<sup>23</sup>, (ii) empirical modeling based on the full time course of dissolution (this work), and (iii) detailed mechanistic modeling (both this and previous work<sup>22</sup>).

The empirical modeling over the full time course of Lp dissolution at pH 7.0 with Fe(II) added 1800 s after 20 or 50  $\mu\text{M}$  DFOB was conducted so that apparent rates constants ( $k_{\text{app}}$ ) for the full time course could be compared with those derived previously for initial dissolution. We applied a pseudo first order model that assumes that the rate of dissolution ( $R_C$ ) is proportional to the free ligand concentration in the solution. In short, the increase in  $[\text{Fe}]_{\text{diss}}$  over time can be expressed in terms of a single adjustable parameter  $k_{C,\text{app}}$  [ $\text{s}^{-1}$ ] and the fixed parameter  $L_T$  (total added  $[\text{L}]$ ) where the reaction rate decreases as  $[\text{Fe}]_{\text{diss}}$  approaches  $L_T$

$$R_C = \frac{d[\text{Fe}]_{\text{diss}}}{dt} = k_{C,\text{app}}(L_T - [\text{Fe}]_{\text{diss}})$$

Note that, for this analysis, the dissolution rate with the ligand in the absence of Fe(II),  $R_L$ , is assumed to be negligible in comparison with  $R_C$ .

For detailed mechanistic kinetic modeling, we used the kinetic program ACUCHEM<sup>37</sup> and MATLAB (MATLAB, The Math Works Inc., Natick, Massachusetts, United States, [www.mathworks.com](http://www.mathworks.com)). The model was used to determine whether the proposed mechanisms (i.e., reactions included in the model) could explain the measured data. The Nelder Mead Simplex Optimization routine in MATLAB was applied to optimize the rate coefficients of rate determining reactions by minimization of the sum of squared differences between measured data points and model output for several experiments simultaneously.

## Results and Discussion

### Dissolution of Lp in a carbonate buffer

Dissolution experiments were conducted with Lp (1125  $\mu\text{M}$ ) at pH 7.0 in a carbonate buffer for comparison with previous studies in MOPS buffer and to compare previously-reported<sup>23</sup> dissolution rates (based on the initial reaction) with rates describing the full course of the dissolution reaction. As seen in Figure 1, addition of either 20 or 50  $\mu\text{M}$  DFOB alone (grey diamonds) resulted in only a very slow increase of dissolved Fe concentrations ( $[\text{Fe}]_{\text{diss}}$ ) over time. In experiments where 1-5  $\mu\text{M}$  Fe(II) was added after DFOB, accelerated dissolution was observed. Note that the time interval between addition of the two reactants, here DFOB first followed by Fe(II), was always 1800 s.

Because of the low solubility of Fe(III) at pH 7, dissolved Fe measured in the Lp suspensions can be assumed to be Fe(III) complexed by DFOB. The extent of Lp dissolution is ultimately limited by the total ligand concentration ( $[\text{L}]_{\text{T}}$ ). With addition of 5  $\mu\text{M}$  Fe(II),  $[\text{Fe}]_{\text{diss}}$  (green squares) increased rapidly indicating accelerated dissolution and reached a plateau within 8000 s at values approaching the total concentration of DFOB (i.e., 20  $\mu\text{M}$  in Fig. 1a and 50  $\mu\text{M}$  in Fig. 1b). At lower added Fe(II) of 1 or 2  $\mu\text{M}$ , Lp dissolution proceeded more slowly (blue circles and orange triangles) and did not reach a plateau within the experimental timeframe.

An empirical kinetic model with a single adjustable parameter  $k_{\text{C},\text{app}}$  [ $\text{s}^{-1}$ ] and the fixed parameter  $L_{\text{T}}$  (see the sub-section Kinetic modeling in the Materials and Methods section) is sufficient to describe the full time course of the dissolution experiments at both DFOB concentrations and all three concentrations of added Fe(II). The fits to this empirical model are shown by the lines in Figure 1. The later time course of the experiments (particularly for 50  $\mu\text{M}$  DFOB) tends to be underestimated by the model. This suggests that, at longer times, some Fe(II) in the system may be lost to oxidation by trace contamination with fugitive oxygen, thus interfering with the catalytic effect of Fe(II).

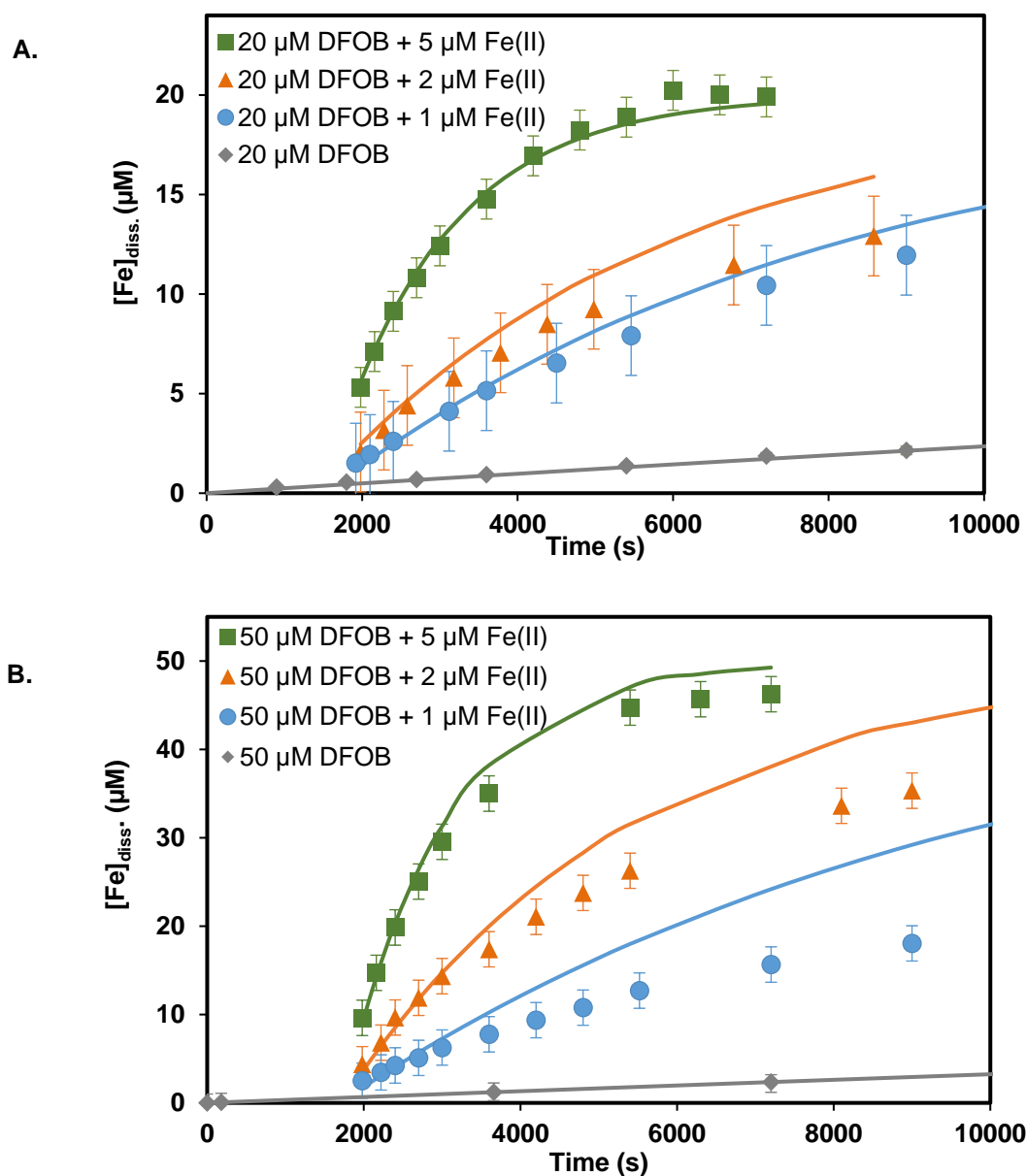


**Figure 1.** Lepidocrocite (Lp) dissolution after addition of Fe(II) to a Lp suspension (1125  $\mu\text{M}$ ) in the presence of (A) 20  $\mu\text{M}$  DFOB and (B) 50  $\mu\text{M}$  DFOB, under anoxic conditions at pH 7 (carbonate-buffered). Error bars correspond to the standard deviations of ICP-MS measurements obtained from repeated calibrations. Fe(II) was added 1800 s after DFOB addition. Solid lines represent empirical model fits.

The extraction of the apparent rate coefficient,  $k_{C,app}$  [ $\text{s}^{-1}$ ], from the data shown in Figure 1 provides the basis to examine the consistency of these data. As shown in Figure 2, the values of  $k_{C,app}$  agree within 95% for 20 and 50  $\mu\text{M}$  DFOB and increase linearly with the added Fe(II) concentrations over the range studied.

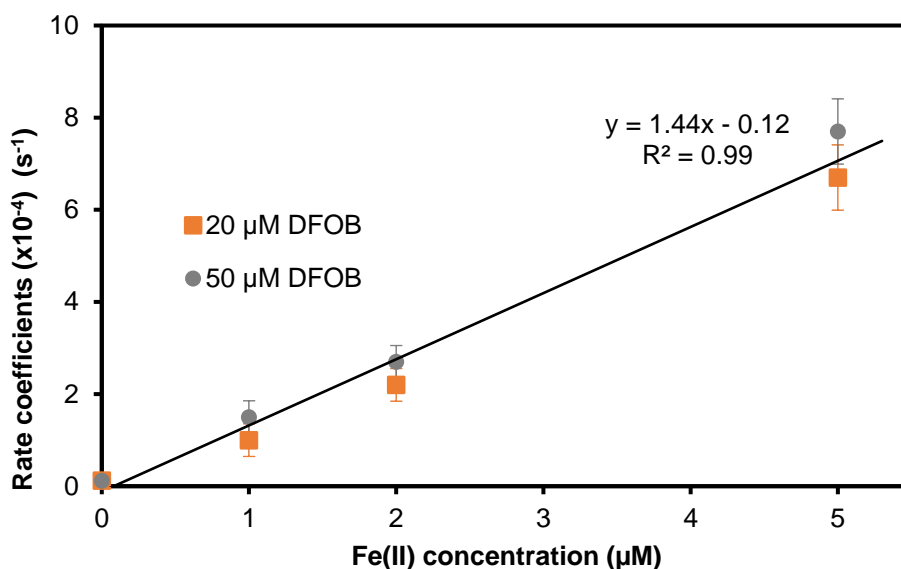


**Figure 2.** Rate coefficients ( $k_{app.}$ ) as a function of added Fe(II) concentrations at pH 7 (carbonate-buffered).  $k_{L,app.}$  (when  $[Fe(II)] = 0 \mu M$ ), and  $k_{C,app.}$  (when  $[Fe(II)] = 1, 2, 5 \mu M$ ) were determined from the fits to the empirical model. Solid lines represent linear fits.

This empirical model also provides a basis for comparison with the observations reported in our previous study conducted in MOPS buffer. In that study, we defined a catalytic effect (CE) as the ratio of  $R_C$  to  $R_L$ , where, in both cases, the reaction was far from completion. (For the definitions of  $R_C$  and  $R_L$ , see the sub-section “Kinetic modelling” in the “Materials and Methods” section.) The comparison of CE values derived from the current study and those reported previously<sup>23</sup> shows that CE is larger in carbonate- than in MOPS -buffered systems (Table S3 and Fig. S1).

### <sup>57</sup>Fe isotope exchange and lepidocrocite (Lp) dissolution

The use of <sup>57</sup>Fe as an isotopic tracer provides additional insight into the process of accelerated Lp dissolution process. Experiments were conducted at pH 6.0 (MES), 7.0 (carbonate and MOPS) and 8.5 (PIPES) with 2 μM <sup>57</sup>Fe(II) and 50 μM DFOB. The order of addition of <sup>57</sup>Fe(II) and DFOB was varied with one reactant added 1800 s before the other. In all cases, rapid increase in the dissolved concentration of <sup>56</sup>Fe ( $[^{56}Fe]^*_{diss.}$ ) corresponding to the natural abundance Fe released from Lp (shown as triangles in Figure 3) was observed only after both Fe(II) and DFOB had been added, without regard to the order of addition. In contrast, the order of addition of Fe(II) and DFOB did have a significant effect on the time course of the dissolved concentrations of tracer <sup>57</sup>Fe ( $[^{57}Fe]_{tracer, diss.}$ ) shown as the open and closed squares in Figure 3.



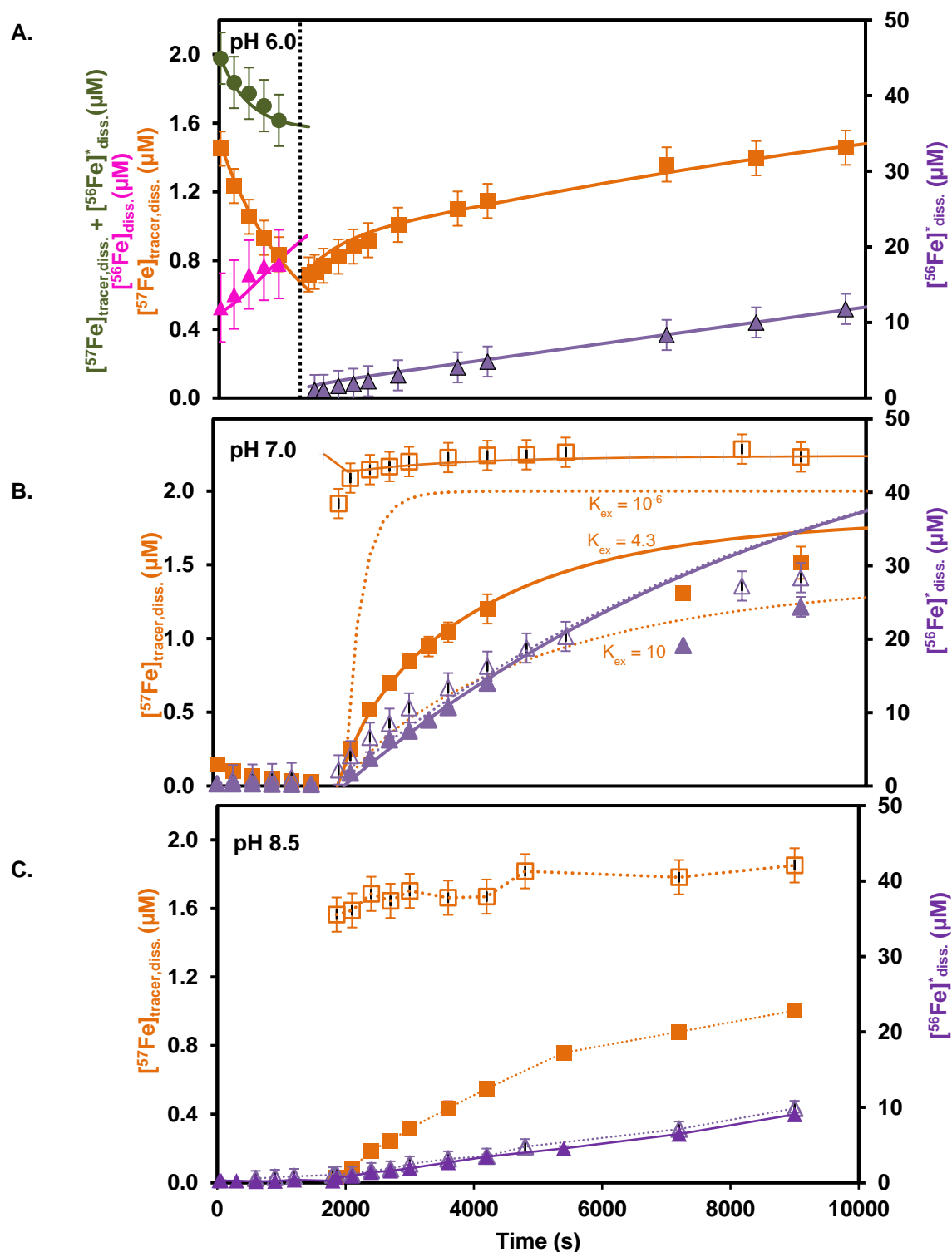


**Figure 3.**  $^{57}\text{Fe}$  isotope exchange and Lp dissolution under anoxic conditions as a function of time at (A) pH 6 (MES), (B) pH 7 (carbonate buffer), and (C) pH 8.5 (PIPES). 2  $\mu\text{M}$   $^{57}\text{Fe}(\text{II})$  was added to a Lp suspension (1125  $\mu\text{M}$ ) 1800 s before (filled symbols; error bars correspond to the ranges of duplicate experiments) or after (empty symbols; error bars as in Fig.1) 50  $\mu\text{M}$  DFOB addition. Symbols: purple triangles (right axis): concentration of Fe released into solution by Lp dissolution ( $^{56}\text{Fe}^*$  diss.); orange squares (left axis): dissolved concentration of tracer  $^{57}\text{Fe}$  corrected for the natural

abundance of  $^{57}\text{Fe}$  in Lp ( $[^{57}\text{Fe}]_{\text{tracer, diss.}}$ ); pink triangles (left axis): concentration of  $^{56}\text{Fe}^*$  in solution resulting from isotopic exchange of  $^{57}\text{Fe}$  with  $^{56}\text{Fe}$  in Lp ( $t < 1800$  s); green circles (left axis): sum of dissolved concentration of Fe measured as  $[^{57}\text{Fe}]_{\text{tracer, diss.}}$  and  $[^{56}\text{Fe}]_{\text{diss.}}^*$  ( $t < 1800$  s).

Lines in Figure 3 A and B represent the kinetic model fits to the measured data (solid lines show model fits to filled symbols, dotted lines to empty symbols). In Figure 3A and 3B, the orange lines show the fit to the  $^{57}\text{Fe}$  data with the optimized equilibrium for exchange between  $(\equiv\text{Fe}^{\text{III}})^{57}\text{Fe}^{\text{II}}$  and  $(\equiv^{57}\text{Fe}^{\text{III}})\text{Fe}^{\text{II}}$  sites ( $K_{\text{ex}} = [(\equiv^{57}\text{Fe}^{\text{III}})\text{Fe}^{\text{II}}] / [(\equiv\text{Fe}^{\text{III}})^{57}\text{Fe}^{\text{II}}] = 4.3\text{--}4.6$  (pH 7) or  $4.2\text{--}4.5$  (pH 6); R6 in the kinetic model). The dashed orange lines show release of  $^{57}\text{Fe}$  that is too fast with no exchange ( $K_{\text{ex}} = 10^{-6}$ ), or too slow with more exchange ( $K_{\text{ex}} = 10$ ).

**$^{57}\text{Fe(II)}$  added first.** When  $^{57}\text{Fe(II)}$  was added first (i.e., before DFOB),  $[^{57}\text{Fe}]_{\text{tracer, diss.}}$  (solid orange squares) decreased over time at pH 6.0 and was nearly or completely undetectable at pH 7.0 and 8.5. At pH 6.0 (Fig. 3A), a concurrent increase in  $[^{56}\text{Fe}]_{\text{diss.}}^*$  (pink filled triangles) was observed. The sum of  $[^{57}\text{Fe}]_{\text{tracer, diss.}}$  and  $[^{56}\text{Fe}]_{\text{diss.}}^*$  (green circles) corresponds to the added  $^{57}\text{Fe(II)}$  concentration ( $2.0\text{ }\mu\text{M}$ ) at  $t=0$  and then decreases (over  $1800$  s) by 20%. This suggests that some of the added  $^{57}\text{Fe(II)}$  is immediately adsorbed to the surface and undergoes isotopic exchange with surface-bound Fe(III) resulting in detectable concentrations of dissolved  $^{56}\text{Fe}$ , which is presumably still in the +II oxidation state. Further adsorption appears to occur more slowly and also to be accompanied by isotopic exchange. These observations agree with our previously reported<sup>22</sup> finding with  $^{57}\text{Fe(II)}$  and Lp and with studies on isotope exchange with Gt<sup>28, 32</sup> and hematite<sup>27, 33</sup>. At pH 7.0 (Fig. 3B) and 8.5 (Fig. 3C),  $[^{56}\text{Fe}]_{\text{diss.}}^*$  was nearly or completely undetectable (i.e., before DFOB addition). This is consistent with the immediate and (nearly) complete loss of tracer  $^{57}\text{Fe(II)}$  from solution at these pH values.

Upon addition of  $50\text{ }\mu\text{M}$  DFOB, accelerated dissolution, shown by increasing  $[^{56}\text{Fe}]_{\text{diss.}}^*$  (filled purple triangles) over time, was observed at all pH values. Lp dissolution was more rapid and proceeded further toward completion at pH 7.0 than at either pH 6.0 or 8.5. In all cases, between 50% (pH 8.5) and 85% (pH 7.0) of the  $^{57}\text{Fe}$  tracer was released back into solution by the end of the experimental time period.

**DFOB added first.** As already discussed for the results shown in Fig. 1, addition of DFOB alone causes only very slow Lp dissolution. Upon addition of  $^{57}\text{Fe(II)}$ , increasing  $[^{56}\text{Fe}]_{\text{diss.}}^*$  (open purple triangles) was observed over time. The overlap of filled and open purple triangles in Figs. 3B

and C indicate that the order of  $^{57}\text{Fe(II)}$  and DFOB addition did not affect the accelerated Lp dissolution process. In contrast, the behavior of the  $^{57}\text{Fe(II)}$  tracer was distinctly different when DFOB was added before rather than after  $^{57}\text{Fe(II)}$ . The open orange squares in Figs. 3B and C show that, at pH 7.0 and 8.5, 75-100% of the added  $^{57}\text{Fe}$  tracer is measured as  $[\text{}^{57}\text{Fe}]_{\text{tracer, diss.}}$  over the entire experimental period. Pre-equilibration of Lp with DFOB inhibits the adsorption of  $^{57}\text{Fe(II)}$  and presumably also the isotopic exchange with surface Fe(III) that was observed in the absence of DFOB. A reasonable fit to the data at pH 6.0 and 7.0 was achieved with the detailed, mechanistic kinetic model (lines in Fig. 3) as described below.

### Kinetic model

In our recent study, we presented a kinetic model for the dissolution of Lp with EDTA at pH 6.0 that was able to describe the entire course of the dissolution.<sup>22</sup> Here, we extended this model to the dissolution of Lp with DFOB and added reactions to describe the observed adsorption and release of  $^{57}\text{Fe}$ . We also tested possible explanations for the delayed release of  $^{57}\text{Fe}$  when  $^{57}\text{Fe(II)}$  was added before the ligand. In particular, the model allows us to estimate the charge delocalization between added  $^{57}\text{Fe(II)}$  and  $^{56}\text{Fe(III)}$  in Lp before and during the dissolution process. Table 1 lists important reactions steps in the kinetic model describing the dissolution of Lp with DFOB and the acceleration by added Fe(II).

When DFOB is added before  $^{57}\text{Fe(II)}$ , it adsorbs reversibly to the surface at Fe(III)-sites (R1) and causes slow, ligand-controlled dissolution (R2). Upon addition of  $^{57}\text{Fe(II)}$ , dissolved  $^{57}\text{Fe(II)DFOB}$  is formed quickly (R3). Adsorption of  $^{57}\text{Fe(II)DFOB}$ , ET, and detachment of  $^{57}\text{Fe(III)DFOB}$  are aggregated in reaction R4. We assume that upon adsorption, negative charge is transferred to Lp, due to strongly reducing properties of Fe(II) complexed to DFOB, but we cannot resolve the individual reaction steps experimentally. After detachment from the surface,  $^{57}\text{Fe(III)DFOB}$  does not undergo further reactions.

When  $^{57}\text{Fe(II)}$  is added first, it is reversibly adsorbed (R5) and charge transfer to Fe(III) can occur at the surface (R6). In the absence of DFOB, adsorption, charge transfer and desorption (R5-R7) can explain the isotope exchange between  $^{57}\text{Fe(II)}$  and Fe(II), which was observable in solution at pH 6.0. It was not measurable at pH 7.0 because dissolved equilibrium concentrations are too low. Note

that we assumed that charge transfer at the surface is fast and that equilibration of charge between Fe- and  $^{57}\text{Fe}$ -surface is reached quickly, while adsorption and desorption reactions are slower.

Table.1. Kinetic model with list of reactions and equilibrium constants (K) and rate coefficients (k).

Nr.	Reaction <sup>(a)</sup>			Description	K/ k <sup>(b)</sup> pH 7	K/ k <sup>(b)</sup> pH 6
R1	$\equiv\text{Fe}^{\text{III}} + \text{L}$	$\rightleftharpoons$	$\equiv\text{Fe}^{\text{III}}\text{L}$	Adsorption of ligand (L) on surface $\text{Fe}^{\text{III}}$	$3.0e5$ <sup>(c)</sup>	$3.0e4$ - $3.0e5$ <sup>(c)</sup>
R2	$\equiv\text{Fe}^{\text{III}}\text{L}$	$\rightarrow$	$\equiv\text{Fe}^{\text{III}} + \text{Fe}^{\text{III}}\text{L}$	Non-catalyzed dissolution	$3.5e-5$	n.d. <sup>(d)</sup>
R3	$^{57}\text{Fe}^{\text{II}} + \text{L}$	$\rightleftharpoons$	$^{57}\text{Fe}^{\text{II}}\text{L}$	Dissolved $^{57}\text{Fe}^{\text{II}}\text{L}$ complex formation	$3.79e2$ <sup>(e)</sup>	$5.26e4$ <sup>(e)</sup>
R4	$\equiv\text{Fe}^{\text{III}} + ^{57}\text{Fe}^{\text{II}}\text{L}$	$\rightarrow$	$\equiv\text{Fe}^{\text{II}} + ^{57}\text{Fe}^{\text{III}}\text{L}$	ET from $^{57}\text{Fe}^{\text{II}}\text{L}$ to surface $\text{Fe}^{\text{III}}$ and detachment of $^{57}\text{Fe}^{\text{III}}\text{L}$	$5.2e3$	200-600
R5	$\equiv\text{Fe}^{\text{III}} + ^{57}\text{Fe}^{\text{II}}$	$\rightleftharpoons$	$\equiv\text{Fe}^{\text{III}}\text{-O-}^{57}\text{Fe}^{\text{II}}$	Adsorption and desorption of $^{57}\text{Fe}^{\text{II}}$ on surface $\text{Fe}^{\text{III}}$	$7.2e6$	$6.3e4$
R6	$\equiv\text{Fe}^{\text{III}}\text{-O-}^{57}\text{Fe}^{\text{II}}$	$\rightleftharpoons$	$\equiv^{57}\text{Fe}^{\text{III}}\text{-O-Fe}^{\text{II}}$	ET between $^{57}\text{Fe}$ and $^{56}\text{Fe}$ on the surface ( $K_{\text{ex}}$ ).	$4.3$ - $4.6$ <sup>(f)</sup>	$4.2$ - $4.5$ <sup>(f)</sup>
R7	$\equiv^{57}\text{Fe}^{\text{III}} + \text{Fe}^{\text{II}}$	$\rightleftharpoons$	$\equiv^{57}\text{Fe}^{\text{III}}\text{-O-Fe}^{\text{II}}$	Adsorption and desorption of $\text{Fe}^{\text{II}}$ on surface $^{57}\text{Fe}^{\text{III}}$	$7.2e6$	$6.3e4$
R8	$\equiv\text{Fe}^{\text{III}}\text{-O-}^{57}\text{Fe}^{\text{II}} + \text{L}$	$\rightarrow$	$\equiv\text{Fe}^{\text{II}} + ^{57}\text{Fe}^{\text{III}}\text{L}$	Adsorption of L on adsorbed $^{57}\text{Fe}^{\text{II}}$ , ET and detachment	81	<5
R9	$\equiv^{57}\text{Fe}^{\text{III}}\text{-O-Fe}^{\text{II}} + \text{L}$	$\rightarrow$	$\equiv^{57}\text{Fe}^{\text{II}} + \text{Fe}^{\text{III}}\text{L}$	Adsorption of L on adsorbed $\text{Fe}^{\text{II}}$ , ET and detachment	81	<5
R10 <sup>(g)</sup>	$\equiv\text{Fe}^{\text{II}} + \text{Bulk}$	$\rightarrow$	$\equiv\text{Fe}^{\text{III}}\text{-O-Fe}^{\text{II}}$	Re-formation of surface site with adsorbed $\text{Fe}^{\text{II}}$	$1e10$	$1e10$
R11 <sup>(g)</sup>	$\equiv^{57}\text{Fe}^{\text{II}} + \text{Bulk}$	$\rightarrow$	$\equiv\text{Fe}^{\text{III}}\text{-O-}^{57}\text{Fe}^{\text{II}}$	Re-formation of surface site with adsorbed $^{57}\text{Fe}^{\text{II}}$	$1e10$	$1e10$

<sup>(a)</sup> In the surface complexation reactions, the type of surface complex (e.g. monodentate and/or bidentate) is not specified. Surface hydroxyl groups are thus omitted and reactions are not balanced for  $\text{OH}^-$ ,  $\text{H}^+$  and  $\text{H}_2\text{O}$ . For example in R1,  $\equiv\text{Fe}^{\text{III}} + \text{L} \rightarrow \equiv\text{Fe}^{\text{III}}\text{L}$  represents the sum of surface complexation reactions, such as  $\equiv\text{Fe}^{\text{III}}\text{OH} + \text{HL} \rightarrow \equiv\text{Fe}^{\text{III}}\text{L} + \text{H}_2\text{O}$  and  $\equiv\text{Fe}^{\text{III}}(\text{OH})_2 + \text{H}_2\text{L} \rightarrow \equiv\text{Fe}^{\text{III}}\text{L} + 2\text{H}_2\text{O}$ . Bonds between Fe-ion that might consist of several ( $\mu$ -oxo) and ( $\mu$ -hydroxo) bonds are represented in simplified form as Fe-O-Fe.

$^{56}\text{Fe}$  is abbreviated as Fe. All reactions with Fe and  $^{57}\text{Fe}$  isotopes in solution and on the surface include the additional of the four possible permutations. For example in R4:  $(\equiv\text{Fe}^{\text{III}}) + ^{57}\text{Fe}^{\text{II}}\text{L} \rightarrow (\equiv\text{Fe}^{\text{II}}) + ^{57}\text{Fe}^{\text{III}}\text{L}$  also R4b:  $(\equiv\text{Fe}^{\text{III}}) + \text{Fe}^{\text{II}}\text{L} \rightarrow (\equiv\text{Fe}^{\text{II}}) + \text{Fe}^{\text{III}}\text{L}$ , R4c:  $(\equiv^{57}\text{Fe}^{\text{III}}) + \text{Fe}^{\text{II}}\text{L} \rightarrow (\equiv^{57}\text{Fe}^{\text{II}}) + \text{Fe}^{\text{III}}\text{L}$ , and R4d:  $(\equiv^{57}\text{Fe}^{\text{III}}) + ^{57}\text{Fe}^{\text{II}}\text{L} \rightarrow (\equiv^{57}\text{Fe}^{\text{II}}) + ^{57}\text{Fe}^{\text{III}}\text{L}$ . The full list of reactions is provided in Table S4.

<sup>(b)</sup> K and k are fitted equilibrium constants and rate coefficients (units in mol/L and s). Numbers in normal font are fitted values; numbers in slanted font are values from previous work, from the literature, or are non-rate determining rate coefficients. More explanations are provided in the SI.

<sup>(c)</sup> Values from Borer et al. 2009; <sup>(d)</sup> Fitted value for pH 7.0, not determined for pH 6.0. (Not critical for model fits at pH 6.0); <sup>(e)</sup> Calculated with DFOB complex formation constants reported by Kim et al., 2010.<sup>39</sup> See SI for more information.

<sup>(f)</sup>  $K_{\text{ex}}$  is the “equilibrium” constant quantifying the equilibration of negative charge between  $^{57}\text{Fe}$  and  $^{56}\text{Fe}$  of  $^{57}\text{Fe}$  adsorbed on the surface. Note that this equation does not imply a thermodynamic preference, but a factor for the probability of charge residing on  $^{56}\text{Fe}$  and  $^{57}\text{Fe}$  in a system of connected sites.  $(\equiv^{57}\text{Fe}^{\text{III}})\text{Fe}^{\text{II}}$  and  $(\equiv\text{Fe}^{\text{III}})^{57}\text{Fe}^{\text{II}}$  do not have to be neighboring sites, only rapid charge transfer between the sites has to be possible.

<sup>(g)</sup> In the model, bulk-Lp contains only  $^{56}\text{Fe}$  (again, abbreviated as Fe) (reactions R10 and R11). This is in agreement with the experimental results, in which the measured  $^{56}\text{Fe}$  concentrations are scaled to represent the concentrations of the sum of Fe-isotopes in Lp.

Ligand that is added after Fe(II) or is present in excess over added Fe(II) (which was always the case in our experiments) can react with surface-bound Fe(II). Ligand adsorption to surface-bound Fe(II), charge transfer, and detachment are summarized in reactions R8 and R9. We again assumed that charge transfer is rapid (due to strongly reducing properties of Fe(II) complexed to DFOB). Once formed, the adsorbed Fe(III)L detaches more quickly than in reaction R2, due to weaker Fe(II)-O-Fe(III) bonds to neighboring atoms compared to Fe(III)-O-Fe(III) bonds. The larger rate coefficients associated with reactions R7 and R8 compared to dissolution in the absence of Fe(II) (R3) account for the Fe(II)-catalyzed accelerated dissolution. Reactions R6 and R8-R9 explain the release of  $^{57}\text{FeL}$  and FeL and their ratios over the course of the dissolution. Finally, reactions R10 and R11 describe rapid formation of new surface sites.

As explained in Table 1 (see footnotes), some equilibrium constants and rate coefficients were fixed (*italic font*) and others optimized (*normal font*). Modelling was performed to determine whether the suggested reactions steps could fit the measured data. Values for these parameters could not be uniquely determined because of correlations among them. For example, the values for the adsorption equilibrium constants in R1, R3 and R5 cannot be determined independently from the values of the rate coefficients for dissolution in R2, R4, R8 and R9. However, equilibrium constants obtained in previous work can be used to constrain fitted values of rate coefficients. We are most confident regarding the value of the equilibrium constant  $K_{\text{ex}}$  for the exchange of charge in reaction R6. Without appreciable charge migration ( $K_{\text{ex}} = 10^{-6}$ ), the model predicts a very quick release of  $^{57}\text{Fe}$  after addition of the ligand (dashed orange line in Figure 3B), in disagreement with the data. With the optimized value ( $K_{\text{ex}} = 4.3$ ) we obtain a good fit to the data (solid orange line), while a larger value ( $K_{\text{ex}} = 10$ ) leads to a much slower release of  $^{57}\text{Fe}$  than experimentally observed (dashed orange line).

The validity of the assigned values for  $K_{\text{ex}}$  is also illustrated by the plot of  $[^{57}\text{Fe}]_{\text{tracer, diss}}$  as a function of  $[^{56}\text{Fe}]_{\text{diss}}^*$  (Fig. 4). The data for pH 7.0 and 8.5 (for both 20 and 50  $\mu\text{M}$  DFOB and for both carbonate and MOPS buffers) collapse onto a single curve. The offset of the curve for pH 6.0 corresponds to the presence of some dissolved Fe(II) at the time of DFOB addition. At the start of the dissolution, the ratio of  $^{57}\text{Fe}/^{56}\text{Fe}$  (i.e., the slope of the line for pH 7.0) is 0.23, which means that the release of  $^{56}\text{Fe}$  is 4.3-fold greater than that of  $^{57}\text{Fe}$  independent of DFOB concentration (or pH). During dissolution, the ratio of  $^{57}\text{Fe}/^{56}\text{Fe}$  in solution continually decreases because less and less  $^{57}\text{Fe}$  is present at the surface, as new surface sites are formed from bulk  $^{56}\text{Fe}$  (R11).

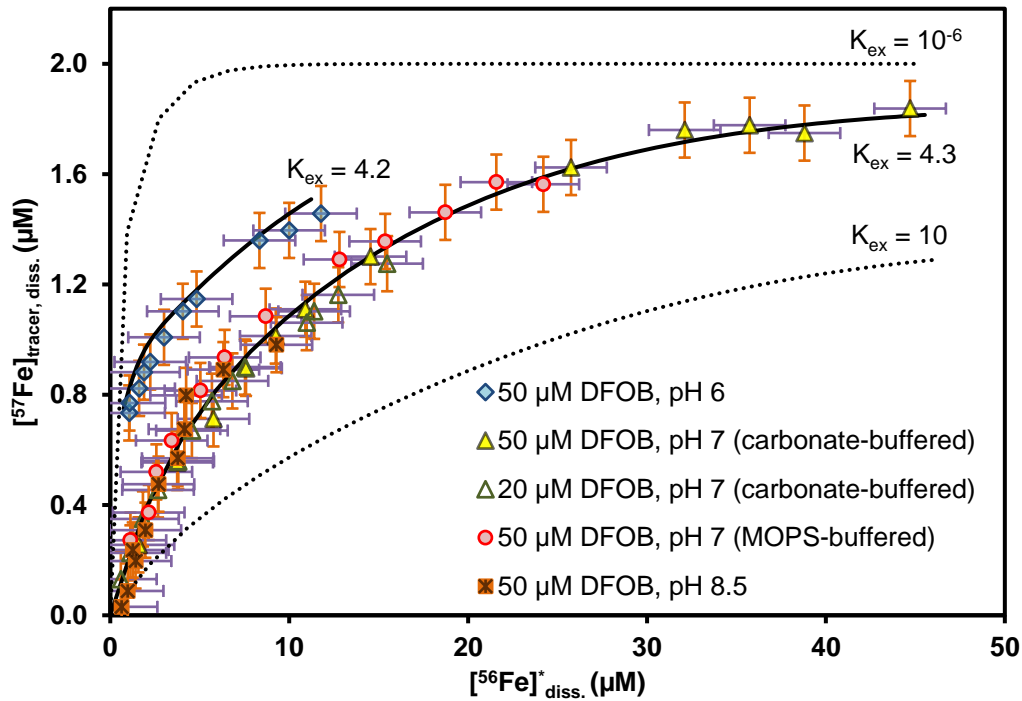


**Figure 4.** Release of tracer  $^{57}\text{Fe}$  in solution as a function of dissolved  $^{56}\text{Fe}^*$  (Fe released from Lp) during accelerated Lp dissolution ( $t > 1800$  s).  $2 \mu\text{M}$   $^{57}\text{Fe}(\text{II})$  was added 1800 s before DFOB addition under anoxic conditions. Most data were already shown in Figure 3 except data for 50  $\mu\text{M}$  DFOB in MOPS system and 20  $\mu\text{M}$  DFOB in carbonate system. The data with time course are shown in SI, Figure S2. The tracer  $^{57}\text{Fe}$  corrected for the natural abundance of  $^{57}\text{Fe}$  in Lp. The thick black line shows the fit to the  $^{57}\text{Fe}$  data at pH 6.0 and 7.0 with the optimized equilibrium for exchange between  $(\equiv\text{Fe}^{\text{III}})^{57}\text{Fe}^{\text{II}}$  and  $(\equiv^{57}\text{Fe}^{\text{III}})\text{Fe}^{\text{II}}$  sites ( $K_{\text{ex}} = [(\equiv^{57}\text{Fe}^{\text{III}})\text{Fe}^{\text{II}}] / [(\equiv\text{Fe}^{\text{III}})^{57}\text{Fe}^{\text{II}}] = 4.3\text{--}4.6$  (pH 7) or  $4.2\text{--}4.5$  (pH 6); R6 in the kinetic model). The thin lines show release of  $^{57}\text{Fe}$  that is too fast with no exchange ( $K_{\text{ex}} = 10^{-6}$ ), or too slow with more exchange ( $K_{\text{ex}} = 10$ ).

Our combined data thus shows that adsorption of Fe(II) to Lp leads to exchange of charge on the surface before and during dissolution, largely independent of pH and ligand concentrations. As the model fits (solid lines in Figure 3A and 3B) show, the model is able to explain our observed dissolution rates in the absence and presence of Fe, and the isotope exchange and release of  $^{57}\text{Fe}$  and  $^{56}\text{Fe}$  during dissolution.

### **$^{57}\text{Fe}$ isotope exchange and goethite (Gt) dissolution.**

Several previous studies<sup>28, 32, 40</sup> reported  $^{57}\text{Fe(II)}$  isotope exchange with Gt in the absence of ligand over time scales of days to months, leading to ET and isotope exchange between aqueous  $^{57}\text{Fe(II)}$  and solid  $^{56}\text{Fe}$ . Here we examine isotope exchange only on shorter time scales of minutes to hours. When  $^{57}\text{Fe(II)}$  was added before DFOB,  $[\text{}^{57}\text{Fe}]_{\text{tracer, diss.}}$  (solid orange squares) decreased over time at pH 7.0 as shown in Figure 5. Since adsorption was almost complete within 1800 s,  $[\text{}^{57}\text{Fe}]_{\text{tracer, diss.}}$  and possible formation of  $[\text{}^{56}\text{Fe}]_{\text{diss.}}^*$  could not be detected.

Addition of 50  $\mu\text{M}$  DFOB led to accelerated dissolution, shown by increasing  $[\text{}^{56}\text{Fe}]_{\text{diss.}}^*$  (filled purple triangles) and total dissolved Fe (green filled circles). Notably,  $[\text{}^{57}\text{Fe}]_{\text{tracer, diss.}}$  increased at a similar rate as  $[\text{}^{56}\text{Fe}]_{\text{diss.}}^*$ , in contrast to Lp where  $[\text{}^{56}\text{Fe}]_{\text{diss.}}^*$  increased by a factor of around 4 faster than  $[\text{}^{57}\text{Fe}]_{\text{tracer, diss.}}$ . This indicates that within our experimental time scale, the extent of isotope exchange was much more limited in Gt as compared to Lp. As also reported in our previous work<sup>23</sup>, dissolution of Gt is slower than that of Lp at pH 7.0, at a rate which is in good agreement with our previously reported rate. Figure S3 shows the data from this study together with those from our previous work. We did not attempt to apply our kinetic model to Gt, because the dissolution was slow and there was not sufficient data on the progress of dissolution.

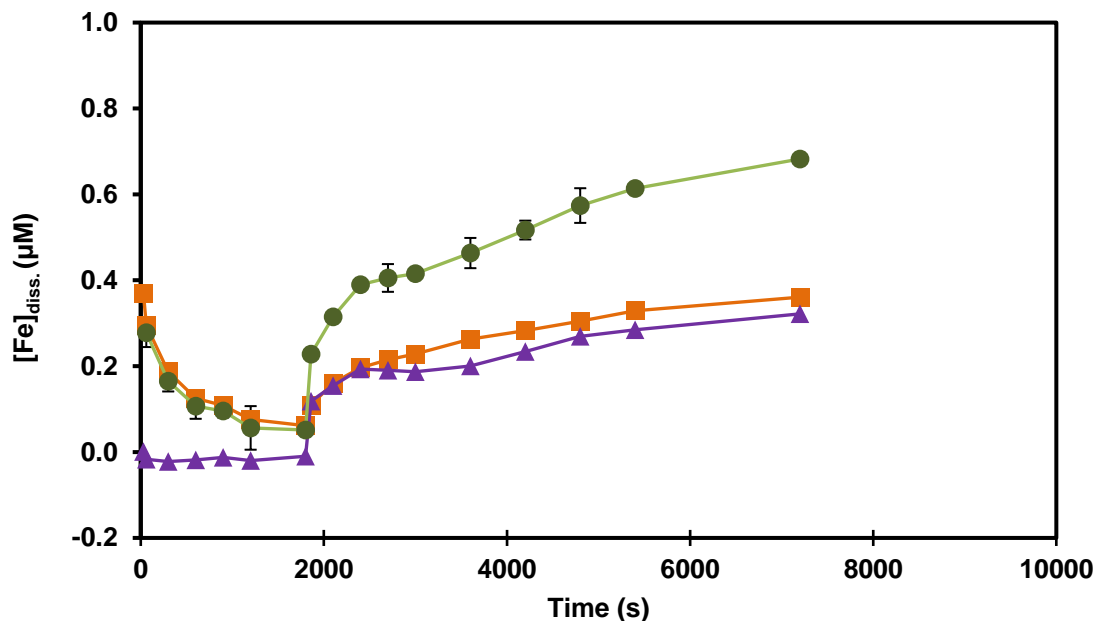


**Figure 5.**  $^{57}\text{Fe}$  isotope exchange and goethite dissolution at pH 7 (carbonate-buffered) under anoxic conditions.  $2\ \mu\text{M}$   $^{57}\text{Fe}(\text{II})$  was added to a goethite suspension ( $1125\ \mu\text{M}$ ) 1800 s before  $50\ \mu\text{M}$  DFOB addition. Error bars correspond to the range of duplicate measurements. Data points under negative values represent measurements which were below the detection limit. Lines serve as visual-guides. Symbols: purple triangles (right axis): concentration of Fe released into solution by goethite dissolution ( $[\text{Fe}]_{\text{diss.}}^*$ ); orange squares (left axis): dissolved concentration of tracer  $^{57}\text{Fe}$  corrected for the natural abundance of  $^{57}\text{Fe}$  in goethite ( $[\text{Fe}]_{\text{tracer, diss.}}$ ); green circles (left axis): sum of dissolved concentration of Fe measured as  $[\text{Fe}]_{\text{tracer, diss.}}$  and  $[\text{Fe}]_{\text{diss.}}^*$  representing the total dissolved Fe concentration.

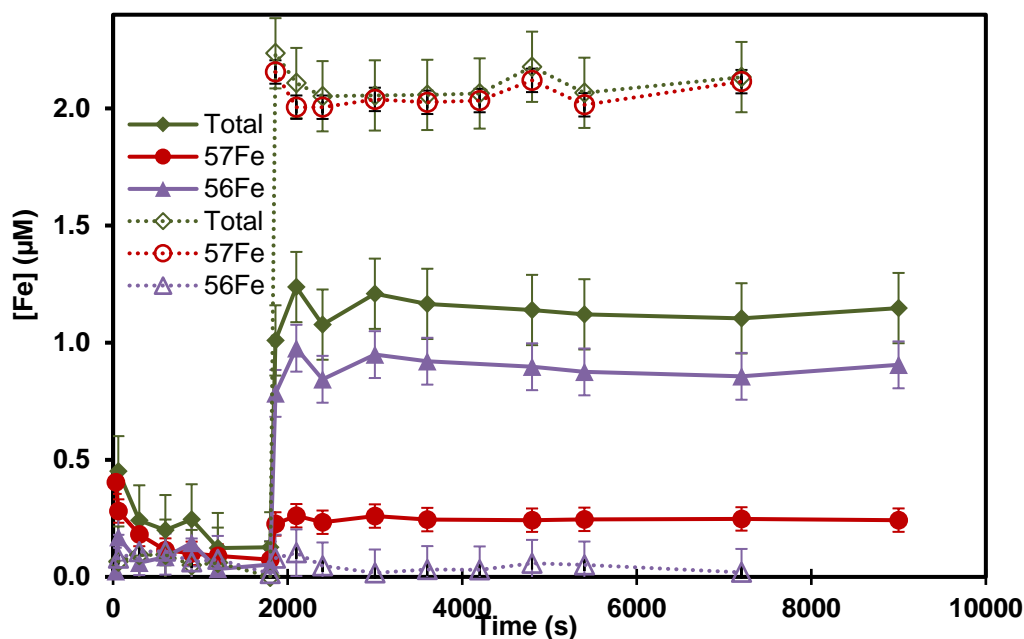
### $^{57}\text{Fe}$ isotope exchange without dissolution

Phenanthroline was added after adsorption of  $^{57}\text{Fe}(\text{II})$  in order to desorb Fe(II) and to allow analysis of its isotopic composition. Control experiments were performed with phenanthroline added before  $^{57}\text{Fe}(\text{II})$ .

**Lepidocrocite.** As shown in Figure 6A,  $^{57}\text{Fe}(\text{II})$  added before phenanthroline was almost completely adsorbed within 1800s, consistent with the data shown in Figure 3B. Upon addition of  $100\ \mu\text{M}$  phenanthroline,  $1.15\ \mu\text{M}$  total Fe(II), of which 22% was  $^{57}\text{Fe}(\text{II})$  and 78% was  $^{56}\text{Fe}(\text{II})$ , was desorbed. Although only 60% of the added Fe(II) was desorbed, the ratio of  $[\text{Fe}(\text{II})]_{\text{diss.}}^* / [\text{Fe}]_{\text{tracer, diss.}}$  of 3.6 indicates that extensive charge transfer occurred and the ratio is comparable to the ratio of around 4.3 at the start of accelerated Lp dissolution with DFOB. In a control experiment with  $^{57}\text{Fe}(\text{II})$  added after phenanthroline, all added  $^{57}\text{Fe}$  (open circles) remained in solution.



## A. Lepidocrocite



## B. Goethite

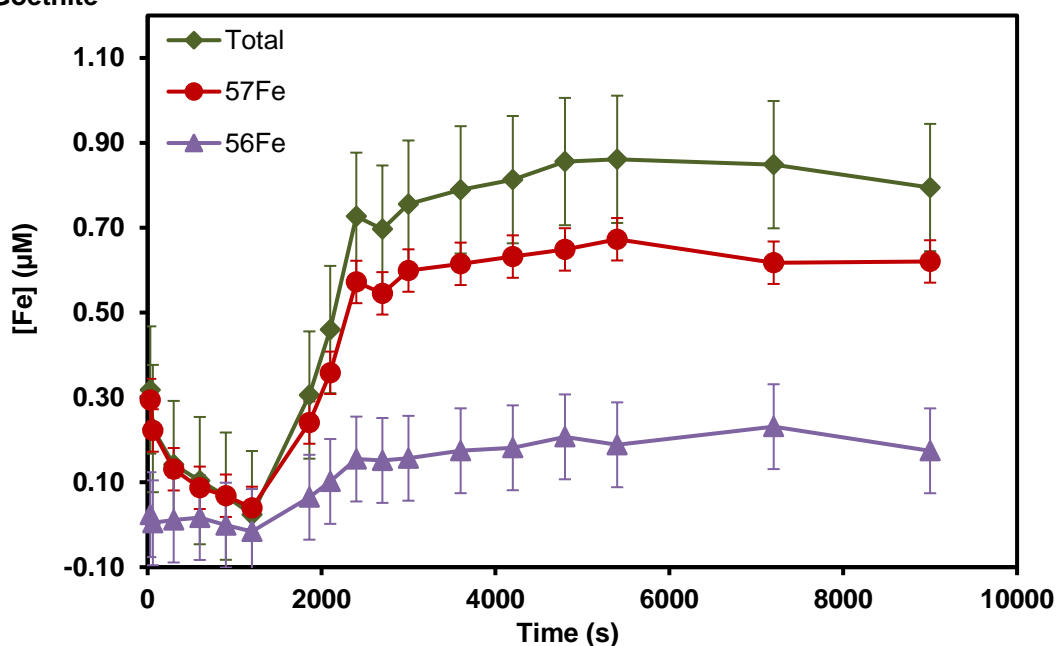


**Figure 6.** Adsorption and desorption of  $^{57}\text{Fe}$  (tracer) and  $^{56}\text{Fe}^*$  on (A) lepidocrocite and (B) goethite at pH 7 (carbonate-buffered) under anoxic conditions.  $2\text{ }\mu\text{M}$   $^{57}\text{Fe}(\text{II})$  was added to (A) lepidocrocite or (B) goethite suspension ( $1125\text{ }\mu\text{M}$ ) 1800 s before (filled symbols) or after (empty symbols)  $100\text{ }\mu\text{M}$  phenanthroline addition. Data points under negative values represent measurements which were below the detection limit. Error bars correspond to the range of duplicate measurements. Lines are to guide eyes through the data points. When phenanthroline was added after  $^{57}\text{Fe}(\text{II})$  addition ( $t > 1800\text{ s}$ ), most of  $^{56}\text{Fe}^*$  released back to solution for Lp. Conversely, most of tracer  $^{57}\text{Fe}$  released back into solution for goethite. In both the cases, only half of the (added) Fe released back to solution.

**Goethite.** Very different results were obtained with Gt, as shown in Figure 6B.  $^{57}\text{Fe(II)}$  added before phenanthroline was again almost completely adsorbed, with no detectable release of  $^{56}\text{Fe}$ . Addition of phenanthroline lead to release of adsorbed Fe(II), although more slowly than with Lp. In contrast to Lp, much more  $^{57}\text{Fe(II)}$  than  $^{56}\text{Fe}$  was released. From 4000-9000 s, 0.85  $\mu\text{M}$  total Fe(II), of which 76% was  $^{57}\text{Fe(II)}$  and 24% was  $^{56}\text{Fe(II)}$ , was desorbed. The ratio of  $[\text{}^{56}\text{Fe(II)}]_{\text{diss}}^* / [\text{}^{57}\text{Fe}]_{\text{tracer, diss}}$  was 0.31, in contrast to the ratio in Lp of 3.6. These contrasting results show that much less charge transfer from added  $^{57}\text{Fe}$  to  $^{56}\text{Fe}$  in the solid must have occurred with Gt than with Lp.

### Possible Mechanism for Lp dissolution and Pathways for $^{57}\text{Fe}$ Isotope Exchange

**DFOB added first.** In the presence of the ligand, interaction of dissolved  $^{57}\text{Fe(II)}$ DFOB with the surface leads fast transfer of charge to surface Fe(III) and formation of dissolved  $^{57}\text{Fe(III)}$ DFOB. This proposed mechanism is supported by the observation that virtually all the  $^{57}\text{Fe}$  added after DFOB remains in solution. Excess dissolved ligand can then complex surface-bound Fe(II), causing fast ET to a neighboring Fe(III) and subsequent detachment of Fe(III)DFOB. The ET and detachment steps can then repeat until all the free DFOB is consumed.

**$^{57}\text{Fe(II)}$  added first.** Adsorption of  $^{57}\text{Fe(II)}$  is most likely to occur at a terrace edge. Charge can be transferred along the surface layer and possibly also into the bulk solid. Addition of DFOB again leads to complexation of Fe(II) at the surface, fast transfer of charge to neighboring Fe(III) sites, and detachment of Fe(III)DFOB. The ratio of  $[\text{}^{57}\text{Fe}]_{\text{tracer, diss}}$  to  $[\text{}^{56}\text{Fe}]_{\text{diss}}^*$  corresponds to the fraction of the charge that resides on  $^{56}\text{Fe}$  and  $^{57}\text{Fe}$  at the Lp surface. The model fits indicate that  $^{56}\text{Fe(II)}$  is 4.3 times more abundant than  $^{57}\text{Fe(II)}$  at the surface.

Assuming equal probabilities for charge distribution over available surface sites, this would mean that each unit of negative charge is in average distributed over 5.3 Fe-sites. In our previous study, we assumed a surface site concentration of 17.5  $\mu\text{M}$  (calculated for 100 mg Lp/L and 1.67 active site per  $\text{nm}^2$ ). With 2  $\mu\text{M}$  of added Fe(II) and charge distribution over 5.3 sites per added Fe(II), the charge would be distributed over 10.6  $\mu\text{M}$  surface sites and thus over most of the surface. The release of  $^{57}\text{Fe}$  at pH 7 with DFOB occurred more slowly than at pH 6.0 in our recent study with EDTA, indicating that charge distribution at pH 7.0 before and during dissolution was more extensive. This can be rationalized by the nearly complete adsorption of Fe(II) at pH 7.0, compared to only

around 20% adsorption at pH 6.0. Even after dissolution of 38  $\mu\text{m}$  Fe(III), which is over two times the concentration of surface sites, we observed the reappearance of only 85-90% of added  $^{57}\text{Fe}$  in solution. The model accounts for this by “dilution” of  $^{57}\text{Fe}$  sites through the regeneration of surface sites from the bulk solid.

It is also possible that some of the charge migrates into the solid and is thus unlikely to be released by dissolution. A few studies<sup>39-42</sup> have shown that induced negative charge might “heal” defect sites in structurally defective crystal surfaces such that adsorbed  $^{57}\text{Fe}$  is incorporated into more stable surface sites or into the bulk, from which it is released more slowly.

## Environmental Significance

We found that, in anoxic, carbonate-buffered suspensions at pH 7.0, micromolar concentrations of added Fe(II) can accelerate the rates of Lp dissolution with DFOB up to a factor of 80. The catalytic effect observed at pH 7.0 in carbonate- buffered suspensions was larger than our recently reported effects in MOPS-buffered system. Since aquatic systems are generally carbonate buffered, it is likely that the acceleration of ligand-controlled dissolution by traces of Fe(II) in natural waters would be at least as large as observed in laboratory experiments with MOPS and other Good’s buffers. Our results are most relevant for soils and surface waters with pH values around 7. Recent analytical developments have demonstrated that strong organic ligands found in the ocean contain compounds with structures similar to DFOB.<sup>41</sup> Thus the mechanisms identified for DFOB may also be important for ligands secreted by marine biota.

The interfacial Fe(II)/Fe(III) ET plays a crucial role in numerous natural processes, for example, in Fe cycling and bioavailability, (trace) metal incorporation and release. We show that ET and isotope exchange during sorption and accelerated dissolution are very different for Lp and Gt, presumably reflecting the difference in structure and mineralogy. We suggest that future studies are extended to different Fe(III)(oxyhydr)oxide phases. Fe(III) phases formed under natural conditions are often less crystalline and contain co-precipitated cations and anions.<sup>42</sup> Future work should test if these phases are also susceptible to Fe(II)-accelerated dissolution. The application of  $^{57}\text{Fe}$  isotope tracer and dissolution experiments can provide relevant information about the mobility and effect of negative

charge in Fe(III)phases and there dissolution behavior in the presence of ligands and low concentrations of Fe(II).

## Acknowledgements

We gratefully acknowledge Thomas Rüttimann (Eawag) for ICP-MS analyses and for technical assistance. This project was financially supported by the Swiss National Science Foundation under contracts Nos. 200021L\_150150 “Synergistic effects of redox processes and ligand controlled dissolution of iron(hydr)oxide phases” Mathematics, Natural sciences and Engineering (Division II). S.M.K., W.D.C.S., and K.K. were supported by the Austrian Science Fund (FWF, Grant No.: I 1528-N19).

## References

1. Watteau, F.; Berthelin, J., Microbial Dissolution of Iron and Aluminum from Soil Minerals - Efficiency and Specificity of Hydroxamate Siderophores Compared to Aliphatic-Acids. *European Journal of Soil Biology* **1994**, 30, (1), 1-9.
2. Hersman, L.; Maurice, P.; Sposito, G., Iron acquisition from hydrous Fe(III)-oxides by an aerobic *Pseudomonas* sp. *Chemical Geology* **1996**, 132, (1-4), 25-31.
3. Kraemer, S. M.; Hering, J. G., Influence of solution saturation state on the kinetics of ligand-controlled dissolution of oxide phases. *Geochimica et Cosmochimica Acta* **1997**, 61, (14), 2855-2866.
4. Neubauer, U.; Furrer, G.; Schulin, R., Heavy metal sorption on soil minerals affected by the siderophore desferrioxamine B: the role of Fe(III) (hydr)oxides and dissolved Fe(III). *European Journal of Soil Science* **2002**, 53, (1), 45-55.
5. Cervini-Silva, J.; Sposito, G., Adsorption of desferrioxamine-B and oxalate on Al-goethite: Implications for microbial dissolution processes. *Geochimica et Cosmochimica Acta* **2002**, 66, (15a), A127-A127.
6. Kearns, J. P.; Cervini-Silva, J.; Banfield, J. F., Siderophores may simultaneously influence iron and phosphorus bioavailability in soils. *Geochimica et Cosmochimica Acta* **2004**, 68, (11), A395-A395.
7. Kraemer, S. M., Iron oxide dissolution and solubility in the presence of siderophores. *Aquatic Sciences* **2004**, 66, (1), 3-18.
8. Kraemer, S. M.; Butler, A.; Borer, P.; Cervini-Silva, J., Siderophores and the dissolution of iron-bearing minerals in marine systems. In *Reviews in Mineralogy and Geochemistry*, 2005; Vol. 59, pp 53-84.
9. Kraemer, S. M.; Crowley, D. E.; Kretzschmar, R., Geochemical aspects of phytosiderophore-promoted iron acquisition by plants. *Advances in Agronomy, Vol 91* **2006**, 91, 1-46.

10. Zhong, L.; Yang, J.; Liu, L.; Li, X., Desferrioxamine-B promoted dissolution of an Oxisol and the effect of low-molecular-weight organic acids. *Biology and Fertility of Soils* **2013**, *49*, (8), 1077-1083.
11. Colombo, C.; Palumbo, G.; He, J. Z.; Pinton, R.; Cesco, S., Review on iron availability in soil: Interaction of Fe minerals, plants, and microbes. *Journal of Soils and Sediments* **2014**, *14*, (3), 538-548.
12. Akafia, M. M.; Harrington, J. M.; Bargar, J. R.; Duckworth, O. W., Metal oxyhydroxide dissolution as promoted by structurally diverse siderophores and oxalate. *Geochimica et Cosmochimica Acta* **2014**, *141*, 258-269.
13. Cheah, S. F.; Kraemer, S. M.; Cervini-Silva, J.; Sposito, G., Steady-state dissolution kinetics of goethite in the presence of desferrioxamine B and oxalate ligands: Implications for the microbial acquisition of iron. *Chemical Geology* **2003**, *198*, (1-2), 63-75.
14. Dehner, C. A.; Awaya, J. D.; Maurice, P. A.; DuBois, J. L., Roles of Siderophores, Oxalate, and Ascorbate in Mobilization of Iron from Hematite by the Aerobic Bacterium *Pseudomonas mendocina*. *Applied and Environmental Microbiology* **2010**, *76*, (7), 2041-2048.
15. Lemanceau, P.; Bauer, P.; Kraemer, S.; Briat, J. F., Iron dynamics in the rhizosphere as a case study for analyzing interactions between soils, plants and microbes. *Plant and Soil* **2009**, *321*, (1-2), 513-535.
16. Loring, J. S.; Simanova, A. A.; Persson, P., Highly mobile iron pool from a dissolution-readsorption process. *Langmuir* **2008**, *24*, (14), 7054-7057.
17. Reichard, P. U.; Kretzschmar, R.; Kraemer, S. M., Dissolution mechanisms of goethite in the presence of siderophores and organic acids. *Geochimica et Cosmochimica Acta* **2007**, *71*, (23), 5635-5650.
18. Sandy, M.; Butler, A., Microbial iron acquisition: Marine and terrestrial siderophores. *Chemical Reviews* **2009**, *109*, (10), 4580-4595.
19. Hersman, L.; Lloyd, T.; Sposito, G., Siderophore-Promoted Dissolution of Hematite. *Geochimica et Cosmochimica Acta* **1995**, *59*, (16), 3327-3330.
20. Yoshida, T.; Hayashi, K.; Ohmoto, H., Dissolution of iron hydroxides by marine bacterial siderophore. *Chemical Geology* **2002**, *184*, (1-2), 1-9.
21. Stewart, A. G.; Hudson-Edwards, K. A.; Dubbin, W. E., Mechanisms of goethite dissolution in the presence of desferrioxamine B and Suwannee River fulvic acid at pH 6.5. *Geochimica et Cosmochimica Acta* **2013**, *115*, 1-14.
22. Biswakarma, J.; Kang, K.; Borowski, S. C.; Schenkeveld, W. D. C.; Kraemer, S. M.; Hering, J. G.; Hug, S. J., Fe(II)-Catalyzed Ligand-Controlled Dissolution of Iron(hydr)oxides. *Environmental Science & Technology* **2019**, *53*, (1), 88-97.
23. Kang, K.; Schenkeveld, W. D. C.; Biswakarma, J.; Borowski, S. C.; Hug, S. J.; Hering, J. G.; Kraemer, S. M., Low Fe(II) Concentrations Catalyze the Dissolution of Various Fe(III)

- (hydr)oxide Minerals in the Presence of Diverse Ligands and over a Broad pH Range. *Environmental Science & Technology* **2019**, 53, (1), 98-107.
24. Williams, A. G. B.; Scherer, M. M., Spectroscopic evidence for Fe(II)-Fe(III) electron transfer at the iron oxide-water interface. *Environmental Science & Technology* **2004**, 38, (18), 4782-4790.
  25. Pedersen, H. D.; Postma, D.; Jakobsen, R.; Larsen, O., Fast transformation of iron oxyhydroxides by the catalytic action of aqueous Fe(II). *Geochimica et Cosmochimica Acta* **2005**, 69, (16), 3967-3977.
  26. Larese-Casanova, P.; Scherer, M. M., Fe(II) sorption on hematite: New insights based on spectroscopic measurements. *Environmental Science & Technology* **2007**, 41, (2), 471-477.
  27. Yanina, S. V.; Rosso, K. M., Linked reactivity at mineral-water interfaces through bulk crystal conduction. *Science* **2008**, 320, (5873), 218-222.
  28. Handler, R. M.; Beard, B. L.; Johnson, C. M.; Scherer, M. M., Atom exchange between aqueous Fe(II) and goethite: An Fe isotope tracer study. *Environmental Science and Technology* **2009**, 43, (4), 1102-1107.
  29. Catalano, J. G.; Fenter, P.; Park, C.; Zhang, Z.; Rosso, K. M., Structure and oxidation state of hematite surfaces reacted with aqueous Fe(II) at acidic and neutral pH. *Geochimica et Cosmochimica Acta* **2010**, 74, (5), 1498-1512.
  30. Gorski, C. A.; Handler, R. M.; Beard, B. L.; Pasakarnis, T.; Johnson, C. M.; Scherer, M. M., Fe Atom Exchange between Aqueous Fe<sup>2+</sup> and Magnetite. *Environmental Science & Technology* **2012**, 46, (22), 12399-12407.
  31. Latta, D. E.; Gorski, C. A.; Scherer, M. M., Influence of Fe<sup>2+</sup>-catalysed iron oxide recrystallization on metal cycling. *Biochemical Society Transactions* **2012**, 40, (6), 1191-1197.
  32. Handler, R. M.; Friedrich, A. J.; Johnson, C. M.; Rosso, K. M.; Beard, B. L.; Wang, C.; Latta, D. E.; Neumann, A.; Pasakarnis, T.; Premaratne, W. A. P. J.; Scherer, M. M., Fe(II)-catalyzed recrystallization of goethite revisited. *Environmental Science and Technology* **2014**, 48, (19), 11302-11311.
  33. Friedrich, A. J.; Helgeson, M.; Liu, C. S.; Wang, C. M.; Rosso, K. M.; Scherer, M. M., Iron Atom Exchange between Hematite and Aqueous Fe(II). *Environmental Science & Technology* **2015b**, 49, (14), 8479-8486.
  34. Joshi, P.; Gorski, C. A., Anisotropic Morphological Changes in Goethite during Fe<sup>2+</sup>-Catalyzed Recrystallization. *Environmental Science and Technology* **2016**, 50, (14), 7315-7324.
  35. Zarzycki, P.; Rosso, K. M., Stochastic Simulation of Isotopic Exchange Mechanisms for Fe(II)-Catalyzed Recrystallization of Goethite. *Environmental Science and Technology* **2017**, 51, (13), 7552-7559.
  36. Buchholz, A.; Laskov, C.; Haderlein, S. B., Effects of Zwitterionic Buffers on Sorption of Ferrous Iron at Goethite and Its Oxidation by CCl<sub>4</sub>. *Environmental Science & Technology* **2011**, 45, (8), 3355-3360.

37. W. Braun, J. T. H., D.K. Kahaner, Acuchem: A computer program for modeling complex chemical reaction systems. *International Journal of Chemical Kinetics* **1988**, 20, 51-62.
38. Borer, P.; Kraemer, S. M.; Sulzberger, B.; Hug, S. J.; Kretzschmar, R., Photodissolution of lepidocrocite ( $\gamma$ -FeOOH) in the presence of desferrioxamine B and aerobactin. *Geochimica et Cosmochimica Acta* **2009**, 73, (16), 4673-4687.
39. Kim, D.; Duckworth, O. W.; Strathmann, T. J., Reactions of aqueous iron-DFOB (desferrioxamine B) complexes with flavin mononucleotide in the absence of strong iron(II) chelators. *Geochimica et Cosmochimica Acta* **2010**, 74, (5), 1513-1529.
40. Joshi, P.; Fantle, M. S.; Larese-Casanova, P.; Gorski, C. A., Susceptibility of Goethite to Fe<sup>2+</sup>-Catalyzed Recrystallization over Time. *Environmental Science and Technology* **2017**, 51, (20), 11681-11691.
41. Boiteau, R. M.; Mende, D. R.; Hawco, N. J.; McIlvin, M. R.; Fitzsimmons, J. N.; Saito, M. A.; Sedwick, P. N.; DeLong, E. F.; Repeta, D. J., Siderophore-based microbial adaptations to iron scarcity across the eastern Pacific Ocean. *Proceedings of the National Academy of Sciences of the United States of America* **2016**, 113, (50), 14237-14242.
42. Senn, A. C.; Kaegi, R.; Hug, S. J.; Hering, J. G.; Mangold, S.; Voegelin, A., Composition and structure of Fe(III)-precipitates formed by Fe(II) oxidation in water at near-neutral pH: Interdependent effects of phosphate, silicate and Ca. *Geochimica et Cosmochimica Acta* **2015**, 162, 220-246.

## Supporting Information

---

- Table S1. List of chemicals
- Table S2. List of experiments and experimental conditions
- Table S3. Lepidocrocite dissolution rates and catalytic effects
- Table S4. Kinetic model with list of reactions and fitted equilibrium constants or rate coefficients
- Figure S1.  $^{57}\text{Fe}$  isotope exchange and Lp dissolution at pH 7.0 : comparison of carbonate- and MOPS- buffered conditions.
- Figure S2.  $^{57}\text{Fe}$  isotope exchange and Lp dissolution at pH 7.0
- Figure S3. Fe(II)-catalyzed goethite dissolution at pH 7.0 in the presence of (20 or 50  $\mu\text{M}$ ) DFOB



Table S1. List of chemicals used for the current study

Chemical Name	Chemical formula	Supplier	Purity	Stock solution (mM)
Sodium Chloride	NaCl	Merck	>99%	10
Iron(II) Chloride	FeCl <sub>2</sub> · 4H <sub>2</sub> O	Sigma-Aldrich	>99%	10
Iron(III) Chloride	FeCl <sub>3</sub> · 6H <sub>2</sub> O	Sigma-Aldrich	>98%	10
Iron ( <sup>57</sup> Fe- 95 atom %, <sup>54</sup> Fe 0.04 %, <sup>56</sup> Fe 3.04 %, <sup>58</sup> Fe 1.86 %)	<sup>57</sup> Fe	Sigma-Aldrich	≥99.9%	20
Iron -10,000 µg/ml	Fe	J.T Baker	ICP-MS standard	
Mesylate salt of Desferrioxamine B	C <sub>25</sub> H <sub>48</sub> N <sub>6</sub> O <sub>8</sub> · CH <sub>3</sub> O <sub>3</sub> S	Sigma-Aldrich	>92.5%	100
MES (2-morpholino-ethane sulfonic acid monohydrate)	C <sub>6</sub> H <sub>13</sub> NO <sub>4</sub> S · H <sub>2</sub> O	Fluka	>99%	100
MOPS (3-(N-) morpholino propane sulfonic acid)	C <sub>7</sub> H <sub>15</sub> NO <sub>4</sub> S	Sigma-Aldrich	>99%	100
PIPES (Piperazine-1,4-bis(2-ethane sulfonic acid))	C <sub>8</sub> H <sub>18</sub> N <sub>2</sub> O <sub>6</sub> S <sub>2</sub>	Sigma-Aldrich	>99%	100
Sodium (bi)carbonate	NaHCO <sub>3</sub>	Sigma-Aldrich	>99%	3
o-Phenanthroline	C <sub>12</sub> H <sub>8</sub> N <sub>2</sub> · H <sub>2</sub> O	Fluka	>99%	10

Table S2. List of experiments and experimental conditions. All experiments were conducted under anoxic conditions in duplicates ( $n = 2$ ). The initial concentration of lepidocrocite or goethite was 1125  $\mu\text{M}$ . (To read the table below: column “Experiments” = first reactant + second reactant; the first reactant was added 1800 s before the second reactant)

Nr.	Experiments <sup>(a)</sup>	[DFOB] ( $\mu\text{M}$ )	[Fe(II)] ( $\mu\text{M}$ )	[ <sup>57</sup> Fe(II)] ( $\mu\text{M}$ )	Buffers (/pH)
1	20 $\mu\text{M}$ DFOB	20	0	NA	Carbonate (3 mM $\text{NaHCO}_3$ , $p(\text{CO}_2) = 0.02\text{atm}$ )  (pH 7.0)
2	20 $\mu\text{M}$ DFOB + 1 $\mu\text{M}$ Fe(II)	20	1		
3	20 $\mu\text{M}$ DFOB + 2 $\mu\text{M}$ Fe(II)	20	2		
4	20 $\mu\text{M}$ DFOB + 5 $\mu\text{M}$ Fe(II)	20	5		
5	50 $\mu\text{M}$ DFOB	50	0		
6	50 $\mu\text{M}$ DFOB + 1 $\mu\text{M}$ Fe(II)	50	1		
7	50 $\mu\text{M}$ DFOB + 2 $\mu\text{M}$ Fe(II)	50	2		
8	50 $\mu\text{M}$ DFOB + 5 $\mu\text{M}$ Fe(II)	50	5		
9	20 $\mu\text{M}$ DFOB + 2 $\mu\text{M}$ <sup>57</sup> Fe(II)	20	-	2	Carbonate (3 mM $\text{NaHCO}_3$ , $p(\text{CO}_2) = 0.02\text{atm}$ )  (pH 7.0)
10	2 $\mu\text{M}$ <sup>57</sup> Fe(II) + 20 $\mu\text{M}$ DFOB	20		2	
11	50 $\mu\text{M}$ DFOB + 2 $\mu\text{M}$ <sup>57</sup> Fe(II)	50		2.2	
12	2 $\mu\text{M}$ <sup>57</sup> Fe(II) + 50 $\mu\text{M}$ DFOB	50		2	
13	2 $\mu\text{M}$ <sup>57</sup> Fe(II) + 50 $\mu\text{M}$ DFOB	50	-	2	MES (5 mM) (pH 6.0)
14	50 $\mu\text{M}$ DFOB + 2 $\mu\text{M}$ <sup>57</sup> Fe(II)	50	-	2.2	MOPS (5 mM) (pH 7.0)
15	2 $\mu\text{M}$ <sup>57</sup> Fe(II) + 50 $\mu\text{M}$ DFOB	50		2	
16	50 $\mu\text{M}$ DFOB + 2 $\mu\text{M}$ <sup>57</sup> Fe(II)	50	-	2	PIPES (5 mM) (pH 8.5)
17	2 $\mu\text{M}$ <sup>57</sup> Fe(II) + 50 $\mu\text{M}$ DFOB	50		2	
18	2 $\mu\text{M}$ <sup>57</sup> Fe(II) + 50 $\mu\text{M}$ DFOB	50	-	2	Carbonate (3 mM $\text{NaHCO}_3$ , $p(\text{CO}_2) = 0.02\text{atm}$ ) (pH 7.0)
19	2 $\mu\text{M}$ <sup>57</sup> Fe(II) + 100 $\mu\text{M}$ phenanthroline	NA		2	
20	2 $\mu\text{M}$ <sup>57</sup> Fe(II) + 100 $\mu\text{M}$ phenanthroline	NA		2	

<sup>(a)</sup> Exp. Nr. 1-17 and 20 were conducted with lepidocrocite (Lp), except exp. nr. 18-19 with goethite. Exp. Nr. 1-8 were conducted to examine the effect of added Fe(II) in carbonate-buffered suspensions. Exp. Nr. 9-18 were conducted to study the isotope exchange and dissolution. Exp. Nr. 19-20 were conducted to assess the isotopic exchange at pH 7.0 without dissolution.

Table S3. Dissolution rates of lepidocrocite and catalytic effect of Fe(II), in the presence of DFOB (20  $\mu\text{M}$  or 50  $\mu\text{M}$ ) with varied Fe(II) concentrations. Listed dissolution rates from Kang et al. (2018) were used in order to compare with the empirical model fits to the measured data of this study. The catalytic effect is defined as the ratio of the rate of dissolution in the presence of ligand and Fe(II) over the rate of dissolution in the presence of the ligand alone.

Experiments	[Fe(II)]	Rate of Dissolution <sup>§</sup>		Catalytic Effect	Buffers (/pH)
		$\mu\text{M}$	$\text{nM s}^{-1}$ $\text{nmol s}^{-1} \text{m}^{-2}$		
20 $\mu\text{M}$ DFOB	0	0.21	0.03	1	Carbonate (pH 7.0)
20 $\mu\text{M}$ DFOB + 1 $\mu\text{M}$ Fe(II)	1	2.71	0.43	13	
20 $\mu\text{M}$ DFOB + 2 $\mu\text{M}$ Fe(II)	2	3.37	0.53	16	
20 $\mu\text{M}$ DFOB + 5 $\mu\text{M}$ Fe(II)	5	8.63	1.37	41	
20 $\mu\text{M}$ DFOB	0	-	0.07	1	MOPS (pH 7.0) (Kang et.al., 2018)
20 $\mu\text{M}$ DFOB + 2 $\mu\text{M}$ Fe(II)	2	-	0.29	4	
50 $\mu\text{M}$ DFOB	0	0.31	0.05	1	Carbonate (pH 7.0)
50 $\mu\text{M}$ DFOB + 1 $\mu\text{M}$ Fe(II)	1	5.59	0.89	18	
50 $\mu\text{M}$ DFOB + 2 $\mu\text{M}$ Fe(II)	2	11.66	1.85	38	
50 $\mu\text{M}$ DFOB + 5 $\mu\text{M}$ Fe(II)	5	27.17	4.31	88	
50 $\mu\text{M}$ DFOB	0	0.20	0.03	1	MOPS (pH 7.0)
50 $\mu\text{M}$ DFOB + 2 $\mu\text{M}$ Fe(II)	2	2.03	0.32	10	
2 $\mu\text{M}$ Fe(II) +50 $\mu\text{M}$ DFOB	2	0.97	0.15	-	MES (pH 6.0)
50 $\mu\text{M}$ DFOB	0	0.47	0.08		PIPES (pH 8.5)
50 $\mu\text{M}$ DFOB + 2 $\mu\text{M}$ Fe(II)	2	0.94	0.15	2	

<sup>§</sup>  $R_C = k_{C,app}(L_T - [Fe]_{diss})$ ;  $k_{C,app}$  is apparent rate constant that was obtained from the empirical model fits to the measured data. The listed rates of accelerated dissolution were calculated at the second data points after the addition of Fe(II), with  $L_T - [Fe]_{diss}$  (free ligand concentration) at these time points (see Fig. 1 in main chapter). There was no difference b/w Fe(II)- and  $^{57}\text{Fe(II)}$ - added rates. The order of addition of Fe(II) (i.e., before or after or DFOB addition) had no significant effect on rates. The rates of the non-catalyzed dissolution (i.e. ligand alone) were determined from linear fits to the data without addition of Fe(II).

Table S4. Kinetic model with list of complete reactions

Nr.	Reaction			Description	K/ k pH 7	K/ k pH 6
R1	$\equiv\text{Fe}^{\text{III}} + \text{L}$	$\rightleftharpoons$	$\equiv\text{Fe}^{\text{III}}\text{L}$	Adsorption of ligand $\text{L}$ on surface $\text{Fe}^{\text{III}}$	$3.0e5$	$3.0e4$ - $3.0e5$
R2	$\equiv\text{Fe}^{\text{III}}\text{L}$	$\rightarrow$	$\equiv\text{Fe}^{\text{III}} + \text{Fe}^{\text{III}}\text{L}$	Non-catalyzed dissolution	$3.5e-5$	n.d.
R3	$^{57}\text{Fe}^{\text{II}} + \text{L}$	$\rightleftharpoons$	$^{57}\text{Fe}^{\text{II}}\text{L}$	Dissolved $^{57}\text{Fe}^{\text{II}}\text{L}$ complex formation	$3.79e2$	$5.26e4$
R3b	$\text{Fe}^{\text{II}} + \text{L}$	$\rightleftharpoons$	$\text{Fe}^{\text{II}}\text{L}$	Dissolved $\text{Fe}^{\text{II}}\text{L}$ complex formation	$3.79e2$	$5.26e4$
R4	$\equiv\text{Fe}^{\text{III}} + ^{57}\text{Fe}^{\text{II}}\text{L}$	$\rightarrow$	$\equiv\text{Fe}^{\text{II}} + ^{57}\text{Fe}^{\text{III}}\text{L}$	ET from $^{57}\text{Fe}^{\text{II}}\text{L}$ to surface $\text{Fe}^{\text{III}}$ and detachment of $^{57}\text{Fe}^{\text{III}}\text{L}$	$5.2e3$	200-600
R4b	$\equiv\text{Fe}^{\text{III}} + \text{Fe}^{\text{II}}\text{L}$	$\rightarrow$	$\equiv\text{Fe}^{\text{II}} + \text{Fe}^{\text{III}}\text{L}$	ET from $\text{Fe}^{\text{II}}\text{L}$ to surface $\text{Fe}^{\text{III}}$ and detachment of $\text{Fe}^{\text{III}}\text{L}$	$5.2e3$	200-600
R4c	$\equiv^{57}\text{Fe}^{\text{III}} + \text{Fe}^{\text{II}}\text{L}$	$\rightarrow$	$\equiv^{57}\text{Fe}^{\text{II}} + \text{Fe}^{\text{III}}\text{L}$	ET from $\text{Fe}^{\text{II}}\text{L}$ to surface $^{57}\text{Fe}^{\text{III}}$ and detachment of $\text{Fe}^{\text{III}}\text{L}$	$5.2e3$	200-600
R4d	$\equiv^{57}\text{Fe}^{\text{III}} + ^{57}\text{Fe}^{\text{II}}\text{L}$	$\rightarrow$	$\equiv^{57}\text{Fe}^{\text{II}} + ^{57}\text{Fe}^{\text{III}}\text{L}$	ET from $^{57}\text{Fe}^{\text{II}}\text{L}$ to surface $^{57}\text{Fe}^{\text{III}}$ and detachment of $^{57}\text{Fe}^{\text{III}}\text{L}$	$5.2e3$	200-600
R5	$\equiv\text{Fe}^{\text{III}} + ^{57}\text{Fe}^{\text{II}}$	$\rightleftharpoons$	$\equiv\text{Fe}^{\text{III}}\text{-O-}^{57}\text{Fe}^{\text{II}}$	Adsorption and desorption of $^{57}\text{Fe}^{\text{II}}$ on surface $\text{Fe}^{\text{III}}$	$7.2e6$	$6.3e4$
R5b	$\equiv\text{Fe}^{\text{III}} + \text{Fe}^{\text{II}}$	$\rightleftharpoons$	$\equiv\text{Fe}^{\text{III}}\text{-O-Fe}^{\text{II}}$	Adsorption and desorption of $\text{Fe}^{\text{II}}$ on surface $\text{Fe}^{\text{III}}$	$7.2e6$	$6.3e4$
R6	$\equiv\text{Fe}^{\text{III}}\text{-O-}^{57}\text{Fe}^{\text{II}}$	$\rightleftharpoons$	$\equiv^{57}\text{Fe}^{\text{III}}\text{-O-Fe}^{\text{II}}$	ET between $^{57}\text{Fe}$ and $^{56}\text{Fe}$ on the surface	4.3-4.6	4.2-4.5
R7	$\equiv^{57}\text{Fe}^{\text{III}} + \text{Fe}^{\text{II}}$	$\rightleftharpoons$	$\equiv^{57}\text{Fe}^{\text{III}}\text{-O-Fe}^{\text{II}}$	Adsorption and desorption of $\text{Fe}^{\text{II}}$ on surface $^{57}\text{Fe}^{\text{III}}$	$7.2e6$	$6.3e4$
R7b	$\equiv^{57}\text{Fe}^{\text{III}} + ^{57}\text{Fe}^{\text{II}}$	$\rightleftharpoons$	$\equiv^{57}\text{Fe}^{\text{III}}\text{-O-}^{57}\text{Fe}^{\text{II}}$	Adsorption of and desorption of $^{57}\text{Fe}^{\text{II}}$ on surface $^{57}\text{Fe}^{\text{III}}$	$7.2e6$	$6.3e4$
R8	$\equiv\text{Fe}^{\text{III}}\text{-O-}^{57}\text{Fe}^{\text{II}} + \text{L}$	$\rightarrow$	$\equiv\text{Fe}^{\text{II}} + ^{57}\text{Fe}^{\text{III}}\text{L}$	Adsorption of $\text{L}$ on adsorbed $^{57}\text{Fe}^{\text{II}}$ , ET and detachment	81	<5
R8b	$\equiv\text{Fe}^{\text{III}}\text{-O-Fe}^{\text{II}} + \text{L}$	$\rightarrow$	$\equiv\text{Fe}^{\text{II}} + \text{Fe}^{\text{III}}\text{L}$	Adsorption of $\text{L}$ on adsorbed $\text{Fe}^{\text{II}}$ , ET and detachment	81	<5
R9	$\equiv^{57}\text{Fe}^{\text{III}}\text{-O-Fe}^{\text{II}} + \text{L}$	$\rightarrow$	$\equiv^{57}\text{Fe}^{\text{II}} + \text{Fe}^{\text{III}}\text{L}$	Adsorption of $\text{L}$ on adsorbed $\text{Fe}^{\text{II}}$ , ET and detachment	81	<5
R9b	$\equiv^{57}\text{Fe}^{\text{III}}\text{-O-}^{57}\text{Fe}^{\text{II}} + \text{L}$	$\rightarrow$	$\equiv^{57}\text{Fe}^{\text{II}} + ^{57}\text{Fe}^{\text{III}}\text{L}$	Adsorption of $\text{L}$ on adsorbed $^{57}\text{Fe}^{\text{II}}$ , ET and detachment	81	<5
R10	$\equiv\text{Fe}^{\text{II}} + \text{Bulk}$	$\rightarrow$	$\equiv\text{Fe}^{\text{III}}\text{-O-Fe}^{\text{II}}$	Re-formation of surface site with adsorbed $\text{Fe}^{\text{II}}$	$1e10$	$1e10$
R11	$\equiv^{57}\text{Fe}^{\text{II}} + \text{Bulk}$	$\rightarrow$	$\equiv\text{Fe}^{\text{III}}\text{-O-}^{57}\text{Fe}^{\text{II}}$	Re-formation of surface site with adsorbed $^{57}\text{Fe}^{\text{II}}$	$1e10$	$1e10$

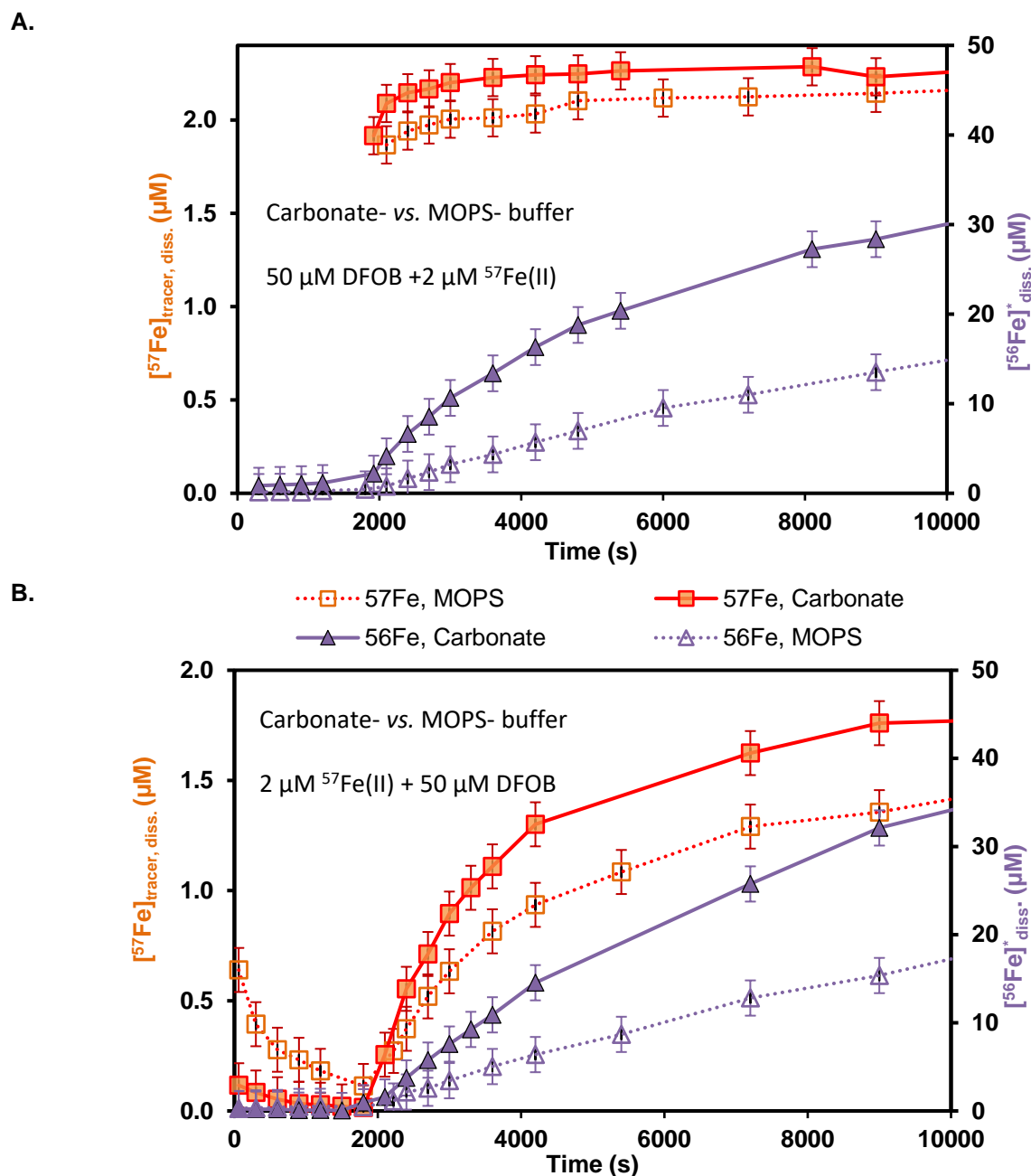


Figure S1.  $^{57}\text{Fe}$  isotope exchange and Lp dissolution as a function of time (anoxic conditions; pH 7.0). Comparison of carbonated-buffered (filled symbols) and MOPS-buffered (empty symbol) systems. (A)  $2\ \mu\text{M}\ ^{57}\text{Fe}(\text{II})$  was added 1800 s after  $50\ \mu\text{M}$  DFOB addition. (B)  $2\ \mu\text{M}\ ^{57}\text{Fe}(\text{II})$  was added 1800 s before  $50\ \mu\text{M}$  DFOB addition. All experiments were conducted in duplicates. Error bars correspond to the standard deviations of ICP-MS measurements obtained from repeated calibrations. Lines are to guide eyes through the data points. Symbols: triangles (right axis): concentration of Fe released into solution by Lp dissolution ( $[\text{}^{56}\text{Fe}]^*_{\text{diss.}}$ ); squares (left axis): dissolved concentration of tracer  $^{57}\text{Fe}$  corrected for the natural abundance of  $^{57}\text{Fe}$  in Lp ( $[\text{}^{57}\text{Fe}]_{\text{tracer, diss.}}$ ).

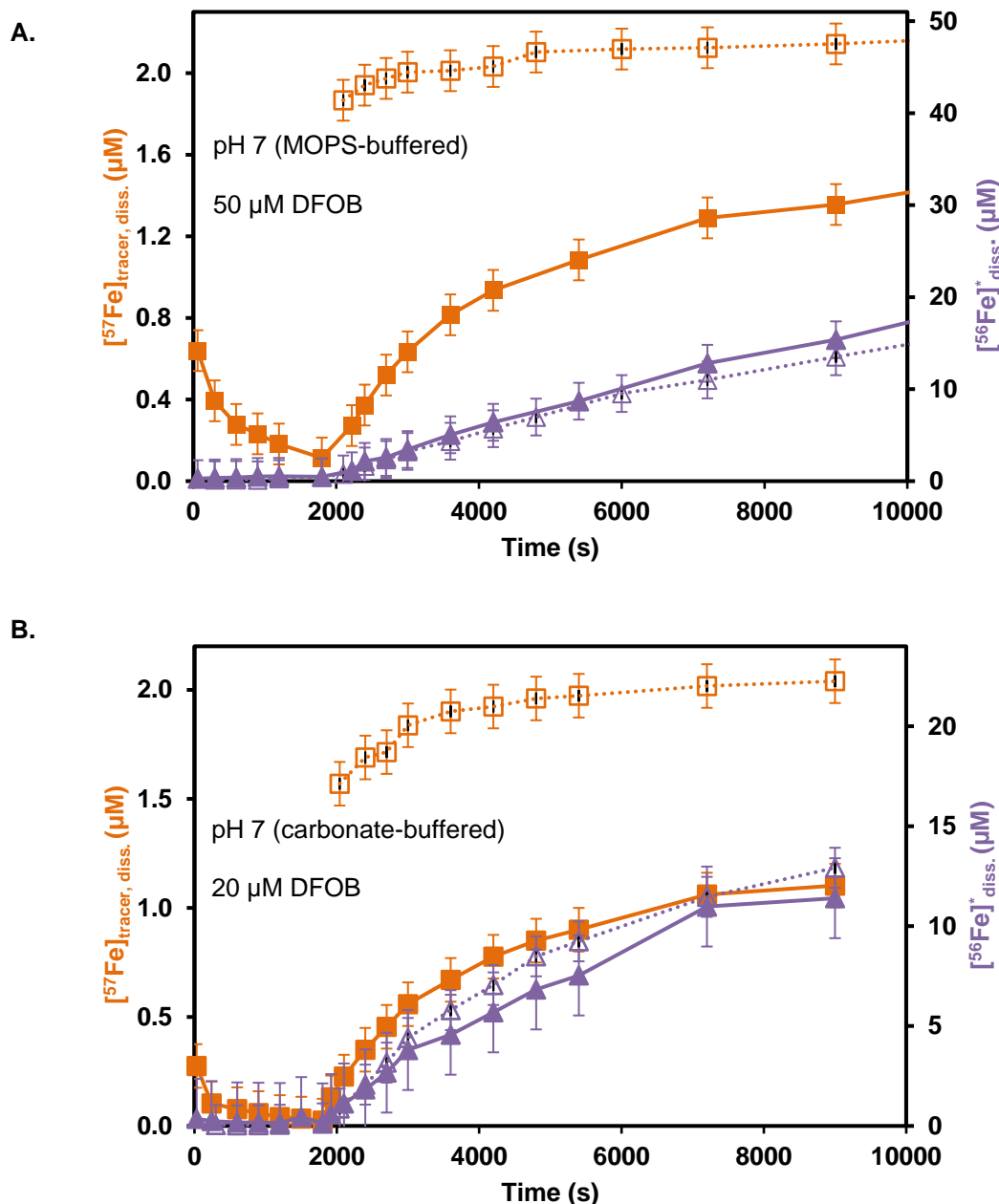


Figure S2.  $^{57}\text{Fe}$  isotope exchange and Lp dissolution as a function of time (A) with 50  $\mu\text{M}$  DFOB at pH 7.0 (MOPS- buffered), and (B) with 20  $\mu\text{M}$  DFOB at pH 7 (carbonate-buffered). 2  $\mu\text{M}$   $^{57}\text{Fe}(\text{II})$  was added to a Lp suspension (1125  $\mu\text{M}$ ) 1800 s before (filled symbols) or after (empty symbols) DFOB addition under anoxic conditions. Error bars correspond to the standard deviations of ICP-MS measurements obtained from repeated calibrations. Lines serve as visual guide. The data for  $^{57}\text{Fe}$  (filled squares) and  $^{56}\text{Fe}$  (filled triangles) after 1800 s are also shown in main Fig. 4.

Symbols: (purple) triangles (right axis): concentration of Fe released into solution by Lp dissolution ( $[^{56}\text{Fe}]^*_{\text{diss.}}$ ); (orange) squares (left axis): dissolved concentration of tracer  $^{57}\text{Fe}$  corrected for the natural abundance of  $^{57}\text{Fe}$  in Lp ( $[^{57}\text{Fe}]_{\text{tracer, diss.}}$ ).

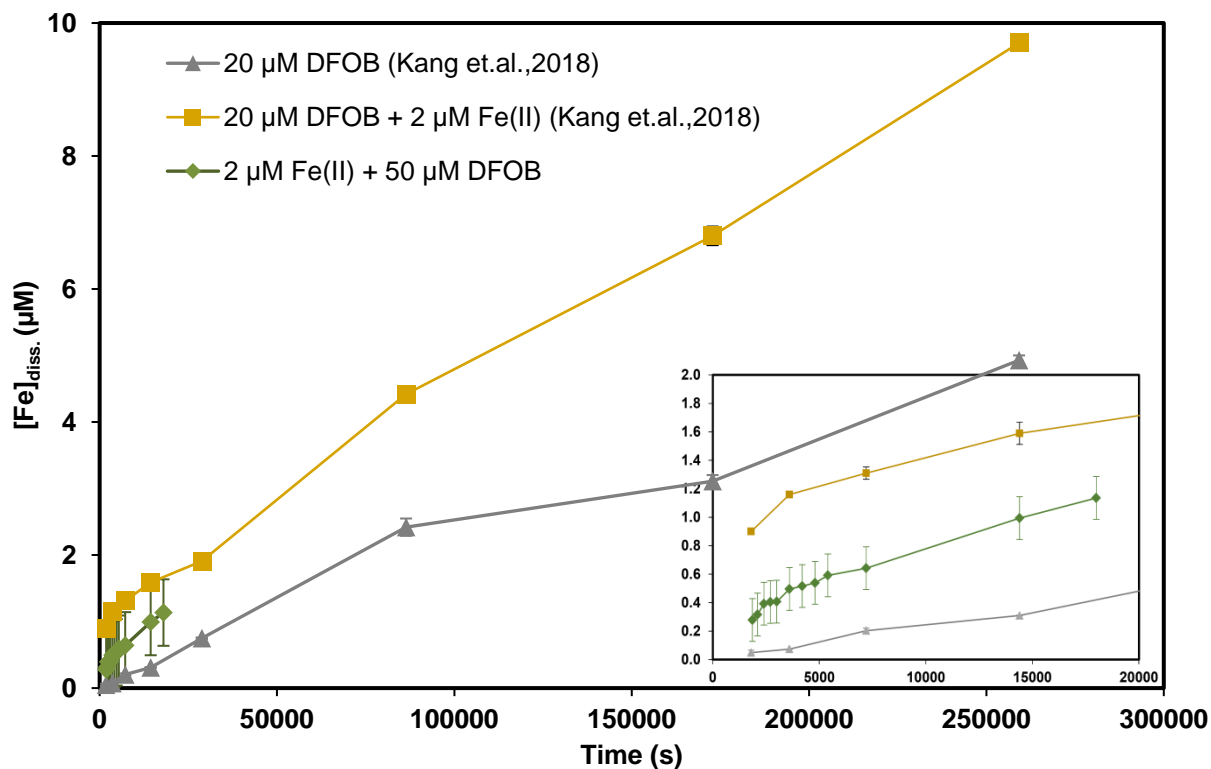


Figure S3. Goethite dissolution at pH 7 under anoxic condition.  $^{57}\text{Fe}(\text{II})$  was added, as a tracer for Fe(II), 1800 s before DFOB (50  $\mu\text{M}$ ) to a goethite suspension (1125  $\mu\text{M}$ ) in carbonate-buffered system. Experiments were conducted in duplicates ( $n=2$ ). Note that Kang. et. al conducted goethite dissolution experiments in MOPS-buffered conditions by adding both DFOB and Fe(II) at a same time. The inset figure is to highlight the first 20 000 s measurements. Lines serve as visual guides.

Goethite dissolution is slower than Lp dissolution (Kang et. al.). Our results show that only 1.14  $\mu\text{M}$  goethite dissolution was measured after 5 hr. (20 000 s), when  $^{57}\text{Fe}(\text{II})$  was added 1800 s before 50  $\mu\text{M}$  DFOB. When compared to measurements by Kang et. al., goethite dissolution within the same time frame was found almost in agreement. Although the concentration of dissolved Fe measured as 1.57  $\mu\text{M}$  by Kang et. al., the differences in measurements could be due to the difference in the applied DFOB concentrations and to the reversed addition of Fe(II). Currently we lack experiments to explain these differences. However, the key purpose of applying  $^{57}\text{Fe}(\text{II})$  before DFOB was to examine the release of  $^{57}\text{Fe}$  during accelerated goethite dissolution (as shown by Fig. 5 in the main chapter).

## Chapter 4

# Photochemically Induced Fe(II)-Catalyzed Ligand-Controlled Dissolution of Iron(hydr)oxides

---

Jagannath Biswakarma, Kyounglim Kang, Walter D.C. Schenkeveld,

Stephan M. Kraemer, Janet G. Hering and Stephan J. Hug

*Manuscript in preparation*



## Abstract

In sunlit environments, Fe(II) can be continuously formed on the surface of iron(hydr)oxides, at rates that depend on the presence of adsorbed organic ligands. Previous studies addressed the photo-induced dissolution of iron(hydr)oxides, but did not distinguish between photochemical formation of dissolved Fe(II) and Fe(II)-accelerated formation of dissolved Fe(III) that can continue after illumination stops. Here we studied the effect of photochemically produced Fe(II) on the dissolution of lepidocrocite (Lp) and goethite (Gt) (1.13 mM) with 50  $\mu$ M EDTA or DFOB, mainly at pH 7.0 in bicarbonate-CO<sub>2</sub> buffered suspensions. The rate of photochemical Fe(II) production in the absence of EDTA or DFOB, was more than 25 fold higher in Lp than in Gt. Fe(II) formation rates in the presence of EDTA was higher than that of DFOB. Continuous illumination with UV-A light (320-420 nm) increased Lp dissolution rates with EDTA or DFOB by factors up to 30 under anoxic condition, in contrast to factors of up to 5.5 under oxic condition. Short periods (5 min or 15 min) of illumination increased dissolution rates by 10- 40 fold; under anoxic conditions, accelerated dissolution persisted in dark after illumination ceased. Under oxic conditions, dissolution rates increased only during illumination, but quickly decreased to nearly pre-illumination levels after illumination stopped. Light-absorption (which occurred to over 98% in our suspensions) thus led to formation of Fe(II) that efficiently catalyzes dissolution, but is not protected from oxidation. Under oxic conditions, dissolved Fe(III) reached 35  $\mu$ M with DFOB after 10 h of continuous illumination, while with EDTA, only 15  $\mu$ M dissolved iron was formed after 280 min and then decreased to below 2  $\mu$ M after 10 h. While different ligands can accelerate dissolution by photochemical Fe(II) formation, only photo-stable ligands such as DFOB can maintain Fe(III) in solution during extended exposure to UV-light under oxic conditions. Accelerated dissolution of Fe(III)-phases by photochemically formed Fe(II) is most likely to be relevant at anoxic/oxic interfaces in shallow lakes, ponds and flooded areas (e.g. rice paddies) and in algal bloom environments.

## Introduction

Dissolution of Fe(III)(oxyhydr)oxides is one of the key biogeochemical processes in the cycling and (bio)availability of Fe in environment. Under sunlight, photochemical reactions can lead to reduction of Fe(III) to Fe(II), for example in surface water<sup>1-3</sup>, seawater<sup>4-6</sup>, atmospheric dust<sup>7-10</sup>, and ice<sup>11</sup>. Laboratory studies have demonstrated that (solar) UV light induces photo reductive dissolution of Fe(III)(oxyhydr)oxides in the presence of organic compounds such as ligands secreted by phytoplankton and algae in oceans, and by microbes and plants in soils.<sup>7, 12-15</sup> These light-induced processes are of interest as they influence the redox speciation of Fe(II)/Fe(III) in the environment and indirectly affect the mobility of (trace) elements that are associated with Fe(III) phases.

In the presence of ligands, the photo-reductive dissolution of iron(hydr)oxides can be explained by two possible processes, which can also occur in parallel. Adsorbed ligands can act as electron hole scavengers on the surface of semiconducting Fe(III) phases, and/or light induced ligand to metal charge transfer (LMCT) in surface complexes can form Fe(II) on the surface and induce dissolution.<sup>15-17</sup> Thus, solar UV illumination can lead to formation of Fe(II), which under oxic conditions is oxidized by dissolved oxygen. Under continuous illumination, steady state concentrations of Fe(II) are established quickly and depend on the relative rates of photochemical formation and oxidation of Fe(II) by oxygen. The rates of photo reductive dissolution in the presence of ligands were reported to be higher than their corresponding dark reduction rates.<sup>12, 18-20</sup> In previous studies, dissolved Fe(II) and total dissolved Fe were quantified while mineral suspensions were continuously exposed to solar UV illuminations.<sup>17, 21-23</sup> However, the possibility that photo-produced Fe(II) could continue to accelerate dissolution even after illumination ceased was not considered.

In our recent studies,<sup>24-26</sup> we examined the effect of added Fe(II) on dissolution of Fe(III)(oxyhydr)oxides, showing that micro-molar concentrations of Fe(II) could lead to up to a 30-fold acceleration of dissolution rates under anoxic conditions. We further demonstrated that photochemically formed Fe(II) also accelerates dissolution rates under both anoxic and oxic conditions. By measuring lepidocrocite (Lp) dissolution *in situ* with infrared spectroscopy, we were able to observe accelerated dissolution during intermittent UV illumination in the presence of the synthetic ligand ethylenediamine tetraacetic acid (EDTA) at pH 6. After UV illumination, accelerated

dissolution was observed to continue in the dark under anoxic conditions but not under oxic conditions.

Here, we extend our previous work by quantifying photo-produced Fe(II) in the absence of solid dissolution, comparing the solids Lp and goethite (Gt), and comparing the synthetic ligand EDTA with the biogenic siderophore desferrioxamine B (DFOB). As in our previous work, we conducted experiments under both anoxic and oxic conditions and at pH 6.0 (MES buffered), 7.0 (CO<sub>2</sub>-carbonate buffered) and 8.5 (PIPES-buffered). In contrast to our previous, *in situ* studies, we conducted batch dissolution experiments under both intermittent (5 or 15 min) and continuous UV illumination. Experiments with continuous UV illumination were particularly helpful for the interpretation of experiments with intermittent illumination under oxic conditions where only subtle effects could be observed.

## Materials and Methods

### Chemicals and Solutions

All chemicals used were of analytical grade and are listed in the Supporting Information (SI), Table S1. Aqueous solutions were prepared using high-purity doubly-deionized (DDI) water (Barnstead Nanopure). The synthesis and characterization of Lp and Gt were described in our recent studies.<sup>24, 25</sup>

### Photochemical experiments

Suspensions of Lp and Gt with EDTA or DFOB (100 ml) were irradiated in 120 ml Pyrex bottles with UV-A light in a box with 8 Philips TL20W/05 (actinic blue) lamps. The lamps have a broad emission spectrum from 310-450 nm (maximum at 365 nm) and closely simulate solar illumination in the UV-A spectral range.<sup>27</sup> The emission spectrum of the UV-source and the spectra of Lp, Fe(III)EDTA and Fe(III)DFOB are shown in the SI (Figure S1).

**Photon flux.** The photon flux entering the Pyrex bottles was measured by ferrioxalate actinometry.<sup>28</sup> 100 ml of a 6 mM ferrioxalate actinometer solution (which absorbed all incoming light of our UV-A light source) was exposed to UV-light. The light flux was determined as 1.37  $\mu\text{mol photons/s}$ , which is comparable to the light flux of 1.63  $\mu\text{mol photons/s}$  measured when the

actinometer was exposed to sunlight on a clear day (11:30 am, November 7, 2018). Over 95% of the light in this spectral range was absorbed by the 1.13 mM suspensions of Lp and Gt (Figure S1).

**Photoproduction of Fe(II).** The photoproduction of Fe(II) was measured at pH 7.0 under anoxic conditions, by adding 470  $\mu$ M phenanthroline (phen) to the Lp or Gt suspensions (without and with 50  $\mu$ M EDTA or DFOB). We assume that with the large excess of phen, all photochemically formed Fe(II) forms dissolved Fe(II)(phen)<sub>3</sub> complexes. Fe(II)(phen)<sub>3</sub> in filtered samples was quantified by measuring UV-spectra and calculation of concentrations from the absorbance at 510 nm ( $\epsilon_{510\text{ nm}} = 11000\text{ M}^{-1}\text{cm}^{-1}$ ).

**Formation of FeEDTA and FeDFOB from Lp and Gt.** All experiments were conducted with initially 100 ml suspensions containing 100 mg/L (1.125 mM) FeOOH (Lp or Gt) and 50  $\mu$ M EDTA or DFOB. For pH 7.0, the background electrolyte was 3 mM NaHCO<sub>3</sub>. Before and during illumination, suspensions were continuously purged with a mixture of 2% CO<sub>2</sub> in N<sub>2</sub> (anoxic) or 2% CO<sub>2</sub> in air (oxic) for the experiments at pH 7.0 (buffered by CO<sub>2</sub> and 3 mM NaHCO<sub>3</sub>). Experiments at pH 6.0 (9.5 mM NaCl and 5 mM MES) and at pH 8.5 (9.5 mM NaCl and 5 mM PIPES) were sparged with N<sub>2</sub> (anoxic) or synthetic air (oxic). Suspensions were irradiated either continuously or intermittently; the periods of intermittent illumination were mainly 5 min for experiments with EDTA (except as noted in the text or figure captions) and 15 min for experiments with DFOB. Samples were withdrawn periodically with a syringe and immediately filtered through 0.1  $\mu$ M Nylon filters. Subsequently, UV-VIS spectra (200-800 nm) were measured to quantify the formed Fe(III)EDTA or Fe(III)DFOB complexes in 1 cm path-length quartz cuvettes. Examples of data processing are shown in SI, Figure S3, S4. Note that with this method, we measure the sum of Fe(II) and Fe(III) complexes, as both Fe(II)EDTA and Fe(II)DFOB are quickly oxidized upon contact with air. We thus refer to dissolved iron as [Fe]<sub>diss</sub> in the figures and the discussion of the experiments, although at higher concentrations Fe(III)EDTA or Fe(III)DFOB dominate over the Fe(II) species, because only a few  $\mu$ M of Fe(II) were produced by UV-illumination. In the oxic experiments, all dissolved Fe(III) is present as Fe(III)EDTA or Fe(III)DFOB.

## Results and Discussion

### Photochemical formation of Fe(II) in Lp and Gt suspensions without and with dissolution-promoting ligands

Photochemical Fe(II) formation was quantified by adding a large excess of the Fe(II)-complexing ligand phen. Suspensions were illuminated intermittently for 5 min; concentrations of Fe(II)(phen)<sub>3</sub> subsequently (i.e., without illumination) reached stable values ( $\pm 5\%$ ) as shown for Lp and DFOB in Figure S2. As shown in Figure 1, the concentration of Fe(II)(phen)<sub>3</sub> in suspensions of either Lp and Gt increases linearly as a function of the duration of illumination. This linear increase confirms that the low concentrations of Fe(II)(phen)<sub>3</sub> formed in our experiments did not lead to significant light adsorption or interactions with Lp or Gt. Photochemical Fe(II) formation rates were determined from the slopes of the linear fits as indicated in Figure 1 and tabulated in Table 1.

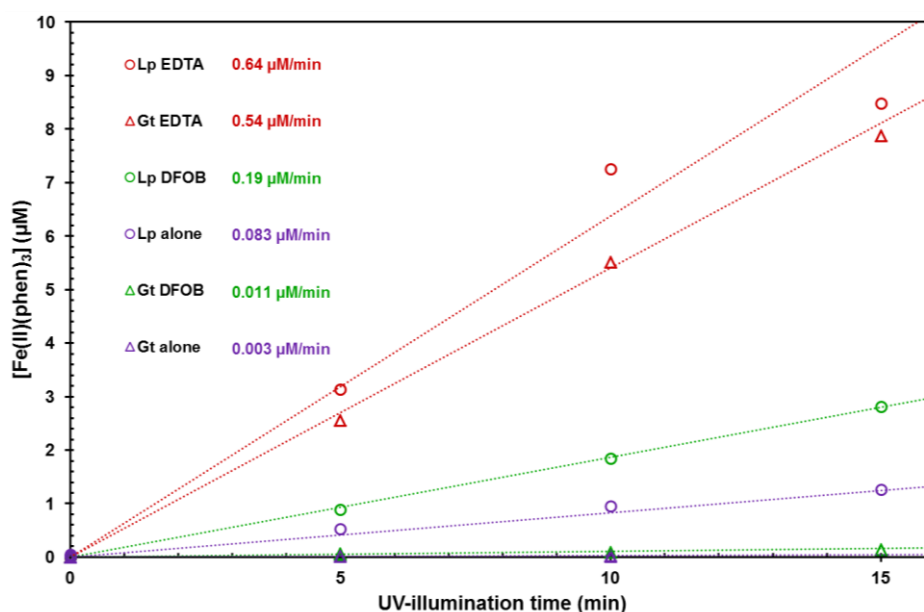


**Figure 1.** Fe(II) produced in 5 min illumination intervals with UV-A light in 1.13 mM lepidocrocite (Lp) and goethite (Gt) suspensions. The Fe(II) production was measured with phenanthroline in the absence of ligands, and in the presence of 50  $\mu\text{M}$  EDTA or DFOB at pH 7.0 (carbonate-buffered, anoxic).

**Table 1.** Dissolution rates and catalytic effects ( $CE_p$ ) of Fe(III)(hydr)oxides (before, during and after illumination) in the presence of 50  $\mu\text{M}$  ligand mainly at pH 7.0; rates at pH 6.0 and 8.5 are reported in *italic* font. Photochemically produced Fe(II) was quantified with phen at pH 7.0 under anoxic conditions.

Rate of photon absorption during illumination: 1,038,000 (nM/min)									
Illumin. time  (min)			Sum of Fe(II) produced (anoxic) (μM)	Fe(II) formation Rate (anoxic) (nM/min)			Quantum yield of Fe(II) formation  ΦFe(II)		
Photochem. Fe(II) Formation									
Lp	EDTA	5	3.2	640	-	-	6.2 x 10 <sup>-4</sup>	-	
Lp	DFOB	15	2.9	193	-	-	1.9 x 10 <sup>-4</sup>	-	
Gt	EDTA	5	2.7	540	-	-	5.2 x 10 <sup>-4</sup>	-	
Gt	DFOB	15	0.17	10	-	-	-	-	
Lp	none	15	1.25	83	-	-	7.7 x 10 <sup>-5</sup>	-	
Gt	none	15	0.05	3	-	-	-	-	
				Dissolution rates (nM/min)		CE <sub>p</sub>	CE <sub>p</sub>	Dissolution rates (% h <sup>-1</sup> )	
				anoxic	oxic	anoxic	oxic	anoxic	oxic
[Fe(III)] <sub>diss</sub> formation in the dark									
Lp	EDTA	-	-	31	25	-	-	0.17	0.13
Lp	DFOB	-	-	19	19	-	-	0.10	0.10
Gt	EDTA	-	-	1.3	-	-		0.01	-
Gt	DFOB	-	-	-	-			-	-
[Fe] <sub>diss</sub> formation during continuous UV-A									
Lp	EDTA			831	121	27	4.8	4.43	0.65
	DFOB			312	105	16	5.5	1.66	0.56
[Fe] <sub>diss</sub> formation after intermittent UV-A									
Lp	EDTA	5	3.2	238	-	8	-	1.27	-
	EDTA	5	3.2	-	-		-	-	-
	EDTA	5	3.2	-	-		-	-	-
	EDTA	15	9.6	427	-	14	-	2.28	-
Lp	DFOB	15	2.9	173	-	9	-	0.92	-
	DFOB	15	2.9	198	-	10	-	1.06	-
	DFOB	15	2.9	131	-	7	-	0.70	-
Gt	EDTA	5	2.7	51	-	39	-	0.27	-
	EDTA	5	2.7	55	-	42	-	0.29	-
	EDTA	5	2.7	37	-	28	-	0.20	-
pH 6.0, Lp/ EDTA in the dark				26	26	-	-	0.14	0.14
Lp/ EDTA after 5 min intermittent UV-A				859	-	33	-	4.58	
pH 8.5									
Lp	DFOB	none (i.e. dark)		39	30			0.21	0.16
Lp	DFOB	5		84		2		0.45	
	DFOB	5		88		2		0.47	
	DFOB	5		79		2		0.42	

In the absence of the dissolution-promoting ligands EDTA or DFOB, 0.05  $\mu\text{M}$   $\text{Fe(II)(phen)}_3$  was measured after Gt was exposed to 15 min of illumination, corresponding to a maximum rate of photochemical  $\text{Fe(II)}$  formation of 0.003  $\mu\text{M}/\text{min}$ . This value was substantially higher with Lp (0.083  $\mu\text{M}/\text{min}$ ; note that reported value in table is calculated for 15 min) consistent with the intrinsic photochemical activity of Lp reported previously by Borer et al. and ascribed to light absorption in the bulk with formation of mobile charge carriers and  $\text{Fe(II)}$  and OH-radicals on the surface.<sup>17</sup>

Higher rates of photochemical  $\text{Fe(II)}$  formation were observed in the presence of EDTA and DFOB for both solids. The most significant enhancement was observed for Gt in the presence of EDTA, which increased the rate of photochemical  $\text{Fe(II)}$  formation by at least a factor of 180 in comparison with the solid alone. With Lp, the rate of photochemical  $\text{Fe(II)}$  formation was increased by a factor of 7.7 by EDTA but only by a factor of 2.3 by DFOB. The effect of DFOB on photochemical  $\text{Fe(II)}$  formation rates was similar for Gt and Lp.

The pronounced effects of EDTA may be due to the high photoreactivity of its surface complexes or to efficient hole scavenging by adsorbed EDTA. In order to produce comparable concentrations of around 3  $\mu\text{M}$   $\text{Fe(II)}$  in subsequent Lp dissolution experiments, we applied intermittent illumination periods of 5 min for EDTA and 15 min for DFOB (see Table 1).

### Effect of UV-A illumination on Lp dissolution

***In the presence of EDTA.*** Figure 2 shows the measured concentrations of total, dissolved Fe ( $[\text{Fe}]_{\text{diss.}}$ ) in Lp suspensions in the presence of EDTA as a function of time at pH 6 and 7 under anoxic and oxic. Note that all dissolved Fe is assumed to be complexed by EDTA (see Materials and Methods). The initial 90 min of the reaction was allowed to proceed without any UV illumination. During this initial period, Lp dissolution was very slow under all conditions (see Table 1 for rates), in good agreement ( $\pm 20$  % relative difference) to the rates reported in our previous study.<sup>24</sup> (Dissolution rates of this study with previous study are listed in SI, Table S2)

Anoxic suspensions were exposed to a single, 5-min illumination period (90-95 min). At both pH 6 and 7, a distinct increase in  $[\text{Fe}]_{\text{diss.}}$  was observed immediately after the illumination period (no samples were collected during illumination). Continued increases in  $[\text{Fe}]_{\text{diss.}}$  were observed after illumination ceased indicating continuing accelerated dissolution of Lp. At pH 6, the reaction reached

completion within 150 min;  $[\text{Fe}]_{\text{diss}}$  (orange squares in Fig. 2) approached the total concentration of EDTA (i.e., 50  $\mu\text{M}$ ). At pH 7,  $[\text{Fe}]_{\text{diss.}}$  increased more slowly (orange triangles in Fig. 2), but accelerated dissolution also persisted after illumination and the reaction reached completion at 420 min.

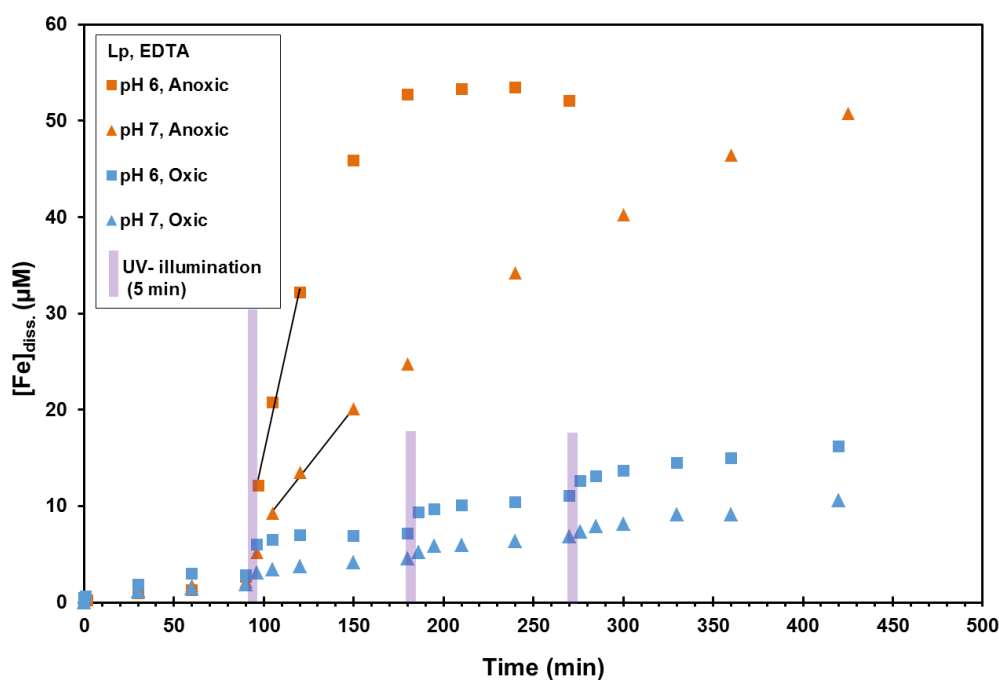


**Figure 2.** Lp dissolution in the presence of 50  $\mu\text{M}$  EDTA. UV-A intermittent illumination intervals of 5 min (shown by purple bars) applied to Lp (1125  $\mu\text{M}$ ) suspension at pH 6 and 7. A single illumination (90-95 min) was applied under anoxic conditions, and three intermittent illuminations (90-95, 180-185, 270-275 min) were applied under oxic conditions. After 5 min illumination, accelerated Lp dissolution (anoxic) occurred rapidly until all free ligand was complexed with Fe in the dark. In contrast, Lp dissolution under oxic conditions was not faster after illumination than before illumination, at both pH 6 and 7. Slopes were determined from the linear fits to the data points, as shown by solid lines.

Dissolution rates (Table 1) were computed from linear regression lines as shown in figures. The rate of Lp dissolution were 8 times faster after than before illumination in the presence of EDTA at pH 7. The persistence of accelerated dissolution at pH 7 after the cessation of illumination under anoxic conditions is consistent with the photochemical production of 3.2  $\mu\text{M}$  Fe(II) in Lp suspensions with 50  $\mu\text{M}$  EDTA measured in the presence of a large excess of phen (Fig. 1). At pH 6, the rate of Lp dissolution was 31 times faster after than before 5 min illumination.



Under oxic conditions at both pH 6 and 7, intermittent illuminations resulted in slight increases in  $[\text{Fe}]_{\text{diss.}}$  at the end of the illumination period, but further dissolution was not significantly accelerated compared to that prior to illumination. The (apparent) step increase in  $[\text{Fe}]_{\text{diss.}}$  is consistent with our prior *in situ* observation of accelerated Lp dissolution during illumination under oxic conditions. Our prior experiments also showed no persistence of the accelerated dissolution subsequent to illumination. Adsorbed Fe(II) and dissolved complexed Fe(II)EDTA are known to be oxidized quickly by dissolved oxygen.<sup>19, 29</sup> Thus our observations indicate that photochemically formed Fe(II) (whether in the bulk or on the surface of Lp) is not protected from fast oxidation.

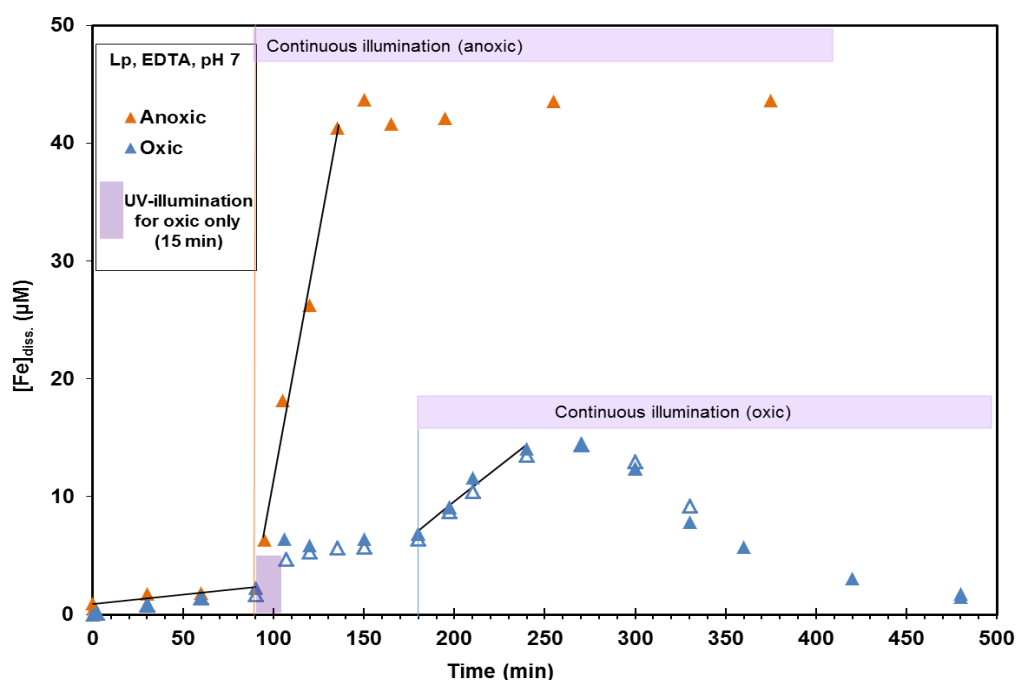


**Figure 3.** Comparison of Lp dissolution with 50  $\mu\text{M}$  EDTA at pH 7.0, under anoxic and oxic conditions. Under anoxic conditions, continuous UV-illumination was applied from 90-400 min. Under oxic conditions, a single illumination of 15 min from 90-105 min was followed by continuous illumination from 180-500 min. Replicate experiments are shown with open symbols. Slopes were determined from the linear fits to the data points, as shown by solid lines. Anoxic continuous illumination led to very rapid formation of  $\text{Fe}_{\text{diss}}$  up to  $43\mu\text{M}$ , while oxic continuous illumination led to slower formation of only  $15\mu\text{M}$   $\text{Fe}_{\text{diss}}$  and a decrease of  $[\text{Fe}]_{\text{diss}}$  with longer illumination times.

Observations under continuous illumination (Fig. 3) can provide additional insight into the effects of intermittent illumination. Under anoxic conditions,  $[\text{Fe}]_{\text{diss}}$  in Lp exposed to continuous illumination in the presence of EDTA at pH 7 increased rapidly and nearly linearly to a final concentration of  $43\mu\text{M}$  (orange triangles). The dissolution rate during illumination was 27 times faster

than the initial rate (prior to UV illumination). A less pronounced effect (5-fold increase) was observed under oxic conditions. The rate under continuous illumination is consistent with the step change in  $[\text{Fe}]_{\text{diss.}}$  observed after 15-min intermittent illumination (Fig. 3, blue triangles). Under continuous illumination,  $[\text{Fe}]_{\text{diss.}}$  reached a maximum value of 15  $\mu\text{M}$  at 240 min and then decreased, suggesting photolysis of Fe(III)EDTA complexes.

**In the presence of DFOB.** Figure 4 shows comparable experiments (though conducted at pH 7 and 8.5) with DFOB instead of EDTA. Before illumination,  $[\text{Fe}]_{\text{diss.}}$  increased only slowly and at the same rates (Table 1) under anoxic (orange) and oxic (blue) conditions. The dissolution rate was 2 times faster at pH 8.5 than at pH 7.0. The dissolution rate at pH 7 under anoxic condition is in good agreement with our previously-reported values.<sup>26</sup> (see SI, Table S2)

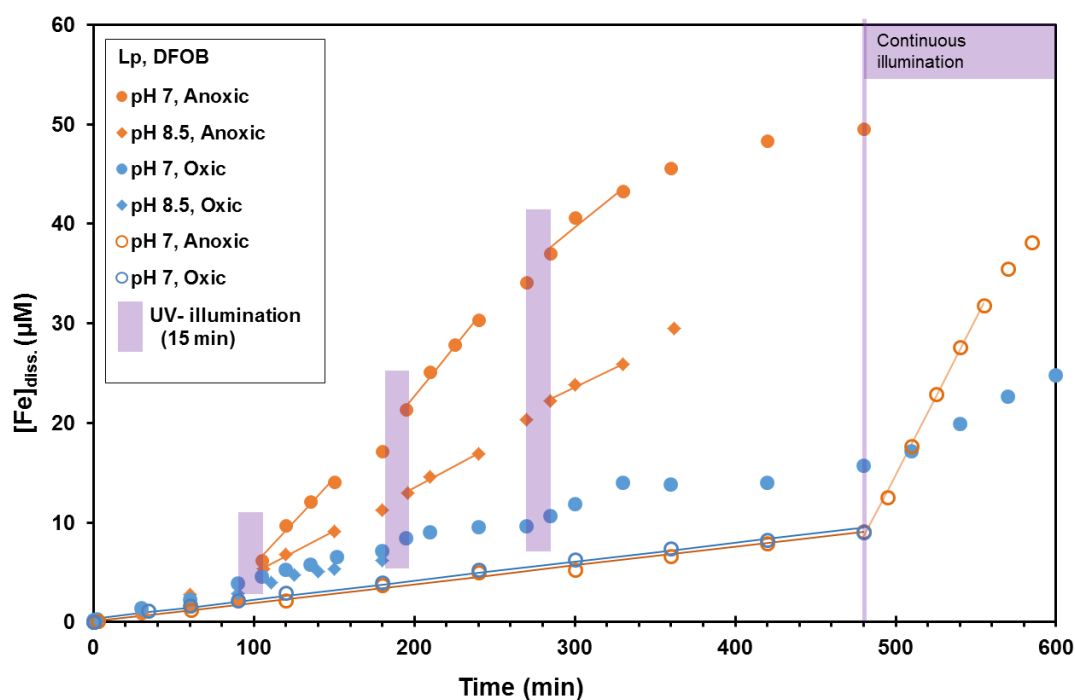


**Figure 4.** Lp dissolution in the presence of 50  $\mu\text{M}$  DFOB. Three intermittent illuminations with UV-A of 15 min each, are indicated with purple bars (90-105, 180-195, 270-285 min).  $\text{Fe}_{\text{diss}}$  was formed at accelerated rates after intermittent illuminations under anoxic, but not under oxic conditions, both at pH 7.0 and pH 8.5. Note that no data was collected during intermittent illumination. Continuous illumination was applied from 480-600 min. For pH 7.0, anoxic (open orange circles) and oxic (open blue circles) no intermittent illuminations were applied prior to continuous illumination (480-600 min), which led to accelerated dissolution under both anoxic and oxic conditions. The acceleration was a factor of 2-3 larger under the anoxic condition. Colored solid lines represent the linear fits to selected data points for slope determination.

Under anoxic conditions, intermittent UV-illumination periods led to accelerated Lp dissolution that persisted in the dark. At pH 7,  $[\text{Fe}]_{\text{diss}}$  (orange circles) reached 50  $\mu\text{M}$  in 450 min in response to three intermittent 15 min illuminations, corresponding to a ca. 9-fold increase in the dissolution rate. Our measurements with phen indicate that 2.9  $\mu\text{M}$  of Fe(II) were produced during each 15 min illumination. In our previous study,<sup>26</sup> addition of 1  $\mu\text{M}$  Fe(II) resulted in an 18-fold increase in Lp dissolution in the presence of DFOB. Although the effect with added Fe(II) is larger than we observed in the photochemical experiments, it is possible that some photo-produced Fe(II) might be oxidized due to concurrent formation of oxidants such as  $\text{H}_2\text{O}_2$ . Figure 4 also shows the result of exposing Lp suspensions in the presence of DFOB (pH 7) to continuous illumination without prior intermittent illumination (orange open circles). Under continuous illumination, the Lp dissolution rate was accelerated by a factor of 16 (nearly twice that observed with intermittent illumination). At pH 8.5, nearly-linear Lp dissolution continued with the first 15-min UV illumination at a rate 2-fold the initial dissolution rate (prior to UV illumination) (Table 1).

Under oxic conditions, reliable estimates of accelerated dissolution rates could be obtained only under continuous illumination. This was examined only for pH 7, where a 5.5-fold increase in the dissolution rate was observed. This dissolution rate is roughly consistent with the step changes in  $[\text{Fe}]_{\text{diss}}$  observed after intermittent illumination.

**EDTA vs DFOB (Oxic).** Since dissolution under oxic conditions is more easily assessed during continuous illumination, we conducted such experiments with DFOB at pH 7. In Figure 5, results with DFOB are shown together with the results with EDTA (previously shown as blue triangles in Fig. 3). In contrast with EDTA,  $[\text{Fe}]_{\text{diss}}$  in the presence of DFOB does not decline after reaching a maximum value. The Lp dissolution rate under continuous illumination (initially 5.5-fold faster than the rate without UV illumination) appears to slow down after 480 min with  $[\text{Fe}]_{\text{diss}}$  reaching a plateau at ca. 35  $\mu\text{M}$ . Thus, both DFOB and EDTA appear to have similar effects on Lp dissolution under continuous illumination initially; the persistence of the accelerating effect with DFOB is consistent with its being a more photo-stable ligand<sup>17, 21</sup> than EDTA. Although DFOB appears to be able to complex Fe(III) over time periods of hours in irradiated solutions, the decrease in dissolution rate and the eventual plateau in  $[\text{Fe}]_{\text{diss}}$  suggests that Fe(II) may react with oxidants accumulated during the

illumination (e.g.  $\text{H}_2\text{O}_2$ )<sup>17</sup> and/or that DFOB may undergo some photo-degradation over longer periods or illumination.

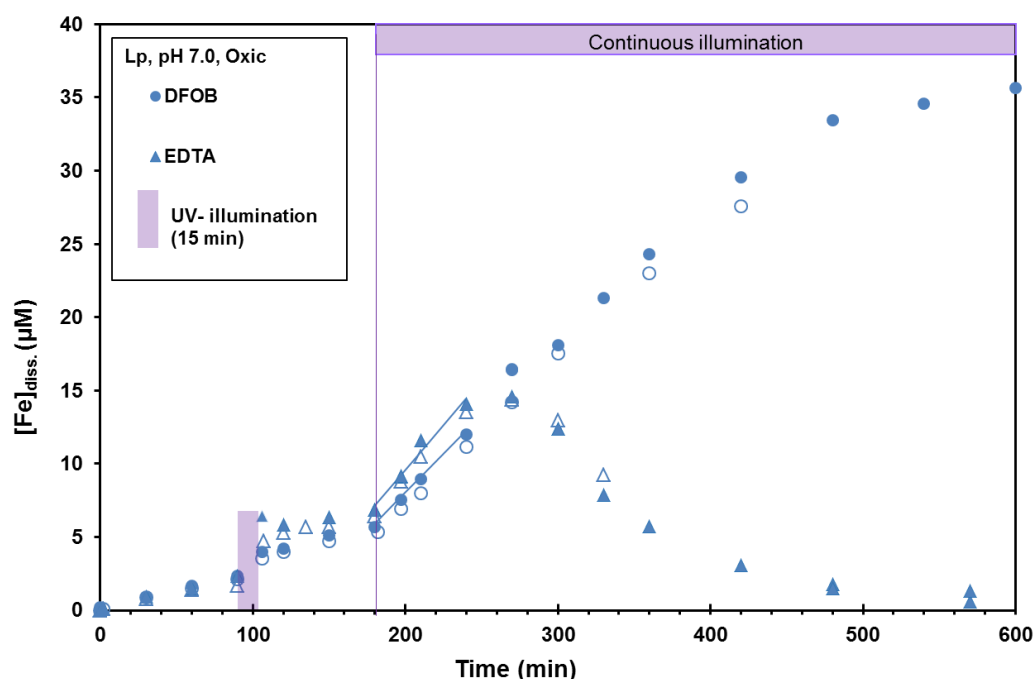


**Figure 5.** Lp dissolution (oxic; pH 7.0) in the presence of 50  $\mu\text{M}$  EDTA or DFOB. One intermittent illumination from 90-105 min is indicated by a purple bar. From 180-600 min, continuous illumination was applied. Replicate experiments are shown with open symbols. Note that data for EDTA was shown already in Fig. 3. Lp dissolution with DFOB continued in the light, indicating that Fe(III)DFOB complexes are not or only slowly photolyzed. With EDTA,  $[\text{Fe}]_{\text{diss}}$  declines rapidly after 280 min, due to photolysis of Fe(III)EDTA complexes and degradation of EDTA. Slopes were determined from the linear fits to the data points, as shown by solid lines.

As discussed above, the effects of intermittent illumination under oxic conditions are very difficult to assess. Additional experiments with both EDTA and DFOB (Fig. S5) showed only inconsistent effects. Transformation of Lp to any other Fe(III) phase was not detected with IR (infrared) spectroscopy after continuous illumination of Lp in the presence of either EDTA or DFOB (Fig. S6).

**EDTA vs DFOB (anoxic).** Figure 6 shows a comparison of the effects of EDTA and DFOB for single UV illuminations of 5 and 15 min at pH 7. The data for the 5 min illumination with EDTA was also shown in Figure 2 (filled orange triangles). For both illumination periods, the effect of EDTA is greater than that of DFOB; this is particularly noticeable when the illumination period is the

same for both ligands. This effect of the illumination period for EDTA as well as the difference between EDTA and DFOB are consistent with the concentrations of photoproducted Fe(II) shown in Figure 1 for Lp ( $3.2\ \mu\text{M}$  for 5-min and  $>8\ \mu\text{M}$  for 15-min illumination with EDTA and  $2.9\ \mu\text{M}$  for 15-min illumination with DFOB).

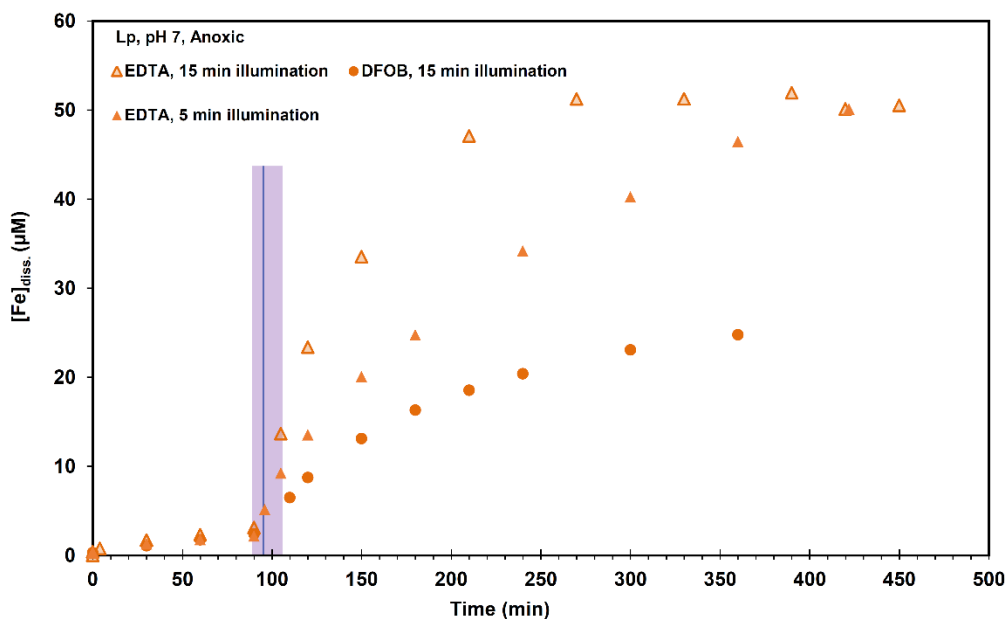


**Figure 6.** Comparison of EDTA vs DFOB in Lp dissolution (anoxic; pH 7.0). UV-A illuminations from 90-105 min for EDTA and DFOB, and 90-95 min for EDTA indicated with purple bar, were applied to  $1.13\ \text{mM}$  Lp suspensions in the presence of  $50\ \mu\text{M}$  DFOB or EDTA. Note that data for EDTA with 5 min illumination was already shown in Figure 2.

### Effect of intermittent UV-A illumination on goethite dissolution

Figure 7 shows Gt dissolution at pH 7 in the presence of EDTA and DFOB before and after intermittent illuminations. Before illumination, Gt dissolution was very slow ( $R = 0.01\% \text{ hr}^{-1}$  with EDTA, and not detectable with DFOB). Intermittent illumination under anoxic conditions with EDTA resulted in a step change in  $[\text{Fe}]_{\text{diss.}}$  (open orange triangles). Accelerated dissolution persisted after illumination ceased. The accelerating effect was roughly 36-fold (average of three rates) for each of the three intermittent illumination periods (Table 1). In contrast, intermittent illumination of Gt in the presence of DFOB had no effect under anoxic conditions (open orange circles); neither was any effect observed under oxic conditions (data not shown).

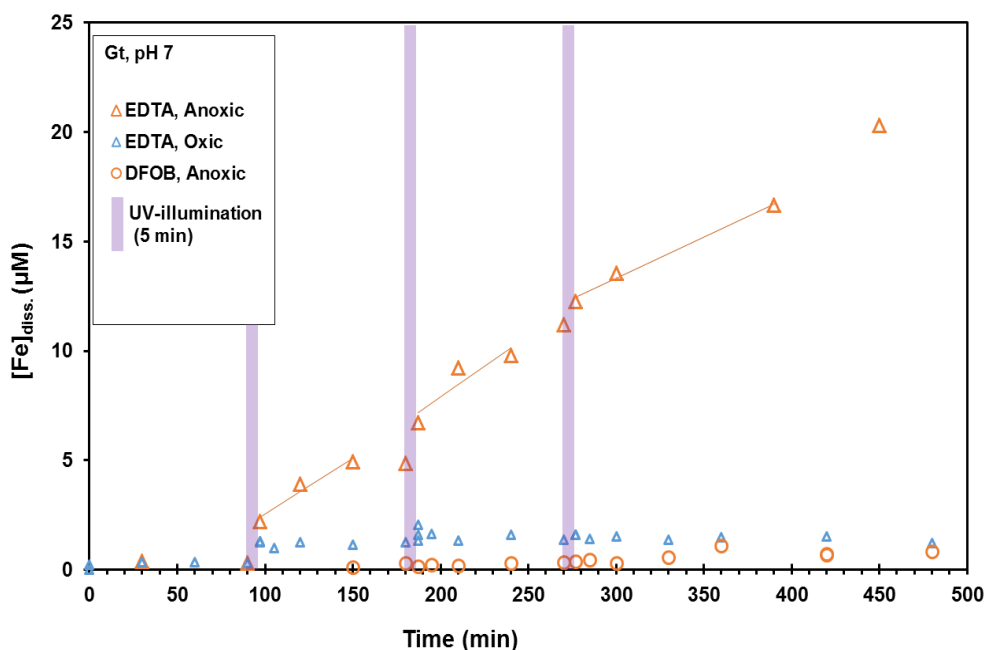


**Figure 7.** Goethite dissolution in the presence of 50  $\mu\text{M}$  EDTA or DFOB at pH 7.0. Intermittent illumination intervals with UV-A, indicated with purple bar, were applied from 90-95, 180-185, 270-275 min. Lines represent the linear fits to the data. Intermittent illumination led to accelerated dissolution in the dark only in the presence of EDTA under anoxic condition. With DFOB,  $[\text{Fe}]_{\text{diss}}$  remained too low for the determination of dissolution rates even under anoxic condition and was not measurable under oxic condition.

Under oxic conditions with EDTA, the first intermittent illumination (5 min) appeared to result in a small step-increase in  $[\text{Fe}]_{\text{diss.}}$  (open blue triangles), but no persistent accelerated dissolution was observed and even the step-increase was not observed in subsequent intermittent illuminations.

### Contrasting photochemical properties of Lp and Gt under anoxic conditions

Because the ligand-promoted (i.e., dark) dissolution rate of Gt was so much slower than that of Lp, the largest effect of intermittent illumination was observed with Gt/EDTA (average 36-fold acceleration). For Lp dissolution, the enhancement with EDTA (under intermittent illumination) was a factor of 8 (see Figure 8). This difference cannot be explained by the photoproduction of Fe(II) since this was nearly the same for both solids: 2.7  $\mu\text{M}$  for Gt and 3.2  $\mu\text{M}$  for Lp in 5 min of illumination (Table 1). In contrast, the lack of any detectable effect of intermittent illumination with DFOB and Gt is consistent with the negligible Fe(II) photoproduction (0.17  $\mu\text{M}$  over 15 min). In addition, the similar effects of EDTA and DFOB on Lp dissolution subject to intermittent illumination for 5 or 15-min

periods was consistent with the concentration of Fe(II) generated photochemically over these illumination periods (3.2  $\mu\text{M}$  for EDTA over 5 min and 2.9  $\mu\text{M}$  for DFOB over 15 min).

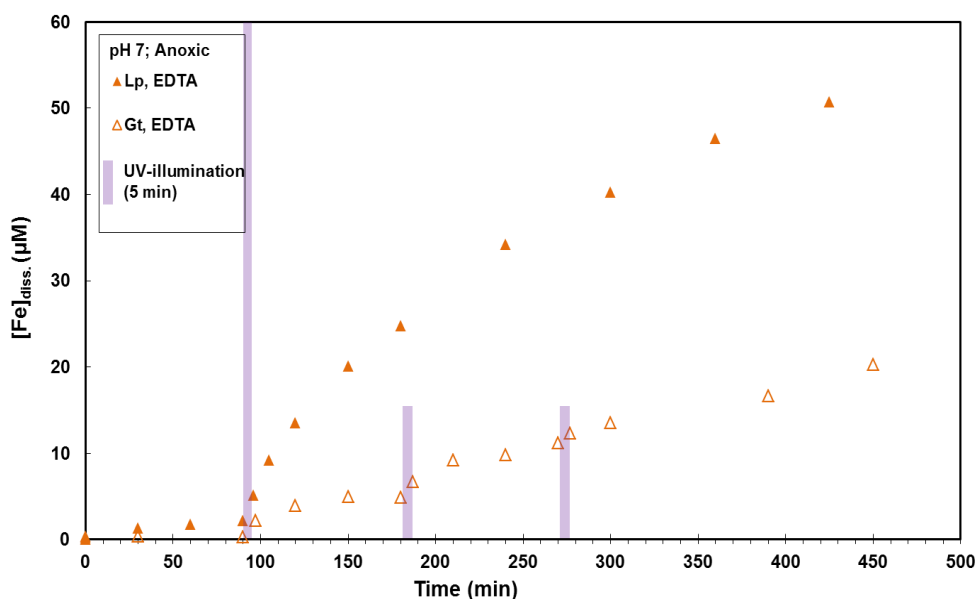


**Figure 8.** Comparison of Lp and Gt dissolution in the presence of 50  $\mu\text{M}$  EDTA at pH 7 under anoxic conditions. The data are already shown for Lp in Fig.2 and for Gt in in Fig. 7. After one 5 min of UV illumination, accelerated Lp dissolution continued until all free EDTA in solution was used up. In contrast, three 5 min intermittent UV illuminations led to only 20  $\mu\text{M}$   $[\text{Fe}]_{\text{diss}}$  in Gt suspension.

## Environmental Implications

Fe(III)(hydr)oxides are ubiquitous on soil-water interfaces and as suspended particles in the water column of aquatic environments that are exposed to sunlight. Understanding the role of photoreactions in the dissolution pathways of Fe(III)(hydr)oxides in redox dynamic environments is an important step to better comprehend the cycles of Fe and other (trace) elements in natural environments. The findings from this study, that Fe(II) produced upon very brief exposure to light can act as a catalyst for continued accelerated dissolution, may allow us to predict the bioavailability of iron and the mobility of associated trace elements in different environments.

Under anoxic conditions, brief periods of illumination accelerate the dissolution of Fe(III)(hydr)oxides (both Lp and Gt) by factors up to 40 with EDTA and DFOB, even after illumination stops. Anoxic environments that can be reached by sunlight exist in shallow lakes<sup>30</sup>, ponds<sup>31</sup> and reservoirs<sup>32, 33</sup>. Spatially limited and transient anoxic zones have been observed in algal bloom environments.<sup>34</sup> Sub-oxic and anoxic micro-environments caused by microbial reduction were

found in overall oxic water in cyanobacterial aggregates in surface blooms<sup>35</sup> or in settling fecal pellets and aggregates<sup>36</sup>. Light-induced dissolution of Fe-phases could thus play an important role in algal blooms, where rapid growth of cyanobacteria can be limited by bio-accessible iron.<sup>34</sup> Concentrations of ligands with reactive hydroxamate moieties were positively correlated to cyanobacterial biomass in lakes with low Fe bioavailability.<sup>37</sup>

Under oxic conditions, intermittent UV-illumination did not lead to accelerated dissolution after illumination stops. Continuous illumination, however, led to acceleration of the dissolution of Lp by factors of around 5 at pH 7.0, for both EDTA and DFOB. The rate of dissolution of Gt under oxic condition was very slow and could not be quantified in our experiments. In the photo-dissolution of Lp, EDTA and DFOB showed strongly contrasting behavior in their ability to mobilize Fe. With EDTA, a peak concentration in  $[\text{Fe}]_{\text{diss}}$  of 14  $\mu\text{M}$  was reached after 240 min then declined. With DFOB, a concentration of 16  $\mu\text{M}$  was reached after 240 min and increased to 35  $\mu\text{M}$  after 600 min. These observations show that photo-stable ligands are required to sustain higher concentrations of dissolved Fe under sunlit conditions. EDTA and most likely similar ligands with photo-active carboxylate groups can accelerate dissolution, but they are photodegraded rapidly. Ligands such as DFOB with hydroxamate groups are more photo-stable and are able to keep Fe in solution. In natural environments, ranges of ligands are present and may have different functions in the mobilization and bioavailability of Fe. The acceleration of dissolution processes by photochemically formed Fe(II) are highly dependent on structure of the Fe phase, the functional groups of the ligand, and the oxygen concentrations.

## Acknowledgements

We thank Thomas Rüttimann (Eawag) for laboratory experiments and technical assistance. This project was financially supported by the Swiss National Science Foundation, project number 200021L\_150150 “Synergistic effects of redox processes and ligand controlled dissolution of iron(hydr)oxide phases” Mathematics, Natural sciences and Engineering (division II). SK, WS and KK were supported by the Austrian Science Fund (FWF, Grant No.: I 1528-N19).



## References

1. Waite, T. D.; Morel, F. M. M., Photoreductive Dissolution of Colloidal Iron Oxides in Natural Waters. *Environ Sci Technol* **1984**, *18*, (11), 860-868.
2. Sulzberger, B.; Laubscher, H., Reactivity of Various Types of Iron(III) (Hydr)Oxides Towards Light-Induced Dissolution. *Mar Chem* **1995**, *50*, (1-4), 103-115.
3. Voelker, B. M.; Morel, F. M. M.; Sulzberger, B., Iron redox cycling in surface waters: Effects of humic substances and light. *Environ Sci Technol* **1997**, *31*, (4), 1004-1011.
4. Wells, M. L.; Mayer, L. M.; Donard, O. F. X.; Sierra, M. M. D.; Ackelson, S. G., The Photolysis of Colloidal Iron in the Oceans. *Nature* **1991**, *353*, (6341), 248-250.
5. Johnson, K. S.; Coale, K. H.; Elrod, V. A.; Tindale, N. W., Iron Photochemistry in Seawater from the Equatorial Pacific. *Mar Chem* **1994**, *46*, (4), 319-334.
6. Kuma, K.; Nakabayashi, S.; Matsunaga, K., Photoreduction of Fe(III) by Hydroxycarboxylic Acids in Seawater. *Water Res* **1995**, *29*, (6), 1559-1569.
7. Pehkonen, S. O.; Siefert, R.; Erel, Y.; Webb, S.; Hoffmann, M. R., Photoreduction of Iron Oxyhydroxides in the Presence of Important Atmospheric Organic-Compounds. *Environ Sci Technol* **1993**, *27*, (10), 2056-2062.
8. Faust, B. C.; Hoigne, J., Photolysis of Fe(III)-Hydroxy Complexes as Sources of Oh Radicals in Clouds, Fog and Rain. *Atmos Environ a-Gen* **1990**, *24*, (1), 79-89.
9. Faust, B. C.; Zepp, R. G., Photochemistry of Aqueous Iron(III) Polycarboxylate Complexes - Roles in the Chemistry of Atmospheric and Surface Waters. *Environ Sci Technol* **1993**, *27*, (12), 2517-2522.
10. Fu, H. B.; Cwiertny, D. M.; Carmichael, G. R.; Scherer, M. M.; Grassian, V. H., Photoreductive dissolution of Fe-containing mineral dust particles in acidic media. *J Geophys Res-Atmos* **2010**, *115*.
11. Kim, K.; Choi, W.; Hoffmann, M. R.; Yoon, H. I.; Park, B. K., Photoreductive Dissolution of Iron Oxides Trapped in Ice and Its Environmental Implications. *Environ Sci Technol* **2010**, *44*, (11), 4142-4148.
12. Goldberg, M. C.; Cunningham, K. M.; Weiner, E. R., Aquatic Photolysis - Photolytic Redox Reactions between Goethite and Adsorbed Organic-Acids in Aqueous-Solutions. *J. Photochem. Photobiol. A* **1993**, *73*, (2), 105-120.
13. Litter, M. I.; Baumgartner, E. C.; Urrutla, G. A.; Blesa, M. A., Photodissolution of Iron Oxides. 3. Interplay of Photochemical and Thermal Processes in Maghemite/Carboxylic Acid Systems. *Environ Sci Technol* **1991**, *25*, (11), 1907-1913.
14. Kraemer, S. M.; Butler, A.; Borer, P.; Cervini-Silva, J., Siderophores and the dissolution of iron-bearing minerals in marine systems. *Rev. Mineral. Geochem.* 2005; Vol. 59, pp 53-84.

15. Barbeau, K.; Rue, E. L.; Trick, C. G.; Bruland, K. T.; Butler, A., Photochemical reactivity of siderophores produced by marine heterotrophic bacteria and cyanobacteria based on characteristic Fe(III) binding groups. *Limnol Oceanogr* **2003**, *48*, (3), 1069-1078.
16. Waite, T. D., Photo-Redox Processes at the Mineral-Water Interface. *Rev Mineral* **1990**, *23*, 559-603.
17. Borer, P.; Sulzberger, B.; Hug, S. J.; Kraemer, S. M.; Kretzschmar, R., Photoreductive dissolution of iron(III) (Hydr)oxides in the absence and presence of organic ligands: Experimental studies and kinetic modeling. *Environ Sci Technol* **2009**, *43*, (6), 1864-1870.
18. Litter, M. I.; Blesa, M. A., Photodissolution of iron oxides. I. Maghemite in EDTA solutions. *J. Colloid Interface Sci.* **1988**, *125*, (2), 679-687.
19. Karametaxas, G.; Hug, S. J.; Sulzberger, B., Photodegradation of EDTA in the Presence of Lepidocrocite. *Environ Sci Technol* **1995**, *29*, (12), 2992-3000.
20. Sulzberger, B.; Laubscher, H., Photochemical Reductive Dissolution of Lepidocrocite - Effect of Ph. In *Aquatic Chemistry - Interfacial and Interspecies Processes*, Huang, C. P.; Omelia, C. R.; Morgan, J. J., Eds. Amer Chemical Soc: Washington, 1995; Vol. 244, pp 279-290.
21. Borer, P. M.; Sulzberger, B.; Reichard, P.; Kraemer, S. M., Effect of siderophores on the light-induced dissolution of colloidal iron(III) (hydr)oxides. *Mar Chem* **2005**, *93*, (2-4), 179-193.
22. Borer, P.; Hug, S. J.; Sulzberger, B.; Kraemer, S. M.; Kretzschmar, R., Photolysis of citrate on the surface of lepidocrocite: An in situ attenuated total reflection infrared spectroscopy study. *J. Phys. Chem. C* **2007**, *111*, (28), 10560-10569.
23. Borer, P.; Hug, S. J., Photo-redox reactions of dicarboxylates and  $\alpha$ -hydroxydicarboxylates at the surface of Fe(III)(hydr)oxides followed with in situ ATR-FTIR spectroscopy. *J. Colloid Interface Sci.* **2014**, *416*, 44-53.
24. Biswakarma, J.; Kang, K.; Borowski, S. C.; Schenkeveld, W. D. C.; Kraemer, S. M.; Hering, J. G.; Hug, S. J., Fe(II)-Catalyzed Ligand-Controlled Dissolution of Iron(hydr)oxides. *Environ Sci Technol* **2019**, *53*, (1), 88-97.
25. Kang, K.; Schenkeveld, W. D. C.; Biswakarma, J.; Borowski, S. C.; Hug, S. J.; Hering, J. G.; Kraemer, S. M., Low Fe(II) Concentrations Catalyze the Dissolution of Various Fe(III) (hydr)oxide Minerals in the Presence of Diverse Ligands and over a Broad pH Range. *Environ Sci Technol* **2019**, *53*, (1), 98-107.
26. Biswakarma, J.; Kang, K.; Borowski, S. C.; Schenkeveld, W. D. C.; Kraemer, S. M.; Hering, J. G.; Hug, S. J., Linking Isotope-Exchange with Fe(II)-Catalyzed Dissolution of Iron (hydr)oxides in the Presence of Bacterial Siderophore Deferoxamine-B. *Environ Sci Technol* **2020**, *54*, (2), 768-777.
27. Hug, S. J.; Canonica, L.; Wegelin, M.; Gechter, D.; Von Gunten, U., Solar oxidation and removal of arsenic at circumneutral pH in iron containing waters. *Environ Sci Technol* **2001**, *35*, (10), 2114-2121.

28. Hatchard, C. G.; Parker, C. A., A New Sensitive Chemical Actinometer .2. Potassium Ferrioxalate as a Standard Chemical Actinometer. *Proc R Soc Lon Ser-A* **1956**, 235, (1203), 518-536.
29. Kari, F. G.; Hilger, S.; Canonica, S., Determination of the Reaction Quantum Yield for the Photochemical Degradation of Fe(III)-EDTA- Implications for the Environmental Fate of EDTA in Surface Waters. *Environ Sci Technol* **1995**, 29, (4), 1008-1017.
30. Oswald, K.; Milucka, J.; Brand, A.; Littmann, S.; Wehrli, B.; Kuypers, M. M. M.; Schubert, C. J., Light-Dependent Aerobic Methane Oxidation Reduces Methane Emissions from Seasonally Stratified Lakes. *Plos One* **2015**, 10, (7).
31. Finlay, B. J.; Maberly, S. C.; Esteban, G. F., Spectacular abundance of ciliates in anoxic pond water: Contribution of symbiont photosynthesis to host respiratory oxygen requirements. *Fems Microbiol Ecol* **1996**, 20, (4), 229-235.
32. Townsend, S. A., The seasonal pattern of dissolved oxygen, and hypolimnetic deoxygenation, in two tropical Australian reservoirs. *Lakes & Reservoirs: Science, Policy and Management for Sustainable Use* **1999**, 4, (1-2), 41-53.
33. Hamre, K. D.; Lofton, M. E.; McClure, R. P.; Munger, Z. W.; Doubek, J. P.; Gerling, A. B.; Schreiber, M. E.; Carey, C. C., In situ fluorometry reveals a persistent, perennial hypolimnetic cyanobacterial bloom in a seasonally anoxic reservoir. *Freshw. Sci.* **2018**, 37, (3), 483-495.
34. Zhang, T.; He, J.; Luo, X., Effect of Fe and EDTA on Freshwater Cyanobacteria Bloom Formation. *Water* **2017**, 9, (5), 326.
35. Ploug, H., Cyanobacterial surface blooms formed by *Aphanizomenon* sp and *Nodularia spumigena* in the Baltic Sea: Small-scale fluxes, pH, and oxygen microenvironments. *Limnol Oceanogr* **2008**, 53, (3), 914-921.
36. Shaked, Y.; Lis, H., Disassembling Iron Availability to Phytoplankton. *Front. Microbiol.* **2012**, 3, (123).
37. Sorichetti, R. J.; Creed, I. F.; Trick, C. G., Iron and iron-binding ligands as cofactors that limit cyanobacterial biomass across a lake trophic gradient. *Freshw. Biol.* **2016**, 61, (1), 146-157.

## Supporting Information

---

- Table S1.** List of chemicals
- Table S2.** List of dissolution rates and catalytic effects from previous studies (Chapter 2 & 3)
- Figure S1.** Emission spectrum of the UV-source and absorbance spectra of Lp, Gt, Fe(III)EDTA and Fe(III)DFOB.
- Figure S2.** Determination of photoproduced Fe(II)
- Figure S3.** Formation of Fe(III)EDTA
- Figure S4.** Formation of Fe(III)DFOB
- Figure S5.** Effect of intermittent illumination (oxic; pH 7.0): Lp dissolution with EDTA vs DFOB
- Figure S6.** Infrared spectra of Lp before and after continuous illumination with UV light in aerated suspensions of Lp and EDTA/DFOB (pH 7.0)

Table S1. List of chemicals used for the current study

<b>Chemical Name</b>	<b>Chemical formale</b>	<b>Supplier</b>	<b>Purity</b>	<b>Stock solution (mM)</b>
Sodium Chloride	NaCl	Merck	>99%	10
Iron(II) Chloride	FeCl <sub>2</sub> . 4H <sub>2</sub> O	Sigma-Aldrich	>99%	10
Iron(III) Chloride	FeCl <sub>3</sub> . 6H <sub>2</sub> O	Sigma-Aldrich	>98%	10
EDTA (Ethylenediamine tetra acetic disodium dihydrate)	C <sub>10</sub> H <sub>14</sub> N <sub>2</sub> Na <sub>2</sub> O <sub>8</sub> . 2H <sub>2</sub> O	Merck	>99%	100
Mesylate salt of Desferrioxamine B	C <sub>25</sub> H <sub>48</sub> N <sub>6</sub> O <sub>8</sub> .CH <sub>4</sub> O <sub>3</sub> S	Sigma-Aldrich	>92.5%	100
MES (2-morpholino-ethane sulfonic acid monohydrate)	C <sub>6</sub> H <sub>13</sub> NO <sub>4</sub> S.H <sub>2</sub> O	Fluka	>99%	100
PIPES (Piperazine-1,4-bis(2-ethane sulfonic acid))	C <sub>8</sub> H <sub>18</sub> N <sub>2</sub> O <sub>6</sub> S <sub>2</sub>	Sigma-Aldrich	>99%	100
Sodium (bi)carbonate	NaHCO <sub>3</sub>	Sigma-Aldrich	>99%	3
o-Phenanthroline	C <sub>12</sub> H <sub>8</sub> N <sub>2</sub> .H <sub>2</sub> O	Fluka	>99%	10

Table S2. List of reported dissolution rates and catalytic effects.

Experimental conditions	Added [Fe(II)]	Lp dissolution rates			Catalytic Effect
	$\mu\text{M}$	% h <sup>-1</sup>	nM min <sup>-1</sup>	nmol s <sup>-1</sup> m <sup>-2</sup>	
Biswakarma et al. 2020 <sup>1</sup>					
20 $\mu\text{M}$ DFOB, pH 7.0	0	0.08	15.2	0.04	1
(carbonate buffer)	1	0.55	103	0.27	7
	2	1.03	194	0.51	13
	5	2.14	40	1.06	26
Kang et al 2019 <sup>2</sup>					
20 $\mu\text{M}$ DFOB, pH 7.0	0	-	-	0.07	1
(MOPS)	2	-	-	0.29	4
Biswakarma et al. 2020 <sup>1</sup>					
50 $\mu\text{M}$ DFOB, pH 7.0	0	0.11	20.2	0.05	1
(carbonate buffer)	1	1.44	270	0.71	13
	2	2.81	527	1.40	26
	5	6.42	1204	3.18	60
50 $\mu\text{M}$ DFOB, pH 7.0	0	0.06	12	0.03	1
(MOPS buffer)	2	0.65	122	0.32	10
50 $\mu\text{M}$ DFOB, pH 8.5	0	0.15	28.4	0.08	1
(PIPES buffer)	2	0.30	56.3	0.15	2
Biswakarma et al. 2019 <sup>3</sup>					
50 $\mu\text{M}$ EDTA, pH 6.0	0.0	0.16		0.08	1
(MES buffer)	0.2	1.07		0.53	7
	0.5	2.29		1.14	14
	1.0	3.08		1.53	19
	2.0	3.56		1.77	22
	4.0	4.13		2.05	26
	6.0	4.17		2.07	26
	10.0	4.97		2.48	31

<sup>1, 2</sup> Rates measured by formation of dissolved Fe in suspensions.<sup>3</sup> Rates measured by decrease of FeOOH infrared bands in ATR-FTIR experiments.

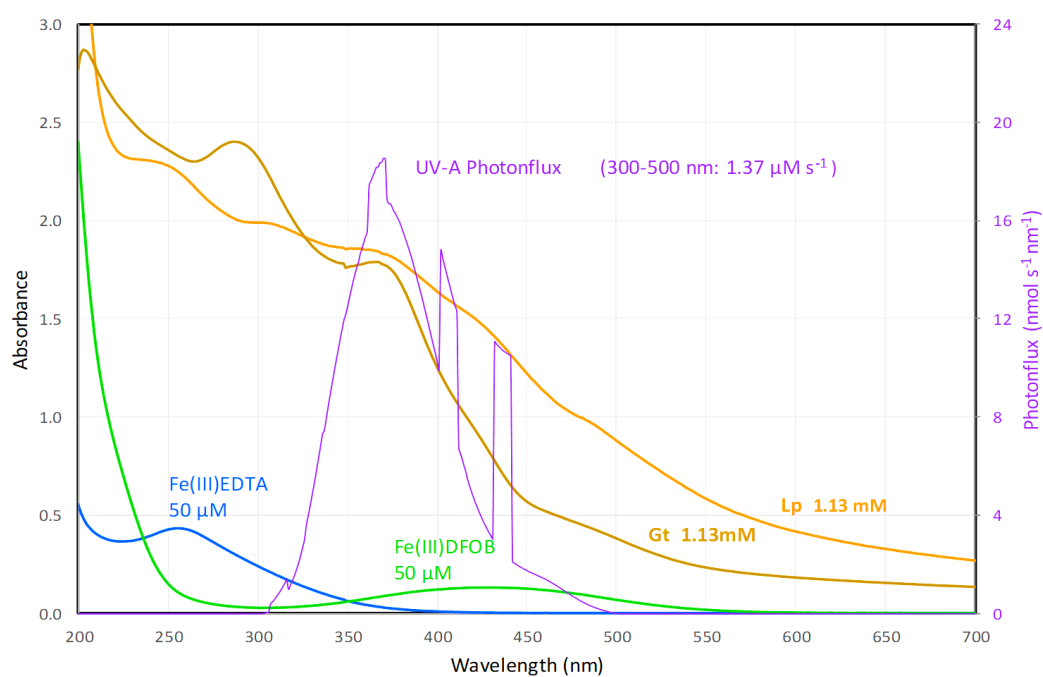


Figure S1. Emission spectrum of the UV-source and absorbance spectra of 1.13 mM Lp, 1.13 mM Gt, 50 μM Fe(III)EDTA and 50 μM Fe(III)DFOB.

The integrated light flux from 300-500 nm was 1.37 μM photons s<sup>-1</sup> and was >98% absorbed by the suspensions in pyrex bottles of 4 cm diameter.

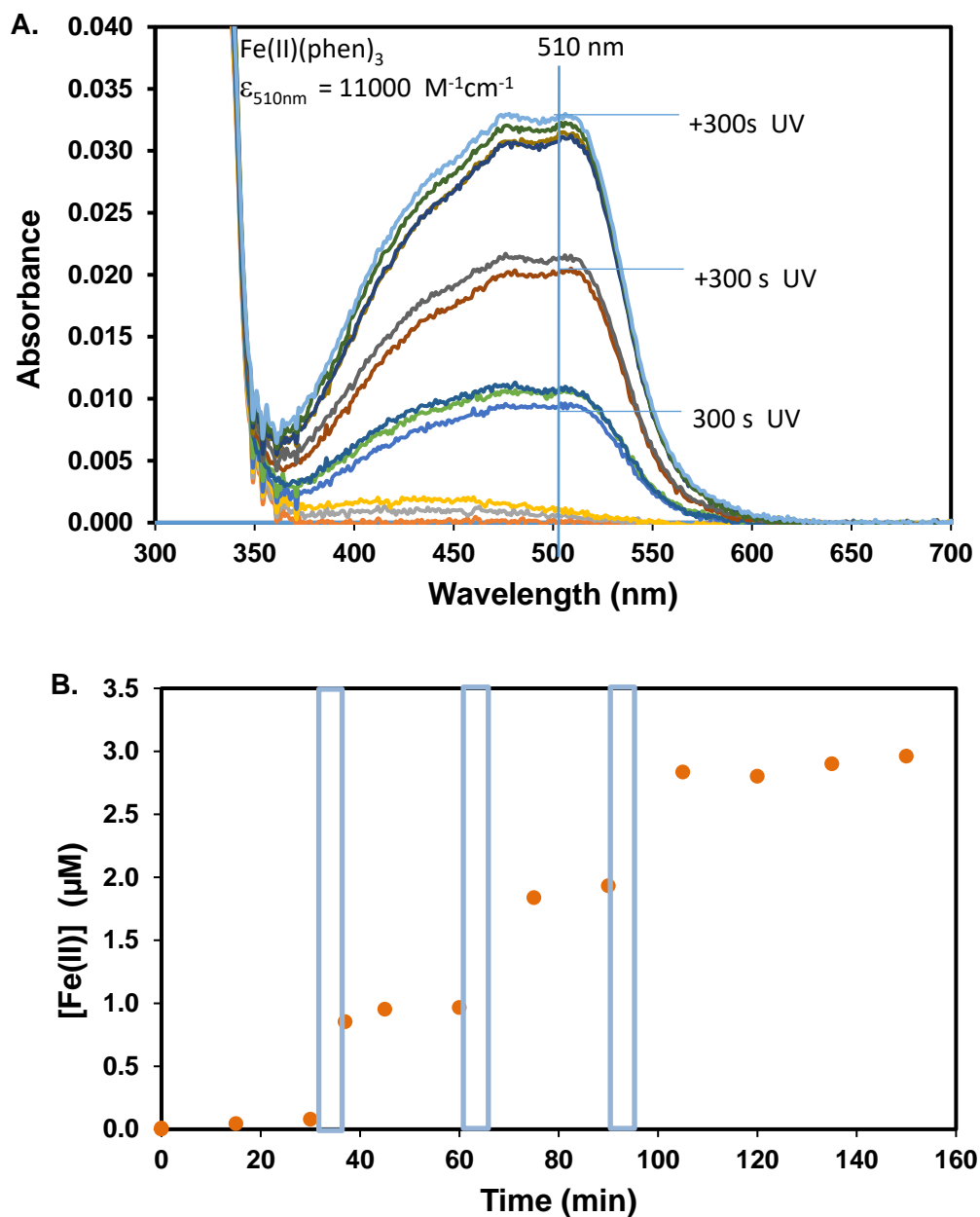


Figure S2. Determination of the photo-produced Fe(II) in a suspension of 10 mg Lp/100 ml (1125  $\mu\text{M}$  Lp) with 50  $\mu\text{M}$  DFOB and 473  $\mu\text{M}$  phenanthroline at pH 7 (3 mM  $\text{NaHCO}_3$ , 2%  $\text{CO}_2$  in  $\text{N}_2$ ). 2.0 ml aliquots were withdrawn and filtered (0.1  $\mu\text{m}$  nylon filter) and spectra were measured in 1 cm quartz-cuvettes. Spectra (baseline corrected) are shown in Fig. S1A (top), corresponding Fe(II)-concentrations (calculated from the absorbance at 510 nm) are shown in Fig. S1B (bottom). Each 5 min illumination produced  $1.0 \pm 0.1 \mu\text{M}$  Fe(II). Illumination periods (300 s) in Fig. S1B (bottom) are indicated with empty blue bars.



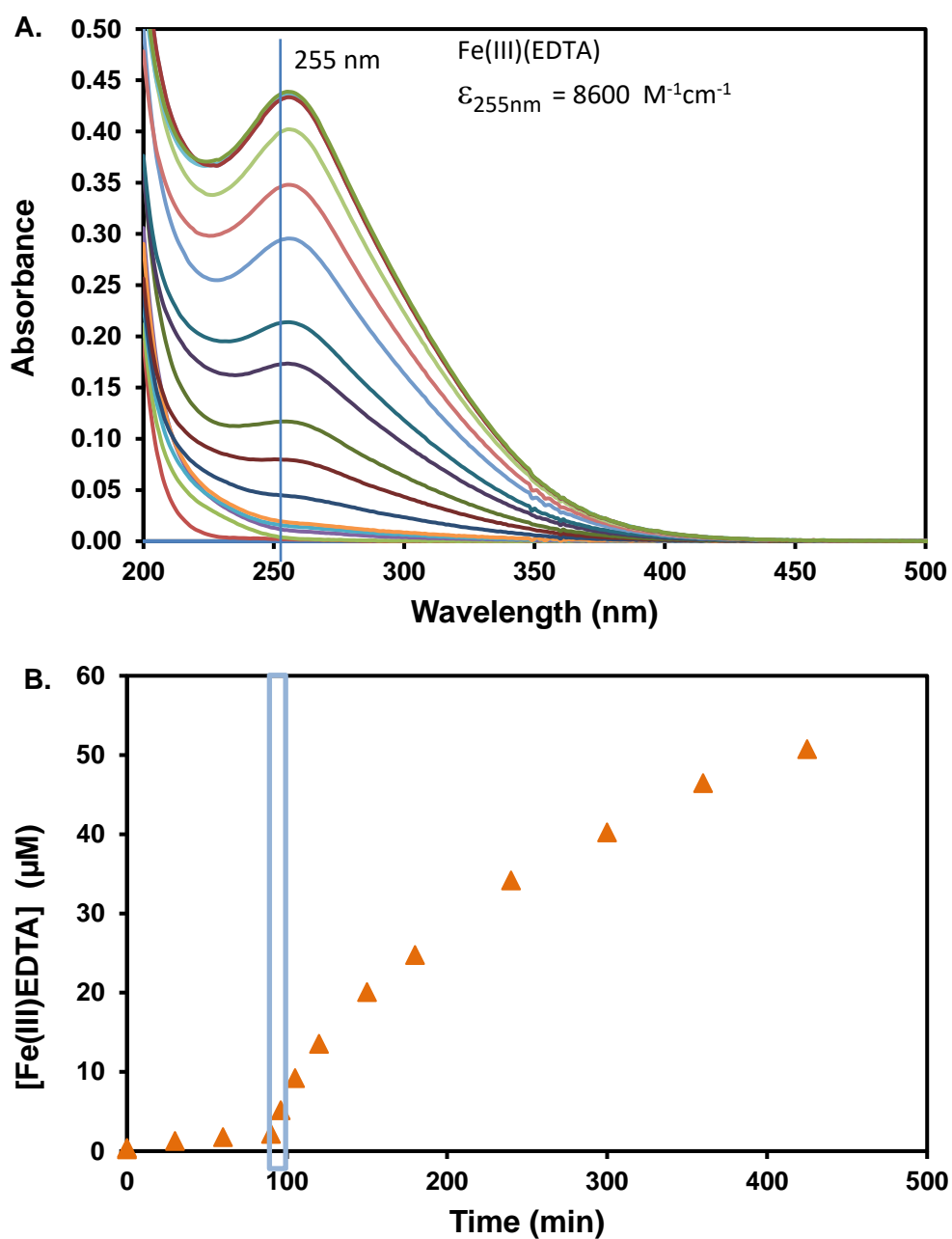


Figure S3. Formation of Fe(III)EDTA in a suspension of 10 mg/100 ml (1125  $\mu\text{M}$  Lp) with 50  $\mu\text{M}$  EDTA at pH 7 (3 mM  $\text{NaHCO}_3$ , 2%  $\text{CO}_2$  in  $\text{N}_2$ ). 2.0 ml aliquots were withdrawn and filtered (0.1  $\mu\text{m}$  nylon filter) and spectra were measured in 1 cm quartz-cuvettes. Spectra (baseline corrected) are shown in Fig. S2A (top), corresponding Fe(III)(EDTA)-concentrations (calculated from the absorbance at 255 nm) are shown in Fig. S2 B (bottom). UV-Illumination periods (90-95 min is indicated with blue rectangles).

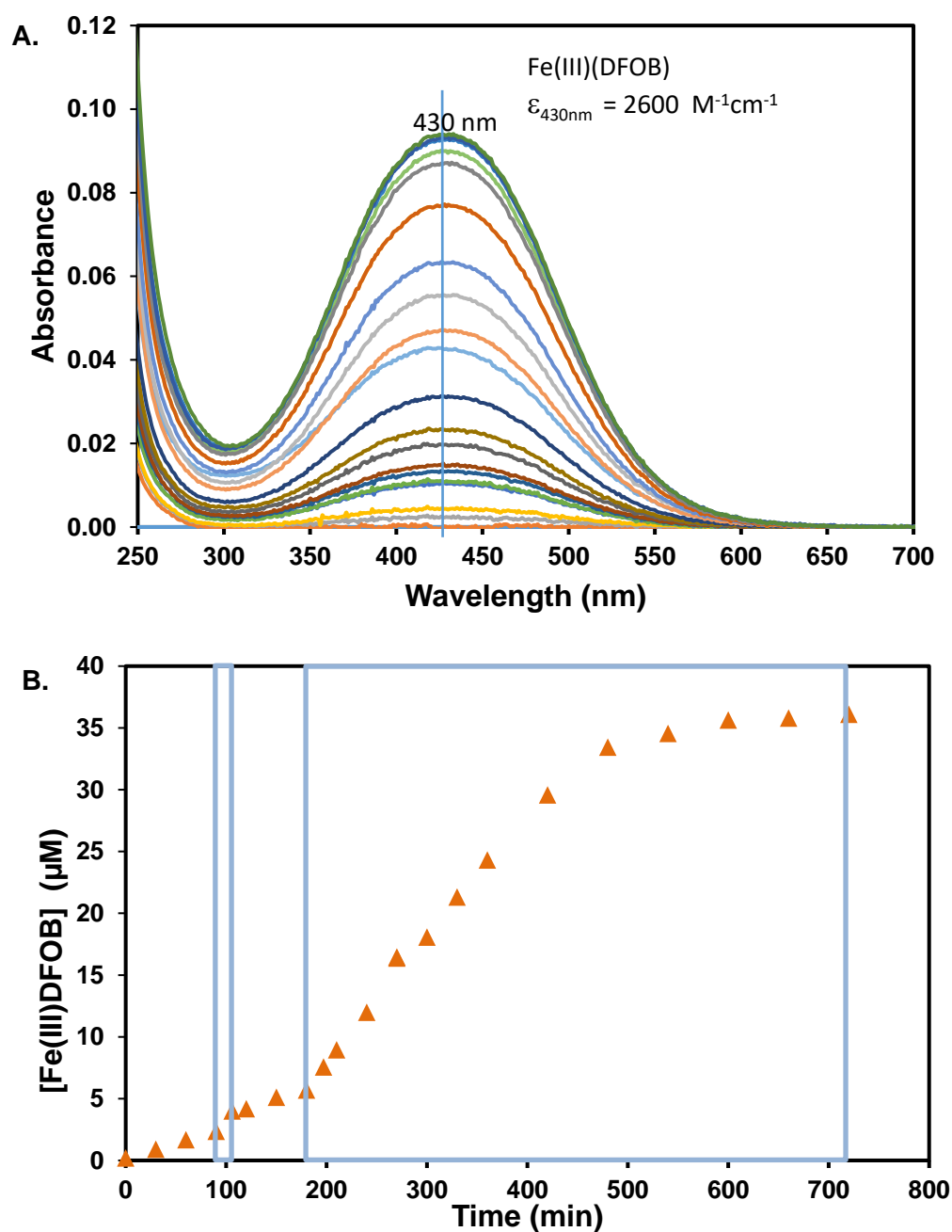


Figure S4. Formation of Fe(III)DFOB in a suspension of 10 mg/100 ml (1125  $\mu\text{M}$  Lp) with 50  $\mu\text{M}$  DFOB at pH 7 (3 mM  $\text{NaHCO}_3$ , 2%  $\text{CO}_2$  in air). 2.0 ml aliquots were withdrawn and filtered (0.1  $\mu\text{m}$  nylon filter) and spectra were measured in 1 cm quartz-cuvettes. Spectra (baseline corrected) are shown in Figure A (top), corresponding Fe(III)(DFOB)-concentrations (calculated from the absorbance at 430 nm) are shown in Figure B (bottom). UV-Illumination periods (90-105 min and 180-720 min) are indicated with blue rectangles.

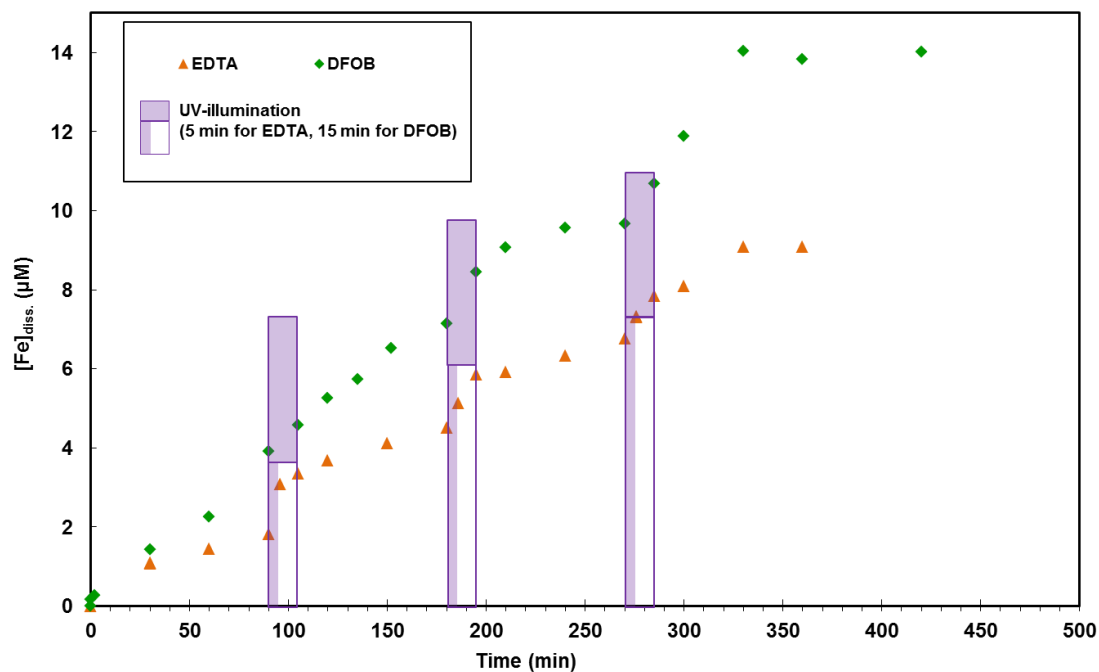


Figure S5. Comparison of EDTA vs DFOB in Lp dissolution (oxic; pH 7.0). Three intermittent illuminations (15 min for DFOB and 5 min for EDTA) were applied to 1.13 mM Lp suspension.  $[\text{Fe}]_{\text{diss.}}$  was minimally increased after each illumination.

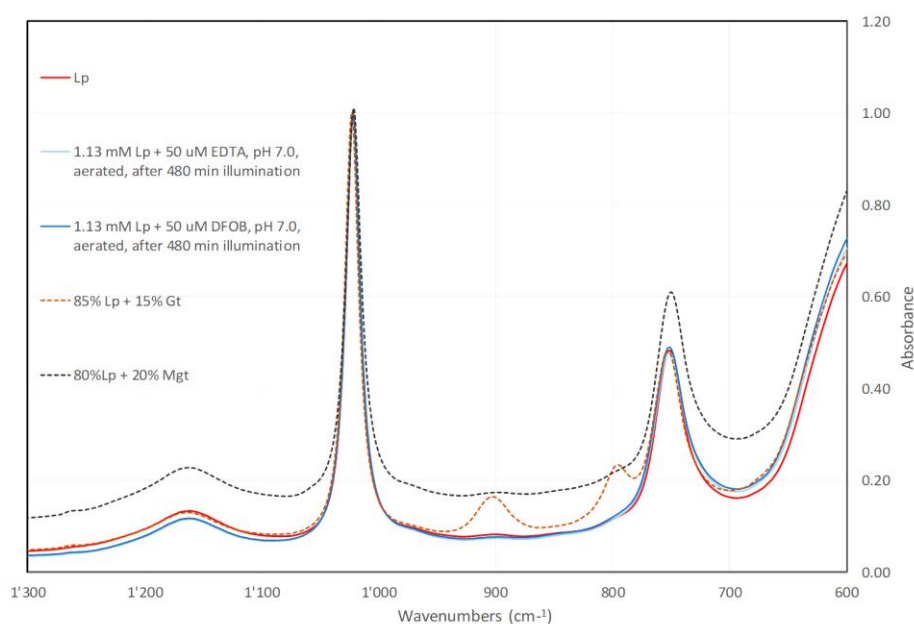


Figure S6. Infrared spectra of Lp before and after 480 min illumination with UV light in aerated suspensions of 1125  $\mu\text{M}$  Lp and 50  $\mu\text{M}$  EDTA or 50  $\mu\text{M}$  DFOB at pH 7.0 (3 mM  $\text{NaHCO}_3$ , 2%  $\text{CO}_2$  in air).

Samples (4 ml) were filtered through 4 mm diameter, 0.1  $\mu\text{m}$  nylon filters. Collected solids in the filter were rinsed with 2 ml  $\text{H}_2\text{O}$  to remove most of the adsorbed ligands, and stored at  $-20^\circ\text{C}$  until measurement of IR-spectra. Solids were re-suspended from the filter with 10-20  $\mu\text{l}$   $\text{H}_2\text{O}$ , and the suspensions were dried in a stream of  $\text{N}_2$  on the 4 mm diameter diamond ATR-disk of the ATR-FTIR instrument (Biorad FTS 575C). The spectra shown are the spectra of dried solids.

The spectra are compared to spectra of Lp before illumination, to Lp mixed with 15% Gt and to Lp with 20% magnetite (Mgt). For easier comparison, spectra were scaled to a common absorbance maximum of 1.0 at  $1121\text{ cm}^{-1}$ . No changes could be detected in the illuminated samples. As shown, formation of Gt or Mgt would have been easily detected by FTIR.

## References

1. Biswakarma, J.; Kang, K.; Borowski, S. C.; Schenkeveld, W. D. C.; Kraemer, S. M.; Hering, J. G.; Hug, S. J., Linking Isotope-Exchange with Fe(II)-Catalyzed Dissolution of Iron (hydr)oxides in the Presence of Bacterial Siderophore Deferoxamine-B *Environ Sci Technol* **2020**, *54* (2), 768-777.
2. Kang, K.; Schenkeveld, W. D. C.; Biswakarma, J.; Borowski, S. C.; Hug, S. J.; Hering, J. G.; Kraemer, S. M., Low Fe(II) Concentrations Catalyze the Dissolution of Various Fe(III) (hydr)oxide Minerals in the Presence of Diverse Ligands and over a Broad pH Range. *Environ Sci Technol* **2019**, *53*, (1), 98-107.
3. Biswakarma, J.; Kang, K.; Borowski, S. C.; Schenkeveld, W. D. C.; Kraemer, S. M.; Hering, J. G.; Hug, S. J., Fe(II)-Catalyzed Ligand-Controlled Dissolution of Iron(hydr)oxides. *Environ Sci Technol* **2019**, *53*, (1), 88-97.

## **Chapter 5**

### **CONCLUSION**

---

Iron (Fe) is an essential micro-nutrient for all living organisms. Despite the high abundance of Fe on our planet, the bioavailability of Fe at circumneutral to alkaline pH is limited. Low solubility and slow dissolution processes of Fe(III)(oxyhydr)oxides in oxic conditions cause Fe-limitations, which leads to Fe deficiencies for organisms.<sup>1</sup> Under Fe-deficient conditions, plants and micro-organisms can acquire Fe by releasing ligands (L) that promote the dissolution of Fe(III)(oxyhydr)oxides. Previous studies have demonstrated synergistic effects on ligand-promoted dissolution of Fe(III)(oxyhydr)oxides with two or more ligands of synthetic and/or natural origin.<sup>2-4</sup> Earlier studies reported accelerated rates of dissolution under anoxic conditions at low pH (3-5) by addition of Fe(II) in the presence of a ligand.<sup>5-7</sup> Recent laboratory studies have observed the synergistic effect between a ligand and a reductant on accelerated dissolution at circumneutral pH.<sup>8,9</sup> No systematic investigations, however, on the effect of Fe(II) on ligand-controlled dissolution at high pH (> 5) had been conducted before this doctoral study was performed.

More recent studies have shown that adsorption of Fe(II), in the absence of ligands, at circumneutral pH leads to phase transformations and recrystallization of Fe(III)(oxyhydr)oxides with no net dissolution. The process of recrystallization has been explained in terms of a “conveyor belt” model.<sup>10-13</sup> In this model, after the adsorption of Fe(II) electron conduction through the bulk solid leads to release of Fe(II) at a distant site. This model suggests that negative charge could reside in the bulk where the charge is protected from oxidation under oxic conditions. If this is the case, Fe(II) might accelerate dissolution processes also under oxic conditions and at circumneutral pH range. However, studies on the possibility of electron conduction through bulk solid in the presence of dissolution-promoting ligands had not been performed before this thesis was conducted.

This doctoral thesis systematically examined the accelerating effect of Fe(II) on Fe(III)(hydr)oxide dissolution in the presence and absence of dissolution-promoting ligands. The effect was studied at pH 6.0, 7.0 and 8.5, which is more relevant to natural systems than studies at low pH (3-5) conditions. Under these conditions, oxic and anoxic conditions were compared to account for the effects of Fe(II) oxidation which is much faster than at pH 3-5.

The overall aim of the thesis was to mechanistically understand the effect of Fe(II) on ligand-controlled dissolution. Specific aim was to investigate whether bulk electron conduction through solids, *if it occurs*, could retard the oxidation of Fe(II) and cause accelerated dissolution of Fe(III)(hydr)oxides under oxic conditions.

The study was conducted with two structurally different and laboratory synthesized Fe(III)(hydr)oxide minerals: 1.13 mM lepidocrocite (Lp;  $\gamma$ -FeOOH) and goethite (Gt;  $\alpha$ -FeOOH). Two ligands with different functional groups, ethylenediamine tetra acetic acid (EDTA) and the biogenic ligand- desferrioxamine (DFOB) were used as ligands that thermodynamically drive FeOOH dissolution by forming stable Fe(III)-L complexes in solution. To test whether electron transfer on the surface or through the bulk occurs, we conducted studies with  $^{57}\text{Fe}$  isotopes. In selected experiments, Fe(II) was added as  $^{57}\text{Fe(II)}$  and the release of  $^{57}\text{Fe}$  and  $^{56}\text{Fe}$  isotopes in the presence and absence of ligands was followed.

In main, there are two different experimental designs, which we applied in the thesis:

1) Experiments with added Fe(II) (see details in Table 1)

A) Batch measurements with Fe(II)/DFOB,  $^{57}\text{Fe(II)}$ /EDTA and  $^{57}\text{Fe(II)}$ /DFOB

B) Spectroscopic measurements with Attenuated Total Reflectance Fourier Transformed Infrared spectroscopy (ATR-FTIR) with added Fe(II)/EDTA

2) Experiments with photochemically produced Fe(II) (see details in Table 2)

A) Batch measurements with EDTA and DFOB

B) ATR-FTIR with EDTA

A parallel companion study was conducted by Kang et. al to explore the effect of Fe(II) on the dissolution of Lp, two types of Gt, 2-line ferrihydrite and hematite with N,N'-di(2-hydroxybenzyl)-ethylene-diamine-N,N'-diacetate (HBED) and DFOB.<sup>14</sup> Batch dissolution experiments were conducted under anoxic conditions with the same mineral suspension concentrations as we applied in our experiments.



**Table 1.** Summary of experimental conditions in which added Fe(II) or  $^{57}\text{Fe(II)}$  was applied to investigate lepidocrocite (Lp) and goethite (Gt) dissolution under anoxic conditions. A. Batch dissolution experiments. B. Spectroscopic measurements were performed with ATR-FTIR. The effect of Fe(II) on Lp dissolution was examined under anoxic conditions followed by addition of oxygen.

Description/Code <sup>a</sup>			Ligand (L)	Fe(II) or $^{57}\text{Fe(II)}$	pH	Chapter
			( $\mu\text{M}$ )	( $\mu\text{M}$ )	(Buffers <sup>b</sup> )	
A. Batch experiments (1125 $\mu\text{M}$ Lp or Gt)	Ligand before $^{57}\text{Fe(II)}$	Lp-L-Fe(II)	DFOB (20; 50)	0, 1, 2, 5	7.0 (carbonate)	3
		Lp-L- $^{57}\text{Fe(II)}$	EDTA (50)	1	6.0	2
			DFOB (20; 50)	2	6.0; 7.0 <sup>c</sup> ; 8.5	3
		Gt-L- $^{57}\text{Fe(II)}$	DFOB (50)	2	7.0 (carbonate)	3
	$^{57}\text{Fe(II)}$ before ligand	Lp- $^{57}\text{Fe(II)}$ -L	EDTA (50)	1	6.0	2
			DFOB (20; 50)	2	6.0; 7.0 <sup>c</sup> ; 8.5	3
		Gt- $^{57}\text{Fe(II)}$ -L	DFOB (50)	2	7.0 (carbonate)	3
		Lp- $^{57}\text{Fe(II)}$ -phen	phen (100)	2	7.0 (carbonate)	3
		Gt- $^{57}\text{Fe(II)}$ -phen	phen (100)	2	7.0 (carbonate)	3
	B. ATR-FTIR measurements (17 $\mu\text{M}$ Lp)	Lp-L-Fe(II)-IR	EDTA (50)	0, 0.2, 0.5, 1, 2, 4, 6, 10	6.0	2
			EDTA (50)	10	7.0	

<sup>a</sup> Code= Fe(III)(hydr)oxide-1<sup>st</sup> reactant-2<sup>nd</sup> reactant-method.

<sup>b</sup> MES buffer at pH 6.0; MOPS or carbonate buffer at pH 7.0; PIPES buffer at pH 8.5.

<sup>c</sup> Experiments were conducted both with MOPS and carbonate buffer at pH 7.0.

**Table 2.** Summary of main experimental conditions in order to assess the effect of photochemically produced Fe(II) ( $\text{Fe(II)}_{\text{hv}}$ ) on dissolution. UV-lamps were used to produce Fe(II) through either intermittent or continuous illumination into the system. A. Batch dissolution experiments were conducted and samples were analyzed with UV-VIS spectrometry and ICP-MS, as discussed in the Chapter 4. B. Spectroscopic measurements were performed with ATR-FTIR, as described in the Chapter 2.

Description/Code		Ligand (L) ( $\mu\text{M}$ )	continuous/intermittent UV-illumination ( $\text{Fe(II)}_{\text{hv}}$ )	pH	oxic/anoxic
A. Batch experiments	Lp-L- $\text{Fe(II)}_{\text{cont. hv}}$	EDTA; DFOB (50)	continuous	7.0	anoxic
					oxic
	Lp-EDTA- $\text{Fe(II)}_{\text{hv}}$	EDTA (50)	intermittent (3.2 $\mu\text{M}$ / 5min)	6.0; 7.0	anoxic
					oxic
	Lp-DFOB- $\text{Fe(II)}_{\text{hv}}$	DFOB (50)	intermittent (2.9 $\mu\text{M}$ / 15min)	7.0; 8.5	anoxic
					oxic
	Gt-EDTA- $\text{Fe(II)}_{\text{hv}}$	EDTA (50)	intermittent (2.7 $\mu\text{M}$ / 5min)	7.0	anoxic
					oxic
B. ATR-FTIR measurements	Lp-EDTA- $\text{Fe(II)}_{\text{hv}}$ -IR	EDTA (50)	intermittent	6.0; 7.0	anoxic
					Oxic

## Key Results

**Fe(II) accelerates Fe(III)(hydr)oxide dissolution with ligands at high pH (6.0, 7.0, 8.5) under anoxic conditions.**

*Effect of added Fe(II).* In the absence of Fe(II), DFOB alone led to very slow Lp and Gt dissolution rates which are in agreement with the rates reported by Kang et. al.<sup>14</sup> EDTA alone also led to very slow Lp dissolution which is in agreement with previous studies.<sup>15, 16</sup> Conversely, in the presence of micromolar concentrations of added Fe(II), accelerated Lp dissolution rates were observed with DFOB by up to 60- fold (refer to experimental conditions in Table 1; Lp-L-Fe(II) : DFOB was added 30 min before Fe(II) at pH 7.0 (carbonate buffer)). In the parallel study, Kang et. al reported accelerated Lp dissolution rates with DFOB and Fe(II) at pH 7.0 (MOPS buffer), which is in good agreement to our reported rates with MOPS-buffered systems. The rate of Lp dissolution is higher in carbonate- than in MOPS- buffered systems.

In spectroscopic measurements (Lp-L-Fe(II)-IR; Table 1), accelerated Lp dissolution with EDTA up to 31- fold was observed by submicromolar concentrations of added Fe(II) at pH 6.0. No phase changes in the Lp occurred during dissolution experiments.

Overall, the effect of added Fe(II) on Lp dissolution with biogenic ligand DFOB was higher at pH 7.0 than at pH 6.0 and pH 8.5. The effect with synthetic ligand EDTA was higher at pH 6.0 than at pH 7.0, possibly due to weaker adsorption of EDTA onto Lp at pH 7.0 than at pH 6.0.

*Effect of photochemically produced Fe(II).* Continuous UV-illumination led to accelerated dissolution with Lp/EDTA and with Lp/DFOB (Lp-L-Fe(II)<sub>cont. hv</sub>; Table 2). Intermittent illumination under anoxic conditions resulted in the accelerated Lp dissolution which persisted in the dark (Lp-EDTA-Fe(II)<sub>hv</sub> and Lp-DFOB-Fe(II)<sub>hv</sub>; Table 2). Brief doses of intermittent illuminations can drive the accelerated dissolution upto completion of the reaction in the dark rapidly with Lp/EDTA, but only slowly with Lp/DFOB and Gt/EDTA. The effect of photochemically produced Fe(II) on dissolution was much higher with continuous illumination (up to 40 fold acceleration) than with intermittent illumination (up to 8 fold acceleration).

### **Fe(II)-catalyzed dissolution rate is decreased or (nearly) ceased under oxic conditions.**

Addition of synthetic air decreased the Fe(II)-accelerated rates of Lp dissolution (Lp-L-Fe(II)-IR; Table 1), which was observed under anoxic conditions as mentioned above.

Photochemical experiments conducted under oxic conditions (Lp-L-Fe(II)<sub>cont.</sub> hv; Table 2), showed that continuous illumination led to accelerated Lp dissolution with DFOB and EDTA. With EDTA after certain period, dissolution rates decreased, indicating that EDTA and associated complexes could be photolyzed, which is in contrast to DFOB. Intermittent illuminations (Lp-EDTA-Fe(II)<sub>hv</sub>, Lp-DFOB-Fe(II)<sub>hv</sub>, and Gt-EDTA-Fe(II)<sub>hv</sub>; Table 2) did not lead to any accelerated dissolution which continued in the dark. Similar results were obtained in our spectroscopic measurements (Lp-EDTA-Fe(II)<sub>hv</sub>-IR; Table 2). Overall, results indicate that electron transfer on the surface or in the bulk does not lead to formation of Fe(II) that is protected from oxidation under oxic conditions.

### **Using isotopically-labelled Fe(II) to interrogate isotope exchange at the mineral surface.**

*Fate of added Fe(II) is dependent on order of addition.* The fate of added Fe(II) and isotopic exchange before and during dissolution are strongly dependent on the order of Fe(II) addition, as shown with Lp/EDTA in Chapter 2 and with Lp/DFOB in Chapter 3.

When <sup>57</sup>Fe(II) was added after ligand (Lp-L-<sup>57</sup>Fe(II); Table 1), <sup>57</sup>Fe remained in solution suggesting no to minimal isotopic exchange between solution and surface. When <sup>57</sup>Fe(II) was added before ligands (Lp-<sup>57</sup>Fe(II)-L; Table 1), <sup>57</sup>Fe(II) adsorption and the predominant <sup>56</sup>Fe(II) desorption occurred from Lp, indicating extensive isotopic exchange at pH 6.0. At pH 7.0 and 8.5, tracer <sup>57</sup>Fe(II) was lost immediately from solution due to nearly complete adsorption of tracer <sup>57</sup>Fe(II). Subsequent concentrations of desorbed Fe(II) in the absence of ligands were too low for determination of isotopic composition. We, therefore, probed the isotopic composition of adsorbed Fe(II) at pH 7.0 with phenanthroline (phen), which is a ligand that preferentially complexes with Fe(II) and thus lead to desorption of Fe(II), but not to dissolution. Addition of phen caused the release of both <sup>56</sup>Fe(II) and <sup>57</sup>Fe(II) in solution, but the concentration of <sup>56</sup>Fe was higher than <sup>57</sup>Fe(II) indicating the occurrence of isotope exchange on the surface of Lp (Lp-<sup>57</sup>Fe(II)-phen; Table 1).

When ligand was added after  $^{57}\text{Fe(II)}$  addition, the previously exchanged/sorbed tracer  $^{57}\text{Fe}$  reappeared into solution at pH 6.0, 7.0, 8.5, implying that the site of adsorption of added  $^{57}\text{Fe(II)}$  and dissolution might be the same or neighboring sites. In our study, bulk electron conduction would possibly not occur as most of the exchanged/sorbed tracer  $^{57}\text{Fe}$  released back to solution with the concurrent release of  $^{56}\text{Fe}$ - complexed to ligand. These observations indicate that the Fe(II)-catalyzed ligand-controlled dissolution can be faster process than Fe(II)-catalyzed recrystallization.

*Fate of added Fe(II) is dependent on Fe(III) phases.* When tracer  $^{57}\text{Fe(II)}$  was added before ligand to Gt suspension, rapid decrease of  $^{57}\text{Fe}$  observed in solution due to the adsorption (Gt- $^{57}\text{Fe(II)}$ -L; Table 1). Like for Lp, the subsequent release of Fe(II) was also not detectable for Gt due to very low concentration of desorbed Fe(II). When phen was added, the substantial desorption of  $^{57}\text{Fe(II)}$ -phen complexes were observed which is in contrast to our observations with Lp (Gt- $^{57}\text{Fe(II)}$ -phen; Table 1). This might indicate that isotope exchange occurs in Gt within a longer time scale than in Lp.

Upon ligand addition, the rates of  $^{57}\text{Fe}$  release and  $^{56}\text{Fe}$  were in similar range for Gt, in contrast to Lp. These contrasting fates of added tracer  $^{57}\text{Fe}$  during Lp and Gt dissolution can be attributed to the differences in the structure and mineralogy of solids. Isotope tracer experiments with different Fe(III) phases thus enable us to understand mechanistic differences of Fe(II)- catalyzed dissolution processes of different Fe(III) phases.

In recent recrystallization studies, the release Fe(II) was suggested to occur from a distant site through bulk electron conduction mechanism within a long time scale (hrs to weeks).<sup>13, 17</sup> Note that in our study the reaction time between  $^{57}\text{Fe(II)}$  and Fe(III) was only 1800 s. On the short time scale of our experiments, and with low Fe(II) concentrations, we most likely observe isotope exchange only on the surface. Our time scales are not sufficiently long and the Fe(II) concentrations are not sufficiently high to observe isotope exchange with the bulk.

### Using kinetic models to identify possible reaction mechanisms

Kinetic models were developed to explain the experimental data and to discuss possible reaction mechanisms of accelerated dissolution and isotope exchange. A (pseudo) first order empirical model, which considers the entire course of dissolution, was applied to determine the accelerated dissolution rates. The model assumed that the accelerated rate of dissolution is directly proportional to the added Fe(II) and free ligand concentration in solution. A simple rate coefficient was derived, as discussed in Chapter 3, from the model to further determine the rates of dissolution.

Two detailed mechanistic kinetic models were developed to describe different reaction steps in dissolution process of Lp with EDTA and DFOB (Chapter 2 and 3). The model, as discussed in Chapter 2, showed that the Fe(II)-catalyzed dissolution can be explained by formation of surface Fe(II)-L complexes (both by adsorption of dissolved Fe(II)-L complexes and by adsorption of dissolved ligand on adsorbed Fe(II)), followed by electron transfer to a neighboring site and detachment of Fe(III)-L complexes. The main difference between two models is that the model for EDTA includes the adsorption of Fe(III)EDTA on the mineral surface, while the model for DFOB does not include adsorption of Fe(III)DFOB. While adsorption of Fe(III)EDTA to Fe(III)(hydr)oxide has been observed<sup>18</sup>, adsorption of Fe(III)DFOB to Lp has shown to be minimal or non-detectable.<sup>19</sup> The second model is an extended model of the first one, which provides new information about electron transfer and charge distribution on the surface of Lp or Gt, which was missing in the model with EDTA. The model can further explain the relative rates of release of <sup>57</sup>Fe and <sup>56</sup>Fe before and during accelerated dissolution by estimating only the distribution of charge on the surface.

## Environmental Significance

In recent times, interfacial electron transfer and isotope exchange with Fe(II)/Fe(III) have widely been investigated due to their possible roles in the wide-spread biogeochemical processes.<sup>13, 20-22</sup> For example, only Fe(II) adsorption on Fe(III)(hydr)oxides can lead to the formation of new or mixed Fe-phases, crystal growth and recrystallization of the mineral.<sup>10, 11, 23, 24</sup> Previous Fe(II) catalyzed recrystallization studies have not considered the mobility of electrons on the surface and possibly in the bulk in the presence of ligands. Such mobility of electrons could possibly lead to Fe(II) that is protected from oxidation by dissolved O<sub>2</sub>, but still leads to accelerated dissolution. It could also lead to preferential dissolution of surfaces different from the surface where the adsorption of Fe(II) occurs.

The results of this thesis show that electron transfer between adsorbed <sup>57</sup>Fe(II) and Fe(III) surfaces sites does occur, but that the mobile charge is not protected from oxidation and does not lead to sustained accelerated dissolution under oxic conditions. Illumination also did not lead to generation of Fe(II) in the bulk or on the surface that leads to accelerated dissolution under oxic conditions. Furthermore, in all our experiments, no evidence for phase transformation of Lp to Gt or magnetite with added Fe(II) was found with ATR-FTIR, in contrast to previous studies with higher concentration of Fe(II).<sup>25, 26</sup> These results signify that the mechanism of bulk electron conduction most likely does not explain the Fe(II)-catalyzed ligand-controlled dissolution.

The accelerating effect of Fe(II) on ligand-controlled dissolution was observed for a variety of ligands and Fe(III)(oxyhydr)oxides. As previous studies suggested,<sup>8, 9</sup> Fe(II)-catalyzed dissolution could be an important pathway in the dissolution of Fe(III) phases in sub- and anoxic environments, for example, in soils and sediments, and in the oxic–anoxic interface in lakes, wetlands and irrigated fields.<sup>4, 9, 27, 28</sup> The reported dissolution rate was larger at pH 7.0 carbonate- than in MOPS- buffered suspensions with biogenic ligand, suggesting that Fe(II)-catalyzed dissolution might be highly relevant pathway in soils and waters with pH values around 7 where Fe-deficiency is usually high in organisms.

In environments that are exposed to sunlight, both photo-reductive and photochemically formed Fe(II) can accelerate dissolution of Fe(III) phases. Continuous UV-A illumination can accelerate dissolution of Fe(III) phases in sunlit oxic environments, for example, in the ocean and in the atmosphere. As the results discussed in Chapter 4, intermittent UV-A light can also efficiently drive the

dissolution of Fe(III) phases at oxic-anoxic interfaces, for example in shallow lakes and ponds with algal bloom and phytoplankton environments. Studies have shown the occurrence of transient anoxic zones and sub-oxic environments in lakes, and ponds.<sup>29, 30</sup> Intermittent exposure of sun light to such environments can possibly lead to accelerated dissolution of Fe(III) phases and to increase the bioavailability of Fe among organisms.

Ligands with carboxylate functional groups (for e.g., EDTA) are likely prone to photolysis on surfaces and in solution, which limits their ability to form stable Fe(III)-L complexes and to keep Fe(III) in solution. Conversely, photo-stable ligands such as DFOB can form dissolved Fe(III)-DFOB complexes under continuous illumination in oxic conditions. The results highlight the importance of those ligands which can stabilize Fe(III) in solution. These results could also be highly relevant to marine biota which are involved acquiring Fe as their micro-nutrient in stress conditions.<sup>31</sup>

Commonly, the dissolution of Fe(III)(oxyhydr)oxides in natural systems is controlled by reductive and ligand-controlled processes. This thesis explored systematically the interplay of redox and ligand-controlled processes occurring at redox dynamic environments. Results presented in this thesis demonstrate consistently large catalytic effect of traces of Fe(II) on Fe(III)(hydr)oxide dissolution in a pH range where dissolution of Fe(III)-phases is slower and Fe(II) adsorption is higher than in acidic pH. Results from this study advances our current mechanistic understanding of dissolution processes in the presence of ligands and reductants as well as their significance in natural systems. Plants and microorganisms thus, as beneficiaries of the interplay of ligands and/or reductant, can acquire Fe in sub- and anoxic aquatic or terrestrial systems in circumneutral to alkaline pH ranges. The Fe(II)-catalysis is thus highlighted here as one of the key processes in biogeochemical Fe cycling and biological Fe acquisition.



## Future Outlook

*Speciation of Fe during initial phase of accelerated dissolution.* Addition of Fe(II) in the presence of ligands leads to the fast formation of dissolved Fe(II)-L complexes. Currently we assume that these Fe(II)-L complex transfers the electron to the same or neighboring site of the solid and releases back as Fe(III)-L complex. However, the oxidation states of added Fe within the initial phase of dissolution remained unknown. This was experimentally challenging to determine due to the strong interference of fast formation of dissolved Fe-L complexes upon addition of submicromolar concentrations of added Fe(II). If we manage to determine oxidation state, we can more precisely comment on the mechanism of dissolution. The one way to tackle this experimental challenge could be to have the UV-VIS spectrometer inside a glovebox and conduct the dissolution experiment in real-time measured with UV-VIS in order to decouple the initial formation of Fe(II)-L and/or Fe(III)-L complexes.

*Theoretical calculation to explain surface structures.* In a collaborative study with oxalate and Lp, we investigated the mechanism of ligand-promoted dissolution with theoretical calculations based on density functional theory (DFT). We specifically explored the structures of surface complexes and their properties with Lp and oxalate.<sup>32</sup> The study demonstrated that ligand-promoted dissolution of Lp with oxalate is not proportional to the total surface concentrations of adsorbed oxalate, but to the concentration of bi-dentate mononuclear complexes (BM) which are the most reactive species during dissolution.

DFT calculations will be useful in order to interpret the spectra we obtained with Lp and EDTA in ATR-FTIR measurements. DFT calculations can identify major structures of surface complexes that agree best with experimental IR results. Comparison of both experimental and theoretical studies can provide us consistent understanding on adsorption mechanisms of ligands and the contributions of various surface complexes and their structures.

It is noteworthy that DFT calculations were challenging to perform with Lp and oxalate as they were time consuming and required much computing power. DFT calculations with the larger ligand EDTA in the presence of Fe(II) were not attempted in this thesis as they can be computationally more demanding.

*Mechanistic exploration of molecular environments.* Experimentally, time-resolved X-ray absorption spectroscopy (TR-XAS) might provide molecular level structural information of Fe(III)(oxyhydr)oxides with Fe(II), which would be helpful to better understand the redox state of Fe and bonding environments with or without ligands. Ultrafast pump-probe technique coupled with optical transient absorption spectroscopy might be the state-of-art technique to track the electrons into surface or bulk solids. Coupled with photochemical experiments, we can better understand the mobility of electrons within a solid in the presence or absence of ligands, which might explain *if at all* electrons conduct through the bulk in the presence of a dissolution-promoting ligand.

Isotope tracer experiments revealed that the fate of added Fe(II) highly depends on the type of Fe(III) phases. This raises a question whether a general mechanism can explain Fe(II)-catalyzed dissolution processes for Fe(III)(oxyhydr)oxides. Therefore, future studies with various Fe(III) phases are necessary to understand the fate of added Fe(II) and relative differences in mechanisms of accelerated dissolution of different Fe(III)-phases in different time scales (hours to months).

*Trace metal release coupled with Fe(II)-catalyzed dissolution.* Fe(II)-catalyzed dissolution might lead to release of (trace) elements in a redox dynamic environment.<sup>33, 34, 35</sup> The application of <sup>57</sup>Fe isotope tracer experiments in investigating isotope exchange and dissolution processes of Fe(III)- phases can most likely build a foundation for further studies on understanding trace metal release in minerals in redox dynamic environments.

*Fe(II)-catalyzed dissolution of amorphous and mixed Fe(III)-phases in the field.* Recent studies have shown that changes in redox conditions often lead to the formation of amorphous to poorly crystalline Fe(III) phases.<sup>36</sup> In this thesis, pure crystalline Fe(III)(hydr)oxide phases were tested. The effect of Fe(II) should also be tested with amorphous to poorly crystalline Fe(III)- phases formed in natural environments. In nature, Fe(III) phases are often available in mixed forms; for example Fe-bearing clay minerals, Fe sulfides, (hydr)oxides of Fe and manganese, Fe mixed with humic substances.<sup>28</sup> The effect of Fe(II) on these mixed Fe phases is worth exploring due to their high relevance in the environments. The synergistic effects of redox and ligand-controlled processes on such systems may also provide new opportunities for understanding the biogeochemical processes of mixed phases at environmental redox interfaces.

## References

1. Kraemer, S. M., Iron oxide dissolution and solubility in the presence of siderophores. *Aquatic Sciences* **2004**, *66*, (1), 3-18.
2. Hersman, L. E.; Huang, A.; Maurice, P. A.; Forsythe, J. E., Siderophore production and iron reduction by *Pseudomonas mendocina* in response to iron deprivation. *Geomicrobiology Journal* **2000**, *17*, (4), 261-273.
3. Cheah, S. F.; Kraemer, S. M.; Cervini-Silva, J.; Sposito, G., Steady-state dissolution kinetics of goethite in the presence of desferrioxamine B and oxalate ligands: Implications for the microbial acquisition of iron. *Chemical Geology* **2003**, *198*, (1-2), 63-75.
4. Reichard, P. U.; Kretzschmar, R.; Kraemer, S. M., Dissolution mechanisms of goethite in the presence of siderophores and organic acids. *Geochimica Et Cosmochimica Acta* **2007**, *71*, (23), 5635-5650.
5. Suter, D.; Siffert, C.; Sulzberger, B.; Stumm, W., Catalytic dissolution of iron(III)(hydr)oxides by oxalic acid in the presence of Fe(II). *Naturwissenschaften* **1988**, *75*, (11), 571-573.
6. Banwart, S.; Davies, S.; Stumm, W., The Role of Oxalate in Accelerating the Reductive Dissolution of Hematite ( $\alpha$ -Fe<sub>2</sub>O<sub>3</sub>) by Ascorbate. *Colloids and Surfaces* **1989**, *39*, (4), 303-309.
7. Suter, D.; Banwart, S.; Stumm, W., Dissolution of Hydrous Iron(III) Oxides by Reductive Mechanisms. *Langmuir* **1991**, *7*, (4), 809-813.
8. Wang, Z.; Schenkeveld, W. D. C.; Kraemer, S. M.; Giammar, D. E., Synergistic Effect of Reductive and Ligand-Promoted Dissolution of Goethite. *Environmental Science and Technology* **2015**, *49*, (12), 7236-7244.
9. Schenkeveld, W. D. C.; Wang, Z. M.; Giammar, D. E.; Kraemer, S. M., Synergistic Effects between Biogenic Ligands and a Reductant in Fe Acquisition from Calcareous Soil. *Environmental Science & Technology* **2016**, *50*, (12), 6381-6388.
10. Williams, A. G. B.; Scherer, M. M., Spectroscopic evidence for Fe(II)-Fe(III) electron transfer at the iron oxide-water interface. *Environmental Science & Technology* **2004**, *38*, (18), 4782-4790.
11. Yanina, S. V.; Rosso, K. M., Linked reactivity at mineral-water interfaces through bulk crystal conduction. *Science* **2008**, *320*, (5873), 218-222.
12. Handler, R. M.; Beard, B. L.; Johnson, C. M.; Scherer, M. M., Atom exchange between aqueous Fe(II) and goethite: An Fe isotope tracer study. *Environmental Science and Technology* **2009**, *43*, (4), 1102-1107.
13. Handler, R. M.; Friedrich, A. J.; Johnson, C. M.; Rosso, K. M.; Beard, B. L.; Wang, C.; Latta, D. E.; Neumann, A.; Pasakarnis, T.; Premaratne, W. A. P. J.; Scherer, M. M., Fe(II)-catalyzed recrystallization of goethite revisited. *Environmental Science and Technology* **2014**, *48*, (19), 11302-11311.
14. Kang, K.; Schenkeveld, W. D. C.; Biswakarma, J.; Borowski, S. C.; Hug, S. J.; Hering, J. G.; Kraemer, S. M., Low Fe(II) Concentrations Catalyze the Dissolution of Various Fe(III) (hydr)oxide

- Minerals in the Presence of Diverse Ligands and over a Broad pH Range. *Environmental Science & Technology* **2019**, 53, (1), 98-107.
15. Sulzberger, B.; Suter, D.; Siffert, C.; Banwart, S.; Stumm, W., Dissolution of Fe(III)(Hydr)Oxides in Natural-Waters - Laboratory Assessment on the Kinetics Controlled by Surface Coordination. *Marine Chemistry* **1989**, 28, (1-3), 127-144.
  16. Wehrli, B.; Sulzberger, B.; Stumm, W., Redox processes catalyzed by hydrous oxide surfaces. *Chemical Geology* **1989**, 78, (3-4), 167-179.
  17. Zarzycki, P.; Rosso, K. M., Stochastic Simulation of Isotopic Exchange Mechanisms for Fe(II)-Catalyzed Recrystallization of Goethite. *Environmental Science and Technology* **2017**, 51, (13), 7552-7559.
  18. Noren, K.; Loring, J. S.; Bargar, J. R.; Persson, P., Adsorption Mechanisms of EDTA at the Water-Iron Oxide Interface: Implications for Dissolution. *Journal of Physical Chemistry C* **2009**, 113, (18), 7762-7771.
  19. Borer, P.; Hug, S. J.; Sulzberger, B.; Kraemer, S. M.; Kretzschmar, R., ATR-FTIR spectroscopic study of the adsorption of desferrioxamine B and aerobactin to the surface of lepidocrocite ( $\gamma$ -FeOOH). *Geochimica Et Cosmochimica Acta* **2009**, 73, (16), 4661-4672.
  20. Gorski, C. A.; Scherer, M. M., Fe<sup>2+</sup> sorption at the Fe oxide-water interface: A revised conceptual framework. In *ACS Symposium Series*, American Chemical Society: 2011; Vol. 1071, pp 315-343.
  21. Gorski, C. A.; Handler, R. M.; Beard, B. L.; Pasakarnis, T.; Johnson, C. M.; Scherer, M. M., Fe Atom Exchange between Aqueous Fe<sup>2+</sup> and Magnetite. *Environmental Science & Technology* **2012**, 46, (22), 12399-12407.
  22. Joshi, P.; Fantle, M. S.; Larese-Casanova, P.; Gorski, C. A., Susceptibility of Goethite to Fe<sup>2+</sup>-Catalyzed Recrystallization over Time. *Environmental Science and Technology* **2017**, 51, (20), 11681-11691.
  23. Catalano, J. G.; Fenter, P.; Park, C.; Zhang, Z.; Rosso, K. M., Structure and oxidation state of hematite surfaces reacted with aqueous Fe(II) at acidic and neutral pH. *Geochimica Et Cosmochimica Acta* **2010**, 74, (5), 1498-1512.
  24. Katz, J. E.; Zhang, X. Y.; Attenkofer, K.; Chapman, K. W.; Frandsen, C.; Zarzycki, P.; Rosso, K. M.; Falcone, R. W.; Waychunas, G. A.; Gilbert, B., Electron Small Polarons and Their Mobility in Iron (Oxyhydr)oxide Nanoparticles. *Science* **2012**, 337, (6099), 1200-1203.
  25. Pedersen, H. D.; Postma, D.; Jakobsen, R.; Larsen, O., Fast transformation of iron oxyhydroxides by the catalytic action of aqueous Fe(II). *Geochimica Et Cosmochimica Acta* **2005**, 69, (16), 3967-3977.
  26. Jones, A. M.; Collins, R. N.; Rose, J.; Waite, T. D., The effect of silica and natural organic matter on the Fe(II)-catalysed transformation and reactivity of Fe(III) minerals. *Geochimica Et Cosmochimica Acta* **2009**, 73, (15), 4409-4422.

27. Schmidt, C.; Kappler, A., Iron cycling in freshwater environments - A theoretical concept on the dynamics of coupled chemical and biological iron redox processes. *Geochimica et Cosmochimica Acta* **2009**, 73, (13), A1178-A1178.
28. Kappler, A.; Straub, K. L., Geomicrobiological cycling of iron. *Molecular Geomicrobiology* **2005**, 59, 85-108.
29. Zhang, T.; He, J.; Luo, X., Effect of Fe and EDTA on Freshwater Cyanobacteria Bloom Formation. *Water* **2017**, 9, (5), 326.
30. Ploug, H., Cyanobacterial surface blooms formed by *Aphanizomenon* sp and *Nodularia spumigena* in the Baltic Sea: Small-scale fluxes, pH, and oxygen microenvironments. *Limnology Oceanography* **2008**, 53, (3), 914-921.
31. Boiteau, R. M.; Mende, D. R.; Hawco, N. J.; McIlvin, M. R.; Fitzsimmons, J. N.; Saito, M. A.; Sedwick, P. N.; DeLong, E. F.; Repeta, D. J., Siderophore-based microbial adaptations to iron scarcity across the eastern Pacific Ocean. *Proceedings of the National Academy of Sciences of the United States of America* **2016**, 113, (50), 14237-14242.
32. Borowski, S. C.; Biswakarma, J.; Kang, K.; Schenkeveld, W. D. C.; Hering, J. G.; Kubicki, J. D.; Kraemer, S. M.; Hug, S. J., Structure and reactivity of oxalate surface complexes on lepidocrocite derived from infrared spectroscopy, DFT-calculations, adsorption, dissolution and photochemical experiments. *Geochimica et Cosmochimica Acta* **2018**.
33. Hinkle, M. A. G.; Wang, Z. M.; Giammar, D. E.; Catalano, J. G., Interaction of Fe(II) with phosphate and sulfate on iron oxide surfaces. *Geochimica Et Cosmochimica Acta* **2015a**, 158, 130-146.
34. Hinkle, M. A. G.; Catalano, J. G., Effect of phosphate and sulfate on Ni repartitioning during Fe(II)-catalyzed Fe(III) oxide mineral recrystallization. *Geochimica Et Cosmochimica Acta* **2015b**, 165, 62-74.
35. Voegelin, A.; Senn, A. C.; Kaegi, R.; Hug, S. J., Reductive dissolution of As(V)-bearing Fe(III)-precipitates formed by Fe(II) oxidation in aqueous solutions. *Geochemical Transactions* **2019**, 20.
36. Senn, A. C.; Kaegi, R.; Hug, S. J.; Hering, J. G.; Mangold, S.; Voegelin, A., Composition and structure of Fe(III)-precipitates formed by Fe(II) oxidation in water at near-neutral pH: Interdependent effects of phosphate, silicate and Ca. *Geochimica Et Cosmochimica Acta* **2015**, 162, 220-246.





## **Curriculum Vitae**

### **JAGANNATH BISWAKARMA**

Eawag, W & T  
Ueberlandstrasse 133  
Duebendorf 8600, CH

## **EDUCATION**

**ETH Zurich**, Zurich, Switzerland, Doctoral student in Environmental Sciences, 2015-present.

**University of Zurich**, Zurich, Switzerland, Master of Science in Environmental Sciences, 2012-2014.

**Bharath University**, Chennai, India, Bachelor of Technology in Industrial Biotechnology, 2006-2010.

## **PROFESSIONAL EXPERIENCE**

**Eawag, Swiss Federal Institute of Aquatic Science & Technology**, Duebendorf, Switzerland, Water Resources and Drinking Water Department, (2015-present) (doctoral) Researcher.

**ETH Zurich**, Zurich, Switzerland, Department of Chemistry and Applied Biosciences, Institute for Chemical and Bioengineering, Safety & Environmental Technology Group, (2013- 2014) Research Assistant.

**University of Zurich**, Zurich, Institute of Evolutionary Biology and Environmental Sciences, (2013) Field Assistant.

**Hiyoshi Corporation**, Omihachiman (Japan), Chennai (India), (May- July 2009) Intern, (2011-2012) Environmental Officer.

**Ministry of New and Renewable Energy** (Govt. of India), Vellore Institute of Technology University, Tamilnadu, India, (2011) Research Fellow.

**Ministry of Defence** (Govt. of India), Defence Research Laboratory, Tezpur, India (December 2009- March 2010) Research Assistant.

## **PROFESSIONAL AFFILIATIONS, AND ACTIVITIES**

**Member:** Geochemical Society; American Chemical Society.

**Reviewer** to Environmental Science & Technology; Environmental Science: Water Research & Technology; Soil Science Society of America Journal

**2017, Co-organizer and co-chair**, IBP PhD Congress, ETH Zurich, Switzerland.

**2009, International Fellowship**, ABK AOTS DOSOKAI, Japan and Hiyoshi Corporation, Japan.





